Lecture Notes:
Topological Condensed Matter Physics

Sebastian Huber and Titus Neupert

Department of Physics, ETH Zürich
Department of Physics, University of Zürich

If you notice mistakes or typos, please report them to michael.denner@physik.uzh.ch or periv@phys.ethz.ch

Contents

List of Figures

List of Tables

Chapter 1

The integer quantum Hall effect I

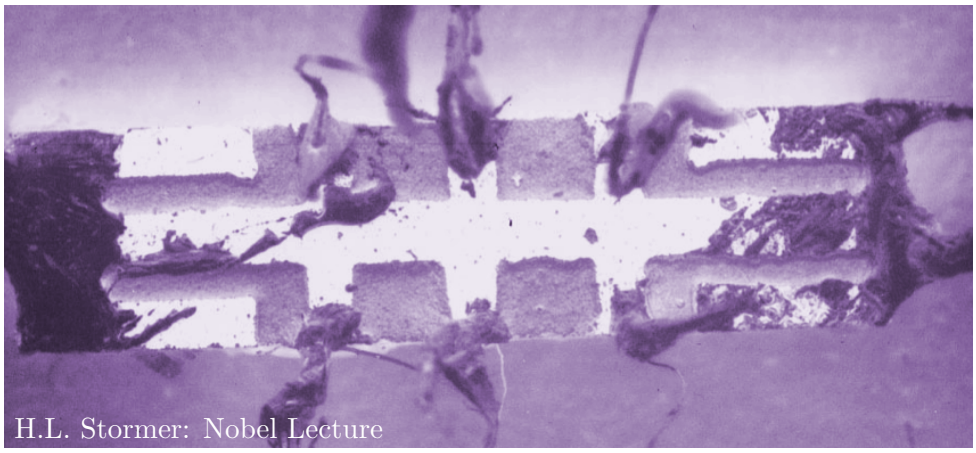

Learning goals

- We know the basic phenomenology of the quantum Hall effect (QHE)
- We know the structure of the lowest Landau level (LLL)
- We understand the role of disorder for the QHE.

- K. von Klitzing, G. Dorda, and M. Pepper, Phys. Rev. Lett. **45**, 494 (1980)

In large parts of this chapter we follow reference [2].

1.1 Preliminaries

The Lorentz force acting on charged particles moving in a two-dimensional plane leads to a build-up of charges perpendicular to the direction of motion. This is the classical Hall effect first discussed by Edwin Hall in 1879 [3]. To understand this, let us consider a two-dimensional system which is translationally invariant. We move to a frame moving with $-\mathbf{v}$ where we therefore see electrons moving with velocity $\mathbf{v}$ and carrying a current

$$\mathbf{J} = -ne\mathbf{v}, \tag{1.1.1}$$

where n is the particle density and e is the electron charge. In the laboratory frame we have $\mathbf{E} = \mathbf{0}$ and $\mathbf{B} = B\hat{\mathbf{z}}$. Hence, in the moving frame we obtain

$$\mathbf{E} = -\mathbf{v} \wedge \mathbf{B} \qquad \text{and} \qquad \mathbf{B} = B\hat{\mathbf{z}}. \tag{1.1.2}$$

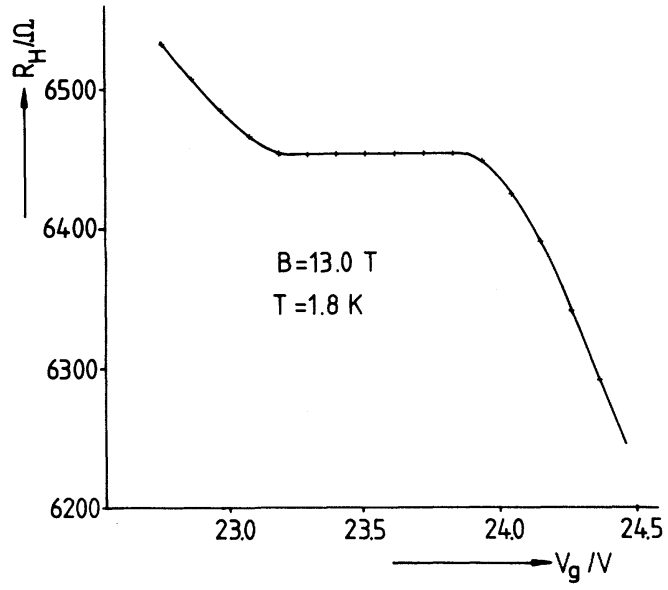

Figure 1.1: Measured Hall resistivity as a function of an applied back-gate which leads to a change in the particle density n. The pronounced plateau is the hallmark of the quantum Hall effect. Figure taken from Ref [1].

We can express the electric field as

$$\mathbf{E} = \frac{B}{ne}\mathbf{J} \wedge \hat{\mathbf{z}}. \tag{1.1.3}$$

The resistivity ρ is defined as the relation between the current and the electric field $E^\mu = \rho_{\mu\nu} J^\nu$. We thus find

$$\rho = \frac{B}{ne}\begin{pmatrix} 0 & 1 \\ -1 & 0 \end{pmatrix} \qquad \Rightarrow \qquad \sigma = \frac{ne}{B}\begin{pmatrix} 0 & -1 \\ 1 & 0 \end{pmatrix}. \tag{1.1.4}$$

We see that owing to the non-zero σ_{xy} the longitudinal resisitivity $\rho_{xx} = \sigma_{xx} = 0$ is equal to the longitudinal conductivity. Moreover, the Hall resistivity is proportional to the magnetic field

$$\rho_{xy} = \frac{B}{ne}. \tag{1.1.5}$$

This is in striking contrast to the seminal discovery of von Klitzing and his co-workers in 1980 [1], see Fig. 1.1. The only ingredient in our theoretical model so far, however, was translational symmetry. In the following, we first take steps towards a quantum mechanical understanding of electrons in a magnetic field before we come back to the issue of translational symmetry breaking via disorder.

1.2 Classical Lagrangian

To motivate how the magnetic field enters our quantum mechanical description, we recall that the classical equations of motions are reproduced by the following Lagrangian $\mathcal{L} = \frac{m}{2}\dot{x}^\mu \dot{x}^\mu - e\dot{x}^\mu A^\mu$.

$$-\frac{d}{dt}\frac{\partial \mathcal{L}}{\dot{x}^\mu} + \frac{\partial \mathcal{L}}{\partial x^\mu} = 0 \qquad \Rightarrow \qquad m\ddot{x} = -eB\dot{y} \quad \text{and} \quad m\ddot{y} = eB\dot{x}. \tag{1.2.1}$$

The canonical momentum is given by $p^\mu = \frac{\partial \mathcal{L}}{\dot{x}^\mu} = m\dot{x}^\mu - eA^\mu$ and therefore the Hamiltonian reads

$$H(x^\mu, p^\mu) = \dot{x}^\mu p^\mu - \mathcal{L}(x^\mu, \dot{x}^\mu) = \frac{1}{2m}\left(p^\mu + eA^\mu\right)\left(p^\mu + eA^\mu\right). \tag{1.2.2}$$

With this small detour into classical mechanics we are now in the position to tackle the quantum mechanical problem of a particle in a magnetic field.

1.3 Landau levels

We have to solve for the eigenstates of the following Hamiltonian

$$H = \frac{1}{2m}(\mathbf{p} + e\mathbf{A})^2. \tag{1.3.1}$$

As only the vector potential $\mathbf{A}$ enters the Hamiltonian we have to chose an appropriate gauge. For now we choose the Landau gauge where $\mathbf{A} = xB\hat{\mathbf{y}}$. We check that $\nabla \wedge \mathbf{A} \equiv \mathbf{B} = (\partial_x A_y - \partial_y A_x)\hat{\mathbf{z}} = B\hat{\mathbf{z}}$. Inserted into the above Hamiltonian we obtain

$$H = \frac{1}{2m}\left[p_x^2 + (p_y + exB)^2\right]. \tag{1.3.2}$$

We immediately observe that this Hamiltonian has a translational symmetry in y direction. We therefore choose the following ansatz for the wave function $\psi(x, y) = e^{iky} f_k(x)$. With this ansatz we obtain a family of one-dimensional problems (one per momentum k in y-direction)

$$h_k = -\frac{\hbar^2\partial_x^2}{2m} + \frac{1}{2}m\omega_c^2\left(x + kl^2\right)^2 \qquad \text{with} \qquad \omega_c = \frac{eB}{m} \qquad \text{and} \qquad l = \sqrt{\frac{\hbar}{eB}}. \tag{1.3.3}$$

We see that we are dealing with a (displaced) one-dimensional harmonic oscillator. The characteristic frequency is known as the the cyclotron frequency ω_c. The displacement is proportional to the y-momentum and measured in the natural length scale, the magnetic length l. Solving the harmonic oscillator we find that

1. $\epsilon_k = \hbar\omega_c\left(s + \frac{1}{2}\right)$ with $s \in \mathbb{N}$.

2. For $s = 0$, i.e., the LLL the wave function is a Gaussian centered at $X_k = -kl^2$

$$\psi(x, y) = \frac{1}{\sqrt{\pi^{1/2}L_y l}} e^{iky} e^{-\frac{1}{2l^2}(x+kl^2)^2} = \frac{1}{\sqrt{\pi^{1/2}L_y l}} e^{iky} e^{-\frac{1}{2l^2}(x-X_k)^2}, \tag{1.3.4}$$

   where L_y is the extent in y-direction as shown in Fig. 1.2.

3. We have a vastly degenerate system. The number of degenerate states in each LL is given by

$$N = \frac{L_y}{2\pi}\int_0^{L_x/l^2} dk = \frac{L_x L_y}{2\pi l^2} = \frac{L_x L_y B}{\Phi_0}, \tag{1.3.5}$$

   where $\Phi_0 = h/e$ is the magnetic flux quantum. In other words, per magnetic flux quantum that penetrates the sample we have one state per Landau level.

Before we continue we should remind ourselves that in the case of huge degeneracies any perturbation might have dramatic effect. Moreover, the choice of basis can facilitate the description of these effects. For the case of a magnetic field, the choice of gauge determined the shape of the basis wave-functions. We will come back to this point later.

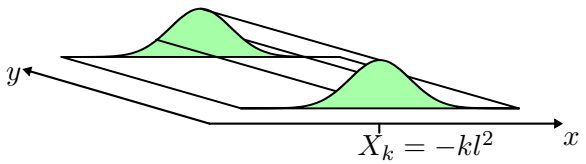

Figure 1.2: Eigenfunctions of the LLL in the Landau gauge.

1.4 Currents

We set out to understand the Hall conductivity. To make further progress, we need to calculate currents. We evaluate the current operator in y direction, $J_y = -\frac{e}{m}(p_y + eA_y)$, in the LLL eigenfunctions

$$\langle\psi|J_y|\psi\rangle = -\frac{e}{m\pi^{1/2}l}\int dx\, e^{-\frac{(x-X_k)^2}{2l^2}}(\hbar k + eBx)e^{-\frac{(x-X_k)^2}{2l^2}} \tag{1.4.1}$$

$$= -\frac{e\omega_c}{\pi^{1/2}l}\int dx\, e^{-\frac{(x-X_k)^2}{l^2}}(x + kl^2) = -\frac{e\omega_c}{\pi^{1/2}l}\int d\alpha\, e^{-\frac{\alpha^2}{l^2}}\alpha = 0. \tag{1.4.2}$$

The last equality holds as the integrand is odd under $\alpha \to -\alpha$. In other words, no net current is flowing as shown in Fig. 1.3.

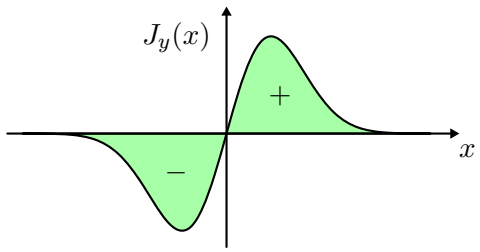

Figure 1.3: Current distribution in the lowest Landau level.

For a current to flow, we need to add an electric field in x-direction $V(x) = eEx$. We still are translationally invariant in y-direction and the one-dimensional problem is changed to

$$h_k = -\frac{\hbar^2\partial_x^2}{2m} + \frac{1}{2}m\omega_c^2\left(x + kl^2\right)^2 + eEx \tag{1.4.3}$$

$$= -\frac{\hbar^2\partial_x^2}{2m} + \frac{1}{2}m\omega_c^2\left(x + kl^2 + \frac{eE}{m\omega_c^2}\right)^2 + eEX_k' + \frac{1}{2}m\bar{v}^2, \tag{1.4.4}$$

where the center of the Gaussians is shifted

$$X_k' = -kl^2 - eE/m\omega_c^2 \tag{1.4.5}$$

and an additional energy $\frac{1}{2}m\bar{v}^2$ with $\bar{v} = -E/B$ arises from the drift of the electrons. The immediate conclusion is that the new energy depends on k, i.e., the huge degeneracy is lifted

$$\epsilon_k = \frac{1}{2}\hbar\omega_c + eEX_k' + \frac{1}{2}m\bar{v}^2. \tag{1.4.6}$$

With an energy that depends on k we can also calculate a non-zero group velocity

$$v_{\text{group}} = \frac{1}{\hbar}\frac{\partial\epsilon_k}{\partial k} = \frac{eE}{\hbar}\frac{\partial X_k'}{\partial k} = -\frac{eE}{\hbar}l^2 = -\frac{E}{B} = \bar{v}. \tag{1.4.7}$$

With this we reach the classical result

$$\langle J_y\rangle = -e\bar{v} \qquad \Rightarrow \qquad \sigma_{xy} = -\frac{ne}{B}. \tag{1.4.8}$$

We reached the same conclusion as with the classical manipulations based entirely on translational symmetry in the beginning of this chapter. In order to make further progress we should take a closer look at the finite extent of a realistic sample as well as on disorder effects to understand the quantization of σ_{xy}.

1.5 Edge states

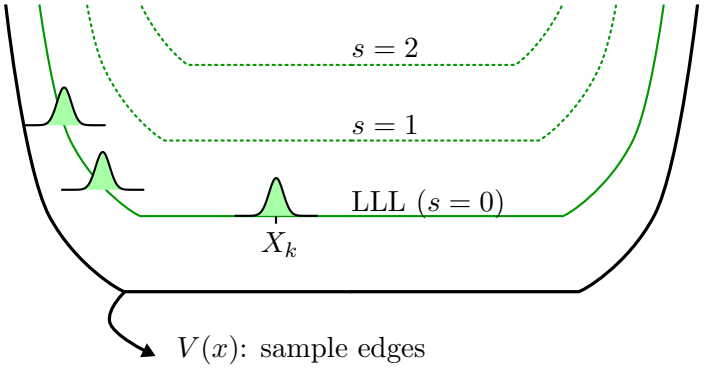

Figure 1.4: Edge states from curved Landau levels.

We try to build an understanding of the influence of the edges of a two dimensional sample by considering a strip which is finite in x-direction and infinite (or periodic) in y-direction. The basis wave functions of the LLL, or equivalently the gauge choice for $\mathbf{A}$, which we used above is optimally tailored to this geometry. Remember that the wave functions are localized in x-direction with a typical extent l. If we now consider a potential $V(x)$ that confines the electrons to a finite region which is smooth over the length-scale l, we can expect the wave function to remain approximately Gaussian. However, the wave functions centered in the vicinity of the edges will be lifted in energy. As the position of the wave function is linked to the momentum k in y-direction we obtain dispersive edge channels.

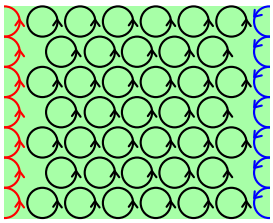
Figure 1.5: Classical skipping orbits.

In order to determine how the current is distributed we again calculate the group velocity.

$$v_{\text{group}} = \frac{1}{\hbar}\frac{\partial \epsilon_k}{\partial k} = \frac{1}{\hbar}\frac{\partial \epsilon_k}{\partial X_k}\frac{\partial X_k}{\partial k} = -\frac{l^2}{\hbar}\frac{\partial \epsilon_k}{\partial X_k} = \begin{cases} < 0 & \text{right edge} \\ > 0 & \text{left edge} \end{cases}. \quad (1.5.1)$$

These simple manipulations reveal that the two opposite edges carry opposite current. This can also be understood from the classical "skipping orbits" picture as shown on the left.

In order to calculate σ_{xy} we now apply a voltage V_H between the two edges (in x-direction) and calculate the resulting current along the sample (in y-direction). Moreover, we assume that the Fermi energy E_{F} lies in between two Landau levels.

The obtain the total current I_y we sum over the contribution ev_k of all occupied states

$$I_y = -e\int_{-\infty}^{\infty}\frac{dk}{2\pi}\frac{1}{\hbar}\frac{\partial \epsilon_k}{\partial k}n_k, \quad (1.5.2)$$

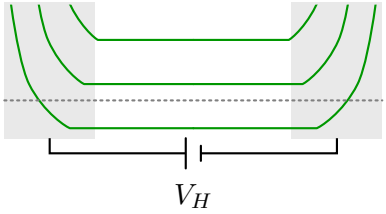

Figure 1.6: Voltage bias.

where n_k is the occupation probability of the k'th mode. Under the assumption that we only fill the LLL and that we are at zero temperature the occupation numbers only take the values $n_k = \{1, 0\}$. Under these assumptions we arrive at

$$I_y = -\frac{e}{h}\int_{\mu_L}^{\mu_R} d\epsilon = -\frac{e}{h}(\mu_R - \mu_L), \quad (1.5.3)$$

where $\mu_{R/L}$ are the respective chemical potentials on the two sides. As we can write $eV_H = \mu_R - \mu_L$ we arrive at

$$I_y = -\frac{e^2}{h}V_H \qquad \Rightarrow \qquad \sigma_{xy} = -\frac{e^2}{h}. \quad (1.5.4)$$

Let us move now the Fermi energy in between any two LL and we immediately conclude that

$$\sigma_{xy} = -\nu\frac{e^2}{h}, \quad (1.5.5)$$

where the integer ν counts the number of filled LL's.

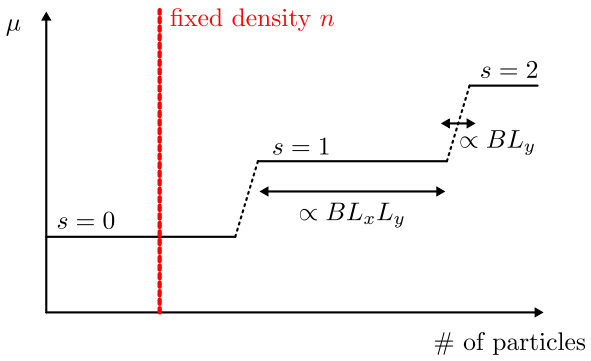

Figure 1.7: Chemical potential stuck to Landau levels.

1.5.1 The effect of disorder*

The above result is strongly suggestive that one dimensional edge channels are responsible for the transport in the quantum Hall effect. Generically the current carried by a one-dimensional channel is given by

$$I = \frac{e^2}{h}|T|^2, \tag{1.5.6}$$

where $|T|^2$ denotes the probability for an electron to be transmitted through a disordered region. However, our edge channels are *chiral* where the electrons have no way to be back-scattered and therefore $|T|^2 = 1$. These arguments explain why even in the case of a disordered sample σ_{xy} can be quantized. However, we did not yet reconcile a quantized σ_{xy} with the general result $\sigma_{xy} = ne/B$ for a clean system.

We assumed the Fermi energy to lie between two Landau levels. Let us see under which conditions this can be the case. We assume the sample to be L_x wide and the edge region which is curved up to extend over the length $W \ll L_x$. From the finite size (or periodic) quantization in y-direction we know that the momentum can take the values $k_i = \frac{2\pi}{L_y} i$ with $i \in \mathbb{Z}$. Hence, we find for the centers of the Localized wave functions $X_i = \frac{2\pi}{L_y} l^2 i$. We now count how many wave functions fit into the bulk and how many into the edge:

$$\text{edge} \quad : \quad \frac{W}{X_i - X_{i-1}} \propto L_y, \qquad \text{bulk} \quad : \quad \frac{L_x}{X_i - X_{i-1}} \propto L_x L_y. \tag{1.5.7}$$

We see that there are extensively many bulk states but only a sub-extensive number of edge states as shown in Fig. 1.7.

Translated to a fixed density but varying magnetic field B we find that for almost all values of B the Fermi energy will lie in the bulk, not the edge! Meaning, our assumption that the we have a completely filled LL and the relevant physics is happening only on the edge was not justified. Hence we need to get a better understanding of disorder effects. We do so in App. A.

Let us here briefly summarize some important effects of disorder. First, it spoils translational symmetry that led to the classical result in contrast with the experimental observation. Second, it lifts the degeneracy of the Landau levels. Disorder broadens the Landau levels in the bulk and provides a reservoir of (localized) states which allow the chemical potential to vary smoothly with density. Since they are localized, these states will not contribute to transport and to the Hall conductance.

References

1. V. Klitzing, K., Dorda, G. & Pepper, M. "New Method for High-Accuracy Determination of the Fine-Structure Constant Based on Quantized Hall Resistance". *Phys. Rev. Lett.* **45,** 494. http://link.aps.org/doi/10.1103/PhysRevLett.45.494 (1980).
2. *Topological aspects of low dimensional systems* (eds Comtet, A., Jolicoeur, T., Ouvry, S. & David, F.) (Springer-Verlag, Berlin, 1999).
3. Hall, E. "On a New Action of the Magnet on Electric Currents". *Amer. J. Math.* **2,** 287. https://www.jstor.org/stable/2369245 (1879).

Chapter 2

The integer quantum Hall effect II

Learning goals

- We know the pumping argument of Laughlin and the concept of spectral flow.
- We know that there is always a delocalized state in each LL.
- We know that σ_{xy} is given by the Chern number.
- We understand why the Chern number is an integer.

- R. B. Laughlin, Phys. Rev. B **23**, 5632. (1981).
- D. J. Thouless, M. Kohmoto, M. Nightingale & M. den Nijs, Phys. Rev. Lett. **49**, 405 (1982)

2.1 Laughlin's argument for the quantization of σ_{xy}

In the following we try to understand the pumping argument presented by R. Laughlin [1].

2.1.1 Spectral flow

The idea of *spectral flow* is central to the pumping argument of Laughlin. We try to understand this idea on the example of a particle on a ring of unit radius $r = 1$ threaded by a flux Φ[1]

$$H = \frac{\hbar^2}{2m}\left(-\mathrm{i}\partial_\phi + \frac{\Phi}{\Phi_0}\right)^2 \quad \Rightarrow \quad \psi_n(\phi) = \frac{1}{\sqrt{2\pi}}e^{\mathrm{i}n\phi} \qquad \text{with} \qquad \epsilon_n = \frac{\hbar^2}{2m}\left(n - \frac{\Phi}{\Phi_0}\right)^2. \quad (2.1.1)$$

After the insertion of a full flux quantum $\Phi_0 = h/e$, the Hamiltonian returns to itself. However, if we follow each state adiabatically, we see that the first excited and the ground state exchanged their positions. This situation is called spectral flow: While the spectrum has to be the same for $\Phi = 0$ and $\Phi = \Phi_0$, the adiabatic evolution does not need to return the ground state to itself! This is illustrated in Fig. 2.1. While the example of a particle on a ring is particularly simple, the same situation can occur for a general setup where after the insertion of a flux Φ_0 the original ground state is adiabatically transferred to an excited state. Let us now see how this spectral flow effect applies to the quantum Hall problem.

[1] The particle only lives on a ring, so we use polar coordinates and forget about the radial part:

$$H = \frac{1}{2m}\left(-\mathrm{i}\frac{\hbar\partial_\phi}{r} + eA_\phi\right)^2.$$

We write the gauge field as

$$A_\phi(r) = \begin{cases} \frac{Br}{2} & r < r_c, \\ \frac{Br_c^2}{2r} = \frac{\Phi}{2\pi r} = \frac{\hbar}{er}\frac{\Phi}{\Phi_0} & r \geq r_c. \end{cases}$$

At $r = 1$, we find the expression in (2.1.1).

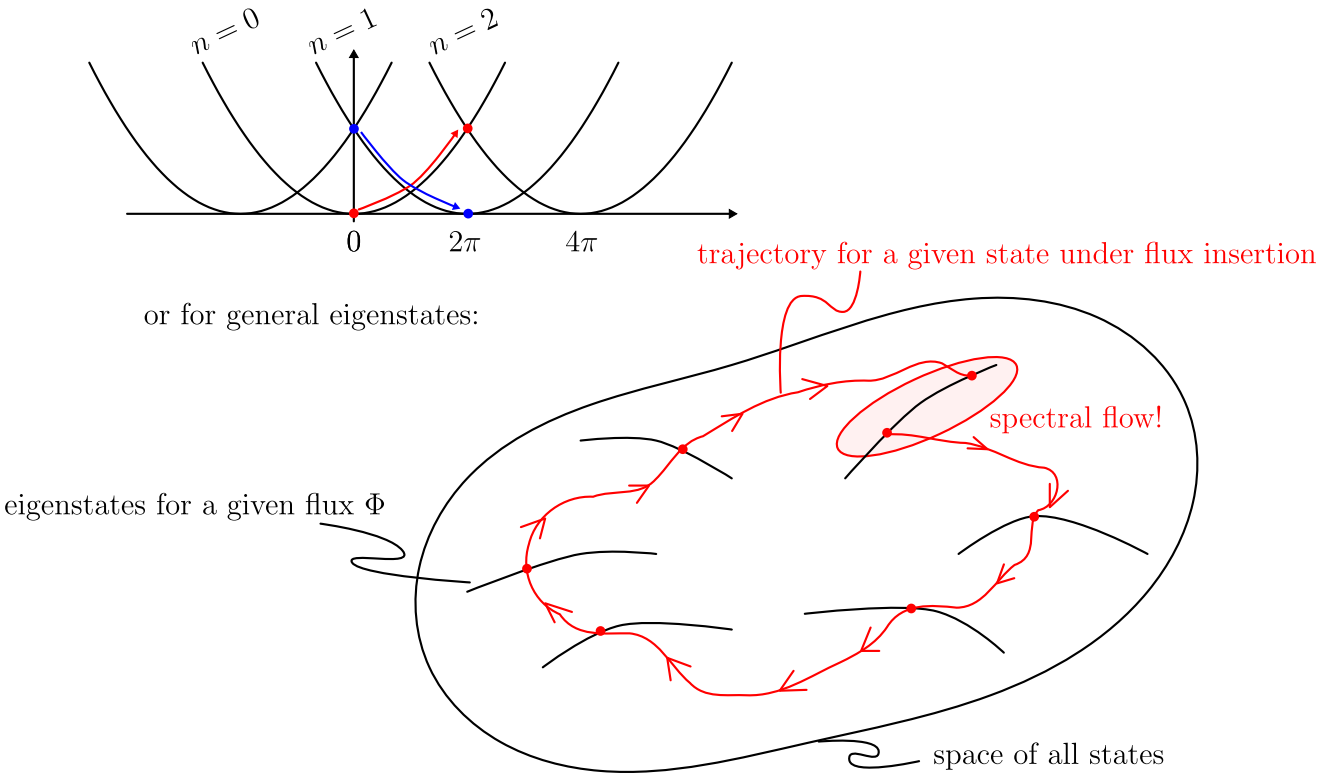

Figure 2.1: Spectral flow.

2.1.2 The ribbon geometry

Laughlin proposed that if σ_{xy} is quantized, it should not depend on the details of the geometry. One is therefore allowed to smoothly deform a rectangular sample as shown in Fig. 2.2. In the last step we replaced the applied voltage $V \to \partial_t \Phi$ with the electromotive force of a time-dependent flux through the opening of the "Corbino" disk.

Let us see what happens when we insert this flux. We make use of the eigenfunctions in the radial gauge $\psi \sim z^m \exp(-z^* z/4)$, where $z = (x - \mathrm{i}y)/l$ which we can also write as $e^{-im\phi} r^m \exp(-r^2/4l^2)$. Again, we see that these are Gaussians in one of the coordinate, however, shifted in radial direction depending on m. By calculating $\partial_r \psi = 0$ we find that they are localized around $r_m = \sqrt{2m}l$. Therefore, the flux enclosed by the m'th wave function is given by

$$\pi r_m^2 B = 2\pi m \frac{\hbar}{eB} B = m\Phi_0. \tag{2.1.2}$$

We now add slowly another flux Φ_0 into the opening of the Corbino disk. Slowly means on a time-scale $t_0 \gg 1/\omega_c$, such that we do not excite any particles into the next LL. From the above considerations we conclude that

$$r_m(\Phi) \to r_m(\Phi + \Phi_0) = r_{m+1}(\Phi). \tag{2.1.3}$$

In other words, by inserting a flux quantum we transferred one state from the inner edge of the disk to the outer perimeter. To reach equilibrium, the system will let the charge relax again and we obtain

$$V_{\hat{\phi}} = -\frac{\partial \Phi}{\partial t} = \frac{h}{et_0}; \qquad I_{\hat{r}} = \frac{e}{t_0} \qquad \Rightarrow \qquad \sigma_{xy} = \frac{I_{\hat{r}}}{V_{\hat{\phi}}} = -\frac{e^2}{h}. \tag{2.1.4}$$

This closes the argument of R. Laughlin [1]: The insertion of one flux quantum transfers a quantized charge across the ribbon and hence leads to the quantized Hall conductance measured

in the experiment. At this point it is in place to review the assumptions that went into this argument

1. $\hbar/t_0 \ll \hbar\omega_c$, i.e., we adiabatically inserted the flux. This is well justified as σ_{xy} describes *linear response*.

2. Spectral flow lead us to an excited state, i.e., the system was sensitive to the flux insertion!

This last statement is somewhat at odds with the comments in the last chapter on the role of disorder: If we need disorder in an essential way to explain the quantization of σ_{xy}, we also have to accept that disorder in two spatial dimensions leads generically to exponentially localized wave-functions [2], which in turn is incompatible with the sensitivity to flux insertion: how can a localized state in the bulk or in the vicinity of the outer edge feel anything of the flux inserted in the middle?
To reconcile this, one has to understand that a basic assumption of the gang-of-four analysis [2], one-parameter scaling, is violated in the presence of a strong magnetic field. More importantly, we should provide a simple, i.e. semi-classical, picture of how to embed at least one extended bulk state in a disordered Landau level.

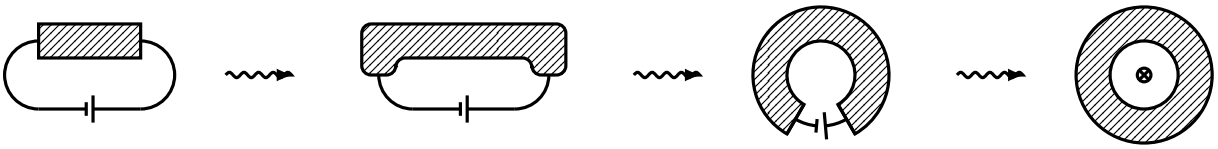

Figure 2.2: Change of geometry for Laughlin's pumping argument.

2.2 The percolation transition

There is a relatively simple picture in terms of percolating clusters that explains the existence of at least one extended state. We know that semi-classical eigenstates in a disordered LL level are given by orbits along equipotential lines.[2] The question is, if there is always an orbit in each LL that connects the two edges of our Corbino disk. If this is the case, this state mediates the sensitivity to the flux insertion and Laughlin's argument goes through also in the disordered case. Luckily the answer to this question is a clear yes!
In Fig. 2.3 an energy landscape for a disordered LLL with a confining potential is shown. Eigenstates are given by equipotential orbits. At low chemical potential μ as shown here, all orbits are "lakes" and hence all states are localized.
When filling in more water (raising μ) we switch at some point from "lakes" to "island". Right at the point where this happens, the shoreline has to connect through the whole sample. This is the sought after extended state in the middle of the sample. Above the center of the LL we are left with "islands" where all states in the bulk are localized. However, we get one edge state on either side of the sample as discussed for the case of no disorder.
We can now summarize our discussion of disorder effects: (i) We found the extended state in the LL needed for Laughlin's pumping argument to hold. (ii) The disorder allows the chemical potential to smoothly change also between the LL's. Therefore, there is an extensive window where the chemical potential lies in the range of the (mobility) gap and hence we find

$$\sigma_{xy} = -\frac{e^2}{h}\nu \qquad \nu \in \mathbb{Z}. \tag{2.2.1}$$

[2] See exercise number one.

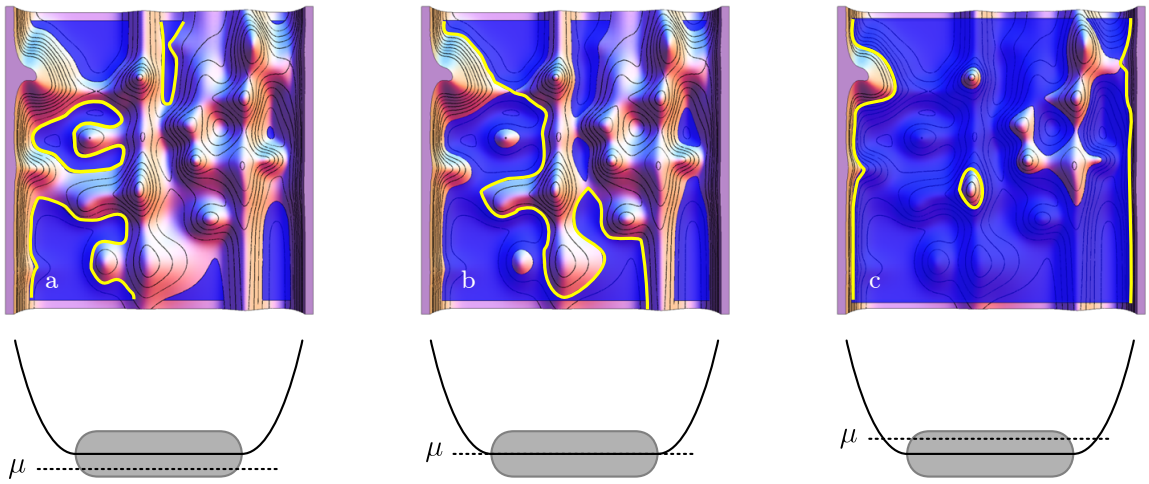

Figure 2.3: (a) Chemical potential below the center of the LL: All states are localized in the form of orbits around lakes. (b) At the percolation threshold there is one shoreline connecting the two sides of the sample. (c) Above the middle of the LL all but the two edge states are localized around islands.

2.3 The TKNN integer

We have now seen that the Hall conductivity has to be quantized in two independent ways. Once, we saw that the edge states of the QHE are chiral one dimensional channels which carry a conductivity of e^2/h. On the other hand, we saw that the pumping argument requires σ_{xy} to be quantized. In both cases the effect was not only stable to disorder but actually required a certain amount of dirt to lift the huge degeneracy of the LL's which made the chemical potential cling to the bulk states. The obvious question is now if there is a deeper, "topological" reason that links these two arguments given above. The answer was given in another seminal paper by Thouless, Kohmoto, Nightingale, and den Nijs (TKNN) in 1982 [3–5].

2.3.1 Landau levels on the torus*

The original paper [3] considered electrons in a periodic potential. Here we want to follow a different route inspired by Avron and Seiler [6] (See also lecture notes by A. Kitaev).

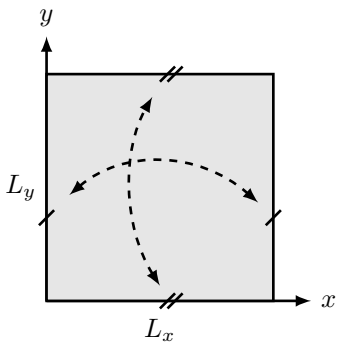

Figure 2.4: Real space torus.

We consider the problem of a magnetic field on a torus. We use the gauge field

$$A_x = \frac{\Phi_x}{L_x}, \quad A_y = \frac{\Phi_y}{L_y} + Bx, \tag{2.3.1}$$

where we added fluxes $\Phi_{x/y}$ through the openings of the torus. The boundary conditions on the torus in the presence of a magnetic field are somewhat non-trivial. Let us define them with respect to the magnetic translation operators which are defined via the canonical momentum operator $(-\mathrm{i}\hbar\nabla - e\boldsymbol{A})$

$$T^A_{\boldsymbol{u}} = e^{\frac{\mathrm{i}}{\hbar}\boldsymbol{u}\cdot\boldsymbol{p}} = e^{\frac{\mathrm{i}}{\hbar}\boldsymbol{u}\cdot(-\mathrm{i}\hbar\nabla - e\boldsymbol{A})}. \tag{2.3.2}$$

Note that these operators depend on the choice of gauge. To derive the boundary conditions,

we now consider $\boldsymbol{u}_1 = (L_x, 0)$ and $\boldsymbol{u}_2 = (0, L_y)$.

$$T^A_{\boldsymbol{u}_1}\psi(x,y) = \psi(x+L_x,y) \stackrel{!}{=} \psi(x,y), \tag{2.3.3}$$

$$T^A_{\boldsymbol{u}_2}\psi(x,y) = e^{-\frac{\mathrm{i}e}{\hbar}BxL_y}\psi(x,y+L_y) \stackrel{!}{=} \psi(x,y). \tag{2.3.4}$$

These two conditions are only compatible if

$$T^A_{\boldsymbol{u}_1}T^A_{\boldsymbol{u}_2} = T^A_{\boldsymbol{u}_2}T^A_{\boldsymbol{u}_1}. \tag{2.3.5}$$

This is only the case for

$$\frac{eB}{\hbar}L_xL_y = \frac{L_xL_y}{l^2} = 2\pi n \tag{2.3.6}$$

with $n \in \mathbb{Z}$. In other words, an integer number of flux quanta has to pierce the surface of the torus (we can only put quantized magnetic monopoles inside the torus). One can also see that the boundary conditions contain a "gluing phase"

$$\psi(0,y) = \psi(L_x,y), \tag{2.3.7}$$

$$\psi(x,0) = e^{-\frac{\mathrm{i}e}{\hbar}BxL_y}\psi(x,L_y). \tag{2.3.8}$$

In order to appreciate the role of (Φ_x, Φ_y) we calculate the Wilson loops

$$W_x(y) = \oint dx\tilde{A}_x(x,y) = -BL_xy + \Phi_x, \tag{2.3.9}$$

$$W_y(x) = \oint dy\tilde{A}_y(x,y) = BL_yx + \Phi_y, \tag{2.3.10}$$

where we absorbed the gluing phase in the vector potential $\tilde{\boldsymbol{A}}$. $\boldsymbol{W} = (W_x(y), W_y(x))$ is a gauge invariant vector and shows that on a torus a magnetic field breaks all translational symmetries. Moreover, we see, that we can view (Φ_x, Φ_y) as a shift in (x, y). Equipped with these details about the problem of a magnetic field on a torus we now want to embark on the calculation of the Hall conductivity.

2.3.2 Kubo formula

For a microscopic calculation of the conductivity we need a bit of linear response theory. We are interested in the (linear) response of a system to a (small) applied perturbation. In our case the response of interest is the current density $\boldsymbol{j}(r) = \frac{e}{2m}\sum_i[\boldsymbol{p}_i\delta(\boldsymbol{r}-\boldsymbol{r}_i) + \delta(\boldsymbol{r}-\boldsymbol{r}_i)\boldsymbol{p}_i)]$. The perturbation is given by an applied electric field $\boldsymbol{E} = -\partial_t\boldsymbol{A}$. The perturbing Hamiltonian can therefore be written as

$$H' = -\int d\boldsymbol{r}\,\boldsymbol{j}(\boldsymbol{r})\cdot\boldsymbol{A}(\boldsymbol{r}), \tag{2.3.11}$$

We are interested in the expectation value of the current density operator

$$\bar{\boldsymbol{j}}(\boldsymbol{r},t) = \langle\psi|U^\dagger(t)\boldsymbol{j}(\boldsymbol{r},t)U(t)|\psi\rangle \qquad \text{with} \qquad U(t) = T_te^{-\frac{\mathrm{i}}{\hbar}\int_{-\infty}^t dt'H'(t')}, \tag{2.3.12}$$

and

$$\boldsymbol{j}(\boldsymbol{r},t) = e^{\frac{\mathrm{i}}{\hbar}\int_{-\infty}^t dt'\,H_0(t')}\boldsymbol{j}(\boldsymbol{r})e^{-\frac{\mathrm{i}}{\hbar}\int_{-\infty}^t dt'\,H_0(t')} \quad \text{and} \quad H'(t) = e^{\frac{\mathrm{i}}{\hbar}\int_{-\infty}^t dt'\,H_0(t')}H'e^{-\frac{\mathrm{i}}{\hbar}\int_{-\infty}^t dt'\,H_0(t')} \tag{2.3.13}$$

Here, T_t is the time-ordering operator and $|\psi\rangle$ is the unperturbed ground state of the original Hamiltonian H_0. As usual for perturbation theory, we switched to the interaction representation. We assume the vector potential in H' to be given by $\boldsymbol{A} = (\Phi_x/L_x, \Phi_y/L_y)e^{t/\tau}$, which corresponds to slowly turning on the fluxes through the opening of the torus. Moreover, we only drive with

a spatially constant field. Note, that $\boldsymbol{A}_0 = Bx\hat{\boldsymbol{y}}$ is not included in H' as this is not considered to be small but part of the unperturbed Hamiltonian H_0. In linear response we can expand the exponent in $U(t)$ to obtain

$$\bar{j}_\alpha(\boldsymbol{r},t) = \frac{\mathrm{i}}{\hbar}\sum_\beta \int_{-\infty}^{t} dt'\, A_\beta(t')\langle[j_\alpha(\boldsymbol{r},t), \int d\boldsymbol{r}' j_\beta(\boldsymbol{r}',t')]\rangle \tag{2.3.14}$$

$$= \frac{\mathrm{i}}{\hbar}\sum_\beta \int_{-\infty}^{t} dt'\, A_\beta(t')\langle[j_\alpha(\boldsymbol{r},t), J_\beta(t')]\rangle. \tag{2.3.15}$$

We write $J_\beta(t')$ for the $\boldsymbol{q}=0$ Fourier-component of the current as it represent the *total* current. Moreover, as we only drive with $\boldsymbol{q}=0$, we only get response at this wave vector. To make this clearer we take the Fourier transform on both side with respect to $\boldsymbol{r}$

$$\bar{J}_\alpha(t) = \frac{\mathrm{i}}{\hbar}\sum_\beta \int_{-\infty}^{t} dt' \underbrace{\frac{\Phi_\beta}{L_\beta} e^{\frac{t'}{\tau}}}_{=\tau E^0_\beta e^{t'/\tau}} \langle[J_\alpha(t), J_\beta(t')]\rangle. \tag{2.3.16}$$

We can now relate the current density[3] to the final driving field E_y^0 to obtain an expression for the Hall conductance

$$\sigma_{xy}(t) = \frac{\mathrm{i}\tau}{\hbar v}\int_{-\infty}^{t} dt'\, e^{\frac{t'}{\tau}}\langle[J_x(t), J_y(t')]\rangle \tag{2.3.17}$$

The result (2.3.17) is known as the *Kubo formula*. Let us review this result again: The first current operator arises as we measure a current. The second one because the perturbing Hamiltonian H' is also proportional to the current. The commutator originates from the perturbation theory where $U(t)$ is once acting from the left and once from the right. The multiplication by τ accounts for the time derivative linking the electric field $\boldsymbol{E}$ and the vector potential $\boldsymbol{A}$. Finally, in our derivation we made the explicit assumption that we turn on the fluxes Φ_α adiabatically. Certainly the Kubo formula is more general and can be derived for an arbitrary time and space dependence of the perturbation.
To make progress we manipulate (2.3.17) further

$$\sigma_{xy} := \sigma_{xy}(t=0) = \frac{\mathrm{i}}{\hbar v}\int_{-\infty}^{0} dt'\, \tau e^{t'/\tau}\langle[J_\alpha(0), J_\beta(t')]\rangle \tag{2.3.18}$$

$$= \frac{\mathrm{i}}{\hbar v}\int_{0}^{\infty} dt_1 \int_{-\infty}^{0} dt_2 \langle[J_x(t_1), J_y(t_2)]\rangle e^{-\frac{t_1-t_2}{\tau}} \tag{2.3.19}$$

$$= \frac{\mathrm{i}}{\hbar}\langle[Q_x^+, Q_y^-]\rangle, \tag{2.3.20}$$

where the operators $Q_\alpha^\pm$ are defined as

$$Q_\alpha^+ = \frac{1}{L_\alpha}\int_0^\infty dt\, e^{-t/\tau} J_\alpha(t), \qquad \text{and} \qquad Q_\alpha^- = \frac{1}{L_\alpha}\int_{-\infty}^0 dt\, e^{t/\tau} J_\alpha(t). \tag{2.3.21}$$

To evaluate the above formula for σ_{xy} we apply the *adiabatic approximation*: We try to exchange the current operators in (2.3.21) with something that explicitly only depends on the *ground state*

[3] Note that by taking the Fourier-transform

$$\bar{J}(\boldsymbol{q}) = \int d\boldsymbol{r} e^{\mathrm{i}\boldsymbol{q}\cdot\boldsymbol{r}}\bar{j}(\boldsymbol{r})$$

we switched from current *density* to the total current. However, σ_{xy} relates the driving field $\boldsymbol{E}$ to the *current density* in $\bar{J}_x/v = \bar{J}_x/L_xL_y$. We account for that by dividing by the volume $v = L_xL_y$.

wave-function $|\psi_t\rangle$ at a given time during the turn-on process. At this point it is convenient to introduce the (dimensionless) phases

$$\varphi_\alpha := 2\pi \frac{\Phi_\alpha}{\Phi_0}. \tag{2.3.22}$$

Inserted into (2.3.11) we have

$$H'(t) = -\int d\boldsymbol{r}\, \boldsymbol{j}(\boldsymbol{r},t)\cdot \boldsymbol{A}(\boldsymbol{r},t) = -\sum_\alpha J_\alpha(t)\frac{\Phi_\alpha}{L_\alpha}e^{t/\tau} = -\sum_\alpha J_\alpha(t)\frac{\hbar}{e}\frac{\varphi_\alpha}{L_\alpha}e^{t/\tau}. \tag{2.3.23}$$

Let us write the ground state wave function at $t=0$ by evolving the $t=-\infty$ wave function assuming φ_α to be small

$$|\psi_0\rangle = \hat{T}_t e^{-\frac{\mathrm{i}}{\hbar}\int_{-\infty}^0 dt'\, H'(t')}|\psi_{-\infty}\rangle \approx |\psi_{-\infty}\rangle + \sum_\alpha \frac{\mathrm{i}}{e}\varphi_\alpha Q_\alpha^-|\psi_{-\infty}\rangle. \tag{2.3.24}$$

We now make use of the adiabatic approximation: We assume that we do not induce any transitions to states above *a postulated energy gap*. Moreover, the state at $t=-\infty$ does not depend on φ_α. When taking the derivative $\partial/\partial\varphi_\alpha$ on both sides of Eq. (2.3.24) we obtain

$$Q_\alpha^-|\psi_{-\infty}\rangle = -\mathrm{i}e\left|\frac{\partial\psi_0}{\partial\varphi_\alpha}\right\rangle. \tag{2.3.25}$$

We achieved our goal to replace the unwanted current operators! For clarity and to make connection to more mathematical literature [7] we introduce the Berry connection

$$\mathcal{A}_\alpha = \mathrm{i}\langle\psi_0|\partial_\alpha\psi_0\rangle, \qquad \text{or} \qquad \boldsymbol{\mathcal{A}} = \mathrm{i}\langle\psi_0|\nabla\psi_0\rangle \tag{2.3.26}$$

and the corresponding Berry curvature

$$\mathcal{F}_{\alpha\beta} = \partial_\alpha\mathcal{A}_\beta - \partial_\beta\mathcal{A}_\alpha \qquad \text{or} \qquad \boldsymbol{\mathcal{F}} = \nabla\wedge\boldsymbol{\mathcal{A}}. \tag{2.3.27}$$

We can now write for σ_{xy}

$$\sigma_{xy} = \frac{e^2}{\hbar}\mathcal{F}_{xy}, \tag{2.3.28}$$

Let us take the step from the adiabatic turning-on of the field to a dc-field. In that case the field $\boldsymbol{A}$ grows linearly in time, or in other words, the phase φ_x winds as a function of time. We therefore average the above result over $\int d\varphi_x/2\pi$. To make matters more symmetric, we also average over φ_y.[4]. This leads us to the formula

$$\sigma_{xy} = \frac{e^2}{\hbar}\int\frac{d\varphi_x d\varphi_y}{(2\pi)^2}\mathcal{F}_{xy} = \frac{e^2}{h}\int\frac{d\varphi_x d\varphi_y}{2\pi}\mathcal{F}_{xy} = \frac{e^2}{h}\frac{\mathsf{C}^{(1)}}{2\pi}, \tag{2.3.29}$$

where we identified the Chern number $\mathsf{C}^{(1)}$ [7]. In order to get a better understanding of Eq. (2.3.29) we related it to the Berry phase of a spin-1/2 in a magnetic field before we motivate it to be quantized to an integer number times the quantum of conductance e^2/h.

[4] You can argue, that the Hall response should not depend on the arbitrary (but constant) flux through the other opening of the torus. This flux averaging has been widely accepted and recently been put on solid grounds [8].

2.4 The Berry phase

We would like to establish the link between the well known Berry phase [4] and the expression for the Hall conductance derived above. Let us assume that we have a Hamiltonian $H[\boldsymbol{R}(t)]$ that depends on time dependent parameters $\boldsymbol{R}(t)$. These parameters are supposed to evolve slowly

$$\hbar \frac{\partial R_i(t)}{\partial t} \ll \Delta, \tag{2.4.1}$$

where Δ is the minimal gap between the instantaneous ground state and the first excited state at any given time t. If we start at $t = 0$ in the ground state, we will always stay in the instantaneous ground state. However, along the way we will pick up a phase

$$e^{\mathrm{i}\varphi(t)}|\psi_0(\boldsymbol{R})\rangle : \qquad \mathrm{i}\hbar\partial_t e^{\mathrm{i}\varphi(t)}|\psi_0(\boldsymbol{R})\rangle = H[\boldsymbol{R}(t)]e^{\mathrm{i}\varphi(t)}|\psi_0(\boldsymbol{R})\rangle. \tag{2.4.2}$$

Multiplying this expression from the left with $\langle\psi_0(\boldsymbol{R})|e^{-\mathrm{i}\varphi(t)}$ we obtain

$$\partial_t\varphi(t) = \mathrm{i}\langle\psi_0(\boldsymbol{R})|\nabla_{\boldsymbol{R}}|\psi_0(\boldsymbol{R})\rangle \cdot \frac{\partial \boldsymbol{R}}{\partial t} - \frac{1}{\hbar}E_0(\boldsymbol{R}). \tag{2.4.3}$$

Integrating this equation leads to

$$\varphi(t) - \varphi(0) = \underbrace{\int_{\boldsymbol{R}(0)}^{\boldsymbol{R}(t)} \langle\psi_0(\boldsymbol{R})|\mathrm{i}\nabla_{\boldsymbol{R}}|\psi_0(\boldsymbol{R})\rangle \cdot d\boldsymbol{R}}_{\text{geometrical phase}} - \underbrace{\frac{1}{\hbar}\int_0^t dt' E_0(t')}_{\text{dynamical phase}} . \tag{2.4.4}$$

If we now consider a path along a closed contour γ, the dynamical phase drops out and we find

$$\varphi_\gamma = \oint_\gamma d\boldsymbol{l}\, \mathrm{i}\langle\psi_0|\nabla_{\boldsymbol{R}}\psi_0\rangle = \oint_\gamma d\boldsymbol{l}\, \boldsymbol{\mathcal{A}} = \int_\Gamma d\boldsymbol{S}\, \boldsymbol{\mathcal{F}}, \tag{2.4.5}$$

where Γ is the area enclosed by the contour γ. With this we see, that σ_{xy} is given by the Berry phase[5] of the ground state when we move the system once around the torus $[0, 2\pi] \times [0, 2\pi]$. Let us gain a deeper understanding of the Berry phase by recalling the example of a spin-1/2 in a magnetic field.

2.4.1 Spin-1/2 in a magnetic field

The Hamiltonian of a spin-1/2 in a magnetic field is given by

$$H = -\boldsymbol{h}\cdot\boldsymbol{\sigma} = -\sum_{\alpha=x,y,z} h_\alpha\sigma_\alpha. \tag{2.4.6}$$

If we write the magnetic field in spherical coordinates

$$h_x = h\sin(\vartheta)\cos(\varphi), \tag{2.4.7}$$
$$h_y = h\sin(\vartheta)\sin(\varphi), \tag{2.4.8}$$
$$h_z = h\cos(\vartheta), \tag{2.4.9}$$

the ground state can be written as

$$|\xi_1\rangle = \begin{pmatrix} \cos(\vartheta/2) \\ e^{\mathrm{i}\varphi}\sin(\vartheta/2) \end{pmatrix} \qquad \text{or} \qquad |\xi_2\rangle = \begin{pmatrix} e^{-\mathrm{i}\varphi}\cos(\vartheta/2) \\ \sin(\vartheta/2) \end{pmatrix}. \tag{2.4.10}$$

[5] Why do we call this a phase? Note that

$$0 = \partial_\eta 1 = \partial_\eta\langle\psi|\psi\rangle = \langle\partial_\eta\psi|\psi\rangle + \langle\psi|\partial_\eta\psi\rangle = \langle\partial_\eta\psi|\psi\rangle + \langle\partial_\eta\psi|\psi\rangle^* = a + a^*.$$

Therefore $a = -a^*$ and hence, $\mathrm{Re}[a] = 0$.

Both states $|\xi_1\rangle$ and $|\xi_2\rangle$ describe the ground state. However, $|\xi_1\rangle$ is singular at $\vartheta = \pi$ (or at the south-pole), while $|\xi_2\rangle$ is singular at the north-pole. In other words, we had to introduce two patches on the sphere to obtain a smooth parameterization of the instantaneous eigenstates, see Fig. 2.5. However, we can glue these two patches together via a gluing phase

$$|\xi_1\rangle = e^{\mathrm{i}\zeta(\varphi)}|\xi_2\rangle \qquad \text{with} \qquad \zeta(\varphi) = \varphi \tag{2.4.11}$$

along the equator. Let us calculate the Berry connection for the two states. Recall that in spherical coordinates the differential operators take the forms

$$\nabla f = \frac{\partial}{\partial r} f\, \hat{\boldsymbol{r}} + \frac{1}{r}\frac{\partial}{\partial \vartheta} f\, \hat{\boldsymbol{\vartheta}} + \frac{1}{r\sin(\vartheta)}\frac{\partial}{\partial \varphi} f\, \hat{\boldsymbol{\varphi}}, \tag{2.4.12}$$

and

$$\nabla \wedge \boldsymbol{A} = \frac{1}{r\sin(\vartheta)}\left\{\frac{\partial}{\partial \vartheta}\left[A_\varphi \sin(\vartheta)\right] - \frac{\partial A_\vartheta}{\partial \varphi}\right\}\hat{\boldsymbol{r}} + \frac{1}{r}\left\{\frac{1}{\sin(\vartheta)}\frac{\partial A_r}{\partial \varphi} - \frac{\partial}{\partial r}\left(rA_\varphi\right)\right\}\hat{\boldsymbol{\vartheta}} + \frac{1}{r}\left\{\frac{\partial}{\partial r}\left(rA_\vartheta\right) - \frac{\partial A_r}{\partial \vartheta}\right\}\hat{\boldsymbol{\varphi}}. \tag{2.4.13}$$

With this we immediately find

$$\boldsymbol{\mathcal{A}} = \frac{1}{2r}\hat{\boldsymbol{\varphi}} \cdot \begin{cases} -\tan(\vartheta/2) & |\xi_1\rangle \\ \cot(\vartheta/2) & |\xi_2\rangle \end{cases} \qquad \text{and} \qquad \boldsymbol{\mathcal{F}} = -\frac{\alpha}{2r^2}\hat{\boldsymbol{r}}. \tag{2.4.14}$$

Here, we introduced $\alpha = 1$ for later purposes. A few remarks are in order: (i) The "$\boldsymbol{B}$"-field $\mathcal{F}_{\varphi\vartheta}$ corresponds to a monopole field of a monopole of strength $-\alpha$ at the origin. This can be seen by integrating $\mathcal{F}_{\varphi\vartheta}$ over the whole sphere S^2

$$\int_{S^2} d\boldsymbol{\Omega}\, \boldsymbol{\mathcal{F}} = -\alpha. \tag{2.4.15}$$

(ii) Integrated over the solid angle $d\boldsymbol{\Omega}$ we obtain a Berry phase $\varphi = -\frac{\alpha}{2}d\Omega$. (iii) The field $\boldsymbol{\mathcal{A}}$ corresponds to a monopole at $\boldsymbol{h} = 0$. At $\boldsymbol{h} = 0$ the Hamiltonian is zero, i.e., the system is *doubly degenerate*. To appreciate this further, we write (see Ref. [4] for details)

$$\boldsymbol{\mathcal{F}} = \boldsymbol{B} = \nabla \wedge \langle\psi|\nabla\psi\rangle = \langle\nabla\psi| \wedge |\nabla\psi\rangle = \sum_{m\neq 0}\langle\nabla\psi|m\rangle \wedge \langle m|\nabla\psi\rangle = \sum_{m\neq 0}\frac{\langle\psi|\nabla H|m\rangle \wedge \langle m|\nabla H|\psi\rangle}{(E_m - E_0)^2}.$$

It is easy to show that $\nabla \cdot \boldsymbol{B} = 0$ if $E_m - E_0 \neq 0$.
To take another step towards understanding the quantization of the Chern number, let us show that α cannot take arbitrary values. We calculate the Berry phase along a path γ that does not contain the south pole. For simplicity, let us take the equator. We can therefore write

$$\varphi_\gamma = \oint_\gamma d\boldsymbol{l}\, \boldsymbol{\mathcal{A}} = \int_\Gamma d\boldsymbol{\Omega}\, \boldsymbol{\mathcal{F}} = -\alpha\Omega(\Gamma)/2 \mod 2\pi, \tag{2.4.16}$$

where $\Omega(\Gamma)$ is the solid angle of the surface Γ. We closed γ such that Γ contains the north pole. Alternatively we could have closed γ to $\Gamma' = S^2 - \Gamma$ and write

$$\varphi_\gamma = -\int_{\Gamma'} d\boldsymbol{\Omega}\, \boldsymbol{\mathcal{F}} = \alpha(4\pi - \Omega(\Gamma))/2 \mod 2\pi. \tag{2.4.17}$$

In order for (2.4.16) and (2.4.17) to yield the same result we require

$$\alpha \in \mathbb{Z}. \tag{2.4.18}$$

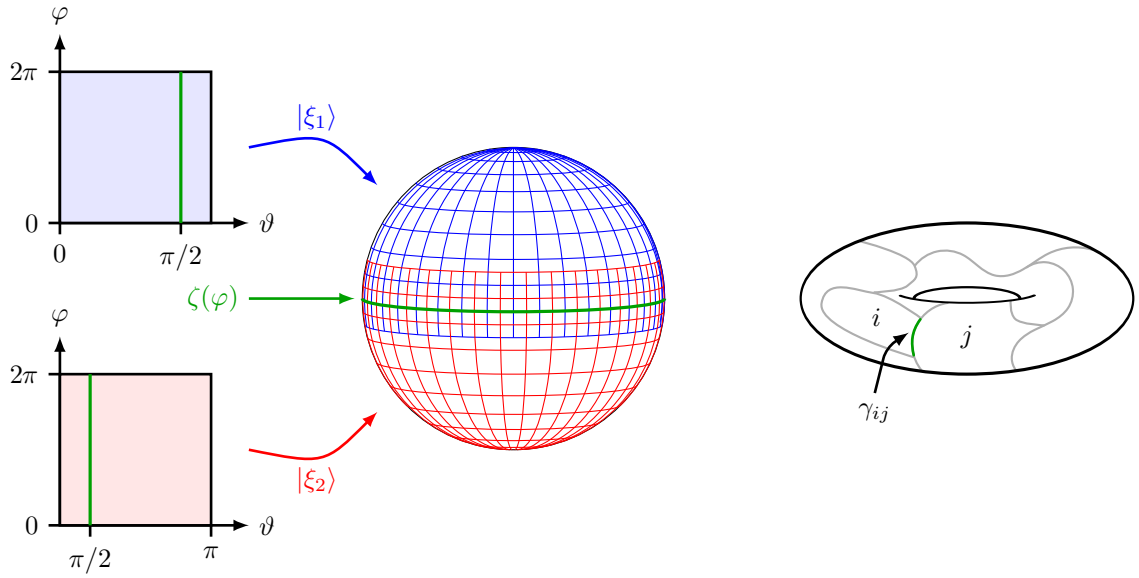

Figure 2.5: Left: Two patches introduced by the gauge choice for the ground state of a spin-1/2 in a magnetic field. No single patch can describe all eigenstate. However, the two patches can be glued together via $\zeta(\varphi)$. Right: Triangulation of the torus where the gluing phase between two individual patches i and j is indicated.

This observation leads us back to the definition of the Chern number

$$\mathsf{C}^{(1)} = \frac{1}{2\pi}\int_M d\boldsymbol{\Omega}\,\boldsymbol{\mathcal{F}} \quad \in \quad \mathbb{Z} \tag{2.4.19}$$

for any "well behaved", compact, two-dimensional manifold M without boundaries. It can be shown that $\mathsf{C}^{(1)}$ is a topological invariant of the *fiber bundle* looking locally like $M \times U(1)$, where $M = S^2$ is the base manifold defined by the parameters of the Hamiltonian (or more precisely, the parameters defining the projectors $|\psi_0\rangle\langle\psi_0|$ onto the ground state) and $U(1)$ is called the fibre defined by the phase of the ground state at any given point on S^2. Note, however, that the fibre bundle we are dealing with only *locally* looks like $S^2 \times U(1)$. To get the full fibre bundle we need to stitch together the two patches defined by $|\xi_{1/2}\rangle$. The role of the gluing phases ζ_{ij} for patches i, j on the compact manifold M can be further highlighted through the formula

$$\mathsf{C}^{(1)} = \frac{1}{2\pi}\sum_{i<j}\int_{\gamma_{ij}} d\zeta_{ij} \quad \in \quad \mathbb{Z}. \tag{2.4.20}$$

In other words, a non-vanishing Chern number $\mathcal{C}$ is intrinsically linked to the inability to chose a smooth gauge, i.e., only if we have to chose several patches that we glue together with ζ_{ij} can $\mathsf{C}^{(1)}$ be non-zero, see Fig. 2.5. A concrete example of this is our example of the spin-1/2 for which we have

$$\mathsf{C}^{(1)} = \frac{1}{2\pi}\int_{S^2} d\boldsymbol{\Omega}\,\boldsymbol{\mathcal{F}} = -1 = \frac{1}{2\pi}\oint_{\text{equator}} d\varphi\,\zeta(\varphi). \tag{2.4.21}$$

For further details we refer to the book by Nakahara [7] for a detailed mathematical exposition or the book by Bohm et al. [9] for a more physical approach. We finish this section by stating the long-sought formula

$$\boxed{\sigma_{xy} = \frac{e^2}{h}\nu \qquad \text{with} \qquad \nu \in \mathbb{Z}.} \tag{2.4.22}$$

2.5 Translation invariant systems

Above we made an effort to formulate the derivation of σ_{xy} free of relations to momentum integrals. This allows our formalism to be applied to disordered or interacting systems [6]. However, much of what will follow in Chern insulators and eventually the so-called "topological insulators" will be formulated in translation-invariant systems.
Both for a systems in free space as well as on a lattice it is easy to see that the (quasi) momentum $\boldsymbol{k}$ is doing nothing but making the wave-function acquire a phase $\exp(\mathrm{i}\boldsymbol{k}\cdot\boldsymbol{x})$ which is linearly growing in $\boldsymbol{x}$. Moreover k_α is the proportionality constant in α-direction. The fluxes (Φ_x, Φ_y) do exactly the same. This can easily be seen by performing a gauge transformation

$$\psi(x) = e^{\mathrm{i}kx} \longrightarrow \psi'(x) = e^{\mathrm{i}\frac{e}{\hbar}\int_0^x dx' A(x')} e^{\mathrm{i}kx} = e^{\mathrm{i}\frac{e}{\hbar}\Phi_x x} e^{\mathrm{i}kx} = e^{\mathrm{i}(k+\varphi)x} = e^{\mathrm{i}k'x}. \tag{2.5.1}$$

We see that therefore the integrals over φ in (2.3.29) are nothing but momentum space integrals for periodic systems [3]. Show to yourself that for a ground state wave-function which is a Slater determinant of momentum eigenstates, the expression (2.3.29) is particularly simple.

2.6 Berry curvature as a magnetic field in momentum space

Before we move on to examples beyond Landau levels which carry a Chern number, we want to get another intuition of what a non-zero Berry curvature represents. We consider electrons in a periodic potential under a weak perturbation. Under the right circumstances one can describe the dynamics in a semiclassical model described by the equations of motion for a wave-packet

$$\dot{\boldsymbol{r}} = \boldsymbol{v}_n(\boldsymbol{k}) = \frac{1}{\hbar}\nabla_{\boldsymbol{k}}\epsilon_n(\boldsymbol{k}), \tag{2.6.1}$$

$$\hbar\dot{\boldsymbol{k}} = -e\left[\boldsymbol{E}(\boldsymbol{r},t) + \dot{\boldsymbol{r}}\wedge\boldsymbol{B}(\boldsymbol{r},t)\right], \tag{2.6.2}$$

where n labels the n'th Bloch band. A proper derivation of these equations is beyond the scope of this course. We refer the reader to Ashcroft & Mermin [10] for a basic introduction and to the excellent review by Xiao, et al. [11]. When band properties are taken more properly into account, one finds the above equations have to be adjusted to read [11]

$$\dot{\boldsymbol{r}} = \boldsymbol{v}_n(\boldsymbol{k}) = \frac{1}{\hbar}\nabla_{\boldsymbol{k}}\epsilon_n(\boldsymbol{k}) - \dot{\boldsymbol{k}}\wedge\boldsymbol{\Omega}_n(\boldsymbol{k}), \tag{2.6.3}$$

$$\hbar\dot{\boldsymbol{k}} = -e\left[\boldsymbol{E}(\boldsymbol{r},t) + \dot{\boldsymbol{r}}\wedge\boldsymbol{B}(\boldsymbol{r},t)\right], \tag{2.6.4}$$

with

$$\boldsymbol{\Omega}_n(\boldsymbol{k}) = \langle\partial_{k_x}\varphi_n(\boldsymbol{k})|\wedge|\partial_{k_y}\varphi_n(\boldsymbol{k})\rangle = \boldsymbol{\mathcal{F}}_n(\boldsymbol{k}) \tag{2.6.5}$$

the Berry curvature of the n'th band and $\varphi_n(\boldsymbol{k})$ the corresponding Bloch eigenfunctions. From these equations we can conclude that the Berry curvature takes the role of a "magnetic field" in $\boldsymbol{k}$-space.

References

1. Laughlin, R. B. "Quantized Hall conductivity in two dimensions". *Phys. Rev. B* **23,** 5632. http://link.aps.org/doi/10.1103/PhysRevB.23.5632 (1981).
2. Abrahams, E., Anderson, P. W., Licciardello, D. C. & Ramakrishnan, T. V. "Scaling Theory of Localization: Absence of Quantum Diffusion in Two Dimensions". *Phys. Rev. Lett.* **42,** 673. http://link.aps.org/doi/10.1103/PhysRevLett.42.673 (1979).

3. Thouless, D. J., Kohmoto, M., Nightingale, M. & den Nijs, M. "Quantized Hall Conductance in a Two-Dimensional Periodic Potential". *Phys. Rev. Lett.* **49,** 405. http://link.aps.org/doi/10.1103/PhysRevLett.49.405 (1982).

4. Berry, M. V. "Quantal Phase Factors Accompanying Adiabatic Changes". *Proc. R. Soc. Lond. A* **392,** 45. http://dx.doi.org/10.1098/rspa.1984.0023 (1984).

5. Simon, B. "Holonomy, the Quantum Adiabatic Theorem, and Berry's Phase". *Physical Review Letters* **51,** 2167. http://link.aps.org/doi/10.1103/PhysRevLett.51.2167 (1983).

6. Avron, J. E. & Seiler, R. "Quantization of the Hall Conductance for General, Multiparticle Schrödinger Hamiltonians". *Phys. Rev. Lett.* **54,** 259. http://link.aps.org/doi/10.1103/PhysRevLett.54.259 (1985).

7. Nakahara, M. *Geometry, Topology and Physics* (Taylor and Francis, New York and London, 2003).

8. Hastings, M. B. & Michalakis, S. "Quantization of Hall Conductance for Interacting Electrons on a Torus". *Commun. Math. Phys.* **334,** 433. https://doi.org/10.1007/s00220-014-2167-x (2015).

9. Bohm, A., Mostafazadeh, A., Koizumi, H., Niu, Q. & Zwanziger, J. *The Geometric Phase in Quantum Systems* (Springer-Verlag, Heidelberg, 2003).

10. Ashcroft, N. W. & Mermin, N. D. *Solid State Physics* (Harcourt, Orlando, 1987).

11. Xiao, D., Chang, M.-C. & Niu, Q. "Berry phase effects on electronic properties". *Rev. Mod. Phys.* **82,** 1959. http://dx.doi.org/10.1103/RevModPhys.82.1959 (2010).

Chapter 3

One-dimensional topological phases

Learning goals

- We know the Su-Schrieffer-Herger model.
- We understand its bulk-boundary correspondence.
- We can characterize its topology through winding number invariants and Wilson loops.
- We understand the connection between Wilson loops, polarization, and the position operator.

- J. Zak, Phys. Rev. Lett. **62**, 2747–2750 (1989)
- L. Fidkowski, T. S. Jackson, and I. Klich, Phys. Rev. Lett. **107**, 036601 (2011)
- N. Marzari, A. A. Mostofi, J. R. Yates, I. Souza, and D. Vanderbilt, Rev. Mod. Phys. **84**, 1419 (2012)

In the following chapters, we are mostly concerned with the topological characterization of non-interacting electron Hamiltonians on a lattice. In general, an insulating topological phase of matter may be defined by the requirement that the many-body ground state of the corresponding Hamiltonian (given by a Slater determinant in the non-interacting case) cannot be adiabatically connected to the atomic limit of vanishing hopping between the sites of the lattice. Further requiring that certain symmetries such as time-reversal are not violated along any such adiabatic interpolation enriches the topological classification, in that phases which were classified as trivial in the previous sense now acquire a topological distinction which is protected by the respective symmetry.
In this chapter we will work towards an initial understanding of the fundamental topological properties of insulating (gapped) topological band structures. We will introduce topological invariants and the bulk-boundary correspondence. These concepts can be found in systems of any dimension and likewise we will introduce the bulk-boundary correspondence for arbitrary dimension, using a Wannier state approach. Specifically, we will learn how to employ Wilson loops as a generalization of the one-dimensional (1D) Berry phase to characterize topological properties of a phase. This provides a framework of topological invariants which makes direct contact with the protected boundary degrees of freedom of a given phase. As a pedagogical example for illustration, we will resort to the simplest case of one dimension and there specifically to the Su-Schrieffer-Heeger model throughout.

3.1 Definitions

In this chapter and the following ones, we will be concerned to a large extend with tight-binding models of non-interacting electron system. Therefore it is useful to clarify some notation first. We work in units where $\hbar = c = e = 1$ and denote by σ_i, $i = x, y, z$, the 2×2 Pauli matrices.

We define $\sigma_0 = \mathbb{1}_{2\times 2}$ for convenience. We express eigenfunctions of a translationally invariant single-particle Hamiltonian in the basis

$$\phi_{\boldsymbol{k},\alpha}(\boldsymbol{r}) = \frac{1}{\sqrt{N}} \sum_{\boldsymbol{R}} e^{\mathrm{i}\boldsymbol{k}\cdot(\boldsymbol{R}+\boldsymbol{r}_\alpha)} \varphi_{\boldsymbol{R},\alpha}(\boldsymbol{r}-\boldsymbol{R}-\boldsymbol{r}_\alpha), \tag{3.1.1}$$

where $\varphi_{\boldsymbol{R},\alpha}$, $\alpha = 1, \cdots, N$, are the orbitals chosen as basis for the finite-dimensional Hilbert space in each unit cell, labelled by the lattice vector $\boldsymbol{R}$, and $\boldsymbol{r}_\alpha$ is the center of each of these orbitals relative to the origin of the unit cell. Including $\boldsymbol{r}_\alpha$ in the exponential corresponds to a convenient choice of gauge when studying the response to external fields defined in continuous real space.
A general non-interacting Hamiltonian then has the Bloch matrix elements

$$\mathcal{H}_{\alpha,\beta}(\boldsymbol{k}) = \int \mathrm{d}^d r \phi^*_{\boldsymbol{k},\alpha}(\boldsymbol{r}) \hat{H} \phi_{\boldsymbol{k},\beta}(\boldsymbol{r}), \tag{3.1.2}$$

as well as energy eigenstates

$$\psi_{\boldsymbol{k},n}(\boldsymbol{r}) = \sum_{\alpha}^{N} u_{\boldsymbol{k};n,\alpha} \phi_{\boldsymbol{k},\alpha}(\boldsymbol{r}), \tag{3.1.3}$$

where

$$\sum_{\beta} \mathcal{H}_{\alpha,\beta}(\boldsymbol{k}) u_{\boldsymbol{k};n,\beta} = \epsilon_n(\boldsymbol{k}) u_{\boldsymbol{k};n,\alpha}, \qquad n = 1, \cdots, N. \tag{3.1.4}$$

In the following, we are interested in situations where the system has an energy gap after the first $M < N$ bands, i.e., $\epsilon_M(\boldsymbol{k}) < \epsilon_{M+1}(\boldsymbol{k})$ for all $\boldsymbol{k}$ in the first Brillouin zone (BZ).

3.2 The the Su-Schrieffer-Heeger model

One of the simplest examples of a topological phase is exemplified by the Su-Schrieffer-Heeger (SSH) model, initially devised to model polyacetylene. It describes electrons hopping on a 1D dimerized lattice with two sites A and B in its unit cell (see Fig 3.1***a***). In momentum space, the Bloch Hamiltonian reads

$$\mathcal{H}(k) = \begin{pmatrix} 0 & t + t' e^{\mathrm{i}k} \\ t + t' e^{-\mathrm{i}k} & 0 \end{pmatrix}. \tag{3.2.1}$$

The model has an inversion symmetry $I\mathcal{H}(k)I^{-1} = \mathcal{H}(-k)$, with $I = \sigma_x$. Since it does not couple sites A to A or B to B individually, it furthermore enjoys a chiral or sublattice symmetry $U_{\mathcal{C}}\mathcal{H}(k)U_{\mathcal{C}}^{-1} = -\mathcal{H}(k)$ with $U_{\mathcal{C}} = \sigma_z$. [Notice some abuse of language here: The chiral symmetry is not a "symmetry" in the sense of a commuting operator on the level of the first quantized Bloch Hamiltonian. Still, as a mathematical fact, this chiral symmetry can be helpful to infer and protect the existence of topological boundary modes.] While a standard discussion of the SSH model would focus on the chiral symmetry and its role in protecting topological phases, here we will first consider the implications of the crystalline inversion symmetry. It will be useful to note that the spectrum is given by

$$\epsilon_{\pm}(k) = \pm\sqrt{t^2 + t'^2 + 2tt'\cos k} \tag{3.2.2}$$

with a gap closing at $k = \pi$ for $t = t'$ and at $k = 0$ for $t = -t'$. When $|t| \neq |t'|$, the system is thus insulating (gapped) and we can study its topological properties. The phases $t > t'$, $-t' < t < t'$, and $t < -t'$ are separated by gap closing and could thus potentially be topological different.

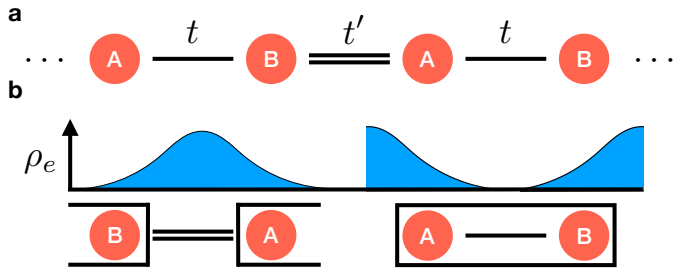

Figure 3.1: ***a*** The model consists of electrons hopping on a dimerized chain with alternating hopping strengths t and t'. For the case of $t' > t$, the model is in its topological phase, which is adiabatically connected to the special case $t' \neq 0$, $t = 0$. In this limit the presence of gapless edge modes is evident when the chain is cut after a full unit cell. ***b*** The polarization is a measure of where charges sit in the unit cell. Shown is the case $\mathsf{P} = 1/2$, where the charge center is displaced by exactly half a lattice spacing. When cutting the system after a full unit cell, the edge hosts a state of charge $1/2$. This is the simplest example of charge fractionalization in topological condensed matter systems.

3.3 Wilson loop and position operator

Introduced in 1984 by Sir Michael Berry, the so-called Berry phase describes a phase factor which arises in addition to the dynamical evolution $e^{\mathrm{i}\int E[\lambda(t)]dt}$ of a quantum mechanical state in an adiabatic interpolation of the corresponding Hamiltonian $H[\lambda(t)]$ along a closed path $\lambda(t)$ in parameter space. It depends only on the geometry of the path chosen, and can be expressed as a line integral of the Berry connection, which we define below for the case where the parameter λ is a single particle momentum. If degeneracies between energy levels are encountered along the path, we have to consider the joint evolution of a set of eigenstates that may have degeneracies. If we consider M such states, the Berry phase generalizes to a $U(M)$ matrix, which may be expressed as the line integral of a non-Abelian Berry connection, and is called non-Abelian Wilson loop.
In the BZ, we may consider momentum $\boldsymbol{k}$ as a parameter of the Bloch Hamiltonian $\mathcal{H}(\boldsymbol{k})$. The corresponding non-Abelian Berry-Wilczek-Zee connection is then given by

$$\boldsymbol{\mathcal{A}}_{m,n}(\boldsymbol{k}) = \mathrm{i}\langle u_{\boldsymbol{k},m}|\boldsymbol{\nabla}_{\boldsymbol{k}}|u_{\boldsymbol{k},n}\rangle, \qquad n,m = 1,\cdots,M. \tag{3.3.1}$$

Note that it is Hermitian.Using matrix notation, we define the Wilson loop, a unitary operator, as

$$W[l] = \overline{\exp}\left[\mathrm{i}\int_l \mathrm{d}\boldsymbol{l}\cdot\boldsymbol{\mathcal{A}}(\boldsymbol{k})\right], \tag{3.3.2}$$

where l is a loop in momentum space and the overline denotes path ordering of the exponential. This unitary operator acts on the occupied band manifold, and can be numerically evaluated

with the formula

$$
\begin{aligned}
W_{n_1,n_{R+1}}[l] &= \lim_{R\to\infty} \sum_{n_2,\cdots n_R=1}^{M} \prod_{i=1}^{R} \Big[\exp\left[\mathrm{i}(\boldsymbol{k}_{i+1}-\boldsymbol{k}_i)\cdot\boldsymbol{\mathcal{A}}(\boldsymbol{k}_{i+1})\right]\Big]_{n_i,n_{i+1}} \\
&= \lim_{R\to\infty} \sum_{n_2,\cdots n_R=1}^{M} \prod_{i=1}^{R} \Big[\delta_{n_i,n_{i+1}} + \mathrm{i}(\boldsymbol{k}_{i+1}-\boldsymbol{k}_i)\cdot\boldsymbol{\mathcal{A}}_{n_i,n_{i+1}}(\boldsymbol{k}_{i+1})\Big] \\
&= \lim_{R\to\infty} \sum_{n_2,\cdots n_R=1}^{M} \prod_{i=1}^{R} \Big[\langle u_{\boldsymbol{k}_{i+1},n_i}|u_{\boldsymbol{k}_{i+1},n_{i+1}}\rangle \\
&\quad -(\boldsymbol{k}_{i+1}-\boldsymbol{k}_i)\cdot\langle u_{\boldsymbol{k}_{i+1},n_i}|\boldsymbol{\nabla}_{\boldsymbol{k}_{i+1}}|u_{\boldsymbol{k}_{i+1},n_{i+1}}\rangle\Big] \qquad (3.3.3) \\
&= \lim_{R\to\infty} \sum_{n_2,\cdots n_R=1}^{M} \prod_{i=1}^{R} \langle u_{\boldsymbol{k}_{i+1},n_i}|u_{\boldsymbol{k}_i,n_{i+1}}\rangle \\
&= \langle u_{\boldsymbol{k}_{R+1},n_1}| \lim_{R\to\infty} \prod_{i=2}^{R} \left(\sum_{n_i}^{M} |u_{\boldsymbol{k}_i,n_i}\rangle\langle u_{\boldsymbol{k}_i,n_i}|\right) |u_{\boldsymbol{k}_1,n_{R+1}}\rangle\,, \qquad (3.3.4)
\end{aligned}
$$

where the path l is sampled into R momenta $\boldsymbol{k}_i$, $i = 1,\cdots,R$, and the limit $R\to\infty$ is taken such that the distance between any two neighboring momentum points goes to zero. Further, $\boldsymbol{k}_1 = \boldsymbol{k}_{R+1}$ are the initial and final momenta along the loop, respectively, on which the Wilson loop matrix depends.

By the last line of Eq. (3.3.3) it becomes clear that $W[l]$ is gauge *covariant*, that is, transforms as an operator under a general gauge transformation $S(\boldsymbol{k}) \in U(M)$ of the occupied subspace given by $|u_{\boldsymbol{k}}\rangle \to S(\boldsymbol{k})\,|u_{\boldsymbol{k}}\rangle$, only for a closed loop l (the case where l is non-contractible is also referred to as the Zak phase). However, the Wilson loop *spectrum* for a closed loop is gauge *invariant*, that is, the eigenvalues of $W[l]$ are not affected by gauge transformations (note that they also do not depend on the choice of $\boldsymbol{k}_i = \boldsymbol{k}_f$) and may therefore carry physical information. We will show in the following that this is indeed the case: the Wilson loop spectrum is related to the spectrum of the position operator projected into the space of occupied bands.

To proceed, we consider a geometry where l is parallel to the x coordinate axis, and winds once around the BZ. Let $\boldsymbol{k}$ denote the $(d-1)$ dimensional vector of remaining good momentum quantum numbers. Then $W(\boldsymbol{k})$ is labelled by these remaining momenta. Denote by $\exp(\mathrm{i}\vartheta_{\alpha,\boldsymbol{k}})$, $\alpha = 1,\cdots,M$, the eigenvalues of $W(\boldsymbol{k})$. The set of phases $\{\vartheta_{\alpha,\boldsymbol{k}}\}$ forms a band structure in the $(d-1)$ dimensional BZ and is often equivalently referred to as the Wilson loop spectrum. Note that all $\vartheta_{\alpha,\boldsymbol{k}}$ are only defined modulo 2π, which makes the Wilson loop spectrum inherently different from the spectrum of a physical Bloch Hamiltonian.

The spectral equivalence we will show relates the eigenvalues of the operator $(-\mathrm{i}/2\pi)\log[W(\boldsymbol{k})]$ with those of the projected position operator

$$P(\boldsymbol{k})\hat{x}P(\boldsymbol{k}), \qquad (3.3.5)$$

where the projector $P(\boldsymbol{k})$ onto all occupied band eigenstates along l (i.e., all states with wave vector $\boldsymbol{k}$) is given by

$$P(\boldsymbol{k}) = \sum_{n}^{M} \int_{-\pi}^{\pi} \frac{\mathrm{d}k_x}{2\pi} |\psi_{\boldsymbol{k},n}\rangle\langle\psi_{\boldsymbol{k},n}|, \qquad (3.3.6)$$

where the states $|\psi_{\boldsymbol{k},n}\rangle$ are given by Eq. (3.1.3). The eigenvalues of the projected position operator have the interpretation of the charge centers in the ground state of the Hamiltonian considered, while the eigenstates are known as hybrid Wannier states, which are localized in the x-direction and plane waves perpendicular to it.

To prove the equivalence, we start with the eigenfunctions of $P(\boldsymbol{k})\hat{x}P(\boldsymbol{k})$, which satisfy

$$\left[P(\boldsymbol{k})\hat{x}P(\boldsymbol{k}) - \frac{\tilde{\vartheta}_{\boldsymbol{k}}}{2\pi}\right]|\Psi_{\boldsymbol{k}}\rangle = 0. \tag{3.3.7}$$

Note that there are M eigenvectors, the form of the corresponding eigenvalues $\tilde{\vartheta}_{\alpha,\boldsymbol{k}}/(2\pi)$, $\alpha = 1,\cdots,M$ has been chosen for later convenience and in particular has not yet been logically connected to the $\vartheta_{\alpha,\boldsymbol{k}}$ making up the Wilson loop spectrum (however, we will do so shortly). An eigenfunction can be expanded as

$$|\Psi_{\boldsymbol{k}}\rangle = \sum_n^M \int \mathrm{d}k_x\, f_{\boldsymbol{k},n}(k_x)|\psi_{\boldsymbol{k},n}\rangle, \tag{3.3.8}$$

where the coefficients $f_{\boldsymbol{k},n}$ satisfy the equation

$$\begin{aligned}
&\langle\psi_{\boldsymbol{k},n}|P(\boldsymbol{k})\hat{x}P(\boldsymbol{k})|\Psi_{\boldsymbol{k}}\rangle \\
=\;& \sum_m \int \mathrm{d}\tilde{k}_x\, \langle\psi_{\boldsymbol{k},n}|(\mathrm{i}\partial_{\tilde{k}_x})f_{\boldsymbol{k},m}(\tilde{k}_x)|\psi_{\tilde{\boldsymbol{k}},m}\rangle \\
=\;& \sum_m \int \mathrm{d}\tilde{k}_x\, \mathrm{i}\frac{\partial f_{\boldsymbol{k},m}(\tilde{k}_x)}{\partial\tilde{k}_x}(\delta_{m,n}\delta_{\tilde{k}_x,k_x}) \\
&+\sum_m \int \mathrm{d}\tilde{k}_x f_{\boldsymbol{k},m}(\tilde{k}_x)\int\frac{\mathrm{d}x}{2\pi}\left\langle u_{\boldsymbol{k},n}\left|e^{-\mathrm{i}k_x x}(\mathrm{i}\partial_{\tilde{k}_x})e^{\mathrm{i}\tilde{k}_x x}\right|u_{\tilde{\boldsymbol{k}},m}\right\rangle \\
=\;& \mathrm{i}\frac{\partial f_{\boldsymbol{k},n}(k_x)}{\partial k_x} - f_{\boldsymbol{k},n}(k_x)\int\frac{\mathrm{d}x}{2\pi}x + \mathrm{i}\sum_m\int\mathrm{d}\tilde{k}_x f_{\boldsymbol{k},m}(\tilde{k}_x)\int\frac{\mathrm{d}x}{2\pi}e^{-\mathrm{i}(k_x-\tilde{k}_x)x}\langle u_{\boldsymbol{k},n}|\partial_{k_x}|u_{\tilde{\boldsymbol{k}},m}\rangle \\
=\;& \mathrm{i}\frac{\partial f_{\boldsymbol{k},n}(k_x)}{\partial k_x} + \mathrm{i}\sum_m f_{\boldsymbol{k},m}(k_x)\langle u_{\boldsymbol{k},n}|\partial_{k_x}|u_{\boldsymbol{k},m}\rangle \\
=\;& \mathrm{i}\frac{\partial f_{\boldsymbol{k},n}(k_x)}{\partial k_x} + \sum_m^M \mathcal{A}_{x;n,m}(\boldsymbol{k})f_{\boldsymbol{k},m}(k_x).
\end{aligned} \tag{3.3.9, 3.3.10}$$

(Note that we have to assume an appropriate regularization to make the term $\int \mathrm{d}x\, x$ vanish in this continuum calculation, reflecting the ambiguity in choosing the origin of the coordinate system.) Then, integrating the resulting Eq. (3.3.7) for $f_{\boldsymbol{k},n}(k_x)$, we obtain

$$f_{\boldsymbol{k},n}(k_x) = e^{-\mathrm{i}(k_x-k_x^0)\tilde{\vartheta}_{\boldsymbol{k}}/(2\pi)}\sum_m^M \overline{\exp}\left[\mathrm{i}\int_{k_x^0}^{k_x}\mathrm{d}\tilde{k}_x\mathcal{A}_x(\tilde{k}_x,\boldsymbol{k})\right]_{n,m} f_{\boldsymbol{k},m}(k_x^0). \tag{3.3.11}$$

We now choose $k_x = k_x^0 + 2\pi$. Periodicity of $f_{\boldsymbol{k},m}(k_x^0)$ as $k_x^0 \to k_x^0 + 2\pi$ yields (choosing $k_x^0 = \pi$ without loss of generality)

$$\sum_m^M W(\boldsymbol{k})_{n,m}f_{\boldsymbol{k},m}(\pi) = e^{\mathrm{i}\tilde{\vartheta}_{\boldsymbol{k}}}f_{\boldsymbol{k},n}(\pi), \tag{3.3.12}$$

showing that the expansion coefficients of an eigenstate of $P(\boldsymbol{k})\hat{x}P(\boldsymbol{k})$ with eigenvalue $\tilde{\vartheta}_{\boldsymbol{k}}/(2\pi)$ form eigenvectors of $W(\boldsymbol{k})$ with eigenvalues $e^{\mathrm{i}\tilde{\vartheta}_{\boldsymbol{k}}}$. This establishes the spectral equivalence $\tilde{\vartheta}_{\boldsymbol{k}} = \vartheta_{\boldsymbol{k}}$.

Note that there are M eigenvalues of the Wilson loop, while the number of eigenvalues of $P(\boldsymbol{k})\hat{x}P(\boldsymbol{k})$ is extensive in the system size. Indeed, for each occupied band (i.e., every Wilson loop eigenvalue $\vartheta_{\alpha,\boldsymbol{k}}$, $\alpha = 1,\cdots,M$) there exists a ladder of eigenvalues of the projected position operator

$$\frac{\vartheta_{\alpha,\boldsymbol{k},X}}{2\pi} = \frac{\vartheta_{\alpha,\boldsymbol{k}}}{2\pi} + X, \qquad X\in\mathbb{Z}, \qquad \alpha = 1,\cdots,M. \tag{3.3.13}$$

Notice that we have set the lattice spacing in the x-direction to 1 for convenience here and in the following.
The eigenstates of the projected position operator are then given by

$$\Psi_{\alpha,\boldsymbol{k}}(x-X)=\sum_{n}^{M}\int\frac{\mathrm{d}k_x}{2\pi}e^{-\mathrm{i}\left[\vartheta_{\alpha,\boldsymbol{k}}/(2\pi)+X\right]}f_{\boldsymbol{k},n;\alpha}(k_x)\psi_{\boldsymbol{k},n}(x), \tag{3.3.14}$$

i.e., they are hybrid Wannier states which are maximally localized in x direction, but take on plane wave form in the perpendicular directions. Note that since the eigenvalues of $W(\boldsymbol{k})$ along any non-contractible loop of $\boldsymbol{k}$ in the BZ define a map $S^1\to U(1)\cong S^1$, their winding number, which is necessarily an integer, provides a topological invariant that cannot be changed by smooth deformations of the system's Hamiltonian.

3.4 Wilson loops, polarization and the winding number invariant in the Su-Schrieffer-Heeger model

So far, this has been a rather formal and general introduction to Wilson loops and their connection to the projected position operator. To illustrate them, we go back to the example of the SSH model. Let us start by calculating the Wilson loop for the case where $(t,t')=(0,1)$. The eigenvectors of $\mathcal{H}(k)$ are then given by

$$|u_{k,1}\rangle=\frac{1}{\sqrt{2}}\begin{pmatrix}-e^{\mathrm{i}k}\\1\end{pmatrix},\quad |u_{k,2}\rangle=\frac{1}{\sqrt{2}}\begin{pmatrix}e^{\mathrm{i}k}\\1\end{pmatrix}, \tag{3.4.1}$$

with energies -1 and $+1$, respectively. Since the occupied subspace is one-dimensional in this case, the Berry connection $A(k)=\mathrm{i}\langle u_{k,1}|\partial_k|u_{k,1}\rangle=-1/2$ is Abelian and given by just a purely imaginary number (remember that it is anti-Hermitian in general). We thus obtain

$$\mathsf{P}:=-\frac{\mathrm{i}}{2\pi}\log W=-\frac{1}{2\pi}\int_0^{2\pi}\mathcal{A}(k)\mathrm{d}k=\frac{1}{2}. \tag{3.4.2}$$

The physical interpretation of P is given within the modern theory of polarization as that of a bulk electrical dipole moment or charge polarization, which is naturally only defined modulo 1 since the coordinate of a center of charge on the lattice is only defined up to a lattice translation (remember that we have chosen the lattice spacing $a=1$). It is directly connected to the Wilson loop spectrum $\vartheta_{\alpha,\boldsymbol{k}}$ by a rescaling which makes sure that the periodicity of the charge centers defined in this way is that of the real-space lattice. See also Fig. 3.1***b***.
The result $\mathsf{P}=1/2$ is by no means accidental: In fact, since the inversion symmetry reverses the path of integration in W, but leaves inner products such as $A(k)$ invariant, the Wilson loop eigenvalues of an inversion symmetric system come in complex conjugate pairs, i.e., for each eigenvalue ϑ there exists another eigenvalue ϑ' such that $e^{\mathrm{i}\vartheta}=e^{-\mathrm{i}\vartheta'}$. In the Abelian case of a single band, this means that P be quantized to 0 ($\vartheta=0$) or $1/2$ ($\vartheta=\pi$). This is an example where a crystalline symmetry such as inversion, which acts non-locally in space, protects a topological phase by enforcing the quantization of a topological invariant to values that cannot be mapped into one another by an adiabatic evolution of the corresponding Hamiltonian. Note that since the eigenstates for the parameter choice $(t,t')=(1,0)$ do not depend on k, we immediately obtain $\mathsf{P}=0$ for this topologically trivial case.
By these considerations it is clear that in fact the full parameter regime where $t<t'$ is topological, while the regime $t>t'$ is trivial. This is because it is possible to perform an adiabatic interpolation from the specific parameter choices $(t,t')\in\{(0,1),(1,0)\}$ considered above to all other values as long as there is no gap closing and no breaking of inversion symmetry, which is true provided that the line $t=t'$ is avoided in parameter space.

In many cases, a topological phase comes with topologically protected gapless boundary modes on boundaries which preserve the protecting symmetry. For inversion symmetry, however, there are no boundaries satisfying this requirement. Even though the model at $(t, t') = (0, 1)$ has zero-mode end states [since in this case, $\mathcal{H}(k)$ does not act at all on the A (B) site in the unit cell at the left (right) edge of the sample], these modes can be removed from zero energy by generic local perturbations even without a bulk gap closing. To protect the end modes, we need to invoke the chiral symmetry, which implies that an eigenstate at any energy E is paired up with an eigenstate at energy $-E$. Eigenstates of the chiral symmetry can then only appear at $E = 0$. A spatially and spectrally isolated boundary mode at $E = 0$ can thus not be removed by perturbations that retain the chiral symmetry.
In fact, in the presence of chiral symmetry, the above discussion can be generalized to arbitrary one-dimensional models. In the eigenbasis of $U_{\mathcal{C}}$, we can write any Hamiltonian with chiral symmetry in the form

$$\mathcal{H}(k) = \begin{pmatrix} 0 & q(k) \\ q^\dagger(k) & 0 \end{pmatrix}, \tag{3.4.3}$$

where for the SSH model the matrix $q(k)$ was given by just a complex number. The chiral symmetry allows for the definition of a winding number

$$\nu = \frac{\mathrm{i}}{2\pi} \int \mathrm{d}k \, \mathrm{Tr} \left[q(k) \partial_k q^{-1}(k) \right] \in \mathbb{Z}. \tag{3.4.4}$$

This winding number is a topological invariant, i.e., a quantized number that is the same in the entire phase. Note that the formulation of Eq. (3.4.4) is only possible when chiral symmetry is present. We can make contact with the overarching concept of Wilson loops by calculating the connection

$$\mathcal{A} = \frac{1}{2} \mathrm{i} q(k) \partial_k q^{-1}(k). \tag{3.4.5}$$

Thus the Wilson loop eigenvalues $e^{\mathrm{i}\vartheta_\alpha}$ satisfy

$$\frac{1}{2\pi} \sum_\alpha \vartheta_\alpha = \frac{\nu}{2} \bmod 1. \tag{3.4.6}$$

In particular, in the Abelian case, chiral symmetry thus implies the quantization of P to half-integer values, just as inversion symmetry did it above. An important distinction to be made is that with inversion symmetry, we have a $\mathbb{Z}_2$ topological classification (P can be either 0 or 1/2), while with chiral symmetry the winding number allows for a $\mathbb{Z}$ classification.

3.5 Bulk-boundary correspondence

As already mentioned, Wilson loops not only provide a convenient formulation of many topological invariants, but are also in one-to-one correspondence with the boundary degrees of freedom of the system considered. We will now show that indeed the spectrum of a Hamiltonian in the presence of a boundary is smoothly connected to the spectrum of its Wilson loop along the direction perpendicular to the boundary. Note that since the Wilson loop is determined entirely by the bulk Bloch Hamiltonian, this relation provides an explicit realization of the bulk-boundary correspondence underlying topological phases.
We consider a semi-infinite slab geometry with a single edge of the system at $x = 0$, while keeping $\boldsymbol{k}$ as good quantum numbers. From a topological viewpoint, the actual energetics of the band structure are irrelevant, and we can always deform the Hamiltonian for the sake of clarity to a spectrally flattened Hamiltonian where all bands above and below the gap are at energy $+1$ and -1, respectively, without closing the gap. It is therefore enough to work with

$$\mathcal{H}_{\mathrm{flat}}(\boldsymbol{k}) = 1 - 2P(\boldsymbol{k}) \tag{3.5.1}$$

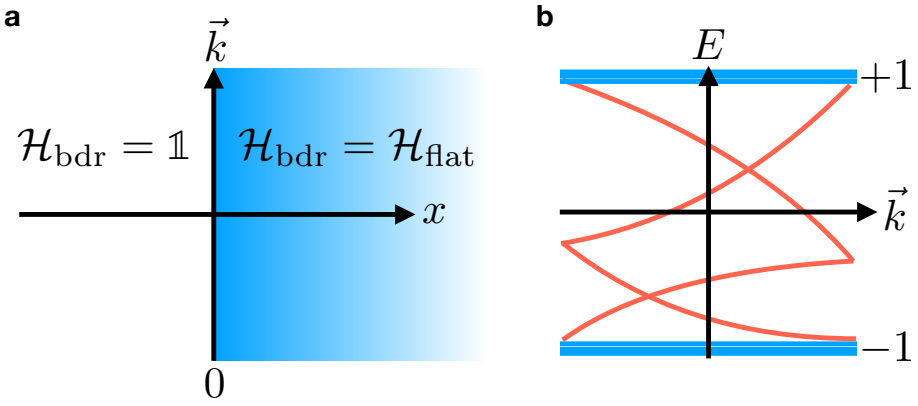

Figure 3.2: ***a*** For $V_0(x)$ as given by Eq. (3.5.4), $\mathcal{H}_{\rm bdr}$ varies discontinuously from a trivial projector in the domain $x < 0$ to $\mathcal{H}_{\rm flat}$ in the domain $x > 0$. Translational symmetry along x is thus broken, however it is preserved along all perpendicular directions, which still have good momentum quantum numbers $\boldsymbol{k}$. ***b*** The spectrum of $\mathcal{H}_{\rm bdr}$ has accumulation points at ± 1, stemming from the semi-infinite regions to the left and right of the domain wall, and a discrete set of bands in between, coming from the finite domain wall region.

to model the bulk system. Here, $P(\boldsymbol{k})$ as defined in Eq. (3.3.6), repeated here for convenience,

$$P(\boldsymbol{k}) = \sum_n^M \int_{-\pi}^{\pi} \frac{\mathrm{d}k_x}{2\pi} |\psi_{\boldsymbol{k},n}\rangle\langle\psi_{\boldsymbol{k},n}|, \tag{3.5.2}$$

is the projector onto the occupied subspace for a given $\boldsymbol{k}$. Note that $\mathcal{H}_{\rm flat}(\boldsymbol{k})$ actually has the same eigenvectors as the original Hamiltonian. To model a system with boundary, we use

$$\mathcal{H}_{\rm bdr}(\boldsymbol{k}) = P(\boldsymbol{k}) V_0(\hat{x}) P(\boldsymbol{k}) + 1 - P(\boldsymbol{k}), \tag{3.5.3}$$

with

$$V_0(x) = \begin{cases} 1 & x < 0 \\ -1 & x > 0 \end{cases} \tag{3.5.4}$$

so that we have $\mathcal{H}_{\rm bdr}(\boldsymbol{k}) \to \mathcal{H}_{\rm flat}(\boldsymbol{k})$ for $x \to +\infty$ and $\mathcal{H}_{\rm bdr}(\boldsymbol{k}) \to 1$ for $x \to -\infty$ (see Fig. 3.2***a***). The latter limit corresponds to a description of the vacuum with the chemical potential chosen so that no electron states will be occupied, which we take to be the topologically trivial limit. Since we take space to be infinitely extended away from the domain wall at $x = 0$, the spectrum of $\mathcal{H}_{\rm bdr}(\boldsymbol{k})$ includes the spectrum of $\mathcal{H}_{\rm flat}(\boldsymbol{k})$, given by ± 1 since $P^2(\boldsymbol{k}) = P(\boldsymbol{k})$, as well as that of the operator 1, trivially given by $+1$. The boundary region is of finite extent and can therefore contribute only a finite number of midgap states as the system has exponentially decaying correlations on either side of the boundary. There are therefore spectral accumulation points at ± 1, but otherwise we are left with a discrete spectrum (see Fig. 3.2***b***). We will focus on this part of the spectrum.

We will now deform the spectrum of $\mathcal{H}_{\rm bdr}(\boldsymbol{k})$ to that of $(-\mathrm{i}/2\pi)\log[W(\boldsymbol{k})]$ by considering an evolution that takes $P(\boldsymbol{k})V_0(\hat{x})P(\boldsymbol{k})$ to $P(\boldsymbol{k})\hat{x}P(\boldsymbol{k})$, the eigenvalues of which were previously shown to be directly related to those of $(-\mathrm{i}/2\pi)\log[W(\boldsymbol{k})]$. The deformation is continuous in $\boldsymbol{k}$ and therefore preserves both discreteness of the spectrum as well as its topological properties. An example for this interpolation is given by

$$V_\lambda(x) = \begin{cases} -\frac{x}{\lambda} & \text{for } |x| < \lambda/(1-\lambda) \\ -\frac{\mathrm{sgn}(x)}{1-\lambda} & \text{for } |x| \geq \lambda/(1-\lambda) \end{cases}, \qquad 0 \leq \lambda \leq 1. \tag{3.5.5}$$

Importantly, for any $\lambda < 1$, $P(\boldsymbol{k})V_\lambda(\hat{x})P(\boldsymbol{k})$ is a finite rank (finite support) perturbation of $(1-\lambda)^{-1}P(\boldsymbol{k})V_0(\hat{x})P(\boldsymbol{k})$, so it will retain the property that the spectrum is discrete. However, the point $\lambda = 1$ deserves closer inspection, as $P(\boldsymbol{k})\hat{x}P(\boldsymbol{k})$ is not a bounded operator. However, we can handle this subtlety by defining

$$h(r) = \begin{cases} r & \text{for} - w < r < w \\ \text{sgn}(r)w & \text{else} \end{cases} \tag{3.5.6}$$

and considering $h[P(\boldsymbol{k})V_\lambda(\hat{x})P(\boldsymbol{k})]$ for some large w. The spectrum evolves uniformly continuously from $h[P(\boldsymbol{k})V_0(\hat{x})P(\boldsymbol{k})]$ to $h[P(\boldsymbol{k})V_1(\hat{x})P(\boldsymbol{k})]$ for any finite w.
The topology of the Wilson loop spectrum and the physical boundary spectrum is thus identical. Protected spectral flow in the former implies gapless boundary modes in the latter, as long as the form of the boundary [i.e., $V(x)$] does not break a symmetry that protects the bulk spectral flow.

References

1. Zak, J. "Berry's phase for energy bands in solids". *Phys. Rev. Lett.* **62,** 2747. https://doi.org/10.1103/PhysRevLett.62.2747 (1989).
2. Fidkowski, L., Jackson, T. & Klich, I. "Model Characterization of Gapless Edge Modes of Topological Insulators Using Intermediate Brillouin-Zone Functions". *Phys. Rev. Lett.* **107,** 036601. https://doi.org/10.1103/PhysRevLett.107.036601 (2011).
3. Marzari, N., Mostofi, A., Yates, J., Souza, I. & Vanderbilt, D. "Maximally localized Wannier functions: Theory and applications". *Rev. Mod. Phys.* **84,** 1419. https://doi.org/10.1103/RevModPhys.84.1419 (2012).

Chapter 4

From Chern insulators to 3D topological insulators

Learning goals

- We know Dirac fermions.
- We know what a Chern insulator is.
- We know the BHZ model.
- We can explain the idea of "pair-switching".

- G. Jotzu, M. Messer, R. Desbuquois, M. Lebrat, T. Uehlinger, D. Greif, and T. Esslinger, Nature **515**, 237 (2014)

Initially, we dealt with systems subject to a magnetic field $\boldsymbol{B}$. We could show how their ground state can be described with a topological invariant, the Chern number. Moreover, we have seen how topological phenomena can be observed in one dimensional systems without a magnetic field. In the present chapter, we try to extend these ideas. The main question we are trying to answer is the following: Can there be lattice systems with Bloch bands that are characterized by a non-zero Chern number even in the absence of a net magnetic field? Such an insulator would be termed a *Chern insulator*. Before we embark on this question, we need to understand a simple continuum problem called the Dirac model. Moreover, can we get rid of time-reversal symmetry breaking all-together and find topological insulators in time reversal invariant (TRI) systems?

4.1 Dirac fermions

Dirac fermions in two dimensions are described by the Hamiltonian

$$\mathcal{H}(\boldsymbol{k}) = \sum_i d_i(\boldsymbol{k})\sigma_i \qquad \text{with} \qquad d_1(\boldsymbol{k}) = k_x,\ \ d_2(\boldsymbol{k}) = k_y,\ \ d_3(\boldsymbol{k}) = m. \tag{4.1.1}$$

The energies and eigenstates are given by

$$\epsilon(\boldsymbol{k})_\pm = \pm d(\boldsymbol{k}) = \pm\sqrt{k^2+m^2} \qquad \text{and} \qquad \psi_\pm(\boldsymbol{k}) = \frac{1}{\sqrt{2d(\boldsymbol{k})[d(\boldsymbol{k})\pm d_3(\boldsymbol{k})]}}\begin{pmatrix} d_3(\boldsymbol{k})\pm d(\boldsymbol{k}) \\ d_1(\boldsymbol{k}) + \mathrm{i}d_2(\boldsymbol{k})\end{pmatrix}.$$

It is straight forward to show (exercise!) that the Berry connection of the lower band can be written as

$$\mathcal{A}_\mu(\boldsymbol{k}) = \mathrm{i}\langle\psi_-(\boldsymbol{k})|\partial_{k_\mu}\psi_-(\boldsymbol{k})\rangle = \frac{1}{2d(\boldsymbol{k})[d(\boldsymbol{k})-d_3(\boldsymbol{k})]}\left[d_2(\boldsymbol{k})\partial_{k_\mu}d_1(\boldsymbol{k}) - d_1(\boldsymbol{k})\partial_{k_\mu}d_2(\boldsymbol{k})\right] \tag{4.1.2}$$

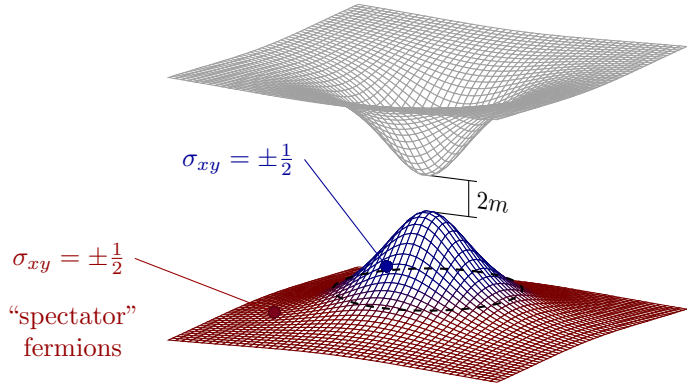

Figure 4.1: Regularization of the Dirac spectrum due to a lattice.

And the corresponding Berry curvature is given by

$$\mathcal{F}_{\mu\nu}(\boldsymbol{k}) = \frac{1}{2}\epsilon_{\alpha\beta\gamma}\hat{d}_\alpha(\boldsymbol{k})\partial_{k_\mu}\hat{d}_\beta(\boldsymbol{k})\partial_{k_\nu}\hat{d}_\gamma(\boldsymbol{k}) \qquad \text{with} \qquad \hat{\boldsymbol{d}}(\boldsymbol{k}) = \frac{\boldsymbol{d}(\boldsymbol{k})}{d(\boldsymbol{k})}. \tag{4.1.3}$$

Using our concrete d-vector we find

$$\mathcal{A}_x = \frac{k_y}{2\sqrt{k^2+m^2}(\sqrt{k^2+m^2}-m)} \qquad \text{and} \qquad \mathcal{A}_y = \frac{-k_x}{2\sqrt{k^2+m^2}(\sqrt{k^2+m^2}-m)}, \tag{4.1.4}$$

and therefore

$$\mathcal{F}_{xy} = -\frac{m}{2(k^2+m^2)^{3/2}}. \tag{4.1.5}$$

Let us plug that into the formula for the Hall conductance

$$\sigma_{xy} = \frac{e^2}{h}\frac{1}{2\pi}\int d\boldsymbol{k}\,\mathcal{F}_{xy} = -\frac{e^2}{h}\int_0^\infty dk k\frac{1}{2}\frac{m}{(k^2+m^2)^{3/2}} = -\frac{e^2}{h}\frac{\text{sign}(m)}{2}. \tag{4.1.6}$$

We can draw several important insights from this results:

1. $\sigma_{xy} \neq 0 \;\Rightarrow$ we must have broken time-reversal invariance. How did this happen?
2. $\sigma_{xy} \neq \frac{e^2}{h}\nu$ with $\nu \in \mathbb{Z}$. How can this be?

Let us start with the first question. We have to make the distinction between two cases. (i) If the σ-matrices encode a real spin-1/2 degree of freedom the time reversal operator is given by

$$\mathcal{T} = \mathrm{i}\sigma_y K,$$

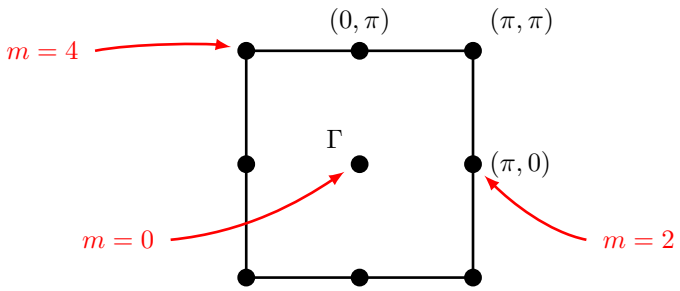

Figure 4.2: Band touching for a simple Chern insulator.

where K denotes complex conjugation. Therefore

$$\mathcal{T}\mathcal{H}(\boldsymbol{k})\mathcal{T}^{-1} = \sum_i -d_i(\boldsymbol{k})\sigma_i = -k_x\sigma_x - k_y\sigma_y - m\sigma_z.$$

If we want to above Hamiltonian to be time reversal invariant we need this to be

$$\mathcal{T}\mathcal{H}(\boldsymbol{k})\mathcal{T}^{-1} \stackrel{!}{=} \mathcal{H}(-\boldsymbol{k}) = -k_x\sigma_x - k_y\sigma_y + m\sigma_z.$$

From this we conclude that the Dirac fermions are only time reversal invariant for $d_3(\boldsymbol{k}) = m = 0$. However, in this case, there is no gap in the spectrum at $\boldsymbol{k} = 0$ and the calculation of σ_{xy} does not make sense. (ii) For the case that the Pauli matrices describe some iso-spin where $\mathcal{T} = K$, we need to have $H^*(\boldsymbol{k}) = H(-\boldsymbol{k})$. Or in other words

$$d_1(\boldsymbol{k}) = d_1(-\boldsymbol{k}), \;\; d_2(\boldsymbol{k}) = -d_2(-\boldsymbol{k}), \;\; d_3(\boldsymbol{k}) = d_3(-\boldsymbol{k}).$$

From these considerations we conclude that our Hamiltonian breaks time reversal invariance in either case and we can indeed expect a non-vanishing Hall conductance.
Let us now address the non-quantized nature of σ_{xy}. The quantization of σ_{xy} arises from the quantized value of the Chern number. We have seen in our derivation, however, that it was crucial that the domain over which we integrated the Berry curvature was closed and orientable. Here we are in a continuum model where the integral over all momenta extends over the whole $\mathbb{R}^2$. We have therefore no reason to expect σ_{xy} to be quantized.
There is value to formula (4.1.6), however. Imagine that the Dirac Hamiltonian arises from some low-energy expansion ($\boldsymbol{k}\cdot\boldsymbol{p}$) around a special point in the Brillouin zone of a lattice model. For the full lattice, the $k \to \infty$ integral would be regularized due to the Brillouin zone boundary. The whole system has a quantized Hall conductivity. However, the region close to the "Dirac-point" contributes $\pm 1/2$ to the Chern number, see Fig. 4.1. Moreover, imagine a gap closing and re-opening transition described by the Dirac Hamiltonian where m changes its value. In such a situation the change in Chern number $\Delta\mathsf{C}^{(1)} = \pm 2\pi$. Therefore, the Dirac model is an excellent way to study *changes in the Chern number*.
Before we continue to the simplest possible Chern insulator we state the following formula without proof (exercise!)

$$\mathcal{H}(\boldsymbol{k}) = \sum_{i,j=1}^{2} A_{ij}k_i\sigma_j + m\sigma_z \qquad \Rightarrow \qquad \sigma_{xy} = -\frac{e^2}{h}\frac{\mathrm{sign}(m)}{2}\mathrm{sign}(\det A). \tag{4.1.7}$$

4.2 The simplest Chern insulator

We obtain the simplest conceivable Chern insulator by elevating the Dirac model to a lattice problem

$$d_1 = k_x \to \sin(k_x), \;\; d_2 = k_y \to \sin(k_y). \tag{4.2.1}$$

The σ matrices now act in a space of orbitals. The fact that the coupling between them is odd in $\boldsymbol{k}$ means that they need to differ by one quantum of angular momentum, e.g., an s-type and a p-type orbital. By symmetry, there can be an even in $\boldsymbol{k}$ term within each orbital, so we add it to our model

$$d_3 = m \to -2 + m + \cos(k_x) + \cos(k_y).$$

The Hamiltonian is gapped ($d(\boldsymbol{k}) \neq 0 \;\forall\, \boldsymbol{k}$) $\forall\, m$ except at the special points in the Brillouin zone shown in Fig. 4.2.
We begin analyzing the Hamiltonian for $m \ll 0$ and $m \gg 4$. For $m = \pm\infty$, the eigenstates of the Hamiltonian are fully localized to single sites and the system certainly shows no Hall conductance. Another way to see this is to observe that

$$\mathsf{C}^{(1)} = \frac{1}{2\pi}\int_{\mathrm{BZ}} d\boldsymbol{k}\, \epsilon_{\alpha\beta\gamma}\hat{d}_\alpha\partial_{k_x}\hat{d}_\beta\partial_{k_y}\hat{d}_\gamma \tag{4.2.2}$$

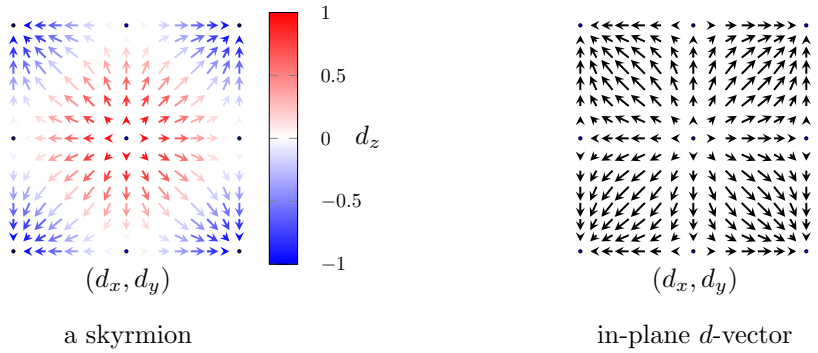

Figure 4.3: Left: spin-configuration of a skyrmion. Right: in-plane d-vector of H.

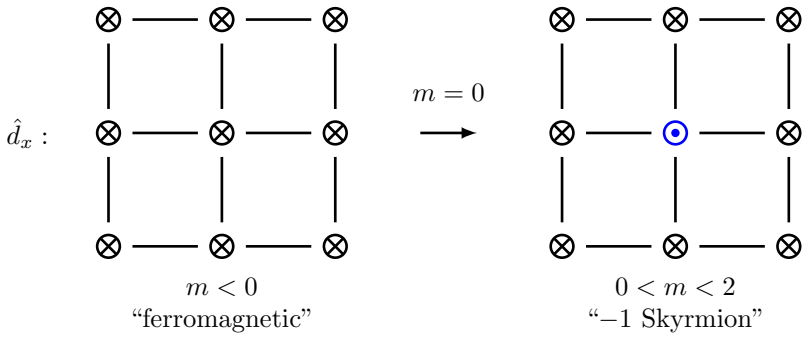

Figure 4.4: Change of the d_3 component at the first critical point.

counts the winding of $\hat{\boldsymbol{d}}(\boldsymbol{k})$ throughout the Brillouin zone, i.e., it provides us what we know as the *skyrmion number*. In Fig. 4.3(a) we show a spin-configuration corresponding to a skyrmion. When we now look at the planar part of the d-vector, we see that we have all laid out for a skyrmion. The only addition we need is a sign change of d_3 at the right places in the Brillouin zone. This does not happen for $m < 0$ or $m > 4$. Note that exactly this sign change closes the gap in a fashion describable by Dirac fermions. Hence we appreciate the importance of the above discussion. It is now trivial to draw the phase diagram.

The case $0 \leq m < 2$: We start from $m = -\infty$ where $\sigma_{xy} = 0$ and go through the gap-closing at $\boldsymbol{k} = 0$ for $m = 0$. Around $\boldsymbol{k} = 0$ we find

$$\mathcal{H} = k_x\sigma_x + k_y\sigma_y + m\sigma_x.$$

Therefore

$$\Delta\sigma_{xy} = -\frac{e^2}{h}\left[\frac{1}{2}\text{sign}(m)\Big|_{m>0} - \frac{1}{2}\text{sign}(m)\Big|_{m<0}\right] = -\frac{e^2}{h} = \sigma_{xy}.$$

The correspoding change in $d_3(\boldsymbol{k})$ is shown in Fig. 4.4.

The case $2 \leq m < 4$: At $m = 2$ the gap closes at $(\pi, 0)$ and $(0, \pi)$. Let us expand the Hamiltonian around these points

$$\mathcal{H}_{(\pi,0)} = \quad k_x\sigma_x - k_y\sigma_y + (-2+m)\sigma_z, \tag{4.2.3}$$
$$\mathcal{H}_{(0,\pi)} = -k_x\sigma_x + k_y\sigma_y + (-2+m)\sigma_z. \tag{4.2.4}$$

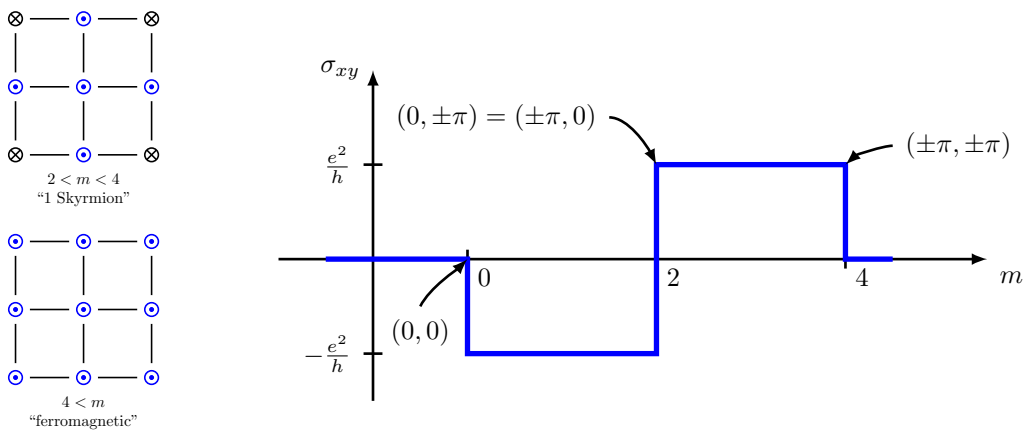

Figure 4.5: Left: d_3 component after the second and third gap closing. Right: Evolution of the topological index as a function of m.

From this we read out the change in σ_{xy}:

$$\Delta\sigma_{xy} = 2\frac{e^2}{h}\left[\frac{1}{2}\text{sign}(-2+m)\Big|_{m>2} - \frac{1}{2}\text{sign}(-2+m)\Big|_{m<2}\right] = 2\frac{e^2}{h}. \tag{4.2.5}$$

Note that the 2 in front stems from the two gap closings, and an additional $-$ sign arises from the odd sign of the determinant A, cf. Eq. (4.1.7). Together with the value of σ_{xy} for $0 < m < 2$ we obtain

$$\sigma_{xy} = +\frac{e^2}{h}.$$

The corresponding $d_3(\boldsymbol{k})$ is shown in Fig. 4.5.

The case $4 \leq m$: The last gap-closing happens at (π, π) for $m = 4$. At this point

$$\mathcal{H}_{(\pi,\pi)} = -k_x\sigma_x - k_y\sigma_y + (-4+m)\sigma_z.$$

As before the change in σ_{xy} is given by

$$\Delta\sigma_{xy} = -\frac{e^2}{h}\left[\frac{1}{2}\text{sign}(-4+m)\Big|_{m>0} - \frac{1}{2}\text{sign}(-4+m)\Big|_{m<0}\right] = -\frac{e^2}{h}.$$

And we arrive again at $\sigma_{xy} = 0$ as expected for a phase connected to the $m = \infty$ limit. Again, $d_3(\boldsymbol{k})$ is shown in Fig. 4.5 together with an overview of the whole analysis.
Before we move on, we also show the energy spectrum of the lattice Dirac Hamiltonian analyzed here. Fig. 4.6 shows such a spectrum for $m = 0.8$ on a half-plane: We calculate the spectrum on a cylinder of length $L = 60$. Around the circumference we use the translation symmetry to label states with respect to $k_\parallel$. If we also apply periodic boundary conditions in the direction where the cylinder has length L (turning the geometry into torus), we find the bulk spectrum shown in the left panel. By opening the boundaries and only selecting states on one side of the open cylinder we obtain the right panel showing the expected chiral edge mode traversing the gap.

4.3 Time reversal invariant topological insulators

In this chapter we try to understand what topological properties can arise for free fermion systems subject to some symmetry constraints. The exposition starts from a the simplest extension

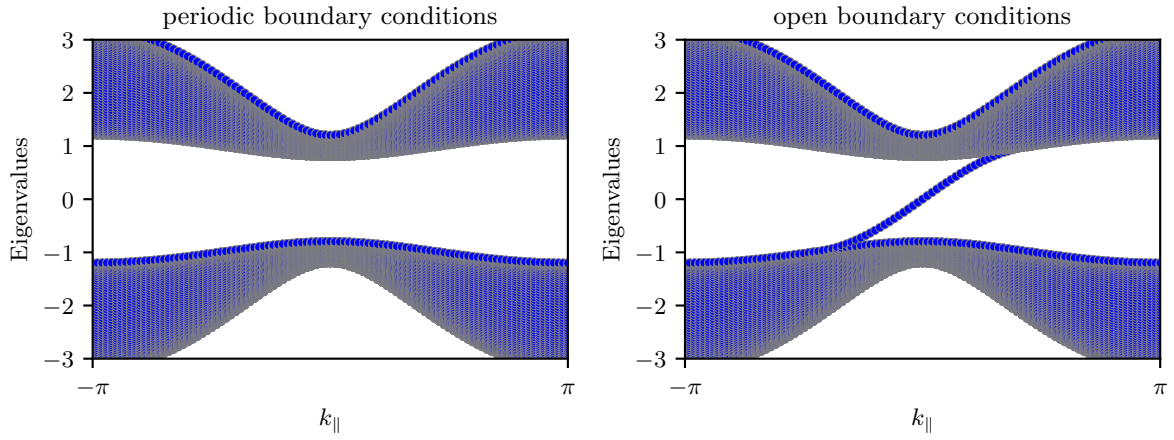

Figure 4.6: Spectrum of the lattice Dirac model for $m = 0.8$. The left panel shows the bulk spectrum as a function of the momentum along one direction ($k_\parallel$). The right panel shows the same setup for a half plane including one edge.

of the lattice Dirac model into a time-reversal invariant version. We then motivate on physical grounds how one can construct a topological index characterizing this new type of band insulator. The so derived topological index for two-dimensional systems readily generalizes to three dimensions. Note, that our path of going from the lattice Dirac model to the Bernevig-Hughes-Zhang model [1] below is not following the historical route. For an account of the two milestone papers by Haldane [2] and Kane and Mele [3], you can consult the App. B. Finally, note that we build in an essential way on Kramers-pairs which require the time reversal operator $\mathcal{T}^2 = -1$ to square to minus one, i.e., we are dealing with spinful electrons.

4.3.1 The BHZ model

We construct a time reversal invariant Hamiltonian from the lattice Dirac model

$$\mathcal{H}_{\mathrm{D}}(\boldsymbol{k}) = [m - 2 + \cos(k_x) + \cos(k_y)]\sigma_z + \sin(k_x)\sigma_x + \sin(k_y)\sigma_y, \tag{4.3.1}$$

by explicitly adding the time-reversed partner

$$\begin{aligned}\mathcal{H}_{\mathrm{BHZ}} &= \begin{pmatrix} \mathcal{H}_{\mathrm{D}}(\boldsymbol{k}) & 0 \\ 0 & \mathcal{H}^*_{\mathrm{D}}(-\boldsymbol{k}) \end{pmatrix} \\ &= \tau_0 \otimes \{[m - 2 + \cos(k_x) + \cos(k_y)]\sigma_z + \sin(k_y)\sigma_y\} + \sin(k_x)\tau_z \otimes \sigma_x. \end{aligned} \tag{4.3.2}$$

Note, that if we use $\boldsymbol{\tau}$ to denote a spin-1/2 degree of freedom, the time reversal operator reads now $\mathcal{T} = \mathrm{i}\tau_y \otimes \sigma_0 K$, where K denotes complex conjugation and $\mathcal{T}^2 = -\tau_0 \otimes \sigma_0$. In other words, this Hamiltonian simply describes two Chern insulators glued together, each with an opposite Chern number. As long as the z-component $\tau_z \otimes \sigma_0$ of the spin is conserved, one can immediately write down a topological index, the spin-Chern number [4]

$$\mathsf{C}_s^{(1)} := \frac{\mathsf{C}_\downarrow^{(1)} - \mathsf{C}_\uparrow^{(1)}}{2} \mod 2 \quad \in \mathbb{Z}_2. \tag{4.3.3}$$

When we look at the edge spectrum of the above Hamiltonian in Fig 4.7, it can be understood why this index is only in $\mathbb{Z}_2$ and not in $\mathbb{Z}$ as the Chern number. The crossing of the two edge states at $k_\parallel = 0$ is protected by the Kramer's degeneracy. This degeneracy arises, as $\boldsymbol{k} = 0$ is itself a time-reversal invariant momentum (TRIM). If we now would have two such Kramers pairs

at $\boldsymbol{k} = 0$, one could unlink the edge states while preserving the double-degeneracy. However, each time one has an odd number of such crossings, one is bound to remain, hence $\mathsf{C}_s^{(1)} \in \mathbb{Z}_2$. We can now add a perturbation that breaks the conservation of S_z, such as

$$\mathcal{H} = \mathcal{H}_{\text{BHZ}} + \lambda \tau_x \otimes \sigma_y. \tag{4.3.4}$$

As this Hamiltonian still commutes with $\mathcal{T}$, we expect the Kramers argument of above to still hold. Indeed, as we see in the right panel of Fig. 4.7, the edge states persists also for $\lambda = 0.1$. Clearly we need a better index than the spin-Chern number defined above. While there is an extension of the spin-Chern number for weakly broken spin-conservation[1], we want to make progress to an index only based on time-reversal symmetry.

4.3.2 $\mathbb{Z}_2$ index

Charge polarization

We revisit Laughlin's pumping argument to make progress towards a $\mathbb{Z}_2$ index for TRI topological insulators. We have seen in the last chapter, that in the simple case of only one filled band in one spatial dimension, the charge polarization can be written as

$$\mathsf{P} := -\frac{\mathrm{i}}{2\pi} \log W = -\frac{1}{2\pi} \int_0^{2\pi} \mathcal{A}(k) \mathrm{d}k. \tag{4.3.5}$$

Two comments are in order:

1. If we re-gauge $|\psi_k\rangle \to e^{\mathrm{i}\varphi(k)} |\psi_k\rangle$ with a $\varphi(k)$ that is winding by $2\pi m$ throughout the Brillouin zone, the corresponding polarization changes to

   $$\mathsf{P} \to \mathsf{P} + m.$$

   This is ok, as charge polarization is anyway only defined up to a lattice constant.

[1] The two filled bands of H_{BHZ} together have a vanishing Chern number. The S_z quantum number, however, allowed us to label the two filled bands individually and calculate a Chern number per spin. Here we show how one can extend this to weak violation of S_z conservation. First, take the two eigenstates of the filled bands

$$P_{\text{filled}}(\boldsymbol{k}) = \begin{bmatrix} \boldsymbol{u}_1(\boldsymbol{k}) & \boldsymbol{u}_2(\boldsymbol{k}) \end{bmatrix},$$

with the two column vectors $\boldsymbol{u}_\alpha(\boldsymbol{k})$, $\alpha = 1, 2$ of the two lower eigenstates of H_{BHZ} per $\boldsymbol{k}$. In case $\tau_z \otimes \sigma_0$ is a symmetry, the two labels are also labelling the eigenstates of S_z with $(1, 2) \to (\uparrow, \downarrow)$. How do we smoothly (as a function of $\boldsymbol{k}$) assign the labels α in case this symmetry is broken? We can project the symmetry into the space of filled states

$$S_z^{\text{filled}}(\boldsymbol{k}) = P_{\text{filled}}(\boldsymbol{k}) \tau_z \otimes \sigma_0 P_{\text{filled}}^\dagger(\boldsymbol{k}).$$

As S_z is not commuting with H_{BHZ}, $S_z^{\text{filled}}(\boldsymbol{k})$ is not diagonal anymore. However, we can diagonalize it

$$\begin{pmatrix} \chi_+ & 0 \\ 0 & \chi_- \end{pmatrix} = M(\boldsymbol{k}) S_z^{\text{filled}}(\boldsymbol{k}) M^\dagger(\boldsymbol{k}).$$

As long as there is a spin gap $\Delta_S = |\chi_+ - \chi_-| > 0$ for all $\boldsymbol{k}$, we can now use the states

$$\begin{bmatrix} \boldsymbol{u}_+(\boldsymbol{k}) & \boldsymbol{u}_-(\boldsymbol{k}) \end{bmatrix} = M(\boldsymbol{k}) P_{\text{filled}}(\boldsymbol{k})$$

to calculate the spin-Chern number [5] via

$$\boldsymbol{\mathcal{A}}_\pm = \mathrm{i} \langle \boldsymbol{u}_\pm(\boldsymbol{k}) | \nabla \boldsymbol{u}_\pm(\boldsymbol{k}) \rangle.$$

It is important to note that there is no well-established bulk-boundary relation for the spin-Chern number defined this way.

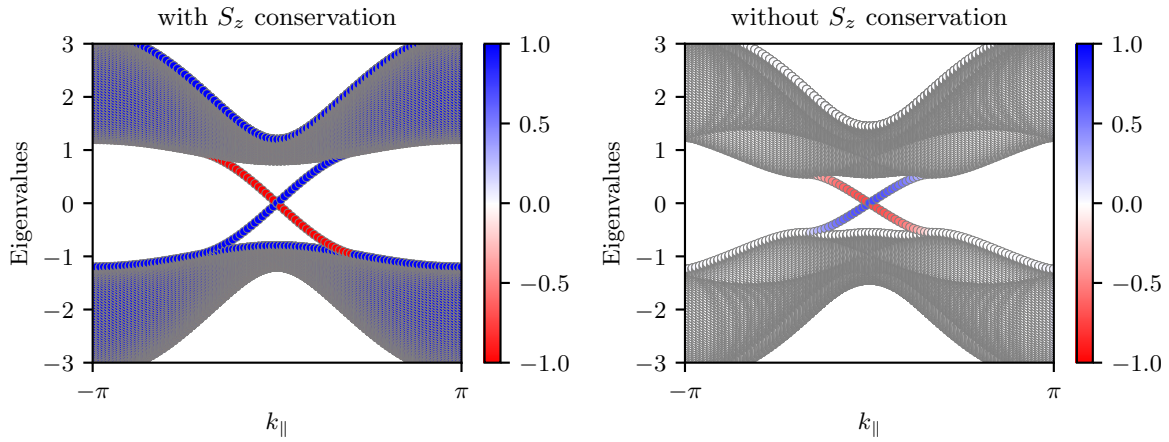

Figure 4.7: Spectrum of the BHZ model for $m = 0.8$. The left panel shows the spectrum for a half plane including only one edge for $\lambda = 0$, where S_z is a good quantum number. The color code indicates the spin S_z (Note, that the bulk has the same number of both red and blue dots). The right panel shows the same spectrum for $\lambda = 0.8$, where the two spin sectors are mixed leading to an un-polarized bulk. Due to the type of coupling, the spin-polarization is largely preserved along the edge.

2. P depends on the chosen gauge. But *changes in* P *by a smooth change in system parameters are gauge independent.* So let us imagine a tuning parameter k_y with

$$\mathcal{H}(k_y) \to \mathcal{H}(k_y')$$

which is slow in time. The change in charge polarization is given by

$$\Delta\mathsf{P} = -\frac{1}{2\pi}\left[\int_{-\pi}^{\pi} dk \mathcal{A}(k, k_y) - \int_{-\pi}^{\pi} dk\, \mathcal{A}(k, k_y')\right] \tag{4.3.6}$$

If we use Stokes' theorem we arrive at

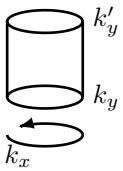

$$\Delta\mathsf{P} = \int_{k_y}^{k_y'} dk_y \int_{-\pi}^{\pi} dk\, \mathcal{F}(k, k_y). \tag{4.3.7}$$

By chosing $k_y' = k_y + 2\pi$, we find for the change in charge polarization $\Delta\mathsf{P} = \mathsf{C}^{(1)}$ where $\mathsf{C}^{(1)}$ is the Chern number. We known, however that $\mathsf{C}^{(1)} \sim \sigma_{xy}$. Indeed, this is nothing but Laughlin's pumping argument for the quantum Hall effect and hence is equal to zero for TRI systems.

Building on the above insight we try to refine the charge pumping of Laughlin to be able to characterize a TRI system.

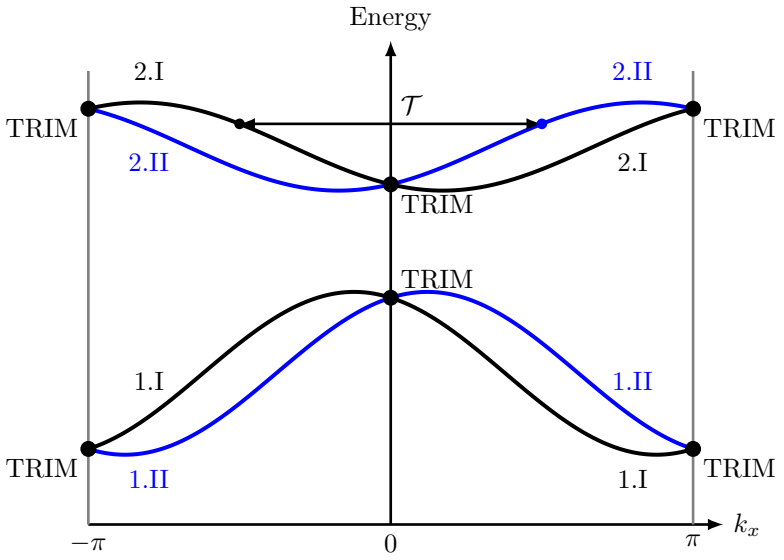

Figure 4.8: Energy levels for a time revesal invariant system.

Time reversal polarization

Let us now try to generalize the charge pumping approach to the TRI setup. For this it is beneficial to look at the structure of a generic energy diagram as shown in Fig 4.8. Under time-reversal, momenta k are mapped to $-k$. Moreover, there are special points in the Brillouin zone which are mapped onto themselves. This is true for all momenta which fulfill $k = -k + G$, where G is a reciprocal lattice vector. This is trivially true for $k = 0$, but also for special points on the borders of the Brillouin zone. On such time reversal invariant momenta (TRIM's), the spectrum has to be doubly degenerate due to Kramer's theorem.
Owing to the symmetry between k and $-k$ we can constrain ourselves to only *half the Brillouin zone*. In this half, we label all bands by 1.I, 1.II, 2.I, 2.II, ... The arabic number simply label pairs of bands. Due to the double degeneracy at the TRIMs, we need an additional (roman number) to label the two (sub)-bands emerging form the TRIMs. One can also say that the roman index labels Kramers pairs

$$\mathcal{T}|\varphi_{n.\mathrm{I}}(k)\rangle = e^{\mathrm{i}\chi_{n,k}}|\varphi_{n.\mathrm{II}}(-k)\rangle. \tag{4.3.8}$$

We now try to construct the polarization for only one of the two labels $s = \mathrm{I}$ or II

$$\mathsf{P}^s = -\frac{1}{2\pi}\int_{-\pi}^{\pi} dk\, \mathcal{A}^s(k) \qquad \text{with} \qquad \mathcal{A}^s(k) = \mathrm{i}\sum_{n \text{ filled}} \langle\varphi_{n.s}(k)|\partial_k|\varphi_{n.s}(k)\rangle. \tag{4.3.9}$$

It is clear that $\mathsf{P} = \mathsf{P}^{\mathrm{I}} + \mathsf{P}^{\mathrm{II}}$ will vanish. However, the same must not hold for the *time reversal polarization*

$$\mathsf{P}^{\mathcal{T}} = \mathsf{P}^{\mathrm{I}} - \mathsf{P}^{\mathrm{II}}. \tag{4.3.10}$$

The problem is, that we assigned the labels I and II. It is not a priori clear if this can be done in a gauge invariant fashion. In particular, the Slater determinant of a band insulator with $2n$ filled bands has a $SU(2n)$ symmetry, as basis changes of filled states do not affect the total wave function. With our procedure we explicitly broke this $SU(2n)$ symmetry. There is a way however, to formulate the same $\mathcal{T}$-polarization $\mathsf{P}^{\mathcal{T}}$ in a way that does not rely on a specific labeling of the Kramers pairs. This can be achieved by the use of the so-called *sewing matrix* [6]

$$B_{mn}(k) = \langle\varphi_m(-k)|\mathcal{T}|\varphi_n(k)\rangle. \tag{4.3.11}$$

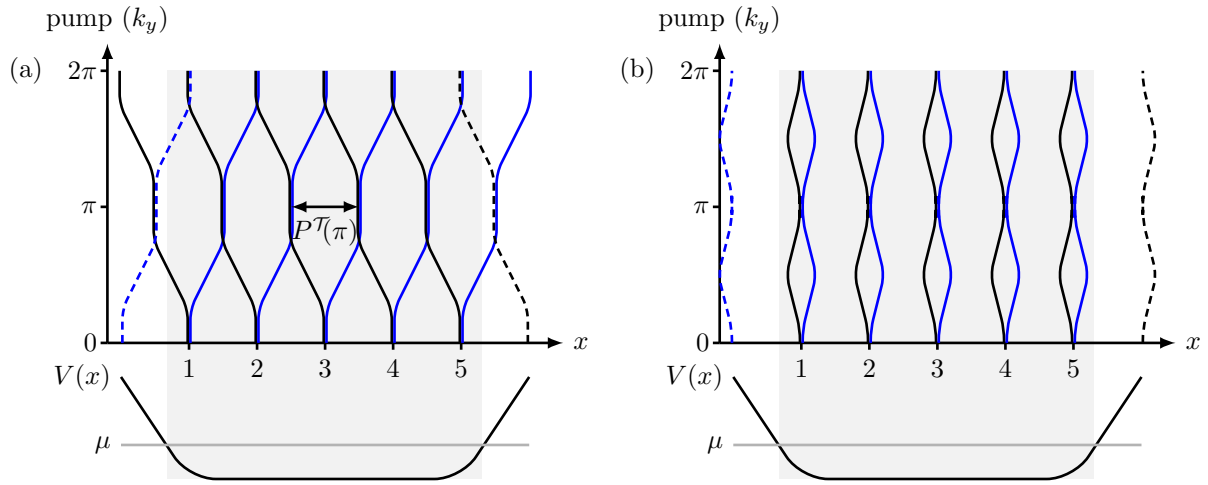

Figure 4.9: (a) Pumping of time reversal polarization in a topologically non-trivial state. (b) Pumping of time reversal polarization in a trivial state.

$B(k)$ has the following properties: (i) it is unitary, and (ii) it is anti-symmetric, i.e., $B^{\mathrm{T}}(k) = -B(k)$, only if k is a TRIM. Using this matrix one can show that

$$\mathsf{P}^{\mathcal{T}} = \frac{1}{\mathrm{i}\pi} \log \left[\frac{\sqrt{\det B(\pi)}}{\mathrm{Pf}\, B(\pi)} \frac{\mathrm{Pf}\, B(0)}{\sqrt{\det B(0)}} \right]. \tag{4.3.12}$$

This expression is manifestly invariant under $SU(2n)$ rotations within the filled bands. Moreover, it only depends on the two TRIMs $k = 0, \pi$, and it is defined modulo two.

The Pfaffian $\mathrm{Pf}\, B(k)$ of a $2n \times 2n$ anti-symmetric matrix matrix B is defined as

$$\mathrm{Pf}\, B = \frac{1}{2^n n!} \sum_{\sigma \in S_{2n}} \mathrm{sign}(\sigma) \prod_{i=1}^{n} b_{\sigma(2i-1),\sigma(1i)} \tag{4.3.13}$$

with the property

$$\mathrm{Pf}^2\, B = \det B. \tag{4.3.14}$$

Let us now see how we can describe changes in the time-reversal polarization under the influence of an additional parameter k_y. Written as in (4.3.12), it is only defined for $k_y = 0, \pi, 2\pi$, i.e, at TRIMs. In Fig. 4.9 we illustrate what we can expect from such a smooth change. We start at $k_y = 0$. If we now change k_y slowly, we know that due to TRI, we cannot build up a charge polarization. However, the Wannier centers of two Kramers pairs will evolve in opposite direction. At $k_y = \pi$, we can check how far these centers evolved away from each other. As $\mathsf{P}^{\mathcal{T}}$ is well defined and equal to 0 or 1 we have two options: (i) Each Wannier center meets up with one coming from a neighboring site [Fig. 4.9(a)]. This gives rise to $\mathsf{P}^{\mathcal{T}}(k_y = \pi) = 1$ and this effect is called *pair switching*. (ii) The centers fall back onto each other again [Fig. 4.9(b)], resulting in $\mathsf{P}^{\mathcal{T}}(k_y = \pi) = 0$.

Let us further assume that we have a smooth confining potential $V(x)$ in x-direction. As in the case of the quantum Hall effect, we see how states can be pushed up-hill or pulled down-hill as a function of k_y. However, as opposed to the quantum Hall effect, we have here the situation that on each edge we have both a state coming down in energy as well as one climbing up! From that we conclude that if we have pair-switching, we expect two counter-propagating edge states on *both sides of the sample*. The same observation can be made by looking at the Wilson loop spectrum as described in the last chapter.

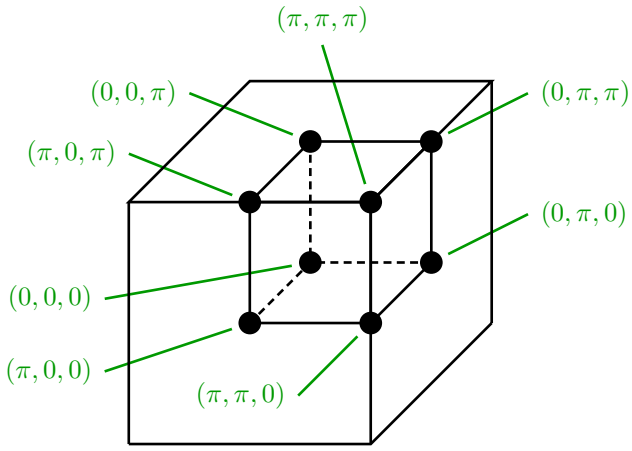

Figure 4.10: TRIMs of the three-dimensional Brillouin zone.

We can now construct a topological index for the two-dimensional system: If the $\mathcal{T}$-polarization at $k_y = 0$ and $k_y = \pi$ differ by one, we expect an odd number of pairs of edge states. Hence, we define

$$\nu = \prod_{l=1}^{4} \frac{\sqrt{\det B(\mathbf{\Lambda}_l)}}{\mathrm{Pf}\, B(\mathbf{\Lambda}_l)} \in \mathbb{Z}_2 \qquad \text{with} \qquad \mathbf{\Lambda}_l \ : \ \text{TRIM}. \tag{4.3.15}$$

4.3.3 Three dimensional topological insulators

The above formulation immediately suggests a three-dimensional generalization of the $\mathbb{Z}_2$ index

$$\nu_s = \prod_{l=1}^{8} \frac{\sqrt{\det B(\mathbf{\Lambda}_l)}}{\mathrm{Pf}\, B(\mathbf{\Lambda}_l)} \in \mathbb{Z}_2 \qquad \text{with} \qquad \mathbf{\Lambda}_l \ : \ \text{TRIM}, \tag{4.3.16}$$

where now the product runs over all eight TRIMs of the three-dimensional Brillouin zone shown in Fig. 4.10. This index is called the *strong* topological index. Additionally, one can think of a three-dimensional system to be made out of planes of two-dimensional topological insulators. In Fig. 4.11 we show how one can attribute a *weak* topological index (ν_x, ν_y, ν_z) corresponding to the stacking directions.
According to our reasoning above, when we cut the system perpendicular to the direction defined by the weak index, we expect *two Dirac cones* on the resulting surface (why?). However, if we have a strong topological index, there is a single Dirac cone irrespective of the way we terminate the bulk system. To wrap up, we mention that one usually gathers the indices to

$$\boldsymbol{\nu} = (\nu_s; \nu_x, \nu_y, \nu_z). \tag{4.3.17}$$

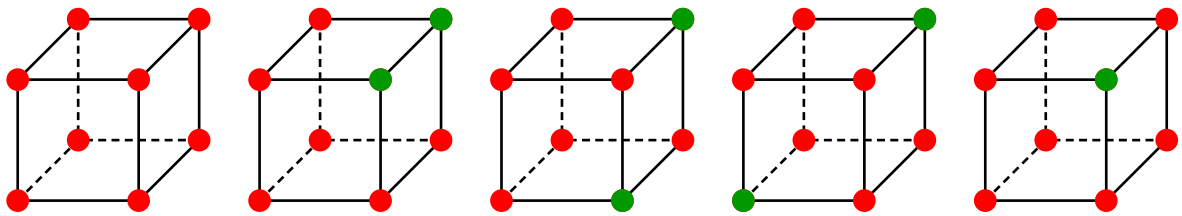

Figure 4.11: Stacking directions of 2D topological insulators.

References

1. Bernevig, B. A., Hughes, T. L. & Zhang, S.-C. "Quantum Spin Hall Effect and Topological Phase Transition in HgTe Quantum Wells". *Science* **15,** 1757. http://dx.doi.org/10.1126/science.1133734 (2006).
2. Haldane, F. D. M. "Model for a Quantum Hall Effect without Landau Levels: Condensed-Matter Realization of the "Parity Anomaly"". *Phys. Rev. Lett.* **61,** 2015. http://link.aps.org/doi/10.1103/PhysRevLett.61.2015 (1988).
3. Kane, C. L. & Mele, E. J. "Quantum Spin Hall Effect in Graphene". *Phys. Rev. Lett.* **95,** 226801. http://link.aps.org/abstract/PRL/v95/e226801 (2005).
4. Sheng, D. N., Weng, Z. Y., Scheng, L. & Haldane, F. D. M. "Quantum Spin-Hall Effect and Topologically Invariant Chern Numbers". *Phys. Rev. Lett.* **97,** 036808. http://dx.doi.org/10.1103/PhysRevLett.97.036808 (2006).
5. Prodan, E. "Robustness of the spin-Chern number". *Phys. Rev. B* **80,** 125327. http://dx.doi.org/10.1103/PhysRevB.80.125327 (2009).
6. Bernevig, B. A. & Hughes, T. L. *Topological insulators and superconductors* (Princeton University Press, 2013).

Chapter 5

One-dimensional Topological Superconductors

Learning goals

- We understand the Bogoliubov-de-Gennes representation of a mean-field superconducting Hamiltonian and its relation to a Majorana fermion representation.
- We know one-dimensional topological superconductors, their topological invariant, boundary modes and topological classification.
- We understand how interactions reduce the topological classification from $\mathbb{Z}$ to $\mathbb{Z}_8$ in one-dimensional topological superconductors.

- A. Kitaev, Phys.-Usp. **44**, 131 (2001)
- L. Fidkowski and A. Kitaev, Phys. Rev. B **83**, 075103 (2011)

5.1 Warmup for superconductivity: 0D superconductors

As a smooth start in the world of superconducting Bogoluibov-de-Gennes mean-field Hamiltonians, we consider impurity sites in s and p-wave superconductors and show that these can experience a transition at which the parity of the many-body ground state changes. To this end, we consider the simplest noninteracting model of a single site and a pair of sites, respectively, but work in its many-body Hilbert space.
In superconductors without further symmetries (which applies to chiral p-wave superconductors) the $\mathbb{Z}_2$ topological index of a 1D superconductor denotes the change in fermion parity of the ground-state as a flux π is inserted through a system with periodic boundary conditions. This parity change can even be observed in zero-dimensional models of isolated impurities and provides basic intuition whether and how a 1D chain of scalar impurities has the potential to undergo a topological phase transition. Here, we discuss this minimal model for a parity changing transition for one and two sites populated with spinless fermions and for a single site populated with spinful fermions.

5.1.1 Spinless fermions

A single spinless fermion cannot exhibit superconducting pairing. Irrespective of that, we see that an on-site chemical potential μ can change the fermion parity P of the ground state (i.e., whether there is an odd or an even number of electrons in the ground state), for the latter is

given by sgnμ. In the occupation basis $(|0\rangle, |1\rangle)$, the Hamiltonian reads

$$H = \begin{pmatrix} 0 & 0 \\ 0 & -\mu \end{pmatrix}. \tag{5.1.1}$$

Any other terms in the Hamiltonian violate the conservation of fermion parity. The ground state is given by $|0\rangle$ and $|1\rangle$ for $\mu < 0$ and $\mu > 0$, respectively, with opposite parity.
The minimal extension to this model that accounts for superconducting pairing includes two sites with spinless fermions. In this case, we can have triplet – but not singlet – superconducting pairing. In the basis $(|0,0\rangle, |1,0\rangle, |0,1\rangle, |1,1\rangle)$, the Hamiltonian reads

$$H = \begin{pmatrix} 0 & 0 & 0 & \Delta \\ 0 & -\mu & t & 0 \\ 0 & t & -\mu & 0 \\ \Delta^* & 0 & 0 & -2\mu \end{pmatrix}, \tag{5.1.2}$$

where t is the hopping integral between the two sites. The energies are

$$\varepsilon^{\text{even}} = \pm\sqrt{|\Delta|^2 + \mu^2} - \mu, \qquad \varepsilon^{\text{odd}} = \pm t - \mu. \tag{5.1.3}$$

The system does not conserve the fermion number anymore, but it conserves its *parity*. Whenever $|t| > |\Delta|$ (commonly referred to as the weak pairing phase), we can induce a parity change of the ground state (protected crossing) by changing the chemical potential at

$$\mu^2 = t^2 - |\Delta|^2. \tag{5.1.4}$$

For smaller $|\mu|$, the ground state has odd parity, for larger $|\mu|$, it has even parity. This is in line with the behavior of bound states of two impurities in p-wave superconductors: They exhibit a protected crossing in the bound state spectrum. The presence of this protected crossing implies the existence of sub-gap Shiba states in the energy spectrum: since a protected crossing has to occur upon varying μ, which could be considered as modeling the scalar impurity strength, it must be that sub-gap $E < |\Delta|$ states exist.

5.1.2 Spinful fermions

A single site with a spinful fermion degree of freedom will allow for singlet superconducting pairing Δ. We also apply a Zeeman field B in the direction of the spin-quantization axis. In the basis $(|0,0\rangle, |\uparrow,0\rangle, |0,\downarrow\rangle, |\uparrow,\downarrow\rangle)$, the Hamiltonian reads

$$H = \begin{pmatrix} 0 & 0 & 0 & \Delta \\ 0 & -\mu + B & 0 & 0 \\ 0 & 0 & -\mu - B & 0 \\ \Delta^* & 0 & 0 & -2\mu \end{pmatrix}. \tag{5.1.5}$$

The energies are

$$\varepsilon^{\text{even}} = \pm\sqrt{|\Delta|^2 + \mu^2} - \mu, \qquad \varepsilon^{\text{odd}} = \pm B - \mu, \tag{5.1.6}$$

and the eigenstates

$$\begin{aligned} |\text{even}, \pm\rangle &= \frac{1}{N_\pm}\left[\left(\mu \pm \sqrt{|\Delta|^2 + \mu^2}\right)|0,0\rangle + \Delta^*|\uparrow,\downarrow\rangle\right], \\ |\text{odd}, -\rangle &= |0,\downarrow\rangle, \qquad |\text{odd}, +\rangle = |\uparrow,0\rangle, \end{aligned} \tag{5.1.7}$$

where $N_\pm$ is an appropriate normalization.

We observe a level crossing protected by parity symmetry at

$$B^2 = |\Delta|^2 + \mu^2. \tag{5.1.8}$$

For smaller $|B|$, the ground state has even parity, for larger $|B|$, it has odd parity. This is congruent with the behavior of a ferromagnetic Shiba chain on an s-wave superconductor. This model also indicates that a density impurity cannot induce a subgap bound state deep in an s-wave superconducting gap, because μ does not induce any phase transition in this model for $B = 0$.

5.1.3 Bogoliubov-de-Gennes formulation and Nambu spinors

Writing out Hamiltonian (5.1.5) in second quantization,

$$H = (B-\mu)c_\uparrow^\dagger c_\uparrow + (-B-\mu)c_\downarrow^\dagger c_\downarrow + \Delta c_\uparrow^\dagger c_\downarrow^\dagger + \Delta^* c_\downarrow c_\uparrow \tag{5.1.9}$$

we find that it cannot be written as a noninteracting Bloch Hamiltonian anymore, but it is still quadratic in the fermion operators. For that reason we can write it as

$$H = \frac{1}{2}\Psi^\dagger h \Psi, \qquad h = \begin{pmatrix} B-\mu & 0 & 0 & \Delta \\ 0 & -B-\mu & -\Delta & 0 \\ 0 & -\Delta^* & -B+\mu & 0 \\ \Delta^* & 0 & 0 & B+\mu \end{pmatrix}, \tag{5.1.10}$$

where $\Psi = (c_\uparrow, c_\downarrow, c_\uparrow^\dagger, c_\downarrow^\dagger)^\mathsf{T}$. This description allows us to reduce the problem to the study of a matrix h (the Bogoliubov-de-Gennes, BdG, Hamiltonian), but it introduces a redundancy in this matrix in the form of an always present PHS

$$\mathcal{P} = U_\mathcal{P}\mathcal{K}, \qquad U_\mathcal{P} = \tau_1 \otimes \sigma_0, \qquad \mathcal{P}h\mathcal{P}^{-1} = -h, \tag{5.1.11}$$

where τ_i, $i = 1, 2, 3$ are the Pauli matrices acting on particle-hole space. Notice that $\mathcal{P}^2 = +1$. Diagonalizing the matrix h yields

$$\begin{aligned} a_{-1} &= \frac{1}{N_+}(0, \mu + \sqrt{\mu^2 + |\Delta|^2}, \Delta^*, 0)^\mathsf{T}, \\ a_1 &= \frac{1}{N_-}(-\mu + \sqrt{\mu^2 + |\Delta|^2}, 0, 0, \Delta^*)^\mathsf{T}, \\ a_{-2} &= \frac{1}{N_+}(-\mu - \sqrt{\mu^2 + |\Delta|^2}, 0, 0, \Delta^*)^\mathsf{T}, \\ a_2 &= \frac{1}{N_-}(0, \mu - \sqrt{\mu^2 + |\Delta|^2}, \Delta^*, 0)^\mathsf{T} \end{aligned} \tag{5.1.12}$$

with eigenvalues $E_1 = -E_{-1} = B + \sqrt{|\Delta|^2 + \mu^2}$, $E_2 = -E_{-2} = -B + \sqrt{|\Delta|^2 + \mu^2}$ and the appropriate normalizations N_+ and N_-. Let un consider the superconducting limit where the energies are ordered for $B > 0$ like $E_{-1} \leq E_{-2} < E_2 \leq E_1$. We can now define the operators

$$\begin{aligned} \gamma_{-1} &:= a_{-1}^*\Psi^\dagger = \frac{1}{N_+}\left[\left(\mu + \sqrt{\mu^2 + |\Delta|^2}\right)c_\downarrow^\dagger + \Delta c_\uparrow\right], \\ \gamma_1 &:= a_1^*\Psi^\dagger = \frac{1}{N_-}\left[\left(-\mu + \sqrt{\mu^2 + |\Delta|^2}\right)c_\uparrow^\dagger + \Delta c_\downarrow\right], \\ \gamma_{-2} &:= a_{-2}^*\Psi^\dagger = \frac{1}{N_+}\left[\left(-\mu - \sqrt{\mu^2 + |\Delta|^2}\right)c_\uparrow^\dagger + \Delta c_\downarrow\right], \\ \gamma_2 &:= a_2^*\Psi^\dagger = \frac{1}{N_-}\left[\left(\mu - \sqrt{\mu^2 + |\Delta|^2}\right)c_\downarrow^\dagger + \Delta c_\uparrow\right]. \end{aligned} \tag{5.1.13}$$

We check that

$$\gamma_{-1}|\text{even},-\rangle = 0, \qquad \gamma_{-2}|\text{even},-\rangle = 0, \tag{5.1.14}$$

i.e., the ground state is annihilated by the negative energy operators. This defines the BCS ground state. Furthermore,

$$\gamma_1|\text{even},-\rangle = -|\text{odd},+\rangle, \qquad \gamma_2|\text{even},-\rangle = |\text{odd},-\rangle, \qquad \gamma_1\gamma_2|\text{even},-\rangle \propto |\text{even},+\rangle, \tag{5.1.15}$$

that is, we can reach all excited states by applying the respective positive energy operators to the ground state.
In the limit where B dominates, for $B > 0$ the energies are ordered as $E_{-1} \leq E_2 < E_{-2} \leq E_1$. In this case, the ground state $|\text{odd},-\rangle = |0,\downarrow\rangle$ is annihilated by the negative energy operators γ_{-1} and γ_2 and excited states can be constructed from this ground state similar to the above.
A more general translational invariant system with Hamiltonian

$$H = \sum_{\boldsymbol{k}} \sum_{s,s'=\uparrow,\downarrow} \left[c^\dagger_{s,\boldsymbol{k}} \left(h_{0,\boldsymbol{k}}\right)_{s,s'} c_{s',\boldsymbol{k}} + c^\dagger_{s,\boldsymbol{k}} \left(\Delta_{\boldsymbol{k}}\right)_{s,s'} c^\dagger_{s',-\boldsymbol{k}} + \text{h.c.} \right] \tag{5.1.16}$$

can be recast as

$$H = \sum_{\boldsymbol{k}} \Psi^\dagger_{\boldsymbol{k}} h_{\boldsymbol{k}} \Psi_{\boldsymbol{k}}, \qquad h_{\text{k}} = \begin{pmatrix} h_{0,\boldsymbol{k}} & \Delta_{\boldsymbol{k}} \\ \Delta^\dagger_{\boldsymbol{k}} & -h^*_{0,-\boldsymbol{k}} \end{pmatrix}, \tag{5.1.17}$$

where $\Psi_{\boldsymbol{k}} = (c_{\uparrow,\boldsymbol{k}}, c_{\downarrow,\boldsymbol{k}}, c^\dagger_{\uparrow,-\boldsymbol{k}}, c^\dagger_{\downarrow,-\boldsymbol{k}})^{\mathsf{T}}$ and $h_{0,\boldsymbol{k}}$ as well as $\Delta_{\boldsymbol{k}}$ are 2×2 matrices. The BCS ground state is then again defined by the unique state that is annihilated by all operators $\gamma_{-1,\boldsymbol{k}}$ and $\gamma_{-2,\boldsymbol{k}}$ with negative energies and excited states are constructed by applying all positive energy operators to it.

5.2 The one-dimensional p-wave superconductor

In the Su-Schrieffer-Heeger model, particle-hole symmetry (and with it the chiral symmetry) is in some sense fine-tuned, as it is lost if generic longer-range hoppings are considered. In superconductors, particle-hole symmetry arises more naturally as a symmetry that is inherent in the redundant description of mean-field Bogoliubov-de-Gennes Hamiltonians.
Before we consider a simplified microscopic model, let us name a set of possible physical ingredients that would be required to realize such a model. They are

- a quasi-1D electronic system
- Rashba spin-orbit coupling
- Zeeman coupling
- proximity-induced s-wave superconductivity.

When corroborating in the correct way, these ingredients yield a 1D system of effectively spinless electrons that are superconducting. A simple first quantized Hamiltonian for the 1D wire with Rashba spin-orbit coupling α and Zeeman coupling B is given by

$$H_{\text{wire}} = \frac{k^2}{2m}\sigma_0 + \alpha k \sigma_y + B\sigma_x - \mu. \tag{5.2.1}$$

The spectrum $\varepsilon_{k,\pm} = \frac{k^2}{2m} - \mu \pm \sqrt{(\alpha k)^2 + B^2}$ has only two Fermi points $k_\pm$ (instead of 4) if $|B| > |\mu|$ and the spin polarization of the two Fermi points is almost opposite in the limit of small B. This means that the two states at the Fermi points are almost Kramers pairs and hence conventional Cooper pairs can effectively couple to this system, gapping out the Fermi points.

5.2.1 The Kitaev wire

Here, we want to consider the simplest model for a topological superconductor that has been studied by Kitaev. The setup is again a 1D chain with one orbital for spinless fermion on each site (the spinless nature is essentially motivated by the fact that at the Fermi points we find eigenstates of a definite spin polarization). Superconductivity is encoded in pairing terms $c_i^\dagger c_{i+1}^\dagger$ that do not conserve particle number. The Hamiltonian is given by

$$H = \sum_{i=1}^{N} \left[-t \left(c_i^\dagger c_{i+1} + c_{i+1}^\dagger c_i \right) - \mu c_i^\dagger c_i + \Delta c_{i+1}^\dagger c_i^\dagger + \Delta^* c_i c_{i+1} \right]. \tag{5.2.2}$$

Here, μ is the chemical potential and Δ is the superconducting order parameter, which we will decompose into its amplitude $|\Delta|$ and complex phase ϑ, i.e., $\Delta = |\Delta| e^{\mathrm{i}\vartheta}$.
The fermionic operators $c_i^\dagger$ obey the algebra

$$\{c_i^\dagger, c_j\} = \delta_{i,j}, \tag{5.2.3}$$

with all other anticommutators vanishing. We can chose to trade the operators $c_i^\dagger$ and c_i on every site i for two other operators a_i and b_i that are defined by

$$a_i = e^{-\mathrm{i}\vartheta/2} c_i + e^{\mathrm{i}\vartheta/2} c_i^\dagger, \qquad b_i = \frac{1}{\mathrm{i}} \left(e^{-\mathrm{i}\vartheta/2} c_i - e^{\mathrm{i}\vartheta/2} c_i^\dagger \right). \tag{5.2.4}$$

These so-called Majorana operators obey the algebra

$$\{a_i, a_j\} = \{b_i, b_j\} = 2\delta_{ij}, \qquad \{a_i, b_j\} = 0 \qquad \forall i, j. \tag{5.2.5}$$

In particular, they square to 1

$$a_i^2 = b_i^2 = 1, \tag{5.2.6}$$

and are self-conjugate

$$a_i^\dagger = a_i, \qquad b_i^\dagger = b_i. \tag{5.2.7}$$

In fact, we can always break up a complex fermion operator on a lattice site into its real and imaginary Majorana components though it may not always be a useful representation. As an aside, note that the Majorana anti-commutation relation in Eq. (5.2.5) is the same as that of the generators of a Clifford algebra where the generators all square to +1. Thus, mathematically one can think of the operators a_i (or b_i) as matrices forming by themselves the representation of Clifford algebra generators.
When rewritten in the Majorana operators, Hamiltonian (5.2.2) takes (up to a constant) the form

$$H = \frac{\mathrm{i}}{2} \sum_{i=1}^{N} \left[-\mu a_i \, b_i + (t + |\Delta|) b_i \, a_{i+1} + (-t + |\Delta|) a_i \, b_{i+1} \right]. \tag{5.2.8}$$

After imposing periodic boundary conditions, it is again convenient to study the system in momentum space. When defining the Fourier transform of the Majorana operators $a_i = \sum_i e^{\mathrm{i}ki} a_k$ we note that the the self-conjugate property (5.2.7) that is local in position space translates into $a_k^\dagger = a_{-k}$ in momentum space (and likewise for the b_k). The momentum space representation of the Hamiltonian is

$$H = \sum_{k \in \mathrm{BZ}} \sum_{\alpha = A,B} (a_k \;\; b_k) \, h_k \begin{pmatrix} a_{-k} \\ b_{-k} \end{pmatrix} \tag{5.2.9a}$$

$$h_k = \begin{pmatrix} 0 & -\frac{\mathrm{i}\mu}{2} + \mathrm{i}t \cos k + |\Delta| \sin k \\ \frac{\mathrm{i}\mu}{2} - \mathrm{i}t \cos k + |\Delta| \sin k & 0 \end{pmatrix} \tag{5.2.9b}$$

$$= \sigma_x |\Delta| \sin k + \sigma_y \left(\frac{\mu}{2} - t \cos k \right), \tag{5.2.9c}$$

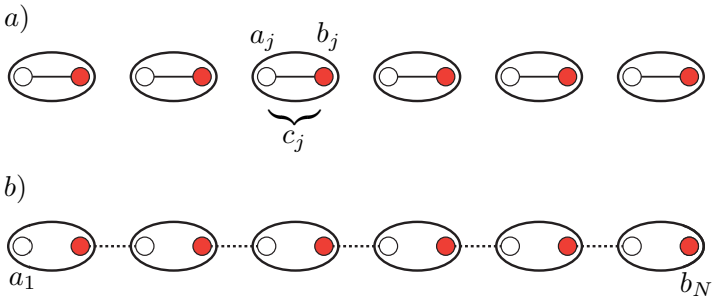

Figure 5.1: Schematic illustration of the lattice p-wave superconductor Hamiltonian in the (a) trivial limit (b) non-trivial limit. The white (empty) and red (filled) circles represent the Majorana fermions making up each physical site (oval). The fermion operator on each physical site (c_j) is split up into two Majorana operators (a_j and b_j). In the non-trivial phase the unpaired Majorana fermion states at the end of the chain are labelled with a_1 and b_N. These are the states which are continuously connected to the zero-modes in the non-trivial topological superconductor phase.

While this Bloch Hamiltonian is formally very similar to that of the SSH model, we have to keep in mind that it acts on entirely different single-particle degrees of freedom, namely in the space of Majorana operators instead of complex fermionic operators. As with the case of the Su-Schrieffer-Heeger model, the Hamiltonian (5.2.9) has a time-reversal symmetry $\mathcal{T} = \sigma_z\mathcal{K}$ and a particle-hole symmetry $P = \mathcal{K}$ which combine to the chiral symmetry $C = \sigma_z$. For the topological properties that we first explore, only the particle-hole symmetry is crucial. We will see that the model has a $\mathbb{Z}_2$ topological classification in this case. We will then take the TRS as a real symmetry in addition, in which case we can again define a winding number, analogous to the SSH model. This results in a $\mathbb{Z}$ topological classification if only Hamiltonians bilinear in the Majorana operators are considered (so-called noninteracting systems).
To determine its topological phases, we notice that Hamiltonian (5.2.9) is gapped except for $|t| = |\mu/2|$. We specialize again on convenient parameter values on either side of this potential topological phase transition

- $\mu = 0$, $|\Delta| = t$: The Bloch matrix h_k takes exactly the same form as that of the SSH model for the parameter choice $\delta = +1$. We conclude that the Hamiltonian (5.2.9) is in a topological phase. The Hamiltonian reduces to

$$H = \mathrm{i}t \sum_j b_j a_{j+1}. \tag{5.2.10}$$

  A pictorial representation of this Hamiltonian is shown in Fig. 5.1 b). With open boundary conditions it is clear that the Majorana operators a_1 and b_N are not coupled to the rest of the chain and are 'unpaired'. In this limit the existence of two Majorana zero modes localized on the ends of the chain is manifest.

- $\Delta = t = 0$, $\mu < 0$: This is the topologically trivial phase, since the Hamiltonian is independent of k so that that the winding number vanishes necessarily. In this case the Hamiltonian reduces to

$$H = -\mu \frac{\mathrm{i}}{2} \sum_j a_j b_j. \tag{5.2.11}$$

  In its ground state the Majorana operators on each physical site are coupled but the Majorana operators between each physical site are decoupled. In terms of the physical

complex fermions, it is the ground state with either all sites occupied or all sites empty. A representation of this Hamiltonian is shown in Fig. 5.1 a). The Hamiltonian in the physical-site basis is in the atomic limit, which is another way to see that the ground state is trivial. If the chain has open boundary conditions there will be no low-energy states on the end of the chain if the boundaries are cut between *physical* sites. That is, we are not allowed to pick boundary conditions where a physical complex fermionic site is cut in half.

These two limits give the simplest representations of the trivial and non-trivial phases. By tuning away from these limits the Hamiltonian will have some mixture of couplings between Majorana operators on the same physical site, and operators between physical sites. However, since the two Majorana modes are localized at different ends of a gapped chain, the coupling between them will be exponentially small in the length of the wire and they will remain at zero energy. In fact, in the non-trivial phase the zero modes will not be destroyed until the bulk gap closes at a critical point.

It is important to note that these zero modes count to a different many-body ground state degeneracy than the end modes of the Su-Schrieffer-Heeger model. The difference is rooted in the fact that one cannot build a fermionic Fock space out of an odd number of Majorana modes, because they are linear combinations of particles and holes. Rather, we can define a *single* fermionic operator out of *both* Majorana end modes a_1 and b_N as $c^\dagger := a_1 + \mathrm{i}b_N$. The Hilbert space we can build out of a_1 and b_N is hence inherently nonlocal. This *nonlocal* state can be either occupied or empty giving rise to a two-fold degenerate ground state of the chain with two open ends. (In contrast, the topological Su-Schrieffer-Heeger chain has a four-fold degenerate ground state with two open ends, because it has one fermionic mode on each end.) The Majorana chain thus displays a different form of fractionalization than the Su-Schrieffer-Heeger chain. For the latter the topological end modes carry fractional charge. In the Majorana chain, the end modes are a fractionalization of a fermionic mode into a superposition of particle and hole (and have no well defined charge anymore), but the states $|0\rangle$ (with $c|0\rangle = 0$) and $c^\dagger|0\rangle$ do have distinct fermion parity. The nonlocal fermionic mode formed by two Majorana end modes is envisioned to work as a qubit (a quantum-mechanical two-level system) that stores quantum information (its state) in a way that is protected against local noise and decoherence.

5.2.2 Topological classification

If we disregard the time-reversal symmetry, and two parallel wires are considered, we can gap out the two end states by a term

$$\mathrm{i}a_1 a_1', \tag{5.2.12}$$

where the primed and unprimed operator are the end states of the first and the second wire, respectively. This implies that, while a single end state is protected, a pair of them is not. The topological classification with only PHS is $\mathbb{Z}_2$. Let us now discuss the topological index for this case. Intuitively, when we consider pairing between opposite momentum eigenstates, the topological invariant should distinguish the two cases where an even number of pairs of Fermi points was present before the pairing was introduced from the situation where an odd number of pairs of Fermi points was present. The former would be topologically trivial, while the latter would be the non-trivial superconductor. The points $k = 0$ and $k = \pi$ are invariant under PHS and it is sufficient to determine the parity of the number of occupied bands at $k = 0$ and $k = \pi$ to deduce the parity of pairs of Fermi points. If the product of the parities of occupied bands is odd, there is an odd number of Fermi points. It is not possible to deduce from the BdG Hamiltonian the parity of the number of occupied bands without particle-hole doubling. In a sense, we would need to take the square root of it in a controlled way and then compute the sign of the square root. From Hamiltonian (5.2.9) we make two observations

1. h_0 and h_π have the form i times an antisymmetric matrix

2. the change of the sign of the upper right (or lower left) element between $k = 0$ and $k = \pi$ is what relates to the change in parity between the two points.

For a general Majorana Hamiltonian,

$$H = \frac{\mathrm{i}}{2} \sum_{r,r'} \gamma_r^{\mathsf{T}} A_{r,r'} \gamma_{r'} \tag{5.2.13}$$

these observations can be generalized by observing that

$$H = \frac{\mathrm{i}}{2} \sum_{k} \tilde{\gamma}_{-k}^{\mathsf{T}} \tilde{A}(k) \tilde{\gamma}_k, \tag{5.2.14}$$

where we have defined

$$\tilde{A}(k) = \sum_{R} e^{\mathrm{i}kR} A_R \tag{5.2.15}$$

assumed translational invariance $A_{r,r'} = A_{r-r'} = A_R$. Since $A_{r,r'}$ is an antisymmetric matrix, $\tilde{A}(k)$ are also antisymmetric for $k = 0, \pi$. For even dimensional antisymmetric matrices, the Pfaffian

$$\mathrm{Pf}(A) := \frac{1}{2^n n!} \epsilon_{i_1,i_2,\cdots,i_{2n}} A_{i_1,i_2} A_{i_3,i_4} \cdots A_{i_{2n-1},i_{2n}}, \tag{5.2.16}$$

is a way of taking the square root of the determinant. The topological $\mathbb{Z}_2$ invariant is given by

$$\nu = \mathrm{sgn} \left\{ \mathrm{Pf}[\tilde{A}(0)] \mathrm{Pf}[\tilde{A}(\pi)] \right\} = \pm 1. \tag{5.2.17}$$

If translational symmetry is not present, this generalizes to

$$\nu = \mathrm{sgn}\, \mathrm{Pf}(A). \tag{5.2.18}$$

If we also insist on the presence of TRS, the chiral symmetry guarantees that the winding number is a well-defined topological invariant similar to the case of the SSH model yielding a $\mathbb{Z}$ topological classification if only bilinear (noninteracting) Hamiltonians are considered. For interacting Hamiltonians, something more interesting happens, as we explore in the next section.

5.2.3 Reduction of the classification by interactions: $\mathbb{Z} \to \mathbb{Z}_8$

When time-reversal symmetry $\mathcal{T} = \mathcal{K}$ is present, the model considered in Sec. 5.2 has a noninteracting $\mathbb{Z}$ topological characterization. We want to explore how interactions alter this classification, following a calculation by Fidkowski and Kitaev. To this end, we consider a collection of n identical 1D topological Majorana chains and only consider their Majorana end modes on one end, which we denote by $a_1, \cdots, a_n$. We will take the point of view that if we can gap the edge, we can continue the bulk to a trivial state (insulator). This is not entirely a correct point of view in general (see 2D topologically ordered states such as the toric code discussed in the next Section), but works for our purposes. Given some integer n, we ask whether we can couple the Majorana modes locally on one end such that no gapless degrees of freedom are left on that end and the ground state with open boundary conditions becomes singly degenerate. We only allow couplings that respect time-reversal symmetry. Let us first derive the action of $\mathcal{T}$ on the Majorana modes. The complex fermion operators are left invariant under time-reversal $\mathcal{T} c \mathcal{T}^{-1} = c$. Hence,

$$\mathcal{T}(a + \mathrm{i}b)\mathcal{T}^{-1} = \mathcal{T} a \mathcal{T}^{-1} - \mathrm{i} \mathcal{T} b \mathcal{T}^{-1} \stackrel{!}{=} a + \mathrm{i}b \quad \Rightarrow \quad \mathcal{T} a \mathcal{T}^{-1} = a, \qquad \mathcal{T} b \mathcal{T}^{-1} = -b. \tag{5.2.19}$$

Thus, when acting on the modes localized on the left end of the wire (which transform like the a's), time-reversal symmetry leaves the Majorana operators invariant.

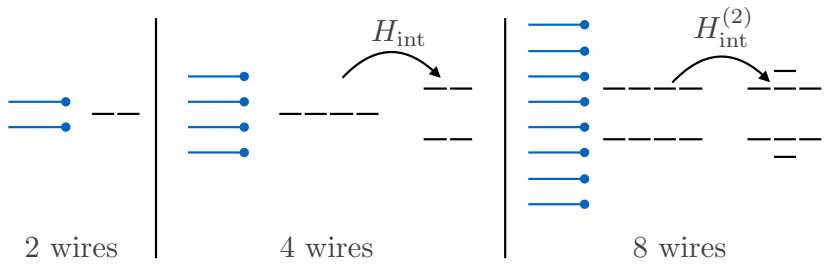

Figure 5.2: Schematic illustration of the many body energy levels for 2, 4, and 8 wires with Majorana end states as well as the (partial) lifting of their degeneracy that is in accordance with time-reversal symmetry.

One now subsequently considers the Majorana end modes from 2,4, and 8 wires and adds suitable perturbations to see whether a unique (many-body) ground state can be obtained while retaining time-reversal symmetry. One finds doubly-degenerate ground state for 2 as well as 4 wires (see exercise). (We note in passing that the ground state from the end states of 4 wires is even 4-fold degenerate if only non-interacting, i.e., Majorana-bilinear terms are allowed.) Going to 8 wires, one can construct an interaction term between them that has a unique ground state (see Fig. 5.2).
This unique ground state can be adiabatically continued to the atomic limit. In this way the noninteracting $\mathbb{Z}$ classification breaks down to $\mathbb{Z}_8$ if interactions are allowed.

References

1. Kitaev, A. Y. "Unpaired Majorana fermions in quantum wires". *Phys.-Usp.* **44,** 131 (2001).
2. Fidkowski, L. "Entanglement Spectrum of Topological Insulators and Superconductors". *Phys. Rev. Lett.* **104,** 130502. http://link.aps.org/doi/10.1103/PhysRevLett.104.130502 (2010).

Chapter 6

Two-dimensional Topological Superconductors

Learning goals

- We know the chiral p-wave superconductor in two dimensions and can argue why it has bound states in vortices.
- We understand the non-Abelian nature of vortex bound states.
- We can motivate Kitaev's 16-fold way classification for 2D superconductors.

- R. Jackiw and P. Rossi, Nuclear Phys. B **190**, 681-691 (1981)
- D. Ivanov, Phys. Rev. Lett. **86**, 268 (2001)
- A. Kitaev, Annals of Physics **321**, 2–111 (2006)

6.1 Lattice and continuum model and their topological invariant

After having studied topological superconductivity in 1D, we now want to move to 2D where we will find qualitatively new physics in the chiral p-wave superconductor. On the level of the noninteracting Bloch Hamiltonian, it is formally similar to a Chern insulator, but we will see that the physical degrees of freedom on which this Hamiltonian acts make the story much richer, bridging to theories with anyonic excitations and topological order. More precisely, the vortices of the chiral p-wave superconductor exhibit anyon excitations which have exotic non-Abelian statistics. For the system to be topologically ordered, these vortices should appear as emergent, dynamical excitations. This requires to treat the electromagnetic gauge field quantum-mechanically. (In fact, since the fermion number conservation is spontaneously broken down to the conservation of the fermion parity in the superconductor, the relevant gauge theory involves only a $\mathbb{Z}_2$ instead of a U(1) gauge field.) However, the topological properties that we want to discuss here can also be seen if we model the gauge field and vortices as static defects, rather than within a fluctuating $\mathbb{Z}_2$ gauge theory. This allows us to study a models very similar to the "noninteracting" topological superconductor in 1D and still expose the non-Abelian statistics. For pedagogy we will use both lattice and continuum models of the chiral superconductor. We begin with the lattice Hamiltonian defined on a square lattice

$$\begin{aligned} H = \sum_{m,n} \Big\{ -t \left(c^\dagger_{m+1,n} c_{m,n} + c^\dagger_{m,n+1} c_{m,n} + \text{h.c.} \right) - (\mu - 4t) c^\dagger_{m,n} c_{m,n} \\ + \left(\Delta c^\dagger_{m+1,n} c^\dagger_{m,n} + \mathrm{i}\Delta c^\dagger_{m,n+1} c^\dagger_{m,n} + \text{h.c.} \right) \Big\} . \end{aligned} \tag{6.1.1}$$

The fermion operators $c_{m,n}$ annihilate fermions on the lattice site (m, n) and we are considering spinless (or equivalently spin-polarized) fermions. We set the lattice constant $a = 1$ for simplicity.

The pairing amplitude is anisotropic and has an additional phase of i in the y-direction compared to the pairing in the x-direction. Because the pairing is not on-site, just as in the lattice version of the p-wave wire, the pairing terms will have momentum dependence. We can write this Hamiltonian in the Bogoliubov-deGennes form and, assuming that Δ is translationally invariant, can Fourier transform the lattice model to get

$$H_{\text{BdG}} = \frac{1}{2}\sum_{\boldsymbol{p}} \Psi^\dagger_{\boldsymbol{p}} \begin{pmatrix} \epsilon(p) & 2\mathrm{i}\Delta(\sin p_x + \mathrm{i}\sin p_y) \\ -2\mathrm{i}\Delta^*(\sin p_x - \mathrm{i}\sin p_y) & -\epsilon(p) \end{pmatrix} \Psi_{\boldsymbol{p}}, \tag{6.1.2}$$

where $\epsilon(p) = -2t(\cos p_x + \cos p_y) - (\mu - 4t)$ and $\Psi_{\boldsymbol{p}} = \begin{pmatrix} c_{\boldsymbol{p}} & c^\dagger_{-\boldsymbol{p}} \end{pmatrix}^{\mathsf{T}}$. For convenience we have shifted the chemical potential by the constant $4t$. As a quick aside we note that the model takes a simple familiar form in the continuum limit ($\boldsymbol{p} \to 0$):

$$H^{(\text{cont})}_{\text{BdG}} = \frac{1}{2}\sum_{\boldsymbol{p}} \Psi^\dagger_{\boldsymbol{p}} \begin{pmatrix} \frac{p^2}{2m} - \mu & 2\mathrm{i}\Delta(p_x + \mathrm{i}p_y) \\ -2\mathrm{i}\Delta^*(p_x - \mathrm{i}p_y) & -\frac{p^2}{2m} + \mu \end{pmatrix} \Psi_{\boldsymbol{p}} \tag{6.1.3}$$

where $m \equiv 1/2t$ and $p^2 = p_x^2 + p_y^2$. We see that the continuum limit has the characteristic $p_x + \mathrm{i}p_y$ chiral form for the pairing potential. The quasiparticle spectrum of $H^{(\text{cont})}_{\text{BdG}}$ is $E_\pm = \pm\sqrt{(p^2/2m - \mu)^2 + 4|\Delta|^2 p^2}$, which, with a nonvanishing pairing amplitude, is gapped across the entire BZ as long as $\mu \neq 0$. This is unlike some other types of p-wave pairing terms [e.g., $\Delta(p) = \Delta p_x$] which can have gapless *nodal* points or lines in the BZ for $\mu > 0$. In fact, nodal superconductors, having gapless quasiparticle spectra, are not topological superconductors by definition (i.e., a bulk excitation gap does not exist).

We recognize the form of $H^{(\text{cont})}_{\text{BdG}}$ as a massive 2D Dirac Hamiltonian, and indeed Eq. (6.1.1) is just a lattice Dirac Hamiltonian which is what we will consider first. In the first quantized notation, the single particle Hamiltonian for a superconductor is equivalent to that of an insulator with an additional particle-hole symmetry (It is thus placed in class D in the classification that we will introduce in the next lecture) and admits a $\mathbb{Z}$ topological classification in 2D. Thus, we can classify the eigenstates of Hamiltonian (6.1.1) by a Chern number – but due to the breaking of U(1) symmetry, the Chern number does not have the interpretation of Hall conductance. However, it is still a topological invariant.

We expect that H_{BdG} will exhibit several phases as a function of Δ and μ for a fixed $t > 0$. For simplicity let us set $t = 1/2$ and make a gauge transformation $c_{\boldsymbol{p}} \to e^{\mathrm{i}\vartheta/2} c_{\boldsymbol{p}}$, $c^\dagger_{\boldsymbol{p}} \to e^{-\mathrm{i}\vartheta/2} c^\dagger_{\boldsymbol{p}}$ where $\Delta = |\Delta| e^{i\vartheta}$. The Bloch Hamiltonian for the lattice superconductor is then

$$\mathcal{H}_{\text{BdG}}(\boldsymbol{p}) = (2 - \mu - \cos p_x - \cos p_y)\,\sigma_z - 2|\Delta|\sin p_x \sigma_y - 2|\Delta|\sin p_y \sigma_x, \tag{6.1.4}$$

where the σ_i, $i = x, y, z$, are the Pauli matrices in the particle/hole basis. Assuming $|\Delta| \neq 0$, this Hamiltonian has several fully-gapped superconducting phases separated by gapless critical points. The quasi-particle spectrum for the lattice model is

$$E_\pm = \pm\sqrt{(2 - \mu - \cos p_x - \cos p_y)^2 + 4|\Delta|^2 \sin^2 p_x + 4|\Delta|^2 \sin^2 p_y} \tag{6.1.5}$$

and is gapped (under the assumption that $|\Delta| \neq 0$) unless the prefactors of all three Pauli matrices vanish simultaneously. As a function of (p_x, p_y, μ) we find three critical points. The first critical point occurs at $(p_x, p_y, \mu) = (0, 0, 0)$. The second critical point has two gap-closings in the BZ for the same value of μ : $(\pi, 0, 2)$ and $(0, \pi, 2)$. The third critical point is again a singly degenerate point at $(\pi, \pi, 4)$. We will show that the phases for $\mu < 0$ and $\mu > 4$ are trivial superconductors while the phases $0 < \mu < 2$ and $2 < \mu < 4$ are topological superconductors with opposite chirality. In principle one can define a Chern number topological invariant constructed from the eigenstates of the lower quasi-particle band to characterize the phases. We will show this calculation below, but first we make some physical arguments as to the nature of the phases.

We will first consider the phase transition at $\mu = 0$. The low-energy physics for this transition occurs around $(p_x, p_y) = (0, 0)$ and so we can expand the lattice Hamiltonian around this point; this is nothing but Eq. (6.1.3). One way to test the character of the $\mu < 0$ and $\mu > 0$ phases is to make an interface between them. If we can find a continuous interpolation between these two regimes which is always gapped then they are topologically equivalent phases of matter. If we cannot find such a continuously gapped interpolation then they are topologically distinct. A simple geometry to study is a domain wall where $\mu = \mu(x)$ such that $\mu(x) = -\mu_0$ for $x < 0$ and $\mu(x) = +\mu_0$ for $x > 0$ for a positive constant μ_0. This is an interface which is translationally invariant along the y-direction, and thus we can consider the momentum p_y as a good quantum number to simplify the calculation. What we will now show is that there exist gapless, propagating fermions bound to the interface which prevent us from continuously connecting the $\mu < 0$ phase to the $\mu > 0$ phase. This is one indication that the two phases represent topologically distinct classes.
The single-particle Hamiltonian in this geometry is

$$\mathcal{H}_{\mathrm{BdG}}(p_y) = \frac{1}{2}\begin{pmatrix} -\mu(x) & 2\mathrm{i}|\Delta|\left(-\mathrm{i}\frac{d}{dx} + \mathrm{i}p_y\right) \\ -2\mathrm{i}|\Delta|\left(-\mathrm{i}\frac{d}{dx} - \mathrm{i}p_y\right) & \mu(x) \end{pmatrix}, \tag{6.1.6}$$

where we have ignored the quadratic terms in p, and p_y is a constant parameter, not an operator. This is a quasi-1D Hamiltonian that can be solved for each value of p_y independently. We propose an ansatz for the gapless interface states:

$$|\psi_{p_y}(x, y)\rangle = e^{\mathrm{i}p_y y} \exp\left(-\frac{1}{2|\Delta|}\int_0^x \mu(x')dx'\right)|\phi_0\rangle \tag{6.1.7}$$

for a constant, normalized spinor $|\phi_0\rangle$. The secular equation for a zero-energy mode at $p_y = 0$ is

$$\mathcal{H}_{\mathrm{BdG}}(0)|\psi_0(x, y)\rangle = 0 \qquad \Longrightarrow \begin{pmatrix} -\mu(x) & -\mu(x) \\ \mu(x) & \mu(x) \end{pmatrix}|\phi_0\rangle = 0. \tag{6.1.8}$$

The constant spinor which is a solution of this equation is $|\phi_0\rangle = 1/\sqrt{2}\,(1, -1)^{\mathsf{T}}$. This form of the constant spinor immediately simplifies the solution of the problem at finite p_y. We see that the term proportional to p_y in Eq. (6.1.6) is $-2|\Delta|p_y\sigma_x$. Since $\sigma_x|\phi_0\rangle = -|\phi_0\rangle$, i.e., the solution $|\phi_0\rangle$ is an eigenstate of σ_x, we conclude that $|\psi_{p_y}(x, y)\rangle$ is an eigenstate of $\mathcal{H}_{\mathrm{BdG}}(p_y)$ with energy $E(p_y) = -2|\Delta|p_y$. Thus, we have found a normalizable bound state solution at the interface of two regions with $\mu < 0$ and $\mu > 0$ respectively. This set of bound states, parameterized by the conserved quantum number p_y is gapless and chiral, i.e., the group velocity of the quasiparticle dispersion is always negative and never changes sign (in this simplified model). The chirality is determined by the sign of the "spectral" Chern number mentioned above which we will calculate below.
These gapless edge states have quite remarkable properties and are not the same chiral complex fermions that propagate on the edge of integer quantum Hall states, but chiral real (Majorana) fermions. Using Clifford algebra representation theory it can be shown that the so-called chiral Majorana (or Majorana-Weyl) fermions can only be found in spacetime dimensions $(8k + 2)$, where $k = 0, 1, 2, \cdots$. Thus, we can only find chiral-Majorana states in $(1 + 1)$ dimensions or in $(9+1)$ dimensions (or higher!). In condensed matter, we are stuck with $(1+1)$ dimensions where we have now seen that they appear as the boundary states of chiral topological superconductors. The simplest interpretation of such chiral Majorana fermions is as half of a conventional chiral fermion, i.e., its real or imaginary part. To show this, we will consider the edge state of a Chern number 1 quantum Hall system for a single edge

$$\mathcal{H}^{(\mathrm{QH})}_{\mathrm{edge}} = \hbar v \sum_p p\, \eta_p^\dagger \eta_p, \tag{6.1.9}$$

where p is the momentum along the edge. The fermion operators satisfy $\left\{\eta_p^\dagger, \eta_{p'}\right\} = \delta_{pp'}$. Similar to the discussion on the 1D superconducting wire we can decompose these operators into their real and imaginary Majorana parts

$$\eta_p = \frac{1}{2}(\gamma_{1,p} + \mathrm{i}\gamma_{2,p}), \qquad \eta_p^\dagger = \frac{1}{2}(\gamma_{1,-p} - \mathrm{i}\gamma_{2,-p}), \tag{6.1.10}$$

where $\gamma_{a,p}$ $(a = 1, 2)$ are Majorana fermion operators satisfying $\gamma_{a,p}^\dagger = \gamma_{a,-p}$ and $\left\{\gamma_{a,-p}, \gamma_{b,p'}\right\} = 2\delta_{ab}\delta_{pp'}$. The quantum Hall edge Hamiltonian now becomes

$$\begin{aligned}
\mathcal{H}_{\text{edge}}^{(\text{QH})} =& \hbar v \sum_{p\geq 0} p(\eta_p^\dagger \eta_p - \eta_{-p}^\dagger \eta_{-p}) \\
=& \frac{\hbar v}{4} \sum_{p\geq 0} p \left\{(\gamma_{1,-p} - \mathrm{i}\gamma_{2,-p})(\gamma_{1,p} + \mathrm{i}\gamma_{2,p}) - (\gamma_{1,p} - \mathrm{i}\gamma_{2,p})(\gamma_{1,-p} + \mathrm{i}\gamma_{2,-p})\right\} \\
=& \frac{\hbar v}{4} \sum_{p\geq 0} p \left(\gamma_{1,-p}\gamma_{1,p} + \gamma_{2,-p}\gamma_{2,p} - \gamma_{1,p}\gamma_{1,-p} - \gamma_{2,p}\gamma_{2,-p}\right) \\
=& \frac{\hbar v}{2} \sum_{p\geq 0} p \left(\gamma_{1,-p}\gamma_{1,p} + \gamma_{2,-p}\gamma_{2,p} - 2\right).
\end{aligned} \tag{6.1.11}$$

Thus

$$\mathcal{H}_{\text{edge}}^{(\text{QH})} = \frac{\hbar v}{2} \sum_{p\geq 0} p \left(\gamma_{1,-p}\gamma_{1,p} + \gamma_{2,-p}\gamma_{2,p}\right) \tag{6.1.12}$$

up to a constant shift of the energy. This Hamiltonian is exactly two copies of a chiral Majorana Hamiltonian. The edge/domain-wall fermion Hamiltonian of the chiral p-wave superconductor will be

$$\mathcal{H}_{\text{edge}}^{(p-\text{wave})} = \frac{\hbar v}{2} \sum_{p\geq 0} p\gamma_{-p}\gamma_p. \tag{6.1.13}$$

Finding gapless states on a domain wall of μ is an indicator that the phases with $\mu > 0$ and $\mu < 0$ are distinct. If they were the same phase of matter we should be able to adiabatically connect these states continuously. However, we have shown a specific case of the more general result that any interface between a region with $\mu > 0$ and a region with $\mu < 0$ will have gapless states that generate a discontinuity in the interpolation between the two regions. The question remaining is: Is $\mu > 0$ or $\mu < 0$ non-trivial? The answer is that we have a trivial superconductor for $\mu < 0$ (adiabatically continued to $\mu \to -\infty$) and a topological superconductor for $\mu > 0$. Remember that for now we are only considering μ in the neighborhood of 0 and using the continuum model expanded around $(p_x, p_y) = (0, 0)$. We will now define a bulk topological invariant for 2D superconductors that can distinguish the trivial superconductor state from the chiral topological superconductor state. For the spinless Bogoliubov-deGennes Hamiltonian, which is of the form

$$H_{\text{BdG}} = \frac{1}{2} \sum_{\boldsymbol{p}} \Psi_{\boldsymbol{p}}^\dagger \left[\boldsymbol{d}(\boldsymbol{p}, \mu) \cdot \boldsymbol{\sigma}\right] \Psi_{\boldsymbol{p}}, \tag{6.1.14a}$$

$$\boldsymbol{d}(\boldsymbol{p}, \mu) = \left(-2|\Delta|p_y, -2|\Delta|p_x, p^2/2m - \mu\right), \tag{6.1.14b}$$

the topological invariant is the spectral Chern number which simplifies, for this Hamiltonian, to the winding number

$$\mathsf{C}^{(1)} = \frac{1}{8\pi} \int \mathrm{d}^2\boldsymbol{p}\, \epsilon^{ij}\, \hat{\boldsymbol{d}} \cdot \left(\partial_{p_i}\hat{\boldsymbol{d}} \times \partial_{p_j}\hat{\boldsymbol{d}}\right) = \frac{1}{8\pi} \int \mathrm{d}^2\boldsymbol{p}\, \frac{\epsilon^{ij}}{|\boldsymbol{d}|^3}\, \boldsymbol{d} \cdot \left(\partial_{p_i}\boldsymbol{d} \times \partial_{p_j}\boldsymbol{d}\right). \tag{6.1.15}$$

We defined the unit vector $\hat{\boldsymbol{d}} = \boldsymbol{d}/|\boldsymbol{d}|$, which is possible since $|\boldsymbol{d}| \neq 0$ due to the existence of a gap. This integral has a special form and is equal to the degree of the mapping from

momentum space onto the 2-sphere S^2 given by $\hat{d}_1^2 + \hat{d}_2^2 + \hat{d}_3^2 = 1$. As it stands, the degree of the mapping $\hat{\boldsymbol{d}} : \mathbb{R}^2 \to S^2$ is not well-defined because the domain is not compact, i.e., (p_x, p_y) is only restricted to lie in the Euclidean plane ($\mathbb{R}^2$). However, for our choice of the map $\hat{\boldsymbol{d}}$ we can define the winding number by choosing an equivalent, but compact, domain. To understand the necessary choice of domain we can simply look at the explicit form of $\hat{\boldsymbol{d}}(\boldsymbol{p})$

$$\hat{\boldsymbol{d}}(\boldsymbol{p}) = \frac{(-2|\Delta|p_y, -2|\Delta|p_x, p^2/2m - \mu)}{\sqrt{4|\Delta|^2 p^2 + (p^2/2m - \mu)^2}}. \tag{6.1.16}$$

We see that $\lim_{|\boldsymbol{p}|\to\infty} \hat{\boldsymbol{d}}(\boldsymbol{p}) = (0, 0, 1)$ and it does not depend on the direction in which we take the limit in the 2D plane. Because of the uniqueness of this limit we are free to perform the *one-point compactification* of $\mathbb{R}^2$ which amounts to including the point at infinity in our domain. The topology of $\mathbb{R}^2 \cup \{\infty\}$ is the same as S^2 and thus we can consider the degree of our map from the compactified momentum space (S^2) to the unit $\hat{\boldsymbol{d}}$-vector space (S^2). Using the explicit form of the $\hat{\boldsymbol{d}}$-vector for this model, we find

$$\mathsf{C}^{(1)} = \frac{1}{\pi} \int \mathrm{d}^2\boldsymbol{p} \frac{|\Delta|^2 \left(\frac{p^2}{2m} + \mu\right)}{\left[4|\Delta|^2 p^2 + \left(\frac{p^2}{2m} - \mu\right)^2\right]^{3/2}}. \tag{6.1.17}$$

The evaluation of this integral can be easily carried out numerically. The result is $\mathsf{C}^{(1)} = 0$ for $\mu < 0$ and $\mathsf{C}^{(1)} = 1$ for $\mu > 0$, i.e., there are two different phases separated by a quantum critical point at $\mu = 0$. Thus we have identified the phase which is in the chiral superconductor state to be $\mu > 0$.

6.2 Argument for the existence of Majorana bound states on vortices

A simple but rigorous argument can show us the presence of zero energy bound states in the core of vortices in a superconductor. Assume we have a chiral $(p + \mathrm{i}p)$ superconductor in two geometries: a disk with an edge and a cylinder with two edges. Since it is a topological superconductor, the system will have chiral dispersing (Majorana) gapless modes along the edges. In Fig. 6.1, the spectra are plotted versus the momentum along the edge, and they are qualitatively very different in the two cases. For an edge of length L, the smallest difference between two momenta along the edge is $2\pi/L$. The energy difference between two levels is $v2\pi/L$, where v is the velocity of the edge mode.

In a single particle superconducting Hamiltonian the number of total single-particle eigenvalues is always even. This is clear from the fact that whatever the spinor of the nonsuperconducting Hamiltonian is, when superconductivity is added, we have a doubled spectrum, so that every energy state at $E > 0$ comes with a counterpart at energy $-E$. When labeled by momentum quantum number, for a system with just one edge, like the disk, there cannot be a single state at momentum $p = 0$ at energy $E = 0$. If such a state was there, the spectrum would contain an odd number of states. Hence the spectrum of the linearized edge mode cannot have a state at $E = 0$, $p = 0$ on the disk. The one way to introduce such a state is to have antiperiodic boundary conditions, with the spectrum of the edge being at momenta $\pi(2n + 1)/L$, $n \in \mathbb{Z}$. On the cylinder, as two edges are present, periodic boundary conditions are allowed (as are antiperiodic, which can be obtained by threading a flux through the cylinder).

We now add a single vortex inside the disk, far away from the edge of the disk. What is the influence of the vortex on the edge? The vortex induces a phase 2π in the units of the superconducting quantum $hc/2e$, which means that the phase of Δ changes by 2π, and that

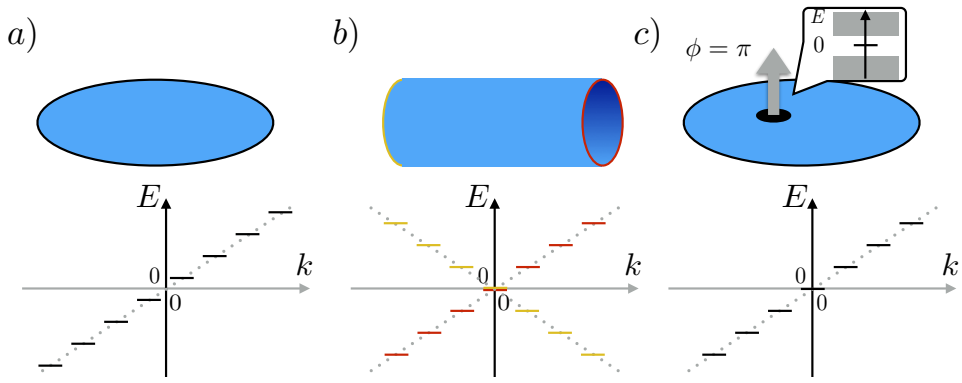

Figure 6.1: Spectra of a Chiral superconductor in different geometries: (a) disk, (b) cylinder, and (c) disk with flux defect. Shown are the spectra of the chiral topological boundary modes including their finite-size quantization with level spacing $v2\pi/L$. If a π flux is inserted in the disk geometry (c), it binds an isolated zero-energy state. At the same time, a single zero-energy state appears on the edge.

of the electronic operators by π upon a full rotation around the edge. This implies that the antiperiodic boundary conditions on the edge without vortex changes to periodic boundary conditions in the presence of the vortex. The spectrum on the edge then is translated by π/L compared to the case without the vortex, making it have an energy level at $p = 0, E = 0$. This would mean that the spectrum has an odd number of levels. However, this cannot be true, as we explained above, since the number of levels is always even. We are hence missing one unpaired level. Where is it? Since the only difference from the case with no vortex is the vortex itself, we draw the conclusion that the missing level is associated with the vortex, and is a bound state on the vortex. We also draw the conclusion that, since it is unpaired and really bound to the vortex, it has to rest exactly at $E = 0$, thereby showing that chiral superconductors have Majorana zero modes in their vortex core.

6.3 Vortices in two-dimensional chiral p-wave superconductors

6.3.1 Explicit bound state solutions

Let us explicitly show that a vortex in a chiral superconductor will contain a zero mode. This calculation, which is a variant of our calculation for the existence of a Majorana mode at the interface between a topological and a trivial superconductor. We consider a disk of radius R which has $\mu > 0$ surrounded by a region with $\mu < 0$ for $r > R$. We know from our previous discussion that there will be a single branch of chiral Majorana states localized near $r = R$, but no exact zero mode. If we take the limit $R \to 0$ this represents a vortex and all the low-energy modes on the interface will be pushed to higher energies. If we put a π-flux inside the trivial region it will change the boundary conditions such that even in the $R \to 0$ limit there will be a zero-mode in the spectrum localized on the vortex.
Now let us take the Bogoliubov-deGennes Hamiltonian in the Dirac limit ($m \to \infty$) and solve the Bogoliubov-deGennes equations in the presence of a vortex located at $r = 0$ in the disk geometry in polar coordinates. Let $\Delta(r, \vartheta) = |\Delta(r)|e^{i\alpha(\boldsymbol{r})}$. The profile $|\Delta(r)|$ for a vortex will depend on the details of the model, but must vanish inside the vortex core region, e.g., for an infinitely thin core we just need $|\Delta(0)| = 0$. We take the phase $\alpha(\boldsymbol{r})$ to be equal to the polar angle ϑ at $\boldsymbol{r}$.
The first step in the solution of the bound state for this vortex profile is to gauge transform the

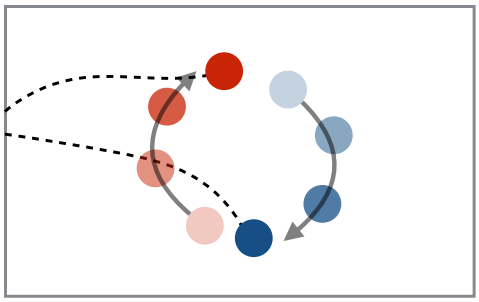

Figure 6.2: Illustration of the exchange of two vortices in a chiral p-wave superconductor. The dotted lines represent branch cuts across which the phase of the superconducting order parameter jumps by 2π.

phase of $\Delta(r,\vartheta)$ into the fermion operators via $\Psi(\boldsymbol{r}) \to e^{\mathrm{i}\alpha(r)/2}\Psi(\boldsymbol{r})$. This has two effects: (i) it simplifies the solution of the Bogoliubov-deGennes differential equations and (ii) converts the boundary conditions of $\Psi(\boldsymbol{r})$ from periodic to anti-periodic around the vortex position $\boldsymbol{r} = 0$. In polar coordinates the remaining single-particle Bogoliubov-deGennes Hamiltonian is simply

$$\mathcal{H}_{\mathrm{BdG}} = \frac{1}{2}\begin{pmatrix} -\mu & 2|\Delta(r)|e^{\mathrm{i}\vartheta}\left(\frac{\partial}{\partial r} + \frac{\mathrm{i}}{r}\frac{\partial}{\partial\vartheta}\right) \\ -2|\Delta(r)|e^{-\mathrm{i}\vartheta}\left(\frac{\partial}{\partial r} - \frac{\mathrm{i}}{r}\frac{\partial}{\partial\vartheta}\right) & \mu \end{pmatrix}. \tag{6.3.1}$$

We want to solve $\mathcal{H}_{\mathrm{BdG}}\Psi = E\Psi = 0$ which we can do with the ansatz

$$\Psi_0(r,\vartheta) = \frac{\mathrm{i}}{\sqrt{r}\mathcal{N}}\exp\left[-\frac{1}{2}\int_0^r \frac{\mu(r')}{|\Delta(r')|}\mathrm{d}r'\right]\begin{pmatrix} -e^{\mathrm{i}\vartheta/2} \\ e^{-\mathrm{i}\vartheta/2}\end{pmatrix} \equiv \mathrm{i}g(r)\begin{pmatrix} -e^{\mathrm{i}\vartheta/2} \\ e^{-\mathrm{i}\vartheta/2}\end{pmatrix}, \tag{6.3.2}$$

where $\mathcal{N}$ is a normalization constant. The function $g(r)$ is localized at the location of the vortex. We see that $\Psi_0(r,\vartheta+2\pi) = -\Psi_0(r,\vartheta)$ as required. From an explicit check one can see that $\mathcal{H}_{\mathrm{BdG}}\Psi_0(r,\vartheta) = 0$. The field operator which annihilates fermion quanta in this localized state is

$$\gamma = \int r\mathrm{d}r\mathrm{d}\vartheta\ \mathrm{i}g(r)\left[-e^{\mathrm{i}\vartheta/2}c(r,\vartheta) + e^{-\mathrm{i}\vartheta/2}c^\dagger(r,\vartheta)\right], \tag{6.3.3}$$

from which we can immediately see that $\gamma = \gamma^\dagger$. Thus the vortex traps a single Majorana bound state at zero-energy.

6.3.2 Non-Abelian statistics of vortices in chiral p-wave superconductors

We have shown in the last Section that on each vortex in a spinless chiral superconductor there exists a single Majorana bound state. If we have a collection of $2N$ vortices which are well-separated from each other, a low-energy subspace is generated which in the thermodynamic limit leads to a ground state degeneracy of 2^N. For example, two vortices give a degeneracy of 2, which can be understood by combining the two localized Majorana bound states into a single complex fermion state which can be occupied or un-occupied, akin to the end states of the superconducting wire. From $2N$ vortices one can form N complex fermion states giving a degeneracy of 2^N, which can be broken up into the subspace of 2^{N-1} states with even fermion parity and the 2^{N-1} states with odd fermion parity. As an aside, since we have operators that mutually anti-commute and square to $+1$ we can define a Clifford algebra operator structure using the set of $2N$ γ_i.

Let us begin with a single pair of vortices which have localized Majorana operators γ_1 and γ_2 respectively and are assumed to be well separated. We imagine that we adiabatically move the

vortices in order to exchange the two Majorana fermions. If we move them slow enough then the only outcome of exchanging the vortices is a unitary operator acting on the two degenerate states which make up the ground state subspace. If we exchange the two vortices then we have $\gamma_1 \to \gamma_2$ and $\gamma_2 \to \gamma_1$. However if we look at Fig. 6.2 we immediately see there is a complication. In this figure we have illustrated the exchange of two vortices and the dotted lines represent branch cuts across which the phase of the superconductor order parameter jumps by 2π. Since our solution of the Majorana bound states used the gauge transformed fermion operators we see that the bound state on the red vortex, which passes through the branch cut of the blue vortex, picks up an additional minus sign upon exchange. Thus the exchange of two vortices is effected by

$$\gamma_1 \to \gamma_2, \qquad \gamma_2 \to -\gamma_1. \tag{6.3.4}$$

In general, if we have $2N$ vortices, we can think of the different exchange operators $T_{ij}(\gamma_a)$ which for our choice of conventions send $\gamma_i \to \gamma_j$, $\gamma_j \to -\gamma_i$, and $\gamma_k \to \gamma_k$ for all $k \neq i, j$. A concept for topological quantum computation arises from using the degenerate Hilbert space spanned by the Majorana particles as quantum bits (qubits) and the exchange operations as multi-qubit gates. Importantly, since the exchange operations preserve Fermion parity (we assume they are adiabatic, so there is no level crossing) we can only work in either the even parity or odd parity subspace and use it as qubits. Let us consider the case of 4 Majoranas, which span a ($\sqrt{2}^4 = 4$)-dimensional Hilbert space. Let us focus on the even-parity sector, which is two-dimensional and consists of the states $|00\rangle$ and $|11\rangle$ where the two occupation numbers are those of the fermions with creation and annihilation operators defined as follows

$$\begin{aligned} a &= \frac{1}{2}(\gamma_1 + \mathrm{i}\gamma_2), \qquad a^\dagger = \frac{1}{2}(\gamma_1 - \mathrm{i}\gamma_2), \\ b &= \frac{1}{2}(\gamma_3 + \mathrm{i}\gamma_4), \qquad b^\dagger = \frac{1}{2}(\gamma_3 - \mathrm{i}\gamma_4). \end{aligned} \tag{6.3.5}$$

Consider now a *double-exchange* of Majoranas γ_2 and γ_4, which results in $\gamma_2 \to -\gamma_2$ and $\gamma_4 \to -\gamma_4$. As a result, $a \leftrightarrow a^\dagger$ and $b \leftrightarrow b^\dagger$. Thus, an initially empty state $|00\rangle$ would now be measured as occupied under both operators a and b and thus the double-exchange of the Majoranas results in $|00\rangle \leftrightarrow |11\rangle$, i.e., a flip of our qubit, also called a Pauli-x gate (because of the matrix representation of the operation in the $|00\rangle, |11\rangle$ basis being the first Pauli matrix). Importantly, the operation defined in Eq. (6.3.4) does not commute with this double-exchange of γ_2 and γ_4, an indication of the *non-Abelian* statistics of Majorana fermions. This property allows for topologically protected, albeit not universal, quantum computation operations.

6.4 The 16-fold way classification of two-dimensional chiral superconductors

We have now noticed that there are two characterizations of a topological superconductor, but they are seemingly different. First, the spectral Chern number is an integer $\mathsf{C}^{(1)} \in \mathbb{Z}$. Directly related to it is the number of chiral Majorana modes on the edge, which in turn is related to an experimental observable, the thermal conductivity on the edge. Hence the system has a $\mathbb{Z}$ index, which becomes obvious when an edge exists. We then saw that a $(p+\mathrm{i}p)$ superconductor (i.e., a topological superconductor with Chern number equal to one) with a vortex threaded through it exhibits a Majorana zero energy mode at the core of the vortex. A $(d+\mathrm{i}d)$ superconductor, with Chern number equal to 2, would exhibit two Majorana modes in the core of the vortex. However, those two Majorana modes would be unstable towards single particle hybridization terms, which would push them away from zero energy, and leave the core of the vortex with no states in it. The generalization tells us that an even Chern number topological superconductor has no Majorana zero modes in the vortex while an odd Chern number topological superconductor has

one Majorana zero mode in its core. This shows that the defects (vortices) in a topological superconductor are classified by a $\mathbb{Z}_2$ number ($\mathsf{C}^{(1)} \mod 2$).
We now show that there is a third classification related to the idea of topological order. In the absence of an edge and in the absence of vortex defects, there is a $\mathbb{Z}_{16}$ classification of topological superconductors indexed by $\mathsf{C}^{(1)} \mod 16$, which can be put on solid grounds by the formalism of topological quantum field theory (TQFT).
We ask how we can classify the system in the absence of an edge. One way would be to compute the phases that wavefunctions can acquire upon taking particles or quasiparticles around each other. However, the system is made out of electrons (its a superconductor), so usually nothing special can happen to phases of electrons. The only "special" excitation of the superconductor is a vortex, so we will look at the phase that two vortices acquire upon exchange. We can calculate this with an argument. Take two copies of the $(p + \mathrm{i}p)$ superconductor governed by the Hamiltonian

$$H = \frac{\mathrm{i}}{4} \sum_{j,k} A_{jk} (\gamma_{1,j}\gamma_{1,k} + \gamma_{2,j}\gamma_{2,k}), \tag{6.4.1}$$

written in terms of Majorana operators $\gamma_{1,j}$ for one copy and $\gamma_{2,j}$ for the other copy. These operators can be combined into an complex fermion $c_j = (\gamma_{1,j} + \mathrm{i}\gamma_{2,j})/2$ in terms of which the Hamiltonian becomes

$$H = \mathrm{i} \sum_{j,k} A_{jk} c_j^\dagger c_k. \tag{6.4.2}$$

This Hamiltonian has a "fake" U(1) symmetry given by our choice of A_{jk} for both Hamiltonians. (Since the system is gapped, we expect our universal conclusions to hold even when this symmetry is stripped away). Thus, the system is a quantum Hall state of Hall conductance $\mathsf{C}^{(1)}$ (in units of e^2/h) if each of the superconductors had Chern number $\mathsf{C}^{(1)}$. We now ask what happens when we thread a superconducting vortex $h/2e$, which is equal to π. Threading a flux 2π in a quantum Hall state of Chern number $\mathsf{C}^{(1)}$ pulls $\mathsf{C}^{(1)}$ electron charges to the vortex core through the Hall effect, hence a π flux pulls $\mathsf{C}^{(1)}/2$ electron charges towards the core. We then try to compute the phase acquired when a vortex is exchanged with another vortex. This is an exchange process, which is half a braid. A braid of two vortices is equivalent to $\mathsf{C}^{(1)}/2$ electrons braided with a π vortex, giving rise to a phase $\pi\mathsf{C}^{(1)}/2$ upon a braid, and $\pi\mathsf{C}^{(1)}/4$ under exchange. Since this is the phase for exchange of vortices in two exactly identical superimposed superconductors, the phase for exchange in one of them is half that, $\pi\mathsf{C}^{(1)}/8 = 2\pi\mathsf{C}^{(1)}/16$. This shows that the phase for vortex exchange is defined only mod 16.
Let us summarize what we have learned about the vortices in chiral superconductors with odd Chern number. We have seen that well-separated vortices hold a Majorana zero mode at their core. When these vortices come together, the two Majorana modes hybridize and split, giving rise to two states which differ by their fermion parity. Let us call the Bogoliubov-deGennes vacuum 1 and the Bogoliubov quasiparticle ψ, and the Majorana fermion of the vortex σ. We can then formalize the fusion of two vortices by writing down a fusion rule

$$\sigma \times \sigma = 1 + \psi, \tag{6.4.3}$$

which basically tells us that combining two Majoranas can either go to a state with no fermion or at one with a fermion – the fermion parity (and density) would be different for the two states. Which one it is depends on the microscopics of the model. Hence a quantum state of two Majoranas has to be described by another quantum number, which describes the "fusion channel" of those two Majoranas – either the vacuum or the Bogoliubov quasiparticle. The fusion rule (6.4.3) allows for multiple fusion channels.This is a manifestation of the fact that the Majoranas are non-Abelian anyons. When two Bogoliubov quasiparticles fuse, they condense (form a Cooper pair) and go to the vacuum

$$\psi \times \psi = 1, \tag{6.4.4}$$

while the fusion of a Bogoliubov and a Majorana quasiparticle basically creates another Majorana

$$\psi \times \sigma = \sigma. \tag{6.4.5}$$

This can be rationalized by thinking of the complex Bogoliubov quasiparticle as made out of two Majoranas which then couple to the third Majorana. The Hamiltonian is a 3×3 antisymmetric matrix that necessarily has a zero eigenvalue which is another Majorana fermion coming as a result of the fusion.

References

1. Ivanov, D. A. "Non-Abelian Statistics of Half-Quantum Vortices in p-Wave Superconductors". *Phys. Rev. Lett.* **86,** 268. http://link.aps.org/doi/10.1103/PhysRevLett.86.268 (2001).
2. Kitaev, A. "Anyons in an exactly solved model and beyond". *Ann. Phys.* **321,** 2. http://dx.doi.org/10.1016/j.aop.2005.10.005 (2005).

Chapter 7

The 10-fold way: Classification with respect to local symmetries

Learning goals

- We know the three symmetries on which the table of topological insulators is based.
- We know how, in principle, one can build the table.
- We know how to derive the indices for each symmetry group.
- We know how to make use of the table in real life.

- C.-K. Chiu et al., Rev. Mod. Phys. **88**, 035005 (2016)

7.1 Motivation and definitions

In the chapters up to now we have seen a variety of systems that can be described with a topological quantum number. While the response to an electric field in the integer quantum Hall effect was described by the Chern number, we have seen how such topological indices also show up in simple one-, two- and three-dimensional toy-models. Moreover, these indices are not restricted to plain electron systems, but superconductors may show topological features as well. Some of these systems did not require any symmetries (the quantum Hall effect), see Chap. 2, while others either required local symmetries such as time reversal, see Chap. 4, or appear on Hilbert spaces that have some symmetries built in, cf. Chap. 6. The Nambu-space of superconductors being an example of the latter.

We now try to understand how one can rationalize the above observations in a bigger framework. Let us review which (topological) classification schemes we already encountered. The first example was the characterization of a spin-1/2 in a magnetic field in Sec. 2.4.1. There, we discussed the geometric phase as a function of a smooth change in parameters of a Hamiltonian. The mathematical structure behind that was a fibre bundle. A fiber bundle is an object which locally looks like $M \times f$, where M is some base manifold and f the "fibre". For our case of the geometric phase, the base manifold was S^2 describing the parameter space of the ground state projector $|\psi_0\rangle\langle\psi_0|$. The fiber $f = U(1)$ was the phase of the ground state $|\psi_0\rangle$ that dropped out when we considered the projector. We have seen that one can classify such fibre bundles via a *Chern* number $\mathsf{C}^{(1)}$. For the example of a spin-1/2 in a magnetic field, the Chern number took the value $\mathsf{C}^{(1)} = -2\pi$. For the quantum Hall effect, we identified the fibre bundle with what looks locally like $\mathbb{T}^2 \times U(1)$ where $\mathbb{T}^2$ is the torus defined by the Aharonov-Bohm fluxes through the openings of the (real space!) torus. We argued that also in this case the fibre bundle is characterized by the Chern number which can take any value in $2\pi\nu$ with $\nu \in \mathbb{Z}$ [1, 2].

We also considered special cases where the Aharonov-Bohm fluxes could be replaced by lattice

momenta (k_x, k_y). Moreover, in the simple case of a two-band Chern insulator the Chern number was shown to be equivalent to the Skyrmion number which characterizes mappings $\mathbb{T}^2 \to S^2$ instead of fibre bundles. In general, we can hope to find the classification of mappings $\mathbb{T}^d \to M$, where $\mathbb{T}^d$ is the d-dimensional Brillouin zone and M is some target manifold.
Attempting a topological classification of free fermion systems really means to define equivalence classes of first quantized Hamiltonians. Not so surprisingly, such equivalence classes depend strongly on the presence of symmetries: If we allow for arbitrary deformations of Hamiltonians (of course without the closing of the gap above the ground state!), we might be able to deform two Hamiltonians into each other that are distinct if we restrict the possible interpolation path by requiring symmetries.
A simple example of such a symmetry constraint we encountered in Chap. 3: Consider the restricted one-dimensional two-band system

$$H = \sum_i d_i(k)\sigma_i \qquad \text{with} \qquad \{H, \sigma_z\} = 0. \tag{7.1.1}$$

This symmetry requirement is identical with the demand that there is no z-component of the d-vector as we have observed for the SSH model. In other words, the normalized d-vector lives on S^1. Thanks to this restriction, or symmetry, each Hamiltonian in this class defines a mapping

$$S^1 \to S^1 \tag{7.1.2}$$

which is characterized by the winding number $\mathsf{W}^{(0)}$. In the absence of the symmetry $\{H, \sigma_z\}$=0, the d-vector could point anywhere on S^2. Mappings

$$S^1 \to S^2 \tag{7.1.3}$$

are all trivial, however, as any closed one-dimensional path defined by the image of S^1 is smoothly contractible to a point. Hence, we cannot define a winding number in this case.
We can now attempt to use arbitrary symmetries for our classification task. In the present chapter we focus on three important local symmetries that we want to introduce carefully in the following. After their introduction we are in the position to outline our classification goals more precisely.

7.1.1 Anti-unitary symmetries

When we discuss symmetry constraints on possible equivalence relations between Hamiltonians we want to consider anti-unitary symmetries such as time reversal invariance with $\mathcal{T}\mathrm{i}\mathcal{T}^{-1} = -\mathrm{i}$. Simple local unitary symmetries S that commute with the Hamiltonian $[H, S] = 0$ are not of interest for us in this chapter for the following reason: We could simply go to combined eigenstates of both the symmetry S and the Hamiltonian. We want to assume that we only deal with such block-diagonal Hamiltonians from the outset. If we deal with anti-unitary symmetries, we do not have the eigenstates at hand and we cannot use this program of decomposing H into symmetric sub-blocks. The same holds for unitary symmetries S that anti-commute with the Hamiltonian, i.e., $\{H, S\} = 0$. We will see how such "symmetries" help us to classify topological insulators.
In the following, we use a first quantized language where we write the single particle Hamiltonian as

$$H = \sum_{AB} \psi_A^\dagger \mathcal{H}_{AB} \psi_B, \tag{7.1.4}$$

where A, B run over all relevant quantum numbers. The object of interest is the matrix $\mathcal{H}_{AB}$. In case we deal with superconducting problems the corresponding matrix is constructed from the Nambu spinor

$$H = \sum_{AB} \begin{pmatrix} \psi_A^\dagger & \psi_{\bar{A}} \end{pmatrix} \mathcal{H}_{AB} \begin{pmatrix} \psi_B \\ \psi_{\bar{B}}^\dagger \end{pmatrix}. \tag{7.1.5}$$

Here A and $\bar{A}$ correspond to the paired quantum numbers: For example for an s-wave superconductor $A = (\boldsymbol{k}, \uparrow)$ and $\bar{A} = (-\boldsymbol{k}, \downarrow)$.

Time reversal

Let us now start with the anti-unitary time reversal symmetry

$$\mathcal{T}: \qquad U_{\mathcal{T}}^{\dagger} \mathcal{H}^* U_{\mathcal{T}} = \mathcal{H}, \qquad \text{with} \qquad U_{\mathcal{T}}^{\dagger} U_{\mathcal{T}} = \mathbb{1}, \tag{7.1.6}$$

for some unitary rotation $U_{\mathcal{T}}$. Using the second quantized language we find for these matrices

$$\mathcal{T} \psi_A \mathcal{T}^{-1} = \sum_B [U_{\mathcal{T}}]_{AB} \psi_B. \tag{7.1.7}$$

Applying this identity twice, and making use of the fact that $\mathcal{T}$ is anti-unitary, we find

$$\mathcal{T}^2 \psi_A \mathcal{T}^{-2} = \sum_B [U_{\mathcal{T}}^* U_{\mathcal{T}}]_{AB} \psi_B = \pm \psi_A, \qquad \text{i.e.,} \qquad U_{\mathcal{T}}^* U_{\mathcal{T}} = \pm \mathbb{1}. \tag{7.1.8}$$

Here we used that $\mathcal{T}^2 = -\mathbb{1}$ or $\mathcal{T}^2 = \mathbb{1}$, depending on whether we deal with systems of half-integer spins or not. The last equation can also be written as

$$U_{\mathcal{T}} = \pm U_{\mathcal{T}}^{\mathsf{T}}. \tag{7.1.9}$$

Charge conjugation

The next (anti-) symmetry we consider is the charge-conjugation, or particle-hole symmetry

$$\mathcal{P}: \qquad U_{\mathcal{P}}^{\dagger} \mathcal{H}^* U_{\mathcal{P}} = -\mathcal{H} \qquad \text{with} \qquad U_{\mathcal{P}}^{\dagger} U_{\mathcal{P}} = \mathbb{1}. \tag{7.1.10}$$

Where again we find $U_{\mathcal{P}}$ via

$$\mathcal{P} \psi_A \mathcal{P}^{-1} = \sum_B [U_{\mathcal{P}}^*]_{AB} \psi_B^{\dagger}. \tag{7.1.11}$$

And also in this case we can either have

$$U_{\mathcal{P}} = \pm U_{\mathcal{P}}^{\mathsf{T}}, \tag{7.1.12}$$

depending on wether $\mathcal{P}^2 = \pm \mathbb{1}$. As this particle hole symmetry is slightly less standard than the time reversal symmetry, we give two concrete examples. First, the Hamiltonian of an s-wave superconductor can be written as

$$H = \sum_k \begin{pmatrix} c_{k\uparrow} & c_{k\downarrow} & c_{-k\uparrow}^{\dagger} & c_{-k,\downarrow}^{\dagger} \end{pmatrix}^{\dagger} \underbrace{\begin{pmatrix} \xi(k) & 0 & 0 & \Delta_s \\ 0 & \xi(k) & -\Delta_s & 0 \\ 0 & -\Delta_s^* & -\xi(k) & 0 \\ \Delta_s^* & 0 & 0 & -\xi(k) \end{pmatrix}}_{\mathcal{H}_s} \begin{pmatrix} c_{k\uparrow} \\ c_{k\downarrow} \\ c_{-k\uparrow}^{\dagger} \\ c_{-k,\downarrow}^{\dagger} \end{pmatrix}. \tag{7.1.13}$$

This Hamiltonian has the anti-symmetry

$$U_{\mathcal{P}}^{\dagger} \mathcal{H}_s^* U_{\mathcal{P}} = -\mathcal{H}_s \qquad \text{with} \qquad U_{\mathcal{P}} = \mathrm{i}\sigma_y \otimes \mathbb{1} \qquad \text{and hence} \qquad U_{\mathcal{P}} = -U_{\mathcal{P}}^{\mathsf{T}}. \tag{7.1.14}$$

On the other hand, a triplet superconductor can be of the form

$$H = \sum_k \begin{pmatrix} c_{k\uparrow} & c_{k\downarrow} & c_{-k\uparrow}^{\dagger} & c_{-k,\downarrow}^{\dagger} \end{pmatrix}^{\dagger} \underbrace{\begin{pmatrix} \xi(k) & 0 & 0 & \Delta_t \\ 0 & \xi(k) & \Delta_t & 0 \\ 0 & \Delta_t^* & -\xi(k) & 0 \\ \Delta_t^* & 0 & 0 & -\xi(k) \end{pmatrix}}_{\mathcal{H}_t} \begin{pmatrix} c_{k\uparrow} \\ c_{k\downarrow} \\ c_{-k\uparrow}^{\dagger} \\ c_{-k,\downarrow}^{\dagger} \end{pmatrix}. \tag{7.1.15}$$

Now the Hamiltonian has the anti-symmetry

$$U_{\mathcal{P}}^{\dagger}\mathcal{H}_t^{*}U_{\mathcal{P}} = -\mathcal{H}_t \qquad \text{with} \qquad U_{\mathcal{P}} = \sigma_x \otimes \mathbb{1} \qquad \text{and hence} \qquad U_{\mathcal{P}} = U_{\mathcal{P}}^{\mathsf{T}}. \tag{7.1.16}$$

Note, that all Bogoliubov-de Gennes (BdG) Hamiltonians of mean-field superconductors have a $\mathcal{P}$-type symmetry built in by construction (via the Nambu formalism).

Chiral symmetry

One more option is for the Hamiltonian to posses the following anti-symmetry

$$\mathcal{C}: \qquad U_{\mathcal{C}}^{\dagger}\mathcal{H}U_{\mathcal{C}} = -\mathcal{H} \qquad \text{with} \qquad U_{\mathcal{C}}^{\dagger}U_{\mathcal{C}} = \mathbb{1}. \qquad \text{and} \qquad U_{\mathcal{C}}^{2} = \mathbb{1}. \tag{7.1.17}$$

This symmetry is called chiral or *sub-lattice* symmetry as it often occurs on bipartite lattice models. Note, that whenever the system has a chiral symmetry and either a particle-hole or time-reversal, it actually posses all three of them (show!).

7.2 The periodic table

Let us now classify all possible symmetry classes according to the above three "symmetries". For the time-reversal and particle-hole symmetry we have three options. Either there is no symmetry, one that squares to $\mathbb{1}$, or one that squares to $-\mathbb{1}$. We denote these cases with $0, 1, -1$. Together, there are $3 \times 3 = 9$ different options. Turning around the argument above that a $\mathcal{P}$ ($\mathcal{T}$) together with a $\mathcal{C}$ type symmetry implies a $\mathcal{T}$ ($\mathcal{P}$) symmetry, we see that $\mathcal{C} = \mathcal{P} \circ \mathcal{T}$. Therefore, for all cases where either $\mathcal{T}$ or $\mathcal{P}$ are present the presence or absence of $\mathcal{C}$ is fixed. Only if both particle-hole and time-reversal symmetry are absent, $\mathcal{C}$ can be either present (1) or absent (0). This yields in total 10 different symmetry classes in Tab. 7.1. We would now like to achieve the

label	**symmetry**			**target space**			**spatial dimension** d							
	$\mathcal{T}$	$\mathcal{P}$	$\mathcal{C}$	X_{evol}	X_σ	$X_{\mathcal{Q}}$	1	2	3	4	5	6	7	8
the complex cases:														
A	0	0	0	C_1	C_0	C_0	0	$\mathbb{Z}$	0	$\mathbb{Z}$	0	$\mathbb{Z}$	0	$\mathbb{Z}$
AIII	0	0	1	C_0	C_1	C_1	$\mathbb{Z}$	0	$\mathbb{Z}$	0	$\mathbb{Z}$	0	$\mathbb{Z}$	0
the real cases:														
AI	1	0	0	R_7	R_4	R_0	0	0	0	$2\mathbb{Z}$	0	$\mathbb{Z}_2$	$\mathbb{Z}_2$	$\mathbb{Z}$
BDI	1	1	1	R_0	R_3	R_1	$\mathbb{Z}$	0	0	0	$2\mathbb{Z}$	0	$\mathbb{Z}_2$	$\mathbb{Z}_2$
D	0	1	0	R_1	R_2	R_2	$\mathbb{Z}_2$	$\mathbb{Z}$	0	0	0	$2\mathbb{Z}$	0	$\mathbb{Z}_2$
DIII	-1	1	1	R_2	R_1	R_3	$\mathbb{Z}_2$	$\mathbb{Z}_2$	$\mathbb{Z}$	0	0	0	$2\mathbb{Z}$	0
AII	-1	0	0	R_3	R_0	R_4	0	$\mathbb{Z}_2$	$\mathbb{Z}_2$	$\mathbb{Z}$	0	0	0	$2\mathbb{Z}$
CII	-1	-1	1	R_4	R_7	R_5	$2\mathbb{Z}$	0	$\mathbb{Z}_2$	$\mathbb{Z}_2$	$\mathbb{Z}$	0	0	0
C	0	-1	0	R_5	R_6	R_6	0	$2\mathbb{Z}$	0	$\mathbb{Z}_2$	$\mathbb{Z}_2$	$\mathbb{Z}$	0	0
CI	1	-1	1	R_6	R_5	R_7	0	0	$2\mathbb{Z}$	0	$\mathbb{Z}_2$	$\mathbb{Z}_2$	$\mathbb{Z}$	0

Table 7.1: Periodic table of topological insulators and superconductors. $\mathbb{Z}_2$ and $\mathbb{Z}$ denote binary and integer topological indices, respectively. $2\mathbb{Z}$ denotes an even integer. The symmetries $\mathcal{T}$, $\mathcal{P}$ and $\mathcal{C} = \mathcal{T} \circ \mathcal{P}$ are explained in the text. A zero denotes the absence of the symmetry and for $\mathcal{T}$ and $\mathcal{P}$, the ± 1 indicates if these symmetries square to $\pm\mathbb{1}$. The target spaces are listed in Tab. 7.2

following goals with respect to Tab. 7.1:

1. We know of three ways to construct this table. This amounts to understand the columns "target spaces". One can do this for systems only respecting the symmetries $\mathcal{T}$, $\mathcal{P}$, $\mathcal{C}$, i.e, for system with spatial disorder, or for Bloch Hamiltonians in lattice systems. We expose the latter in some detail, for the rest we refer to [3–5].

2. We would like to know how one can derive explicit formulas for indices characterizing the various entries in Tab. 7.1. We cover some of these derivations, for the rest we refer to [6].

C_0	C_1	R_0	R_1	R_2	R_3	R_4	R_5	R_6	R_7
$\frac{\mathrm{U}(n+m)}{\mathrm{U}(n)\times\mathrm{U}(m)}$	$\mathrm{U}(n)$	$\frac{\mathrm{O}(n+m)}{\mathrm{O}(n)\times\mathrm{O}(m)}$	$\mathrm{O}(n)$	$\frac{\mathrm{O}(2n)}{\mathrm{U}(n)}$	$\frac{\mathrm{U}(2n)}{\mathrm{Sp}(n)}$	$\frac{\mathrm{Sp}(n+m)}{\mathrm{Sp}(n)\times\mathrm{Sp}(m)}$	$\mathrm{Sp}(n)$	$\frac{\mathrm{Sp}(2n)}{\mathrm{U}(n)}$	$\frac{\mathrm{U}(n)}{\mathrm{O}(n)}$

Table 7.2: List of target spaces used for the definition of the 10-fold way.

Let us start with a quick summary of how to construct the table, not making use of translation symmetry.

7.2.1 Random matrices and non-linear sigma models

For now, we do not impose any further symmetries on the Hamiltonian, such as invariance under translations (a unitary symmetry). Hence, we should think of the Hamiltonian as a *random matrix subject to the symmetry constraint* of a given class. In a seminal work, Altland and Zirnbauer [4] established a one-to-one correspondence between the symmetry classes of Hamiltonians and a classification of symmetric spaces in differential geometry that was obtained by Cartan (see Tab. 7.1 and Tab. 7.2).
Their work is an extension of a classification that goes back to Wigner and Dyson and relied on time-reversal symmetry alone. There are two complex classes which possess no anti-unitary symmetry and eight real classes with at least one anti-unitary symmetry. The nomenclature complex and real corresponds to the fact that the anti-unitary symmetries impose reality constraints for the elements of the latter classes, while the former can be represented by complex matrices.
The column X_{evol} of Tab. 7.1 lists the symmetric spaces X_{evol} to which the time-evolution operators $\exp(-\mathrm{i}tH)$ of each class belong. While the columns noting the symmetries and the target spaces of Tab. 7.1 provide an exhaustive classification of noninteracting fermionic Hamiltonians into symmetry classes, it does as such not provide physical information. The physical manifestation of this classification lies in the correspondence between the topological sector of a bulk Hamiltonian and protected gapless modes at the boundary of the system.
Establishing this connection is the main result of Schnyder *et al.* [5]. It is achieved by studying the problem of Anderson localization of non-interacting electrons that are subject to static disorder potentials on the $(d-1)$-dimensional boundary of the system. For every given symmetry class and every dimension of space, they pose the following question: How many fermionic modes can exist on the boundary that are inert to Anderson localization? It is answered in a long wavelength-approximation by studying non-linear sigma-model field theories. While we do not want to enter the discussion of non-linear sigma models here, we note that the result is determined by two ingredients, (i) the dimension $d-1$ of the boundary and (ii) the target space X_σ in which the dynamical field of the nonlinear sigma model lives. Remarkably, these target spaces are a permutation of the spaces X_{evol} of the time-evolution operator.[1]

[1]The result is that the number of boundary modes that are topologically protected against symmetry-preserving disorder at the $(d-1)$-dimensional boundary belong to the homotopy group $\pi_{d-1}(X_\sigma)$, if $\pi_{d-1}(X_\sigma) = \mathbb{Z}_2$ (in which case a so-called $\mathbb{Z}_2$ term can be added to the nonlinear sigma model to prevent localization) and to the

7.2.2 Flatband Hamiltonians

Let us now move to understanding the target spaces $X_{\mathcal{Q}}$ in a bit more detail. In other words, we now consider on top of the local symmetries also translation symmetry. In particular, we want to exemplify how the symmetric spaces that are listed under $X_{\mathcal{Q}}$ in Tab. 7.1 arise in a physical context from symmetry constraints.

Class A

Let us start with the most generic case of class A, in which no symmetry constraints are imposed on the single-particle Hamiltonian. We consider a Hamiltonian H with the full translational invariance of continuous configuration space with periodic boundary conditions imposed. In second quantization, it has the Bloch representation

$$H = \int \mathrm{d}^d\boldsymbol{k}\, \psi^\dagger_\alpha(\boldsymbol{k})\mathcal{H}_{\alpha,\alpha'}(\boldsymbol{k})\psi_{\alpha'}(\boldsymbol{k}), \tag{7.2.1}$$

where $\psi^\dagger_\alpha(\boldsymbol{k})$ creates a fermion of flavor $\alpha = 1, \cdots, N$ at momentum $\boldsymbol{k}$ in the Brillouin zone (BZ) and the summation over α and α' is implicit. The flavor index may represent orbital, spin, or sublattice degrees of freedom. Energy bands are obtained by diagonalizing the $N \times N$ matrix $\mathcal{H}(\boldsymbol{k})$ at every momentum $\boldsymbol{k} \in \mathrm{BZ}$ with the aid of a unitary transformation $U(\boldsymbol{k})$

$$U^\dagger(\boldsymbol{k})\mathcal{H}(\boldsymbol{k})U(\boldsymbol{k}) = \mathrm{diag}\left[\varepsilon_{m+n}(\boldsymbol{k}), \cdots, \varepsilon_{n+1}(\boldsymbol{k}), \varepsilon_n(\boldsymbol{k}), \cdots, \varepsilon_1(\boldsymbol{k})\right], \tag{7.2.2}$$

where the energies are arranged in descending order on the righthand side and $n, m \in \mathbb{Z}$ such that $n + m = N$. So as to start from an insulating fermi-sea ground state, we assume that there exists an energy gap between the bands n and $n + 1$ and that the chemical potential μ lies in this gap

$$\varepsilon_n(\boldsymbol{k}) < \mu < \varepsilon_{n+1}(\boldsymbol{k}), \qquad \forall \boldsymbol{k} \in \mathrm{BZ}. \tag{7.2.3}$$

The presence of the gap allows us to adiabatically deform the Bloch Hamiltonian $\mathcal{H}(\boldsymbol{k})$ to the flatband Hamiltonian

$$\mathcal{Q}(\boldsymbol{k}) := U(\boldsymbol{k}) \begin{pmatrix} \mathbb{1}_m & 0 \\ 0 & -\mathbb{1}_n \end{pmatrix} U^\dagger(\boldsymbol{k}) \tag{7.2.4}$$

that assigns the energy -1 and $+1$ to all states in the bands below and above the gap, respectively. This deformation preserves the eigenstates, but removes the non-universal information about energy bands from the Hamiltonian. In other words, the degenerate eigenspaces of the eigenvalues ± 1 of $\mathcal{Q}(\boldsymbol{k})$ reflect the partitioning of the single-particle Hilbert space introduced by the spectral gap in the spectrum of $\mathcal{H}(\boldsymbol{k})$. The degeneracy of its eigenspaces equips $\mathcal{Q}(\boldsymbol{k})$ with an extra $\mathrm{U}(n) \times \mathrm{U}(m)$ gauge symmetry: While the $(n + m) \times (n + m)$ matrix $U(\boldsymbol{k})$ of Bloch eigenvectors that diagonalizes $\mathcal{Q}(\boldsymbol{k})$ is an element of $\mathrm{U}(n + m)$ for every $\boldsymbol{k} \in \mathrm{BZ}$, we are free to change the basis for its lower and upper bands by a $\mathrm{U}(n)$ and $\mathrm{U}(m)$ transformation, respectively. Hence $\mathcal{Q}(\boldsymbol{k})$ is an element of the symmetric space C_0 defining a map

$$\mathcal{Q}: \quad \mathrm{BZ} \to C_0 = \frac{\mathrm{U}(n+m)}{\mathrm{U}(n) \times \mathrm{U}(m)}. \tag{7.2.5}$$

The group of topologically distinct maps $\mathcal{Q}$, or, equivalently, the number of topologically distinct Hamiltonians $\mathcal{H}$, is given by the homotopy group

$$\pi_d(C_0) \tag{7.2.6}$$

homotopy group $\pi_d(X_\sigma)$, if $\pi_d(X_\sigma) = \mathbb{Z}$ (in which case a so-called Wess-Zumino-Witten term can be added to the nonlinear sigma model to prevent localization, for a given class X_σ and a given dimension d of space.

The homotopy group is a topological characterization of the symmetric space. Loosely speaking, $\pi_d(X)$, $d = 1, 2, \cdots$, of a symmetric space X is formed by homotopic equivalence classes of maps from the d-dimensional sphere to the symmetric space. Two such maps are homotopic if there exists a continuous function that deforms one map into the other. The homotopy groups for $d = 1, \cdots, 8$ are listed in Tab. 7.1.

for any dimension d of the BZ. For example, in $d = 2$ we have $\pi_2(C_0) = \mathbb{Z}$. A physical example of a family of Hamiltonians that exhausts the topological sectors of this group is found in the quantum Hall effect (QHE). The incompressible ground state with $r \in \mathbb{N}$ filled Landau levels is topologically distinct from the ground state with $\mathbb{N} \ni r' \neq r$ filled Landau levels. Two different patches of space with r and r' filled Landau levels have $|r - r'|$ gapless edge modes running at their interface, reflecting the bulk-boundary correspondence of the topological phases. In contrast, $\pi_3(C_0) = 0$ renders all noninteracting fermionic Hamiltonians in three dimensional space (3D) topologically equivalent to the vacuum, if no further symmetries are imposed.

Class AIII

As a second example, let us discuss a Hamiltonian that has only chiral symmetry and hence belongs to the symmetry class AIII. As above, we assume translational invariance and work directly with the Bloch Hamiltonian $\mathcal{H}(\boldsymbol{k})$ for $\boldsymbol{k} \in \mathrm{BZ}$. The chiral symmetry implies a spectral symmetry of $\mathcal{H}(\boldsymbol{k})$. If gapped, $\mathcal{H}(\boldsymbol{k})$ must have an even number of bands $N = 2n$, $n \in \mathbb{Z}$. When represented in the eigenbasis of the chiral symmetry operator $U_{\mathcal{C}}$, the spectrally flattened Hamiltonian $\mathcal{Q}(\boldsymbol{k})$ and the chiral symmetry operator have the representations

$$\mathcal{Q}(\boldsymbol{k}) = \begin{pmatrix} 0 & q(\boldsymbol{k}) \\ q^\dagger(\boldsymbol{k}) & 0 \end{pmatrix}, \qquad U_{\mathcal{C}} = \begin{pmatrix} \mathbb{1}_n & 0 \\ 0 & -\mathbb{1}_n \end{pmatrix}, \tag{7.2.7a}$$

respectively. From $\mathcal{Q}(\boldsymbol{k})^2 = 1$, one concludes that $q(\boldsymbol{k})$ can be an arbitrary unitary matrix. We are thus led to consider the homotopy group $\pi_d(C_1)$ of the mapping

$$q: \quad \mathrm{BZ} \to C_1 = \mathrm{U}(n). \tag{7.2.7b}$$

For example, in $d = 3$ spatial dimensions $\pi_3(C_1) = \mathbb{Z}$.
With these examples, we have discussed the two complex classes A and AIII. In the real classes, which have at least one antiunitary symmetry, it is harder to obtain the constraints on the spectrally flattened Hamiltonian $\mathcal{Q}(\boldsymbol{k})$. Further, if TRS and PHS are constraining the system, the space of $\mathcal{Q}(\boldsymbol{k})$, $X_{\mathcal{Q}}$, and the target space of the nonlinear sigma model, X_σ, do not agree anymore with one another (see Tab. 7.1). The origin for this complication is that the antiunitary symmetry relates $\mathcal{Q}(\boldsymbol{k})$ and $\mathcal{Q}(-\boldsymbol{k})$ rather than acting locally in momentum space.
One last comment is in order: The homotopy groups of symmetric spaces, as arranged in Tab. 7.1 follow a regular periodic pattern as pointed out by Kitaev, the so-called Bott periodicity. That is, the table is periodic under a shift in d with period two and eight for the complex and real cases, respectively. More precisely, $\pi_d(R_q)$, with q understood modulo 8, depends only on $q + d$

$$\pi_d(R_q) = \pi_{d-p}(R_{q+p}), \qquad p \in \mathbb{Z}. \tag{7.2.8}$$

7.2.3 $\mathbb{Z}$ topological invariants

As mentioned in the last section, for situations other than class A and AIII with relatively simple target spaces, it becomes difficult to work directly with the flat band Hamiltonians $\mathcal{Q}(\boldsymbol{k})$. Therefore, we want to shift gears and approach the complete classification in a way more directly related to differential geometry. To this end, let us quickly remind ourselves of the Gauss-Bonnet theorem for Riemannian manifolds before we extend it the our case of Bloch bands. For convenience, we restrict ourselves to translation invariant systems. All results can be extended to weakly disordered systems, however [3].
In physics, topological attributes refer to *global* properties of physical system that is made out of *local* degrees of freedom and might only have local, i.e., short-ranged, correlations. This parallels the distinction between topology and geometry in mathematics, where the former refers to global structure, while the latter refers to local structure of objects. In differential geometry,

a bridge between topology and geometry is given by the Gauss-Bonnet theorem. It states that for compact 2D Riemannian manifolds M without boundary, the integral over the Gaussian curvature $F(\boldsymbol{x})$ of the manifold is (i) integer and (ii) a topological invariant

$$2(1-g) = \frac{1}{2\pi}\int_M \mathrm{d}^2\boldsymbol{x}\, F(\boldsymbol{x}). \tag{7.2.9}$$

Here, g is the genus of M, e.g., $g=0$ for a 2D sphere and $g=1$ for a 2D torus. The Gaussian curvature $F(\boldsymbol{x})$ can be defined as follows. Attach to every point on M the tangential plane, a two-dimensional vector space (The collection of these tangential spaces is called a vector bundle.). Take some vector from the tangential plane at a given point on M and parallel transport it around a closed loop on M. The angle mismatch of the vector before and after the transport is proportional to the Gaussian curvature enclosed in the loop.
In the physical systems that we want to describe, the manifold M is the BZ and the analogue of the tangent plane on M is a space spanned by the Bloch states at a given momentum $\boldsymbol{k} \in \mathrm{BZ}$. Let us state this fact more precisely. We have seen in Sec. 7.2.2 that the Bloch Hamiltonian defines a mapping from the BZ to some symmetric space. The single-particle Hilbert space $\mathfrak{H}_0$ is the N-dimensional projective space over the complex numbers at every momentum $\boldsymbol{k} \in \mathrm{BZ}$. The Bloch states of the $n < N$ filled bands span at every momentum $\boldsymbol{k} \in \mathrm{BZ}$ an n-dimensional space $\mathfrak{h}_{\boldsymbol{k}}$ that is a subspace of $\mathfrak{H}_0$. In mathematical terms, the $\mathfrak{h}_{\boldsymbol{k}}$ as a set form a vector bundle over the BZ. In contrast to the example from differential geometry above, the "tangent space" $\mathfrak{h}_{\boldsymbol{k}}$ is not a Riemannian metric space and can thus no longer be embedded in the same space as the manifold M itself. At the same time, the Gaussian curvature is generalized to a curvature form, that is called Berry curvature F in physics. In our case, it is given by an $n \times n$ matrix of differential forms that is defined via the Berry connection A as

$$\begin{aligned}
\mathrm{F} &:= \mathcal{F}_{ij}(\boldsymbol{k})\,\mathrm{d}k_i \wedge \mathrm{d}k_j && \text{(7.2.10a)}\\
\mathcal{F}_{ij}(\boldsymbol{k}) &:= \partial_i \mathcal{A}_j(\boldsymbol{k}) - \partial_j \mathcal{A}_i(\boldsymbol{k}) - \mathrm{i}[\mathcal{A}_i(\boldsymbol{k}), \mathcal{A}_j(\boldsymbol{k})], \qquad i,j = 1,\cdots,d, && \text{(7.2.10b)}\\
\mathrm{A} &:= \mathcal{A}_i(\boldsymbol{k})\,\mathrm{d}k_i\,, && \text{(7.2.10c)}\\
\mathcal{A}_i^{(ab)}(\boldsymbol{k}) &:= \mathrm{i}\sum_{\alpha=1}^{N} U^\dagger_{a\alpha}(\boldsymbol{k})\partial_i U_{\alpha b}(\boldsymbol{k}), \qquad a,b = 1,\cdots,n, \qquad i = 1,\cdots,d. && \text{(7.2.10d)}
\end{aligned}$$

The unitary transformation $U(\boldsymbol{k})$ that diagonalizes the Hamiltonian was defined in Eq. (7.2.2), both $\mathcal{A}_i(\boldsymbol{k})$ and $\mathcal{F}_{ij}(\boldsymbol{k})$ are $n \times n$ matrices, we write $\partial_i \equiv \partial/\partial k_i$ and the sum over repeated spatial coordinate components i, j is implicit.
Under a local $\mathrm{U}(n)$ gauge transformation in momentum space that acts on the states of the lower bands and is parametrized by the $n \times n$ matrix $G(\boldsymbol{k})$

$$U_{\alpha a}(\boldsymbol{k}) \longrightarrow U_{\alpha b}(\boldsymbol{k}) G_{ba}(\boldsymbol{k}), \qquad \alpha = 1,\cdots,N, \qquad a = 1,\cdots,n, \tag{7.2.11a}$$

the Berry connection A changes as

$$\mathrm{A} \longrightarrow G^\dagger \mathrm{A} G + \mathrm{i} G^\dagger \mathrm{d} G, \tag{7.2.11b}$$

while the Berry curvature F changes covariantly

$$\mathrm{F} \longrightarrow G^\dagger \mathrm{F} G, \tag{7.2.11c}$$

leaving its trace invariant.
For the spatial dimension $d = 2$, the generalization of the Gauss-Bonnet theorem (7.2.9) in algebraic topology was found by Chern to be

$$\begin{aligned}
2\mathsf{C}^{(1)} &:= \frac{1}{2\pi}\int_{\mathrm{BZ}} \mathrm{tr}\,\mathrm{F} \\
&= 2\frac{1}{2\pi}\int_{\mathrm{BZ}} \mathrm{d}^2\boldsymbol{k}\,\mathrm{tr}\,\mathcal{F}_{12}.
\end{aligned} \tag{7.2.12}$$

This defines a gauge-invariant quantity, the first Chern number $\mathsf{C}^{(1)}$. Remarkably, $\mathsf{C}^{(1)}$ can only take integer values: It counts the number of vortices of the vector field $\mathrm{tr}\,[\boldsymbol{\mathcal{A}}(\boldsymbol{k})]$ in the BZ.

Without chiral symmetry

In order to obtain a topological invariant for any even dimension $d = 2s$ of space, we can use the s-th power of the Berry field F to build a gauge invariant d-form that can be integrated over the BZ to obtain scalar (0-form). Upon taking the trace, this scalar is invariant under the gauge transformation (7.2.11a) and defines the s-th Chern number

$$2\mathsf{C}^{(s)} := \frac{1}{s!}\left(\frac{1}{2\pi}\right)^s \int_{\mathrm{BZ}} \mathrm{tr}\,[\mathrm{F}^s]\,, \tag{7.2.13}$$

where $\mathrm{F}^s = \mathrm{F}\wedge\cdots\wedge\mathrm{F}$. As with the case $s = 1$ that we have exemplified above, $\mathsf{C}^{(s)}$ is integer for any $s = 1, 2, \cdots$. This can be understood as follows. Locally in the BZ, for any $s = 1, 2, \cdots$, the integrand of Eq. (7.2.13) can be written as differential of a $(d-1)$ differential form, the so-called Chern-Simons form $\mathrm{Q}^{(s)}$,

$$\mathrm{tr}\,[\mathrm{F}^s] = \mathrm{tr}\left[\mathrm{d}\mathrm{Q}^{(s)}\right]. \tag{7.2.14}$$

The lowest order Chern-Simons forms are given by

$$\mathrm{Q}^{(1)} := \mathrm{A}, \tag{7.2.15a}$$

$$\mathrm{Q}^{(2)} := \mathrm{A}\wedge\mathrm{dA} - \frac{2\mathrm{i}}{3}\mathrm{A}\wedge\mathrm{A}\wedge\mathrm{A}, \tag{7.2.15b}$$

$$\mathrm{Q}^{(3)} := \mathrm{dA}\wedge\mathrm{dA}\wedge\mathrm{A} - \frac{3\mathrm{i}}{2}\mathrm{dA}\wedge\mathrm{A}\wedge\mathrm{A}\wedge\mathrm{A} - \frac{3}{5}\mathrm{A}\wedge\mathrm{A}\wedge\mathrm{A}\wedge\mathrm{A}\wedge\mathrm{A}. \tag{7.2.15c}$$

Unlike F, $\mathrm{Q}^{(s)}$ depends on the gauge choice. If the Chern number is non-vanishing, there is an obstruction to define $\mathrm{Q}^{(s)}$ globally over the BZ, i.e., to define a globally smooth gauge. (Otherwise, the Chern number would vanish due to Stoke's theorem.) The dual form to $\mathrm{Q}^{(s)}$ can be regarded as a d-dimensional vector field on the BZ. The Chern number $\mathsf{C}^{(s)}$ simply counts the number of point-like singularities in this vector field on the BZ in a given gauge and is hence integer.

From inspection of Tab. 7.1 we see that symmetry classes without chiral symmetry may have integer topological invariants $\mathbb{Z}$ only when the dimension d of space is even. In fact, all the integer invariants of these classes are given by the Chern number $\mathsf{C}^{(s)}$ of the respective dimension. However, not for every even dimension does every symmetry class have a $\mathbb{Z}$ homotopy group. This is in one-to-one correspondence to the vanishing of the Chern numbers under some symmetry constraints, as we will now explain.

Class A The Chern numbers are the topological invariants that characterize a Hamiltonian without symmetry constraints in symmetry class A for *every* even dimension $d = 2s$.

Classes AI and AII If TRS but no PHS is present, as it is the case for classes AI and AII, both the Berry connection and the Berry field satisfy

$$\mathcal{A}_i(\boldsymbol{k}) = +\mathcal{A}_i^{\mathsf{T}}(-\boldsymbol{k}), \qquad i = 1, \cdots, d, \tag{7.2.16a}$$

$$\mathcal{F}_{ij}(\boldsymbol{k}) = -\mathcal{F}_{ij}^{\mathsf{T}}(-\boldsymbol{k}), \qquad i, j = 1, \cdots, d. \tag{7.2.16b}$$

As a consequence, if s is odd, the integrand in Eq. (7.2.13) is an odd function of momentum and the Chern number vanishes. In contrast, if $s = 2s'$, $s' \in \mathbb{Z}$, such that $d = 4s'$, there is no reason for $\mathsf{C}^{(2s')}$ to vanish. Indeed $\mathsf{C}^{(2s')}$ is the integer topological invariant for classes AI and AII *whenever* $d = 4s'$.

Classes C and D* Let us now consider the symmetry classes with PHS but no TRS. If PHS is present, as it is the case for classes C and D, the spectrum of the Hamiltonian is symmetric about the Fermi energy, supporting as many bands below it as above it. The Berry field of the lower bands F is related to the Berry field of the upper bands $\widetilde{\mathsf{F}}$

$$\mathcal{F}_{ij}(\boldsymbol{k}) = -\widetilde{\mathcal{F}}^{\mathsf{T}}_{ij}(-\boldsymbol{k}), \qquad i,j = 1,\cdots,d. \tag{7.2.17}$$

It follows that the Chern number of the lower bands $\mathsf{C}^{(s)}$ and the Chern number of the upper bands $\widetilde{\mathsf{C}}^{(s)}$ [given by Eq. (7.2.13) with $\mathcal{F}_{ij}$ replaced by $\widetilde{\mathcal{F}}_{ij}$] are related by

$$\mathsf{C}^{(s)} = (-1)^s\, \widetilde{\mathsf{C}}^{(s)}. \tag{7.2.18}$$

Further, the topological sector of the full system must be trivial

$$\mathsf{C}^{(s)} + \widetilde{\mathsf{C}}^{(s)} = 0. \tag{7.2.19}$$

We conclude form Eqs. (7.2.18) and (7.2.19) that whenever s is even, the Chern number $\mathsf{C}^{(s)}$ vanishes. In contrast, if $s = 2s'+1$, $s' \in \mathbb{Z}$, such that $d = 4s'+2$ there is no reason for $\mathsf{C}^{(2s'+1)}$ to vanish. Indeed $\mathsf{C}^{(2s'+1)}$ is the integer topological invariant for classes C and D *whenever* $d = 4s'+2$.

With chiral symmetry

In systems with chiral symmetry the energy spectrum is symmetric about the Fermi energy, and there exists a *unitary* transformation $U_{\mathcal{C}}$ that maps states from the lower bands to the upper bands. As a consequence, the Berry field of the lower bands F is related to the Berry field of the upper bands $\widetilde{\mathsf{F}}$

$$\mathcal{F}_{ij}(\boldsymbol{k}) = \widetilde{\mathcal{F}}_{ij}(\boldsymbol{k}), \qquad i,j = 1,\cdots,d. \tag{7.2.20}$$

It follows that the Chern number of the lower bands $\mathsf{C}^{(s)}$ and the Chern number of the upper bands $\widetilde{\mathsf{C}}^{(s)}$ are equal

$$\mathsf{C}^{(s)} = \widetilde{\mathsf{C}}^{(s)}. \tag{7.2.21}$$

This is at odds with the fact that the topological sector of the full system must be trivial [see Eq. (7.2.19)]. We conclude that the Chern numbers of any system with chiral symmetry vanish

$$\mathsf{C}^{(s)} = 0. \tag{7.2.22}$$

However, the chiral symmetry allows us to define an alternative topological characterization. To see how it arises as a natural extension of the above, we consider a different representation of the Chern numbers $\mathsf{C}^{(s)}$. In terms of the flatband projector Hamiltonian $\mathcal{Q}(\boldsymbol{k})$ that was defined in Eq. (7.2.4), we can write

$$\mathsf{C}^{(s)} \propto \varepsilon_{i_1\cdots i_d} \int_{\mathrm{BZ}} \mathrm{d}^d\boldsymbol{k}\, \mathrm{tr}\left[\mathcal{Q}(\boldsymbol{k})\partial_{i_1}\mathcal{Q}(\boldsymbol{k})\cdots\partial_{i_d}\mathcal{Q}(\boldsymbol{k})\right], \qquad d = 2s. \tag{7.2.23}$$

The form of Eq. (7.2.23) allows to interpret $\mathsf{C}^{(s)}$ as the *winding number* of the unitary transformation $\mathcal{Q}(\boldsymbol{k})$ over the compact BZ[2]. One verifies that $\mathsf{C}^{(s)} = 0$ for symmetry classes with chiral

[2]Let us illustrate for the first Chern number the equivalence of the characterizations in terms of the Berry curvature and the flatband Hamiltonian $\mathcal{Q}(\boldsymbol{k})$. The Berry connection is $\mathcal{A}_i^{(\alpha\beta)}(\boldsymbol{k}) = \mathrm{i}\langle\alpha|\,\partial_i\,|\beta\rangle$, where $|\alpha\rangle$ and $|\beta\rangle$ are occupied bands. The Berry curvature can then be written as:

$$\mathcal{F}_{ij}^{(\alpha\beta)} = \mathrm{i}\left(\langle\partial_i\alpha|\partial_j\beta\rangle - \langle\partial_j\alpha|\partial_i\beta\rangle\right) - \mathrm{i}\sum_{\gamma=1}^{n}\left(\langle\partial_i\alpha|\gamma\rangle\langle\gamma|\partial_j\beta\rangle - \langle\partial_j\alpha|\gamma\rangle\langle\gamma|\partial_i\beta\rangle\right). \tag{7.2.24}$$

symmetry by inserting $U_{\mathcal{C}}U_{\mathcal{C}}^\dagger$ at some point in the expression and anticommuting $U_{\mathcal{C}}$ with all $\mathcal{Q}$, using the cyclicity of the trace. After $2s+1$ anticommutations, we are back to the original expression up to an overall minus sign and found $\mathsf{C}^{(s)} = -\mathsf{C}^{(s)}$ implying Eq. (7.2.22).
In odd dimensions of space, we can define a topological invariant by modifying Eq. (7.2.23) and using the chiral operator $U_{\mathcal{C}}$

$$\begin{aligned}\mathsf{W}^{(s)} &:= \frac{(-1)^s s!}{2(2s+1)!}\left(\frac{\mathrm{i}}{2\pi}\right)^{s+1}\varepsilon_{i_1\cdots i_d}\int_{\mathrm{BZ}}\mathrm{d}^d\boldsymbol{k}\,\mathrm{tr}\left[U_{\mathcal{C}}\mathcal{Q}(\boldsymbol{k})\partial_{i_1}\mathcal{Q}(\boldsymbol{k})\cdots\partial_{i_d}\mathcal{Q}(\boldsymbol{k})\right]\\ &= \frac{(-1)^s s!}{(2s+1)!}\left(\frac{\mathrm{i}}{2\pi}\right)^{s+1}\varepsilon_{i_1\cdots i_d}\int_{\mathrm{BZ}}\mathrm{d}^d\boldsymbol{k}\,\mathrm{tr}\left[q(\boldsymbol{k})\partial_{i_1}q^\dagger(\boldsymbol{k})\partial_{i_2}q(\boldsymbol{k})\cdots\partial_{i_d}q^\dagger(\boldsymbol{k})\right], \qquad d=2s+1.\end{aligned} \tag{7.2.31}$$

By anticommuting the chiral operator $U_{\mathcal{C}}$ once with all matrices $\mathcal{Q}$ and using the cyclicity of the trace, one finds that the expression for $\mathsf{W}^{(s)}$ vanishes for even dimensions. The second line of Eq. (7.2.31) allows to interpret $\mathsf{W}^{(s)}$ as the *winding number* of the unitary off-diagonal part of the chiral Hamiltonian $q(\boldsymbol{k})$ that was defined in Eq. (7.2.7a).

Class AIII The chiral winding numbers defined in Eq. (7.2.31) are the topological invariants that characterize a Hamiltonian without symmetry constraints other than chiral symmetry in symmetry class AIII for *every* odd dimension $d = 2s+1$.

Classes BDI and CII* If both TRS and PHS are present and $\mathcal{P}^2 = \mathcal{T}^2$ as it is the case for classes BDI and CII, the flatband Hamiltonian $\mathcal{Q}$ that enters Eq. (7.2.31) satisfies

$$U_{\mathcal{P}}\mathcal{Q}(\boldsymbol{k})U_{\mathcal{P}}^{-1} = -\mathcal{Q}^{\mathsf{T}}(-\boldsymbol{k}), \tag{7.2.32a}$$
$$U_{\mathcal{T}}\mathcal{Q}(\boldsymbol{k})U_{\mathcal{T}}^{-1} = +\mathcal{Q}^{\mathsf{T}}(-\boldsymbol{k}). \tag{7.2.32b}$$

Furthermore,

$$U_{\mathcal{T}} = \pm U_{\mathcal{T}}^{\mathsf{T}}, \qquad U_{\mathcal{T}}^{-1} = \pm\left(U_{\mathcal{T}}^{-1}\right)^{\mathsf{T}}, \tag{7.2.33}$$

We can insert the identity resolution $\sum_{\gamma=1}^{N}|\gamma\rangle\langle\gamma|$ in the first two terms such that only the sum over un-occupied bands survives:

$$\mathcal{F}_{ij}^{(\alpha\beta)} = \mathrm{i}\sum_{\gamma=n+1}^{N}\left(\langle\partial_i\alpha|\gamma\rangle\langle\gamma|\partial_j\beta\rangle - \langle\partial_j\alpha|\gamma\rangle\langle\gamma|\partial_i\beta\rangle\right) \tag{7.2.25}$$

and

$$\mathcal{F}_{ij} = \sum_{\alpha,\beta=1}^{n}|\alpha\rangle F_{ij}^{(\alpha\beta)}\langle\beta| = \mathrm{i}\epsilon_{ij}\left(\partial_i P_-\right)P_+\left(\partial_j P_-\right), \tag{7.2.26}$$

where we introduced the projectors on the occupied bands $P_- = \sum_{\gamma=1}^{n}|\gamma\rangle\langle\gamma|$ and on the unoccupied ones $P_+ = \sum_{\gamma=n+1}^{N}|\gamma\rangle\langle\gamma|$. Note that we have $\mathcal{Q} = P_+ - P_-$ and $P_-^2 = P_-$, $P_+^2 = P_+$. Since $P_-^2 = P_-$, we have:

$$\partial_i P_- = \partial_i P_-^2 = P_-\partial_i P_- + (\partial_i P_-)P_-, \tag{7.2.27}$$

from which follows:

$$\partial_i P_-(\mathbb{1} - P_-) = (\partial_i P_-)P_+ = P_-\partial_i P_-. \tag{7.2.28}$$

We can then write

$$\mathrm{tr}\left[\mathcal{F}_{ij}\right] = \mathrm{i}\epsilon_{ij}\mathrm{tr}\left[P_-\partial_i P_-\partial_j P_-\right]. \tag{7.2.29}$$

Here, we managed to express the trace of the Berry curvature in terms of the projector unto the occupied bands. Let us now see how we can reach a final expression in terms of the flatband Hamiltonian $\mathcal{Q}$. We first notice how $\mathcal{Q} = \mathbb{1} - 2P_-$, hence all derivative operators satisfy $\partial_i\mathcal{Q} = -2\partial_i P_-$. We then have

$$\epsilon_{ij}\mathrm{tr}\left[Q\partial_i Q\partial_j Q\right] = \epsilon_{ij}\mathrm{tr}\left[4(\mathbb{1}-2P_-)\partial_i P_-\partial_j P_-\right] = -8\epsilon_{ij}\mathrm{tr}\left[P_-\partial_i P_-\partial_j P_-\right], \tag{7.2.30}$$

where the terms with $\mathbb{1}$ vanishes because of the cyclicity of the trace and the antisymmetric tensor ϵ_{ij}. We hence succeeded in expressing the first Chern number in terms of the flatband Hamiltonian $\mathcal{Q}$. Similar calculations prove the validity of Eq. (7.2.23) for higher Chern numbers.

with the sign given by $\mathcal{T}^2$. The same relations hold for $U_\mathcal{P}$. As a consequence, the chiral operator $U_\mathcal{C} = U_\mathcal{T}\left(U_\mathcal{P}^{-1}\right)^\mathsf{T}$ transforms as

$$U_\mathcal{T}^{-1} U_\mathcal{C} U_\mathcal{T} = (\mathcal{P}^2\mathcal{T}^2)\, U_\mathcal{C}^\mathsf{T}. \tag{7.2.34}$$

Using the time-reversal symmetry of $\mathcal{Q}$ in Eq. (7.2.31) yields, for d odd,

$$\begin{aligned}
\mathsf{W}^{(s)} &= \frac{(-1)^s s!}{2(2s+1)!}\left(\frac{\mathrm{i}}{2\pi}\right)^{s+1} \varepsilon_{i_1\cdots i_d} \int_{\mathrm{BZ}} \mathrm{d}^d\boldsymbol{k}\, \mathrm{tr}\left[U_\mathcal{T}^{-1} U_\mathcal{C} U_\mathcal{T} \mathcal{Q}^\mathsf{T}(-\boldsymbol{k}) \partial_{i_1} \mathcal{Q}^\mathsf{T}(-\boldsymbol{k}) \cdots \partial_{i_d} \mathcal{Q}^\mathsf{T}(-\boldsymbol{k})\right] \\
&= \frac{(-1)^s s!}{2(2s+1)!}\left(\frac{\mathrm{i}}{2\pi}\right)^{s+1} \varepsilon_{i_1\cdots i_d} \int_{\mathrm{BZ}} \mathrm{d}^d\boldsymbol{k}\, \mathrm{tr}\left[(\mathcal{P}^2\mathcal{T}^2) U_\mathcal{C} \mathcal{Q}(\boldsymbol{k}) \partial_{i_d} \mathcal{Q}(\boldsymbol{k}) \cdots \partial_{i_1} \mathcal{Q}(\boldsymbol{k})\right] \\
&= (-1)^s\, \mathsf{W}^{(s)}, \qquad d = 2s+1,
\end{aligned} \tag{7.2.35}$$

where we used that $\mathcal{Q}$ anticommutes with $U_\mathcal{C}$. If s is odd, as is the case for $d = 3$, $\mathsf{W}^{(s)}$ is bound to vanish for the classes BDI and CII. In contrast, if $s = 2s'$, $s' \in \mathbb{Z}$, such that $d = 4s' + 1$, there is no reason for $\mathsf{W}^{(s)}$ to vanish. Indeed, $\mathsf{W}^{(s)}$ is the integer topological invariant for classes BDI and CII *whenever* $d = 4s' + 1$.

Classes CI and DIII* If both TRS and PHS are present and $\mathcal{P}^2 = -\mathcal{T}^2$ as it is the case for classes CI and DIII, the manipulations of Eq. (7.2.35) still apply, except for the last equality. As $\mathcal{P}^2\mathcal{T}^2 = -1$, it now reads

$$\mathsf{W}^{(s)} = (-1)^{s+1}\, \mathsf{W}^{(s)}, \qquad d = 2s+1. \tag{7.2.36}$$

We conclude that $\mathsf{W}^{(s)}$ is the integer topological invariant for classes CI and DIII *whenever* $d = 4s' + 3$, while it vanishes otherwise.
In summary, we have now given explicit formulas for the topological invariants for all entries $\mathbb{Z}$ in Tab. 7.1.

7.2.4 Dimensional reduction: $\mathbb{Z}_2$ topological invariants

In this section, we will discuss explicit formulas for all entries $\mathbb{Z}_2$ in Tab. 7.1. By inspection of Tab. 7.1, we notice that $\mathbb{Z}_2$ always appears one or two dimensions lower than an entry $\mathbb{Z}$. We will see that the system with $\mathbb{Z}$ is in a sense a parent system from which the lower dimensional $\mathbb{Z}_2$ topological insulators and superconductors, the first and second descendants, can be deduced. First, we will review these dimensional reduction arguments for the real symmetry classes with chiral symmetry. In contrast, for the real symmetry classes without chiral symmetry, we are going to derive more accessible formulas for the topological invariants that do not rely on dimensional reduction.

With chiral symmetry

First descendants For the real classes with chiral symmetry (classes BDI, CI, CII, DIII), we will sketch the so-called dimensional reduction procedure. As an underlying invariant, we will use the winding number $\mathsf{W}^{(s)}[q]$ defined for the off-diagonal projector q in $(2s+1)$-dimensional space in Eq. (7.2.31). In $d = 2s$ dimensions, we can define a relative index between two systems described by the projectors $q_1(\boldsymbol{k})$ and $q_2(\boldsymbol{k})$ by constructing an interpolation $q(\boldsymbol{k}, t)$ that depends on the parameter $t \in [0, \pi]$ such that

$$q(\boldsymbol{k}, t = 0) = q_1(\boldsymbol{k}), \qquad q(\boldsymbol{k}, t = \pi) = q_2(\boldsymbol{k}). \tag{7.2.37}$$

This interpolation is extended for parameter values $t \in [-\pi, 0]$ by demanding that the flatband Hamiltonian $\mathcal{Q}(\boldsymbol{k}, t)$ associated with $q(\boldsymbol{k}, t)$ satisfies the symmetry constraints of the symmetry class that $q_1(\boldsymbol{k})$ and $q_2(\boldsymbol{k})$ belong to in the $(2s+1)$-dimensional space spanned by $\boldsymbol{k}$ and t. Then, the winding number $\mathsf{W}^{(s)}[q]$ is well defined. We can now show that the parity of this winding number is independent of the parametrization $q(\boldsymbol{k}, t)$. To see this, consider a second parametrization $q'(\boldsymbol{k}, t)$ that also satisfies Eq. (7.2.37) and the symmetry constraints of the respective class. Define further the two "twisted" interpolations

$$\widetilde{q}(\boldsymbol{k}, t) := \begin{cases} q(\boldsymbol{k}, -t) & t \in [-\pi, 0] \\ q'(\boldsymbol{k}, t) & t \in (0, \pi] \end{cases}, \qquad \widetilde{q}'(\boldsymbol{k}, t) := \begin{cases} q'(\boldsymbol{k}, t) & t \in [-\pi, 0] \\ q(\boldsymbol{k}, -t) & t \in (0, \pi] \end{cases}. \tag{7.2.38}$$

From this definition of $\widetilde{q}(\boldsymbol{k}, t)$ and $\widetilde{q}'(\boldsymbol{k}, t)$ follows the equality

$$\mathsf{W}^{(s)}[q'] - \mathsf{W}^{(s)}[q] = \mathsf{W}^{(s)}[\widetilde{q}] + \mathsf{W}^{(s)}[\widetilde{q}']. \tag{7.2.39}$$

Further, with the help of TRS, following the steps in Eq. (7.2.35), one can show that $\mathsf{W}^{(s)}[\widetilde{q}] = \mathsf{W}^{(s)}[\widetilde{q}']$. Hence, the winding numbers of any two symmetry-respecting interpolations between $q_1(\boldsymbol{k})$ and $q_2(\boldsymbol{k})$ share the same parity. We can use this parity to define two equivalence classes of Hamiltonians $q(\boldsymbol{k})$ in each of the symmetry classes BDI, CI, CII, and DIII. We are thus lead to define the parity

$$\nu_1[q_1, q_2] := (-1)^{\mathsf{W}^{(s)}[q]} \in \{1, -1\}, \tag{7.2.40}$$

with q being any symmetry-respecting interpolation between q_1 and q_2. The winding number $\mathsf{W}^{(s)}$ of an interpolation between any two trivial Hamiltonians (Hamiltonians without $\boldsymbol{k}$-dependence) vanishes. Thus, the parity of a given off-diagonal projector $q_1(\boldsymbol{k})$ with any trivial reference off-diagonal projector q_0

$$\nu_1[q_1, q_0] \equiv \nu_1[q_1] \tag{7.2.41}$$

constitutes the $\mathbb{Z}_2$ invariant for $q_1(\boldsymbol{k})$, with $\nu_1 = +1$ being the topologically trivial class.

Second descendants* We continue to derive the $\mathbb{Z}_2$ classification of the second descendants for the symmetry classes BDI, CI, CII, and DIII. To this end, consider a pair of off-diagonal projectors $q_{\mathrm{a}}(\boldsymbol{k})$ and $q_{\mathrm{b}}(\boldsymbol{k})$ that belong to the same symmetry class and are defined in a $(d = 2s-1)$-dimensional BZ. We define two interpolations $q_1(\boldsymbol{k}, r)$ and $q_2(\boldsymbol{k}, r)$ that are parametrized by $r \in [0, \pi]$ such that

$$q_i(\boldsymbol{k}, r = 0) = q_{\mathrm{a}}(\boldsymbol{k}), \qquad q_i(\boldsymbol{k}, r = \pi) = q_{\mathrm{b}}(\boldsymbol{k}), \qquad i = 1, 2. \tag{7.2.42}$$

Again, these interpolations are extended for parameter values $t \in [-\pi, 0]$ by demanding that the flatband Hamiltonians $\mathcal{Q}_i(\boldsymbol{k}, r)$ associated with $q_i(\boldsymbol{k}, r)$, $i = 1, 2$, satisfy – in the $2s$-dimensional space spanned by $\boldsymbol{k}$ and r – the symmetry constraints of the symmetry class that $q_{\mathrm{a}}(\boldsymbol{k})$ and $q_{\mathrm{b}}(\boldsymbol{k})$ belong to. Then, the parities $\nu_1[q_1]$ and $\nu_1[q_2]$ are well defined via Eq. (7.2.41). The crucial point is that one can now show $\nu_1[q_1] = \nu_1[q_2]$, that is, $\nu_1[q]$ is independent of the interpolation (7.2.42) and depends only on the endpoints $q_{\mathrm{a}}(\boldsymbol{k})$ and $q_{\mathrm{b}}(\boldsymbol{k})$. To see this, consider an interpolation $q(\boldsymbol{k}, r, t)$ between the interpolations, parametrized by $t \in [0, \pi]$ such that

$$q(\boldsymbol{k}, r, t = 0) = q_1(\boldsymbol{k}, r), \qquad q(\boldsymbol{k}, r, t = \pi) = q_2(\boldsymbol{k}, r), \qquad r \in [-\pi, \pi]. \tag{7.2.43}$$

As before, $q(\boldsymbol{k}, r, t)$ is extended to the interval $t \in [-\pi, 0]$ such that it satisfies the symmetry constraints of the respective class. We have shown in Eq. (7.2.39) that the parity $\nu_1[q_1, q_2]$, computed using Eq. (7.2.40), is independent of the particular choice of interpolation (7.2.37). It follows from Eq. (7.2.37) that

$$q(\boldsymbol{k}, r = 0, t) = q_{\mathrm{a}}(\boldsymbol{k}), \qquad q(\boldsymbol{k}, r = \pi, t) = q_{\mathrm{b}}(\boldsymbol{k}), \qquad t \in [-\pi, \pi], \tag{7.2.44}$$

which is independent of t. We might thus as well think of $\nu_1[q_1, q_2]$ that is computed using Eq. (7.2.40) as a relative parity of the second descendants

$$\nu_2[q_\mathrm{a}, q_\mathrm{b}] := (-1)^{\mathsf{W}^{(s)}[q]} \in \{1, -1\}, \tag{7.2.45}$$

if $q(\boldsymbol{k}, r, t)$ satisfies Eq. (7.2.44) and the respective symmetry constraints. This constitutes the $\mathbb{Z}_2$ index of the second descendants.

Without chiral symmetry*

For real symmetry classes without chiral symmetry, i.e., classes AI, AII, C, and D, the $\mathbb{Z}_2$ invariant is related to the Chern number in one or two dimensions higher. Thus, one could apply the exactly same arguments that lead to Eqs. (7.2.40) and (7.2.45), if one replaces the winding number $\mathsf{W}^{(s)}$ by the Chern number $\mathsf{C}^{(s)}$ of the Hamiltonian. However, to arrive at more explicit formulas for the $\mathbb{Z}_2$ invariants, we will depart from this strategy.

First descendants We consider in $(d = 2s - 1)$-dimensional space the flatband Hamiltonian $\mathcal{Q}(\boldsymbol{k})$ that we want to study and a reference flatband Hamiltonian $\mathcal{Q}_0$ that belongs to the same symmetry class as $\mathcal{Q}(\boldsymbol{k})$, but has no momentum dependence. Instead of constructing an interpolation between these two systems on the level of the Hamiltonians, as was done in the case of the chiral class, let us propose an explicit interpolation between the Berry connection A associated with $\mathcal{Q}(\boldsymbol{k})$ and the vanishing Berry connection of $\mathcal{Q}_0$. The interpolating Berry connection $\widetilde{\mathrm{A}}$ depends on the extra parameter $t \in [-\pi, \pi]$ and reads

$$\widetilde{\mathrm{A}} := \frac{|t|}{\pi}\,\mathrm{A}, \tag{7.2.46a}$$

with

$$\begin{aligned}\widetilde{\mathrm{F}} &:= \mathrm{d}\widetilde{\mathrm{A}} - \mathrm{i}\widetilde{\mathrm{A}} \wedge \widetilde{\mathrm{A}} \\ &= \frac{t}{|t|\pi}\,\mathrm{A} \wedge \mathrm{d}t + \frac{|t|}{\pi}\mathrm{dA} - \mathrm{i}\frac{t^2}{\pi^2}\mathrm{A} \wedge \mathrm{A}\end{aligned} \tag{7.2.46b}$$

being the corresponding curvature form defined for $t \neq 0$. Since $\widetilde{\mathrm{F}}$ is a curvature form on a $2s$-dimensional torus parametrized by $\boldsymbol{k}$ and t, it can be associated to a Chern number $\widetilde{\mathsf{C}}^{(s)}$. Using the fact that $\widetilde{\mathcal{F}}(\boldsymbol{k}, t) = \widetilde{\mathcal{F}}(\boldsymbol{k}, -t)$, we can reduce the t integration from the interval $[-\pi, \pi]$ to the interval $[0, \pi]$ by multiplication with a factor of 2

$$\widetilde{\mathsf{C}}^{(s)} = 2 \times \frac{1}{2s!}\,(12\pi)^s \int\limits_{\mathrm{BZ}\times[0,\pi]} \mathrm{tr}\left[\widetilde{\mathrm{F}}^s\right]. \tag{7.2.47a}$$

Upon explicitly performing the t-integration using the form of $\widetilde{\mathrm{F}}$ in Eq. (7.2.46b), we find that the Chern number is given as an integral of the $(d = 2s - 1)$-forms $\mathrm{Q}^{(s)}$ defined in Eq. (7.2.15c) over the BZ

$$\widetilde{\mathsf{C}}^{(s)} = 2 \times \frac{1}{s!}\left(\frac{1}{2\pi}\right)^s \int\limits_{\mathrm{BZ}} \mathrm{tr}\left[\mathrm{Q}^{(s)}\right]. \tag{7.2.47b}$$

We have thus obtained a form of $\widetilde{\mathsf{C}}^{(s)}$ that is expressed in terms of $\mathcal{Q}(\boldsymbol{k})$ in the $(2s-1)$-dimensional BZ alone. As the Chern-number $\widetilde{\mathsf{C}}^{(s)}$ may only take integer values, the $(2s - 1)$-dimensional polarization

$$\mathsf{P}^{(2s-1)} := \frac{1}{s!}\left(\frac{1}{2\pi}\right)^s \int\limits_{\mathrm{BZ}} \mathrm{tr}\left[\mathrm{Q}^{(s)}\right], \tag{7.2.48}$$

may only take half-integer values. This is a consequence of the symmetry constraints. For systems in symmetry class A, $\mathsf{P}^{(2s-1)}$ is still well defined, but looses its relation to a Chern number in one dimension higher and thus does not need to be quantized. One might wonder whether we have now obtained a $\mathbb{Z}$ classification in terms of $\mathsf{P}^{(2s-1)}$, instead of the $\mathbb{Z}_2$ classification we were aiming at. That this is not the case can be deduced from carefully considering the effect of gauge transformations. The physical gauge transformations to be considered are those affecting the Berry connection A as given by Eq. (7.2.11a). However, these transformations do not take the form of a gauge transformation for the one-form $\widetilde{\mathrm{A}}$ in the auxiliary space $\mathrm{BZ} \times [-\pi, \pi]$. As a consequence, neither transforms $\widetilde{\mathrm{F}}$ gauge covariantly nor is $\widetilde{\mathsf{C}}^{(s)}$ invariant under the physical gauge transformations (7.2.11a) on A. More precisely, the polarization $\mathsf{P}^{(2s-1)}$ changes under such a gauge transformation (7.2.11a) by

$$\mathsf{P}^{(2s-1)} \longrightarrow \mathsf{P}^{(2s-1)} + \frac{1}{s!}\left(\frac{\mathrm{i}}{2\pi}\right)^s \int_{\mathrm{BZ}} \mathrm{tr}\left[(G^\dagger \mathrm{d}G)^{2s-1}\right]. \tag{7.2.49}$$

The additive change is the winding number $\mathsf{W}^{(s-1)}$ of the gauge transformation G over the BZ. As this winding number takes only integer values, the non-integer part of $\mathsf{P}^{(2s-1)}$ is a well-defined quantity, i.e., gauge invariant. Gauge transformations with non-vanishing winding number are referred to as large gauge transformations. This defines two equivalence classes of systems in each of the symmetry classes AI, AII, C, and D, distinguished by the parity

$$\nu_1 := (-1)^{2\mathsf{P}^{(2s-1)}} \in \{1, -1\}. \tag{7.2.50}$$

Between any two systems with different ν_1, there exists no smooth interpolation that respects the symmetry. Any vacuum with $\mathrm{A} = 0$ has $\nu_1 = +1$, rendering this class topologically trivial. We have thus obtained the desired $\mathbb{Z}_2$ classification in terms of the parity index ν_1 for the entries $\mathbb{Z}_2$ to the immediate left of $\mathbb{Z}$ in classes AI, AII, C, and D shown in Tab. 7.1.

Second descendants To directly obtain a convenient form of the topological invariant of the second descendant, we shall construct its index ν_2 from gauge obstruction arguments generalizing the derivation by Fu and Kane.
The TRS and PHS constraints in the symmetry classes AI, AII, C, and D relate the wave function *including the gauge choice* at points $\boldsymbol{k}$ and $-\boldsymbol{k}$ in the $(d = 2s)$-dimensional BZ. Effectively, the system thus only depends on degrees of freedom on one half of momentum space, the effective BZ (EBZ). Without loss of generality, we can define the EBZ as

$$\mathrm{EBZ} := \{\boldsymbol{k} \in \mathrm{BZ} : k_1 \in [0, \pi]\}. \tag{7.2.51}$$

We want to find a topological characterization of the flatband Hamiltonian on the EBZ. In contrast to the BZ, the EBZ is a manifold with boundary, namely a d-dimensional torus cut open in one direction (a cylinder in $d = 2$). Consider a situation where the EBZ is divided into two regions V_1 and V_2, each of which is not necessarily simply connected. Suppose that V_1 and V_2 overlap only at their interface

$$\mathrm{EBZ} = V_1 \cup V_2, \qquad \partial V_1 \setminus \partial\mathrm{EBZ} = \partial V_2 \setminus \partial\mathrm{EBZ}. \tag{7.2.52}$$

Further, suppose that there exists a smooth gauge on each of V_1 and V_2, with A_1 and A_2 being the respective Berry connections. The two gauges are related by a gauge transformation G of the form (7.2.11a) that is defined on the closed surface ∂V_1. We can thus consider its winding number around ∂V_1

$$\mathsf{D}^{(s)} := \frac{1}{s!}\left(\frac{\mathrm{i}}{2\pi}\right)^s \int_{\partial V_1} \mathrm{tr}\left[(G^\dagger \mathrm{d}G)^{2s-1}\right] \tag{7.2.53}$$

which is bound to be integer for a closes surface. As we have seen in Eq. (7.2.49), the integrand of the winding number is the difference between the Chern-Simons forms $\mathrm{Q}_1^{(s)}$ and $\mathrm{Q}_2^{(s)}$ in the two gauges A_1 and A_2, respectively

$$\begin{aligned}\mathsf{D}^{(s)} &= \frac{1}{s!}\left(\frac{1}{2\pi}\right)^s \int\limits_{\partial V_1} \mathrm{tr}\left[\mathrm{Q}_1^{(s)} - \mathrm{Q}_2^{(s)}\right] \\ &= \frac{1}{s!}\left(\frac{1}{2\pi}\right)^s \int\limits_{\partial V_1} \mathrm{tr}\left[\mathrm{Q}_1^{(s)}\right] + \int\limits_{\partial V_2} \mathrm{tr}\left[\mathrm{Q}_2^{(s)}\right] - \int\limits_{\partial \mathrm{EBZ}} \mathrm{tr}\left[\mathrm{Q}_2^{(s)}\right]\end{aligned} \tag{7.2.54a}$$

To obtain the second line in Eq. (7.2.54a), we used that in view of the opposite orientation of the overlap region of ∂V_1 and ∂V_2

$$\int\limits_{\partial \mathrm{EBZ}} = \int\limits_{\partial V_1} + \int\limits_{\partial V_2} . \tag{7.2.54b}$$

As $\mathrm{Q}_i^{(s)}$ is defined smoothly in V_i , $i = 1, 2$, we can use Stokes' theorem to relate it to the Berry curvature via Eq. (7.2.14)

$$\mathsf{D}^{(s)} = \frac{1}{s!}\left(\frac{1}{2\pi}\right)^s \left(\int\limits_{\mathrm{EBZ}} \mathrm{tr}\left[\mathrm{F}^s\right] - \int\limits_{\partial \mathrm{EBZ}} \mathrm{tr}\left[\mathrm{Q}_2^{(s)}\right] \right) . \tag{7.2.55}$$

If any gauge transformation was allowed to be applied to A_2, Eq. (7.2.55) would be meaningless, since the second term would change $\mathsf{D}^{(s)}$ by the winding number of the gauge transformation, an integer. However, for the symmetry classes under consideration, either PHS or TRS restricts the allowed gauge transformations. It turns out that the allowed gauge transformations have even winding number on ∂EBZ. Thus, the parity of $\mathsf{D}^{(s)}$ is a gauge invariant quantity that allows to define the $\mathbb{Z}_2$ index for the second descendants

$$\nu_2 := (-1)^{\mathsf{D}^{(s)}} \in \{1, -1\} . \tag{7.2.56}$$

in symmetry classes AI, AII, C, and D. There is a plethora of different but equivalent formulas for this $\mathbb{Z}_2$ index. For example, the original formulation for class AII in $d = 2$ by Kane and Mele employs the antisymmetric overlap matrix $U^\dagger(\boldsymbol{k})U_{\mathcal{T}}U^*(\boldsymbol{k})$ to establish the formula

$$\mathsf{D}^{(1)} = \frac{\mathrm{i}}{2\pi} \int\limits_{\partial \mathrm{EBZ}} \mathrm{d}\,\log\left\{\mathrm{Pf}\,\left[U^\dagger(\boldsymbol{k})U_{\mathcal{T}}U^*(\boldsymbol{k})\right] + \mathrm{i}\delta\right\} , \tag{7.2.57}$$

where Pf denotes the Pfaffian of a matrix and $\delta > 0$ is a regulator. If the system obeys inversion symmetry, Eq. (7.2.57) reduces to a finite product of parity eigenvalues at inversion-symmetric momenta in the BZ. In this form, the index can be computed numerically very efficiently.

References

1. Nakahara, M. *Geometry, Topology and Physics* (Taylor and Francis, New York and London, 2003).
2. Bohm, A., Mostafazadeh, A., Koizumi, H., Niu, Q. & Zwanziger, J. *The Geometric Phase in Quantum Systems* (Springer-Verlag, Heidelberg, 2003).
3. Kitaev, A. "Periodic table for topological insulators and superconductors". *AIP Conf. Proc.* **1134,** 22. http://link.aip.org/link/doi/10.1063/1.3149495 (2009).

4. Altland, A. & Zirnbauer, M. R. "Nonstandard symmetry classes in mesoscopic normal-superconducting hybrid structures". *Phys. Rev. B* **55,** 1142. https://doi.org/10.1103/PhysRevB.55.1142 (1997).

5. Schnyder, A. P., Ryu, S., Furusaki, A. & Ludwig, A. W. W. "Classification of Topological Insulators and Superconductors". *AIP Conf. Proc.* **1134,** 10. https://doi.org/10.1063/1.3149481 (2009).

6. Ryu, S., Schnyder, A. P., Furusaki, A. & Ludwig, A. W. W. "Topological insulators and superconductors: tenfold way and dimensional hierarchy". *New J. Phys.* **12,** 065010. http://dx.doi.org/10.1088/1367-2630/12/6/065010 (2010).

Chapter 8

Topological Crystalline Insulators I

Learning goals

- We understand how the topological classification of insulators and the bulk-boundary correspondence is enhanced by including crystalline symmetries.
- We know how topological invariants such as mirror-graded winding numbers and the mirror Chern number are defined.
- We have an understanding of higher-order topological insulators.

- L. Fu, Phys. Rev. Lett. **106**, 106802 (2011)
- C. Fang and L. Fu, Phys. Rev. B. **91**, 161105 (2015)
- W. Benalcazar *et al.*, Science **357**, 61–66 (2017)
- F. Schindler *et al.*, Science Adv. **4**, eaat0346 (2018)

Topological crystalline insulators are protected by spatial symmetry transformations which act non-locally such as mirror or rotational symmetries. They are usually identified with two notions: i) their bulk ground state is not adiabatically connected to an atomic limit without breaking the protecting symmetry. ii) they have gapless boundary modes which can only be gapped out by breaking the respective symmetry.
In fact, properties i) and ii) are not equivalent. We have already seen for the case of the SSH model protected by inversion symmetry that it is possible to have a model featuring i) but not ii). [1] The reason was that although the model in its topological phase (as detectable by, e.g., the Wilson loop) is not adiabatically connected to any atomic limit, there is no boundary which is left invariant by inversion symmetry, and thus no protected edge modes (as long as we do not consider chiral symmetry, which is local and therefore non-crystalline). This is a general feature of topological crystalline insulators: gapless symmetry-protected boundary modes also require the boundary on which they are localized to preserve the corresponding symmetry. In the following, we discuss several examples of topological crystalline phases and their invariants.

8.1 2D topological crystalline insulator

Here we show how crystalline symmetries can enrich the topological classification of band structures. We begin with a model with chiral symmetry in 2D. A natural non-local symmetry in 2D

[1] To be more precise, we have to differentiate more carefully: The two inversion-symmetry protected phases of the SSH model are actually both atomic limits, in the sense that the ground state can be written as a single Slater determinant of exponentially localized Wannier functions. However, these two atomic limits differ in the location (Wyckoff position) on which the Wannier function is localized. Therefore these two atomic limits are not adiabatically connected. More details on that point of view will follow in the lecture on topological quantum chemistry.

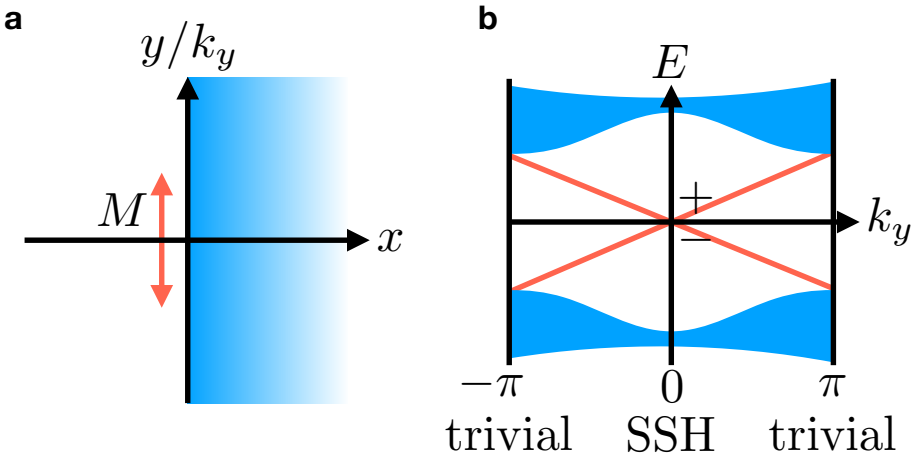

Figure 8.1: Real space geometry and spectrum of the mirror symmetric 2D model of a chiral symmetric topological crystalline insulator. ***a*** We consider a geometry where the system is terminated in x-direction but periodic in y-direction, retaining k_y as momentum quantum number. In particular, note that the surface in this semi-infinite slab geometry is mapped onto itself by the $M = M_y$ mirror symmetry, and therefore hosts gapless modes stemming from the nontrivial topology of the bulk. ***b*** Schematic spectrum of the model given by Eq. (8.1.1) in the presence of the bulk termination in x-direction. There are two counter-propagating chiral modes which are necessarily crossing at $k_y = 0$ due to the chiral symmetry. At hat point, they are also eigenstates of the mirror symmetry with eigenvalue ± 1, respectively. They are therefore protected from hybridization by the mirror symmetry.

we can add is a mirror symmetry, which leaves an edge invariant. While all 2D systems with just chiral symmetry (class AIII in the tenfold way) are topologically trivial, it will turn out that with mirror symmetry this is no longer the case when we require that mirror and chiral symmetry transformations commute.
The model we consider here is defined by the Bloch Hamiltonian

$$\begin{aligned} \mathcal{H}(\boldsymbol{k}) &= \begin{pmatrix} 0 & q(\boldsymbol{k}) \\ q^\dagger(\boldsymbol{k}) & 0 \end{pmatrix}, \\ q(\boldsymbol{k}) &= \begin{pmatrix} (1-\cos k_y) + e^{\mathrm{i}k_x} + \lambda & \sin k_y \\ -\sin k_y & (1-\cos k_y) + e^{-\mathrm{i}k_x} - \lambda \end{pmatrix}. \end{aligned} \tag{8.1.1}$$

The symmetry representations are

$$\begin{aligned} U_{\mathcal{C}}\mathcal{H}(\boldsymbol{k})U_{\mathcal{C}}^{-1} &= -\mathcal{H}(\boldsymbol{k}), \quad M_y\mathcal{H}(k_x,k_y)M_y^{-1} = \mathcal{H}(k_x,-k_y), \\ U_{\mathcal{C}} &= \begin{pmatrix} \mathbb{1}_{2\times 2} & 0 \\ 0 & -\mathbb{1}_{2\times 2} \end{pmatrix}, \quad M_y = \begin{pmatrix} \sigma_z & 0 \\ 0 & \sigma_z \end{pmatrix}, \end{aligned} \tag{8.1.2}$$

where $\mathbb{1}_{2\times 2}$ denotes the 2×2 identity matrix and λ represents a numerically small perturbation that breaks M_x symmetry. When we calculate the winding number along the path $k_x = 0 \to k_x = 2\pi$, $k_y = \text{const.}$ in the BZ, we find $\nu(k_y) = 0\ \forall k_y$. We can most easily see this by evaluating $\nu(0) = 0$ and noting that as the spectrum is gapped throughout the BZ, and the model has chiral symmetry, the result holds for all k_y.
In the presence of mirror symmetry, however, we can refine the topological characterization. Since in our case mirror symmetry satisfies $M_y^2 = 1$, its representation has eigenvalues ± 1. Given any line l_{M_y} in the BZ which is left invariant under the action of M_y, the eigenstates $|u_{\boldsymbol{k},n}\rangle$ of

$\mathcal{H}$ on l_{M_y} can be decomposed into two groups, $\{|u^+_{\boldsymbol{k},l}\rangle\}$ and $\{|u^-_{\boldsymbol{k},l'}\rangle\}$, with mirror eigenvalue ± 1, respectively. We can define the Wilson loop in each mirror subspace as

$$W^{\pm}[l_{M_y}] = \overleftarrow{\exp}\left[\mathrm{i}\int_{l_{M_y}} \mathrm{d}\boldsymbol{l}_{\boldsymbol{M_y}} \cdot \boldsymbol{\mathcal{A}}^{\pm}(\boldsymbol{k})\right], \tag{8.1.3}$$

where we have used the mirror-graded Berry connection

$$\boldsymbol{\mathcal{A}}^{\pm}_{m,n}(\boldsymbol{k}) = \mathrm{i}\langle u^{\pm}_{\boldsymbol{k},m}|\boldsymbol{\nabla}_{\boldsymbol{k}}|u^{\pm}_{\boldsymbol{k},n}\rangle, \qquad n,m = 1,\cdots,M. \tag{8.1.4}$$

For the two mirror invariant paths $l_{M_y} : k_x = 0 \to k_x = 2\pi, k_y = 0, \pi$, the mirror-graded topological polarization invariants evaluate to

$$\mathsf{P}_{M_y}(k_y) = \frac{1}{2}\left[\left(-\frac{\mathrm{i}}{2\pi}\log W^+(k_y)\right) - \left(-\frac{\mathrm{i}}{2\pi}\log W^-(k_y)\right)\right] = \begin{cases} 1/2 & k_y = 0 \\ 0 & k_y = \pi \end{cases}, \tag{8.1.5}$$

as can be directly seen from the relation of the model to two mirror-graded copies of the SSH model in the trivial ($k_y = \pi$) and nontrivial ($k_y = 0$) phase. This confirms that the 2D model is in a topologically nontrivial phase protected by mirror and chiral symmetry. With open boundary conditions, we will therefore find gapless states on both edges with normal to the x-direction (see Fig. 8.1***a*** for such a geometry), because these are mapped onto themselves under M_y. Since the model corresponds to a topological-to-trivial tuning of two copies of the SSH model with opposite winding number, we expect two anti-propagating chiral edge states, which cannot gap out at their crossing at $k_y = 0$ since they belong to different mirror subspaces at this point (see Fig. 8.1***b***). A simple way to see this is that mirror symmetry maps $k_y \to -k_y$, while it does not change the energy E. Therefore it exchanges states pairwise at generic momenta k_y and $-k_y$ and we can form symmetric and anti-symmetric superpositions of them to get mirror eigenstates with eigenvalue $+1$ and -1, respectively. The trace of the representation of M_y on this two-dimensional subspace is therefore 0 at almost all momenta and in particular cannot change discontinuously at $k_y = 0$. Alternatively, direct inspection of the Hamiltonian (8.1.1) at $k_y = 0$ reveals that it is composed of two copies of the SSH model, and in view of the form of the mirror symmetry M_y, the two copies reside in opposite mirror subspaces. As a consequence, their end states (the edge modes at $k_y = 0$) also have opposite mirror eigenvalues and cannot hybridize.

Another 2D system which has two anti-propagating chiral edge modes is the quantum spin Hall effect protected by time-reversal symmetry, where the edge modes are localized on all boundaries. It corresponds to two Chern insulators, one for spin up and one for spin down. The present model may be viewed as a close relative, where the edge modes are protected by mirror and chiral symmetry as opposed to time-reversal, and are only present on edges preserving the mirror symmetry.

8.2 Mirror Chern number

In the previous section, we have witnessed an example of a general scheme to construct topological BZ invariants going beyond the tenfold way for systems protected by crystalline symmetries: since a crystalline symmetry acts non-locally in space, it also maps different parts of the BZ onto each other. However, when there are submanifolds of the BZ which are left invariant by the action of the symmetry considered, we may evaluate a non-crystalline invariant on them, suited for the dimension and symmetry class of the corresponding submanifold, as long as we restrict ourselves to one of the symmetry's eigenspaces.

The most prominent example of this construction is the mirror Chern number C_{m} in three-dimensional systems. Since for a spinful system, mirror symmetry M squares to $M^2 = -1$ its

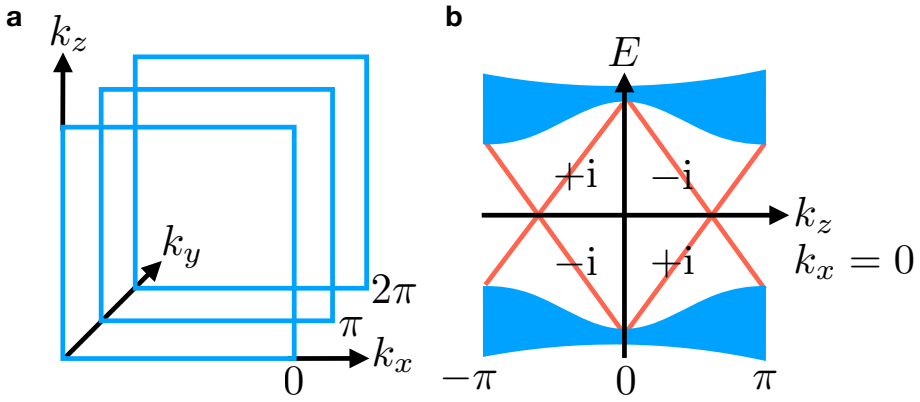

Figure 8.2: Mirror Chern planes in the BZ and schematic surface spectrum for a time-reversal topological crystalline insulator with $\mathsf{C}_\mathrm{m} = 2$. ***a*** For the mirror symmetry M_y, there are two planes in the BZ which are left invariant by it and can therefore be used to define a mirror Chern number: the plane at $k_y = 0$ and the one at $k_y = \pi$. ***b*** A mirror Chern number $C_\mathrm{m} = 2$ enforces the presence of two chiral left-movers and two chiral right-movers along mirror symmetric lines in the surface BZ of any surface mapped onto itself by the mirror symmetry. For M_y, this is, e.g., the case for the surface obtained by terminating the bulk in x-direction and retaining k_y and k_z as momentum quantum numbers. At $k_y = 0$ all bands are eigenstates of the mirror symmetry with eigenvalues as shown, and thus prevented from gapping out. At finite k_y however, hybridization becomes possible and we are left with two Dirac cones in the surface BZ in the case at hand.

representation in this case has eigenvalues $\pm\mathrm{i}$. Let Σ be a surface in the BZ which is left invariant under the action of M, such as the surfaces shown in Fig. 8.2***a*** for M_y. Then, the eigenstates $|u_{\boldsymbol{k},n}\rangle$ of the Hamiltonian on Σ can be decomposed into two groups, $\{|u^+_{\boldsymbol{k},l}\rangle\}$ and $\{|u^-_{\boldsymbol{k},l'}\rangle\}$, with mirror eigenvalues $+\mathrm{i}$ and $-\mathrm{i}$, respectively. Time-reversal symmetry maps one mirror subspace onto the other; if it is present, the two mirror eigenspaces are of the same dimension. We may define the Chern number in each mirror subspace as

$$\mathsf{C}_\pm = \frac{1}{2\pi}\int_\Sigma dk_x dk_z \mathrm{Tr}\left[\mathcal{F}^\pm_{xz}(\boldsymbol{k})\right]. \tag{8.2.1}$$

Here

$$\mathcal{F}^\pm_{ab}(\boldsymbol{k}) = \partial_a \mathcal{A}^+_b(\boldsymbol{k}) - \partial_b \mathcal{A}^+_a(\boldsymbol{k}) - \mathrm{i}\left[\mathcal{A}^+_a(\boldsymbol{k}), \mathcal{A}^+_b(\boldsymbol{k})\right] \tag{8.2.2}$$

is the non-Abelian Berry curvature field in the $\pm\mathrm{i}$ mirror subspace, with $\mathcal{A}^\pm_{a;l,l'}(\boldsymbol{k}) = \mathrm{i}\,\langle u^\pm_{\boldsymbol{k},l}|\partial_a|u^\pm_{\boldsymbol{k},l'}\rangle$, and matrix multiplication is implied. Since $\mathrm{Tr}\left[\mathcal{A}^+_a(\boldsymbol{k}), \mathcal{A}^+_b(\boldsymbol{k})\right] = 0$, this corresponds to the usual Chern number, but restricted to a single mirror subspace. Note that in time-reversal symmetric systems we have $\mathsf{C}_+ = -\mathsf{C}_-$, and can thus define the mirror Chern number

$$\mathsf{C}_\mathrm{m} := (\mathsf{C}_+ - \mathsf{C}_-)/2. \tag{8.2.3}$$

A non-vanishing mirror Chern number implies that the Bloch Hamiltonian on Σ corresponds to a time-reversal pair of Chern insulators. Thus, the full model will host C_m Kramers pairs of gapless modes on an M-invariant line in any surface BZ corresponding to a real space boundary which is mapped onto itself under the mirror symmetry M. These Kramers pairs of modes will be generically gapped out away from the lines in the surface BZ which are invariant under the mirror symmetry, and therefore form surface Dirac cones. Indeed, when C_m is odd in a time-reversal symmetric system, this implies an odd number of Dirac cones in any surface BZ, since then the system realizes a conventional time-reversal invariant topological insulator with the

Dirac cones located at time-reversal invariant surface momenta. When C_m is even, the surface Dirac cones exist only on mirror symmetric surfaces and are located at generic momenta along the mirror invariant lines of the surface BZ (see Fig. 8.2***b***). This inherently crystalline case is realized in the band structure of tin telluride, SnTe.

8.3 $C_2^z\mathcal{T}$-invariant topological crystalline insulator

Here we present another example of a topological crystalline insulator in 3D in order to show that surface Dirac cones protected by crystalline symmetries can also appear at generic, low-symmetry, momenta in the surface BZ. We consider a system that is invariant under the combination $C_2^z\mathcal{T}$ of a two-fold rotation C_2^z around the z axis and time-reversal symmetry $\mathcal{T}$. Note that we take both symmetries to be broken individually.
To understand how this symmetry can protect a topological phase, let us review how time-reversal protects a Dirac cone on the surface of a conventional topological insulator. The effective Hamiltonian on the boundary with surface normal along z of a 3D time-reversal symmetric topological insulator takes the form

$$\mathcal{H}(\boldsymbol{k}) = k_y\sigma_x - k_x\sigma_y. \tag{8.3.1}$$

The symmetries are realized as

$$\begin{aligned} &\mathcal{T}\mathcal{H}(\boldsymbol{k})\mathcal{T}^{-1} = \mathcal{H}(-\boldsymbol{k}), \quad \mathcal{T} = \mathrm{i}\sigma_y K, \\ &C_2^z\mathcal{H}(\boldsymbol{k})(C_2^z)^{-1} = \mathcal{H}(-\boldsymbol{k}), \quad C_2^z = \sigma_z, \end{aligned} \tag{8.3.2}$$

where we denote by K complex conjugation. Now, the unique mass term for $\mathcal{H}(\boldsymbol{k})$ which gaps out the Dirac cone is $m\sigma_z$. This term is forbidden by time-reversal as expected, since it does not commute with $\mathcal{T}$.
If we dispense with $\mathcal{T}$ symmetry and only require invariance under $C_2^z\mathcal{T} = \sigma_x K$, the mass term is still forbidden. However, the addition of other constant terms to the Hamiltonian is now allowed. The freedom we have is to shift the Dirac cone away from the time-reversal symmetric point $\boldsymbol{k} = 0$ by changing the Hamiltonian to

$$\mathcal{H}(\boldsymbol{k}) = (k_y - a)\sigma_x - (k_x - b)\sigma_y, \tag{8.3.3}$$

with some arbitrary parameters a and b. Therefore, the phase stays topologically nontrivial, but has a different boundary spectrum from that of a normal topological insulator. On surfaces preserving $C_2^z\mathcal{T}$ symmetry, any odd number of Dirac cones are stable but are in general shifted away from the time-reversal invariant surface momenta. On the surfaces that are not invariant under $C_2^z\mathcal{T}$, the Dirac cones may be gapped out, since $\mathcal{T}$ is broken. This amounts to a $\mathbb{Z}_2$ topological classification of $C_2^z\mathcal{T}$-invariant 3D topological crystalline insulators.

8.4 Higher-order topological insulators

So far, when we discussed topological systems in d dimensions, we only considered $(d-1)$ dimensional boundaries which could host gapless states due to the nontrivial topology of the bulk. These systems belong to the class of "first-order" topological insulators. In the following, we will give an introduction to second-order topological insulators which have gapless modes on $(d-2)$ dimensional boundaries, that is, on corners in 2D and hinges in 3D, while the boundaries of dimension $(d-1)$ (i.e., the edges of a 2D system and the surfaces of a 3D system) are generically gapped. Higher-order topological insulators require spatial symmetries for their protection and thus constitute an extension of the notion of topological crystalline phases of matter.

8.4.1 2D model with corner modes

A natural avenue of constructing a higher-order topological phase in 2D is to consider a 2D generalization of the SSH model with unit cell as shown in Fig. 8.3***a*** (disregarding the colors in this figure for now) and alternating hoppings t and t' in both the x and y-directions. However, naively the bulk of the model defined this way with all hoppings of positive sign is gapless. This can be most easily seen in the fully atomic limit $t' = 0$, $t \neq 0$, where the Hamiltonian reduces to a sum over intra-unit cell Hamiltonians of the form

$$\mathcal{H} = t \begin{pmatrix} 0 & 1 & 0 & 1 \\ 1 & 0 & 1 & 0 \\ 0 & 1 & 0 & 1 \\ 1 & 0 & 1 & 0 \end{pmatrix}, \tag{8.4.1}$$

which has obviously zero determinant and therefore gapless modes.
This was amended in a model introduced by Benalcazar, Bernevig and Hughes, which gave the first example of a higher-order topological insulator, by introducing a magnetic flux of π per plaquette. A specific gauge choice realizing this corresponds to reversing the sign of the hoppings along the blue lines in Fig. 8.3***a***. The model then has a gapped bulk, but gapless corner modes. This can be most easily seen in the fully dimerized limit $t = 0$, $t' \neq 0$, where one site in each corner unit cell is not acted upon by any term in the Hamiltonian. However, to protect the corner modes we have to include a spatial symmetry in addition to chiral symmetry, since we could otherwise perform an edge manipulation which leaves the bulk (and in particular, its gap) invariant but annihilates one corner mode with another. A natural candidate for this is the pair of diagonal mirror symmetries M_{xy} and $M_{x\bar{y}}$, which each leave a pair of corners invariant and therefore allow for protected gapless modes on them.
Note that we cannot arrive at the same phase by just combining two one-dimensional SSH models glued to the edges of a trivially gapped 2D system: By the mirror symmetry, the two SSH chains on edges that meet in a corner would have to be in the same topological phase. Thus, each would contribute one corner mode. At a single corner, we would therefore have a pair of modes which is not prevented by symmetry from being shifted to finite energies by a perturbation term. This consideration establishes the bulk model we introduced as an intrinsically 2D topological phase of matter. We will now present three alternative approaches to characterize the topology as well as the gapless corner modes of the model.

Elementary mirror subspace analysis

The plaquettes along the $x\bar{y}$ diagonal are the only parts of the Hamiltonian mapped onto themselves by the $M_{x\bar{y}}$ mirror symmetry. In the fully dimerized limit $t' \neq 0$, $t = 0$, we may consider the Hamiltonian as well as the action of $M_{x\bar{y}}$ on a single inter-unit cell plaquette on the diagonal of the system as given by

$$\mathcal{H} = t' \begin{pmatrix} 0 & 1 & 0 & -1 \\ 1 & 0 & 1 & 0 \\ 0 & 1 & 0 & 1 \\ -1 & 0 & 1 & 0 \end{pmatrix}, \quad M_{x\bar{y}} = \begin{pmatrix} 0 & 0 & 1 & 0 \\ 0 & 1 & 0 & 0 \\ 1 & 0 & 0 & 0 \\ 0 & 0 & 0 & -1 \end{pmatrix}. \tag{8.4.2}$$

$M_{x\bar{y}}$ has eigenvectors

$$|+_1\rangle = \begin{pmatrix} 0 \\ 1 \\ 0 \\ 0 \end{pmatrix}, \quad |+_2\rangle = \frac{1}{\sqrt{2}} \begin{pmatrix} 1 \\ 0 \\ 1 \\ 0 \end{pmatrix}, \quad |-_1\rangle = \begin{pmatrix} 0 \\ 0 \\ 0 \\ 1 \end{pmatrix}, \quad |-_2\rangle = \frac{1}{\sqrt{2}} \begin{pmatrix} 1 \\ 0 \\ -1 \\ 0 \end{pmatrix} \tag{8.4.3}$$

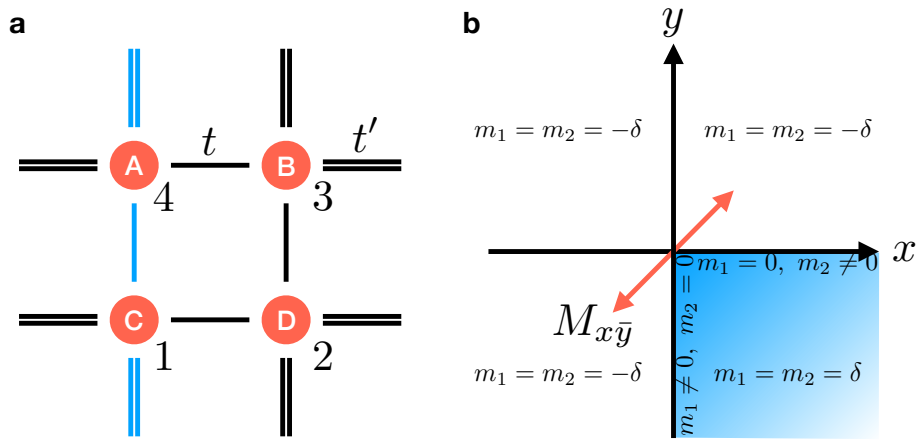

Figure 8.3: Higher-order 2D SSH model. ***a*** The model features intra-unit cell hopping with strength t as well as inter-unit cell hopping with strength t'. For the topological phase we require $t' > t$. In particular, in the fully dimerized limit $t = 0$, $t' \neq 0$ it becomes evident that when we cut the system in two directions to create a corner, there is one dangling site which is not acted upon by any term in the Hamiltonian and therefore provides a zero-mode. The unit cell contains a π-flux per plaquette, which is realized by all blue hoppings being negative, while all black hoppings are positive. ***b*** Vortex geometry of the prefactors of the two masses in Eq. (8.4.9). We imply a smooth interpolation between the mass values given in the bulk, on the edges, and on the outside. At the corner, the masses vanish and they hence form a vortex-like structure around it.

with eigenvalues $+1, +1, -1, -1$, respectively. Since $[\mathcal{H}, M_{x\bar{y}}] = 0$ we know that the Hamiltonian block-diagonalizes into the two mirror subspaces, and we may calculate its form in each Block separately,

$$(\mathcal{H}_+)_{ij} = \langle +_i | \mathcal{H} | +_j \rangle \to \mathcal{H}_+ = \begin{pmatrix} 0 & \sqrt{2} \\ \sqrt{2} & 0 \end{pmatrix} = \mathcal{H}_-. \tag{8.4.4}$$

This, however, is exactly the form taken by a single SSH model in the fully dimerized, and therefore topologically nontrivial, phase (this is because here we have focussed on a plaquette on the diagonal with t' hopping, an adjoining plaquette with t hopping would correspond to the weak bonds in the mirror subspace SSH model). We may therefore interpret our model along one diagonal as two nontrivial SSH models, one for each mirror subspace and protected by the chiral symmetry. Naively this would imply two end modes. However, this is not the case. In the upper left corner, for example, only a single A site is left from an inter-unit cell plaquette (see Fig. 8.3***a***), which happens to have mirror eigenvalue -1. Correspondingly, the lower right corner hosts a dangling D site, which has mirror eigenvalue $+1$. Thus, due to this modified bulk-boundary correspondence of the higher-order topological insulator, each of the two diagonal SSH chains has only one end state at opposite ends. These form the corner modes of the higher-order topological insulator.

Mirror-graded winding number

In analogy to the mirror graded Wilson loop introduced in Sec. 8.1, we can calculate the mirror-graded winding number suited for systems with chiral symmetry. For this we need the full Bloch Hamiltonian, which is given by

$$\mathcal{H}(\boldsymbol{k}) = (1 + \lambda \cos k_x)\tau_0\sigma_x + (1 + \lambda \cos k_y)\tau_y\sigma_y - \lambda \sin k_x \tau_z\sigma_y + \lambda \sin k_y \tau_x\sigma_y. \tag{8.4.5}$$

Note that by a term such as $\sigma_x\tau_0$ we really mean the tensor product $\sigma_x \otimes \tau_0$ of two Pauli matrices. Here, we have chosen $t = 1$ and $t' = \lambda$. The case where $\lambda > 1$ then corresponds to the topological phase. Along the diagonals of the BZ (and only there), the Hamiltonian may again be block-diagonalized by the mirror symmetries. Let us consider for concreteness the $\boldsymbol{k} = (k, k)$ diagonal, which is invariant under M_{xy} with representation

$$M_{xy} = \begin{pmatrix} -1 & 0 & 0 & 0 \\ 0 & 0 & 0 & 1 \\ 0 & 0 & 1 & 0 \\ 0 & 1 & 0 & 0 \end{pmatrix}. \tag{8.4.6}$$

With a transformation that diagonalizes M_{xy}, we can bring the Hamiltonian in the form

$$\tilde{\mathcal{H}}(k,k) = \begin{pmatrix} 0 & q_+(k) & 0 & 0 \\ q_+^\dagger(k) & 0 & 0 & 0 \\ 0 & 0 & 0 & q_-(k) \\ 0 & 0 & q_-^\dagger(k) & 0 \end{pmatrix}, \quad q_\pm(k) = \sqrt{2}(1 + \lambda e^{\mp \mathrm{i}k}). \tag{8.4.7}$$

We see that in the two mirror eigenspaces $\tilde{\mathcal{H}}(k,k)$ takes the form of an SSH model. Defining

$$\nu_\pm = \frac{\mathrm{i}}{2\pi} \int \mathrm{d}k \, \mathrm{Tr}\left[\tilde{q}_\pm(k)\partial_k \tilde{q}_\pm^\dagger(k)\right] \tag{8.4.8}$$

in analogy to our definition of the one-dimensional winding number, where we have appropriately normalized $\tilde{q}_\pm(k) = q_\pm(k)/|q_\pm(k)|$, we obtain $\nu_\pm = \pm 1$ and therefore $\nu_{M_{xy}} = 1$ for the mirror-graded winding number $\nu_{M_{xy}} = (\nu_+ - \nu_-)/2$. As long as the system obeys the mirror symmetry and the chiral symmetry, $\nu_{M_{xy}}$ is a well-defined topological invariant that cannot be changed without closing the bulk gap of the 2D system.

Dirac picture of corner states

An alternative and very fruitful viewpoint of topological phases of matter arises from the study of continuum Dirac Hamiltonians corresponding to a given phase. For example, the band inversion of a first-order topological insulator can be efficiently captured by the Hamiltonian of a single gapped Dirac cone with mass m in the bulk of the material, and mass $(-m)$ in its exterior. One can then show that the domain wall in m binds exactly one gapless Dirac cone to the surface of the material. We want to develop an analogous understanding of higher-order topological phases as exemplified by the model studied in this section.
For the topological phase transition at $\lambda = 1$ in Eq. (8.4.5), there is a gap closing at $\boldsymbol{k}_0 = (\pi, \pi)$. Expanding $\mathcal{H}(\boldsymbol{k})$ around this point to first order and setting $\boldsymbol{k} = \boldsymbol{k}_0 + \boldsymbol{p}$, we obtain

$$\begin{aligned} \mathcal{H}(\boldsymbol{k}) &= (1-\lambda)\tau_0\sigma_x + (1-\lambda)\tau_y\sigma_y + \lambda p_x \, \tau_z\sigma_y - \lambda p_y \, \tau_x\sigma_y \\ &\approx \delta\tau_0\sigma_x + \delta\tau_y\sigma_y + p_x \, \tau_z\sigma_y - p_y \, \tau_x\sigma_y, \end{aligned} \tag{8.4.9}$$

where we have defined $\delta = (1 - \lambda) \ll 1$ and $\lambda \approx 1$. Note that all matrices anticommute and that there are two mass terms, both proportional to δ, in accordance with the gap-closing phase transition at $\delta = 0$. When terminating the system, a boundary is modeled by a spatial dependence of these masses. We consider the geometry shown in Fig. 8.3***b***, where two edges meet in a corner. The mirror symmetry $M_{x\bar{y}}$ maps one edge to the other but leaves the corner invariant. As a result, the mirror symmetry does not pose any restrictions on the masses on one edge, but once their form is determined on one edge, they are also fixed on the other edge by $M_{x\bar{y}}$. In fact, since $M_{x\bar{y}}\tau_0\sigma_x M_{x\bar{y}}^{-1} = \tau_y\sigma_y$ with $M_{x\bar{y}} = (\tau_x\sigma_0 + \tau_z\sigma_0 + \tau_x\sigma_z - \tau_z\sigma_z)/2$ and vice versa, we may consider the particularly convenient choice of Fig. 8.3***b*** for the mass configuration of the corner geometry.

From Fig. 8.3***b***, it becomes evident that the symmetries dictate that the masses, when considered as real and imaginary part of a complex number, wind once around the origin of the corresponding complex plane (at which the system becomes gapless) as we go once around the corner in real space. They are mathematically equivalent to a vortex in a p-wave superconductor, which is known to bind a single Majorana zero-mode. We can therefore infer the presence of a single gapless corner state for the model considered in this section from its Dirac Hamiltonian.
To be more explicit, denoting by $m_1(x,y)$ and $m_2(x,y)$ the position-dependent prefactors of $\sigma_x\tau_0$ and $\sigma_y\tau_y$, respectively, we may adiabatically evolve the Hamiltonian to a form where the mass term vortex is realized in the particularly natural form $m_1(x,y)+\mathrm{i}m_2(x,y) = x+\mathrm{i}y = z$, where z denotes the complex number corresponding to the 2D real space position (x,y). After performing a C_3 rotation about the (111)-axis in τ space, which effects the replacement $\tau_x \to \tau_y \to \tau_z \to \tau_x$, and exchanging the order of τ and σ in the tensor product, the resulting matrix takes on the particularly nice form

$$\begin{aligned} \mathcal{H}(\boldsymbol{k}) &= \begin{pmatrix} 0 & q(\boldsymbol{k}) \\ q^\dagger(\boldsymbol{k}) & 0 \end{pmatrix}, \\ q(\boldsymbol{k}) &= \begin{pmatrix} m_1 - \mathrm{i}m_2 & -\mathrm{i}p_x + p_y \\ -\mathrm{i}p_x - p_y & m_1 + \mathrm{i}m_2 \end{pmatrix} = \begin{pmatrix} \bar{z} & -\partial_{\bar{z}} \\ -\partial_z & z \end{pmatrix} \\ \to \quad q^\dagger(\boldsymbol{k}) &= \begin{pmatrix} z & \partial_{\bar{z}} \\ \partial_z & \bar{z} \end{pmatrix}. \end{aligned} \tag{8.4.10}$$

While for $q^\dagger(\boldsymbol{k})$, there is one zero-energy solution $|\Psi\rangle = e^{-z\bar{z}}(1,1)$, the corresponding solution $|\tilde{\Psi}\rangle = e^{\frac{z^2+\bar{z}^2}{2}}(1,1)$ for $q(\boldsymbol{k})$ is not normalizable. We thus conclude that there is one zero-mode with eigenfunction $(|\Psi\rangle, |0\rangle)$ localized at the corner of the sample.

8.4.2 3D model with hinge modes

To construct a higher-order topological insulator in 3D, we start from a time-reversal invariant topological crystalline insulator with mirror Chern numbers in its bulk BZ. For the sake of simplicity we restrict to the case where only the mirror Chern number C_m belonging to the M_y symmetry is non-vanishing because the argument goes through for each mirror Chern number separately. We will now show that in an open geometry with surface normals along the xy and $x\bar{y}$ direction, $\mathsf{C}_\mathrm{m} = 2$ implies the presence of a single time-reversal pair of gapless chiral hinge modes on the intersection of the (110) and $(1\bar{1}0)$ surfaces (see Fig. 8.4).
As discussed in Sec. 8.2, for M_y symmetry, a nonzero $\mathsf{C}_\mathrm{m} = 2$ enforces two gapless Dirac cones in the surface BZ of the (100) termination, which is mapped onto itself by M_y. Note that on this surface, with normal in x-direction, k_y and k_z are still good momentum quantum numbers. The Hamiltonian for a single surface Dirac cone can be written as

$$\mathcal{H}(k_y, k_z) = v_1\sigma_z k_y + v_z\sigma_x(k_z - k_z^0), \tag{8.4.11}$$

where the mirror symmetry is represented by $M_y = \mathrm{i}\sigma_x$ and thus prevents a mass term of the form $+m\sigma_y$ from appearing. To arrive at a theory describing the intersection of the (110) and $(1\bar{1}0)$ boundaries, we introduce a mirror-symmetric kink in the (100) surface (see Fig. 8.4***a***) and so first consider the intersection of two perturbatively small rotations of the (100) surface, one to a $(1,\alpha,0)$ termination and the other to a $(1,-\alpha,0)$ termination with $\alpha \ll 1$. The Hamiltonian on the $(1,\pm\alpha,0)$ surface becomes

$$\begin{aligned} \mathcal{H}_\pm(k_y, k_z) &= v_1\sigma_z(k_y \pm \rho) + v_z\sigma_x(k_z - k_z^0) \pm m\sigma_y \\ &\equiv v_1\tilde{k}_y^\pm\sigma_z + v_z\tilde{k}_z\sigma_x \pm m\sigma_y, \end{aligned} \tag{8.4.12}$$

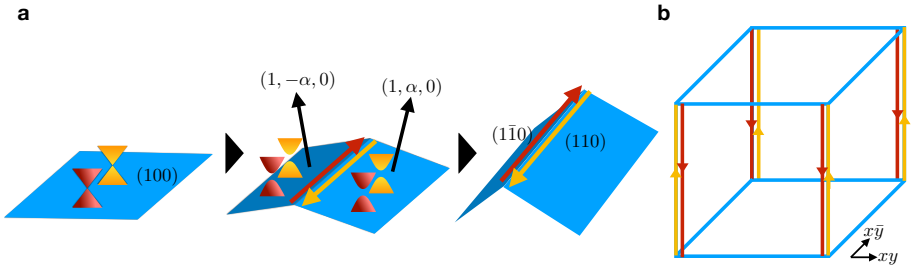

Figure 8.4: Construction of a 3D second-order topological insulator. ***a*** We begin with a surface left invariant by M_y on which $\mathsf{C}_\mathrm{m} = 2$ implies two gapless Dirac cones. When slightly tilting the surface in opposite directions to form a kink, the Dirac cones on the new surfaces on either side of the kink may be gapped out with opposite masses, since the mirror symmetry maps one into the other and anti commutes with the Dirac mass term. Since a domain wall in a Dirac mass binds a single zero-mode, and the two Dirac cones on each surface are mapped into each other by time-reversal, a Kramers pair of gapless hinge modes emerges on the intersection. When continuing to bend the surfaces to create a right angle, these modes cannot vanish since they are protected by the M_y mirror symmetry. ***b*** By this argument we can infer time-reversal paired hinge modes on each hinge along the x (and y, if we also take into account the mirror symmetry M_x along with $\mathsf{C}_\mathrm{m} = 2$) direction.

where m and ρ are small parameters of order α and we have omitted the irrelevant coordinate shifts in the last line. This Hamiltonian describes a gapped Dirac cone, the mass term is now allowed by mirror symmetry since the surfaces considered are no longer invariant under it. Instead, they are mapped onto each other and thus have to carry opposite mass. We note that by this consideration the hinge between the $(1,\alpha,0)$ and $(1,-\alpha,0)$ surfaces constitutes a domain wall in a Dirac mass extended in z-direction, which is known to host a single chiral mode.
We will now explicitly solve for this domain wall mode at $\tilde{k}_z = 0$ by going to real space in y-direction. Making the replacement $\tilde{k}_y^{\pm} \to -\mathrm{i}\partial_y$, the Hamiltonian on either side of the hinge becomes

$$\mathcal{H}_\pm = \begin{pmatrix} -\mathrm{i}v_1\partial_y & \pm \mathrm{i}m \\ \mp \mathrm{i}m & \mathrm{i}v_1\partial_y \end{pmatrix}. \tag{8.4.13}$$

$\mathcal{H}_+$, for which $y > 0$, has one normalizable zero-energy solution given by $|\Psi_+\rangle = e^{-\kappa y}(1,1)$ (where we assume $\kappa = m/v_1 > 0$ without loss of generality). $\mathcal{H}_-$, for which $y < 0$, has another normalizable zero-energy solution given by $|\Psi_-\rangle = e^{\kappa y}(1,1)$. Since the spinor $(1,1)$ of the solutions is the same on either side of the hinge, the two solutions can be matched up in a continuous wave function. We obtain a single normalizable zero-energy solution for the full system at $k_z = 0$, which is falling off exponentially away from the hinge with a real-space dependence given by $|\Psi\rangle = e^{-\kappa|y|}(1,1)$. To determine its dispersion, we may calculate the energy shift for an infinitesimal k_z in first-order perturbation theory to find

$$\Delta E(\tilde{k}_z) = \langle\Psi|\, v_z\tilde{k}_z\sigma_x\,|\Psi\rangle = +v_z\tilde{k}_z \tag{8.4.14}$$

We have therefore established the presence of a single linearly dispersing chiral mode on the hinge between the $(1,\alpha,0)$ and $(1,-\alpha,0)$ surfaces by considering what happens to a single Dirac cone on the $(1,0,0)$ surface when a kink is introduced. The full model, which by $\mathsf{C}_\mathrm{m} = 2$ has two (100) surface Dirac cones paired by time-reversal symmetry, therefore hosts a Kramers pair of hinge modes on the intersection between the $(1,\alpha,0)$ and $(1,-\alpha,0)$ surfaces. These surfaces themselves are gapped. The two modes forming the hinge Kramers pair have opposite mirror eigenvalue. Increasing α non-perturbatively to 1 in a mirror-symmetric fashion cannot change the number of these hinge modes, since the chiral modes belong to different mirror subspaces

and are thus stable to any perturbation preserving the mirror symmetry. By this reasoning, we end up with a pair of chiral modes at each hinge in the geometry of Fig. 8.4***b***.

References

1. Fu, L. "Topological Crystalline Insulators". *Phys. Rev. Lett.* **106,** 106802. http://dx.doi.org/10.1103/PhysRevLett.106.106802 (2011).
2. Fang, C. & Fu, L. "New classes of three-dimensional topological crystalline insulators: Nonsymmorphic and magnetic". *Phys. Rev. B* **91,** 161105(R). https://doi.org/10.1103/PhysRevB.91.161105 (2015).
3. Benalcazar, W. A., Bernevig, B. A. & Hughes, T. L. "Quantized Electric Multipole Insulators". *Science* **357,** 61. https://dx.doi.org/10.1126/science.aah6442 (2017).
4. Serra-Garcia, M. *et al.* "Observation of a phononic quadrupole insulator". *Nature* **555,** 342. https://dx.doi.org/10.1038/nature25156 (2018).

Chapter 9

Topological Crystalline Insulators II: Topological quantum chemistry

Learning goals

- We understand what we mean by Wannierizablity.
- We know how to think of a band as a representation of the space group.
- We know how to construct elementary band representations.
- We can use the Bilbao server to analyze bands according to their symmetry properties.

- B. Bradlyn, L. and Elcoro, J. Cano, M. G. Vergniory, Z. Wang, C. Felser, M. I. Aroyo, and B. A. Bernevig, Nature **537**, 298 (2017)

9.0 Prerequisites

In this chapter we introduce a way to characterize the topology of Bloch bands stabilized by space group symmetries. To this end we will construct representations of the infinite space groups (the group of discrete translations are not closed under a finite number of group elements). As a prerequisite we build on basic knowledge of representation theory. In particular, we assume that you know

1. what an irreducible representation (irrep) is.
2. that irreps of dimension larger than one may split, if the symmetry is reduced. For example the p_x, p_y, p_z orbitals forming the spin-1 triplet

$$+ : p_x + \mathrm{i}p_y \tag{9.0.1}$$
$$0 : p_z \tag{9.0.2}$$
$$- : p_x - \mathrm{i}p_y \tag{9.0.3}$$

   are splitting into the two individual irreps of $p_x \pm \mathrm{i}p_y$ and p_z if $SO(3)$ is reduced to, e.g, C_{4v}.
3. how to use character tables to do this symmetry reduction.
4. about double groups: If spin-1/2 particles are involved, we supplement all group elements to also appear with an additional rotation by 2π. For the irreps where a spin-1/2 particles is involved all characters acquire a minus sign by this. Their names typically carry a bar as for example in $\overline{E}_{1g}$.

9.1 Wannierizability

In a band insulator we are free to choose a basis in which to write down the wave-functions of all filled bands. Let us consider a Bloch problem

$$\sum_{\beta} \mathcal{H}_{\alpha,\beta}(\boldsymbol{k}) u_{\boldsymbol{k};a,\beta} = \epsilon_a(\boldsymbol{k}) u_{\boldsymbol{k};a,\alpha} \tag{9.1.1}$$

where a enumerates the energy bands, $\boldsymbol{k}$ runs over the Brillouin zone and α, β encode some orbital or sub-lattice degree of freedom. We can go from a momentum space picture to a real space description in term of *Wannier functions*

$$\psi_{a,\alpha}(\boldsymbol{r} - \boldsymbol{R}_i) = \int_{\mathrm{BZ}} \mathrm{d}^d\boldsymbol{k}\, u_{\boldsymbol{k};a,\alpha} e^{\mathrm{i}\boldsymbol{k}\cdot(\boldsymbol{r}-\boldsymbol{R}_i)}. \tag{9.1.2}$$

If we want these Wannier functions to serve as a basis for the ground-state, we have to consider all $a \leq n$, where n is the number of filled bands. Already in 1959 Walter Kohn [3] realized, that the Wannier functions are only exponentially decaying if we choose Bloch functions $u_{\boldsymbol{k};a,\alpha}$ which are smooth in $\boldsymbol{k}$.[1] Given what we learned in the last chapters, we immediately observe that $\psi_{a,\alpha}(\boldsymbol{r} - \boldsymbol{R}_i)$ are gauge dependent under a set of U(n) transformations (one per $\boldsymbol{k}$). In other words, we need to choose a *smooth* U(n) *gauge* for the Wannier functions to be exponentially localized. We know, however, that the topological indices introduced in Chap. 7 are only non-vanishing if there is an obstruction to choose a smooth gauge.[2] *Therefore, we can also use the (in-) ability to choose a set of basis functions which are all exponentially localized as a definition for a topological system:* If we can smoothly transform the $\psi_{a,\alpha}(\boldsymbol{r} - \boldsymbol{R}_i)$ to be exponentially localized, i.e., if we can choose an *atomic limit*, we call a system *trivial*. Finally, we have seen that symmetries can give rise to topological phases that would be trivial in their absence, i.e., the adiabatic path to the atomic limit may now be obstructed by the constraints imposed by the symmetry. The same holds here: We demand the atomic limit to be compatible with a set of (crystalline) symmetries.

We are now in the position to define *Wannierizablity*. We call a set of bands Wannierizable if we can find a basis transformation to a set of wave-functions $\psi_{a,\alpha}(\boldsymbol{r} - \boldsymbol{R}_i)$ that are symmetric and exponentially localized. If a set of bands is not Wannierizable, we call it topological.

An important remark is in order: If we formulate a tight-binding model for a set of bands, we implicitly assume that we used exponentially localized wave-functions when we wrote down the Hamiltonian. Therefore, the set of all bands together arising from such a tight-binding model are bound to be trivial. The only option to have topological phases is, if there is more than one band and they are separated by a gap.

With these introductory remarks, we can outline the program of what goes under the name of *topological quantum chemistry* [1]. The symmetries we are dealing with are the 230 space groups, i.e., all symmetry groups arising in crystalline systems. The core idea is, that we can *construct all possible band-structures that can arise from symmetric Wannier functions* positioned in a lattice obeying one of the 230 symmetry groups. Once one achieves this goal, one has, by construction, an *exhaustive list of all trivial bands in each of the space groups*. Using this exhaustive list, we can check for any band-structure we obtain for a concrete problem if and how it fits into this exhaustive table. If it does not, we know we deal with a topological band. As an additional bonus we will see how this approach gives rise to two main classes of topological bands: stable topological and fragile topological. While the latter sounds like an oxymoron, we will see that this type of topology is neither "weak" nor esoteric.

[1] Remember that that the Fourier transformation of a function $u_{\boldsymbol{k}}$ that is s-fold differentiable is falling off at least as $1/|\boldsymbol{x}|^s$. Hence, only for C^∞-functions can we expect exponentially localized Wannier functions.

[2] Remember that the Berry curvature $\boldsymbol{\mathcal{F}}$ can be written as the (higher-dimensional generalizations) curl of a vector field $\boldsymbol{\mathcal{A}}$. Hence, by using Stoke's theorem on a closed manifold (the d-torus) we obtain a zero index if the Berry connection $\boldsymbol{\mathcal{A}}$ is free of divergencies.

In the following, we will introduce all the needed definitions and develop the general strategy. We illustrate all these developments on the example the doubled lattice Dirac model introduced in Chap. 4.

9.2 Space groups

Theory: To introduce space groups we need to fix a few facts about crystals. Crystals are built from Bravais lattices where every *unit cell* in the lattice can be reached by a *discrete translation*

$$\boldsymbol{t} = n_i \, \boldsymbol{a}_i \qquad \text{with} \qquad \boldsymbol{n} \in \mathbb{Z}^d, \tag{9.2.1}$$

where the $\boldsymbol{a}_i$ are the lattice vectors. The Bravais lattice is isomorphic to $\mathbb{Z}^d$ and the group of translations $\{\boldsymbol{t}\}$ on the Bravais lattice is an *infinite group*. Note, that inside the unit cell, atoms can be arranged in arbitrary positions, called Wyckoff positions. The full symmetry group of the crystal can now be written as all operations that leave the crystal invariant and is called a space group G with elements g written as

$$g = \{R|\boldsymbol{r}\}. \tag{9.2.2}$$

The elements of R are in the *crystallographic point group* which leave one point invariant[3] and $\boldsymbol{r}$ are translations. The action of a group element g on a point in space $\boldsymbol{q}$ is given by

$$g\boldsymbol{q} = R\boldsymbol{q} + \boldsymbol{r}. \tag{9.2.3}$$

Note, that the space group generically contains pure translations $\{\mathbb{1}|\mathbf{t}\}$, pure point group operations $\{R|0\}$, as well as non-symmorphic elements which involve, e.g, a mirror operation and a half-lattice translation.
As we intend to investigate what kind of bands can be induced by symmetric orbitals, we need to talk about where we put these orbitals and what it means to be symmetric at the chosen locations. A generic point $\boldsymbol{q}$ inside the unit cell is called a *Wyckoff position*. For the remainder of this chapter we need the "most symmetric" positions called *maximal Wyckoff positions*.[4] Note that a Wyckoff position might not be invariant under all point group operations. The non-trivial images $g\boldsymbol{q} = R^{-1}\boldsymbol{q}$ form the *orbit* of such a position.
Example: We are interested in a system in the space group No. 123, also called $P4/mmm$. In fact, for the purpose of this lecture we are only interested in the planar version of $P4/mmm$. However, we need the out-of plane point group elements to fix the orbitals that we put onto the two-dimensional lattice.
The two dimensional Bravais lattice is generated by the lattice vectors

$$\boldsymbol{a}_1 = (1, 0), \tag{9.2.4}$$
$$\boldsymbol{a}_2 = (0, 1). \tag{9.2.5}$$

The space group $P4/mmm$ does not contain any non-symmorphic elements, i.e, all space group elements can be written as either $\{\mathbb{1}|\boldsymbol{t}\}$ with $\boldsymbol{t} = n_i\boldsymbol{a}_i$ or $\{R|0\}$ with $R \in D_{4h}$, the dihedral point group of $P4/mmm$.

[3] A point group is a symmetry group that leaves a point invariant. A *crystallographic* point group is a point group that is compatible with one of the Bravais lattices. As such, they can only contain discrete rotations, in fact rotations of order 1, 2, 3, 4, and 6. There are only 32 crystallographic point groups.

[4] We can define the *stabilizer group* $G_{\boldsymbol{q}}$, a subgroup of the full group G which leaves the point $\boldsymbol{q}$ invariant. The orbit of a Wyckoff position $\boldsymbol{q}$ is the set of all points generated from $\boldsymbol{q}$ by the application of all $g \in G$ onto that point. This leads to the *multiplicity of a Wyckoff postion*: the number of points in the orbit of $\boldsymbol{q}$. Finally, we can define *maximal Wyckoff positions*: a Wyckoff position $\boldsymbol{q}$ is non-maximal if there exists a group H such that $G_{\boldsymbol{q}} \subset H \subset G$. A Wyckoff position that is not non-maximal is maximal. Examples for maximal Wyckoff positions are those, where $G_{\boldsymbol{q}}$ contains a non-trivial rotation.

In Fig.9.1, we show the unit cell, the maximal Wyckoff positions, and the action of all generators of the group D_{4h}. Note that the maximal Wyckoff positions $1a$ and $1b$ have the full D_{4h} point group as their site-symmetry. At $2c$, the symmetry is reduced to D_{2h}.
While we are at it, we also define the reciprocal lattice vectors $\boldsymbol{K}_i$ via

$$\boldsymbol{K}_i \cdot \boldsymbol{a}_j = 2\pi\delta_{ij}. \tag{9.2.6}$$

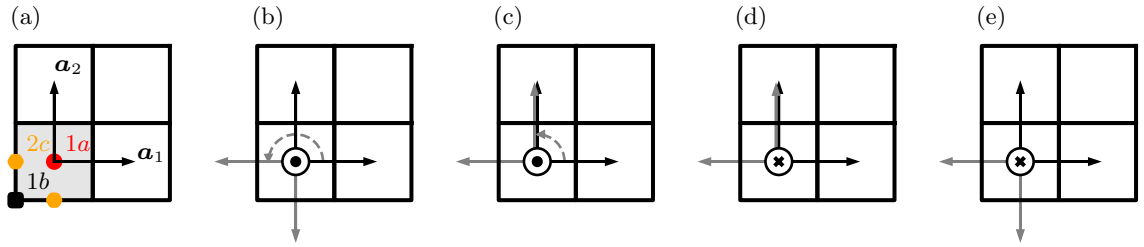

Figure 9.1: The space group $P4/mmm$: (a) The lattice vectors $\boldsymbol{a}_{1/2}$, the unit cell, and the maximal Wyckoff positions $1a$, $1b$, $2c$. (b) The action of the two-fold rotation around the z-axis C_2^z, or in Schönflies notation 2_{001}. (c) The action of a fourfold rotation around the z-axis C_4^z, or in Schönflies notation 4^+_{001}. (d) The action of the two-fold rotation around the y-axis C_2^y, or in Schönflies notation 2_{010}. Note, that for the in-plane drawing, this is identical to a mirror on the y-axis $M_x = I \circ C_2^z \circ C_2^y$, or in Schönflies notation m_{100}. (e) The action of inversion I, or in Schönflies notation -1.

9.2.1 Placing orbitals

Theory: The next step in our program is to place atoms, or more precisely, orbitals at maximal Wyckoff positions.[5] Once we put these orbitals, they will hybridize and form the sought after Bloch bands.
Free atoms are typically symmetric under the action of $SO(3)$. When we place these into the lattice, the symmetry is reduced to the one of the respective Wyckoff positions. This is an example of subduction: The irreducible representations of a larger group (here $SO(3)$) give rise to representations of a smaller group.
Example: Let us put spinful orbitals at the Wyckoff position $1a$. At $1a$ we have the full symmetry D_{4h}, hence we have to consider the double group D_{4h}. A minimal set of characters is given in Tab. 9.1. The Bilbao Crystallographic Server provides most information.
Let us start from the following $SO(3)$ irrep: Out of an s-wave orbital ($L = 0$) and a spin=1/2 ($S = 1/2$) we form the representation with $J = L + S = 1/2$ spanned by $|s,\uparrow\rangle$ and $|s,\downarrow\rangle$. Remember that the representation of a rotation for a general angular momentum state J are given by

$$\rho(\boldsymbol{\Omega}) = e^{\mathrm{i}\boldsymbol{J}\cdot\boldsymbol{\Omega}}, \tag{9.2.7}$$

where $\boldsymbol{J}$ denote the angular momentum matrices $\boldsymbol{J} = (J_x, J_y, J_z)$, $\Omega = |\boldsymbol{\Omega}|$ is the rotation angle

[5] One can of course place atoms at arbitrary Wyckoff positions. However, for the sake of the topological classification of the Bloch bands, the maximal Wyckoff positions suffice [2].

D_{4h}

		$\mathbb{1}$	C_4^z	I	$\bar{C}_4^z$
$\overline{E}_{2g}$	$\overline{GM}_6$	2	$-\sqrt{2}$	2	$-\sqrt{2}$
$\overline{E}_{1g}$	$\overline{GM}_7$	2	$\sqrt{2}$	2	$\sqrt{2}$
$\overline{E}_{2u}$	$\overline{GM}_8$	2	$-\sqrt{2}$	-2	$\sqrt{2}$
$\overline{E}_{1u}$	$\overline{GM}_9$	2	$\sqrt{2}$	-2	$-\sqrt{2}$

D_{2h}

		$\mathbb{1}$	I
$\overline{E}_g$	$\overline{GM}_5$	2	2
$\overline{E}_u$	$\overline{GM}_6$	2	-2

C_s

		$\mathbb{1}$	M_{01}
${}^2\overline{E}$	$\overline{GM}_3$	1	$-\mathrm{i}$
${}^1\overline{E}$	$\overline{GM}_4$	1	i

Table 9.1: Reduced set of characters of the spin-1/2 irreducible representation of the double group D_{4h} and some if its subgroups. The first two columns in each table indicate standard names of the irreps, the following columns contain the characters of the conjugacy classes that we need here. Note that $\bar{C}_4^z = I \circ C_4^z$ is an improper rotation. All other characters not shown are either zero or related by a minus sign due to the addition of a 2π rotation. The generators of all groups can be found on the Bilbao Crystallographic Server for D_{4h}, D_{42h}, C_s, and likewise for the full character tables D_{4h}, D_{2h}, C_s.

and $\hat{\mathbf{\Omega}} = \mathbf{\Omega}/\Omega$ the rotation axis. When using the Pauli matrices $J_i = \frac{1}{2}\sigma_i$ for $J = 1/2$ we obtain

$$\begin{aligned}
\rho(C_2^z) &= \begin{pmatrix} \mathrm{i} & 0 \\ 0 & -\mathrm{i} \end{pmatrix} && \operatorname{tr}\rho(C_2^z) = 0, \\
\rho(C_4^z) &= \begin{pmatrix} e^{\mathrm{i}\pi/4} & 0 \\ 0 & e^{-\mathrm{i}\pi/4} \end{pmatrix} && \operatorname{tr}\rho(C_4^z) = \sqrt{2}, \\
\rho(C_2^y) &= \begin{pmatrix} 0 & 1 \\ -1 & 0 \end{pmatrix} && \operatorname{tr}\rho(C_2^y) = 0, \\
\rho(I) &= \begin{pmatrix} 1 & 0 \\ 0 & 1 \end{pmatrix} && \operatorname{tr}\rho(I) = 2.
\end{aligned} \tag{9.2.8}$$

The last line we extract from the fact that s-orbitals are even under inversion. When comparing the characters with those in Tab. 9.1 we immediately see that we deal with $\overline{E}_{1g}$.
As a second example, let us consider p-orbitals ($L = 1$) and a spin=1/2 ($S = 1/2$). This time, we want to consider $J = L + S = 3/2$. Using the rotation matrices for $J = 3/2$ we obtain

$$\begin{aligned}
\rho(C_2^z) &= \begin{pmatrix} -\mathrm{i} & 0 & 0 & 0 \\ 0 & \mathrm{i} & 0 & 0 \\ 0 & 0 & -\mathrm{i} & 0 \\ 0 & 0 & 0 & \mathrm{i} \end{pmatrix} && \operatorname{tr}\rho(C_2^z) = 0, \\
\rho(C_4^z) &= \begin{pmatrix} e^{3\mathrm{i}\pi/4} & 0 & 0 & 0 \\ 0 & e^{\mathrm{i}\pi/4} & 0 & 0 \\ 0 & 0 & e^{-\mathrm{i}\pi/4} & 0 \\ 0 & 0 & 0 & e^{-3\mathrm{i}\pi/4} \end{pmatrix} && \operatorname{tr}\rho(C_4^z) = 0, \\
\rho(C_2^y) &= \begin{pmatrix} 0 & 0 & 0 & 1 \\ 0 & 0 & -1 & 0 \\ 0 & 1 & 0 & 0 \\ -1 & 0 & 0 & 0 \end{pmatrix} && \operatorname{tr}\rho(C_2^y) = 0, \\
\rho(I) &= \begin{pmatrix} -1 & 0 & 0 & 0 \\ 0 & -1 & 0 & 0 \\ 0 & 0 & -1 & 0 \\ 0 & 0 & 0 & -1 \end{pmatrix} && \operatorname{tr}\rho(I) = -4.
\end{aligned} \tag{9.2.9}$$

Again, the inversion matrix we obtain from the fact that p-orbitals are odd under inversion. We see that by going from $SO(3) \to D_{4h}$ we can further reduce the $J = 3/2$ representation as the states with $m_J = \pm 3/2$ are not mixing with $m_J = \pm 1/2$. We choose the $m_J = \pm 3/2$ sector spanned by $|p_x + \mathrm{i}p_y, \uparrow\rangle$ and $|p_x - \mathrm{i}p_y, \downarrow\rangle$. The representations are given by

$$\begin{aligned}
\rho(C_2^z) &= \begin{pmatrix} -\mathrm{i} & 0 \\ 0 & \mathrm{i} \end{pmatrix} && \operatorname{tr}\rho(C_2^z) = 0, \\
\rho(C_4^z) &= \begin{pmatrix} e^{3\mathrm{i}\pi/4} & 0 \\ 0 & e^{-3\mathrm{i}\pi/4} \end{pmatrix} && \operatorname{tr}\rho(C_4^z) = -\sqrt{2}, \\
\rho(C_2^y) &= \begin{pmatrix} 0 & -1 \\ 1 & 0 \end{pmatrix} && \operatorname{tr}\rho(C_2^y) = 0, \\
\rho(I) &= \begin{pmatrix} -1 & 0 \\ 0 & -1 \end{pmatrix} && \operatorname{tr}\rho(I) = -2.
\end{aligned} \tag{9.2.10}$$

Consulting Tab. 9.1, we see that we work with $\overline{E}_{2u}$. In the following, we want to place these two irreps at $1a$ and investigate what bands can arise from these orbitals.

9.2.2 Inducing a representation of the full space group

Theory: Now that we know which orbitals we place at the maximal Wyckoff positions, we can see how the resulting Bloch wave functions transform under the space group symmetries. To this end, we first take the Fourier transformation back to Bloch states

$$u_{i,\alpha}(\boldsymbol{k}, \boldsymbol{r}) = \frac{1}{\sqrt{N}} \sum_{\mu} e^{\mathrm{i}\boldsymbol{k}\cdot\boldsymbol{t}_\mu} \psi_{i\alpha}(\boldsymbol{r} - \boldsymbol{t}_\mu). \tag{9.2.11}$$

Here, the $\boldsymbol{t}_\mu$ denote the lattice vectors. Note, that opposed to in (9.1.2), we label the orbitals i and the Wyckoff position α individually. We also made the number of unit cells N explicit. Moreover, we do not specify a Hamiltonian yet, so we cannot provide a band label a. All we want to investigate is, how the Bloch states transform under the space group symmetries. As we construct the Bloch states from Wannier states in specific irreps of the point group, we can now deduce how the Bloch states transform. In other words, our procedure of placing well defined irreps at all sites of the crystal and then taking a Fourier transform allows us to *induce a representation* of the (infinte) space group from the irreps of the (finite) point group.
Let us quickly see how we know the transformation of a Wannier state $\psi_{i\alpha}(\boldsymbol{r} - \boldsymbol{t}_\mu)$ under the point group symmetries. For this, we need to know how each orbital transforms around its Wyckoff position. Once we fix this, we will see how they transform in the full lattice.
For the transformation around a single site we reduce all our consideration to the transformation properties of one representative Wyckoff position $\alpha = 1$ in the orbit:

$$g\psi_{i1} = [\rho(g)]_{ji}\psi_{j1}. \tag{9.2.12}$$

For any other Wyckoff position $\boldsymbol{q}_\alpha$ in the orbit of $\boldsymbol{q}_1$ we first bring the Wannier function to position $\alpha = 1$ by the use of

$$\psi_{i\alpha}(\boldsymbol{r}) = g_\alpha \psi_{i1}(\boldsymbol{r}) = \psi_{i1}(g_\alpha^{-1}\boldsymbol{r}) \tag{9.2.13}$$

We then inherit the representation of h at α from the reference position 1

$$h\psi_{i\alpha} = \underbrace{g_\alpha g g_\alpha^{-1}}_{h} g_\alpha \psi_{i1} = g_\alpha g \psi_{i1} = g_\alpha [\rho(g)]_{ji}\psi_{j1} = [\rho(g_\alpha^{-1} h g_\alpha)]_{ji}\psi_{j\alpha}. \tag{9.2.14}$$

This formula is easy to understand. Imagine you consider the Wyckoff $2c$ in $P4/mmm$ which has two points in the orbit: $\alpha = 1: \ (1/2, 0)$ and $\alpha = 2: \ (0, 1/2)$. $2c$ has the site symmetry group D_{2h}. The mirror $h = m_{01}$ at $\alpha = 1$ corresponds to the the mirror $g = m_{10}$ at $\alpha = 2$. The factor $g_\alpha^{-1} h g_\alpha$ is reflecting just that with $g_\alpha = C_4^z$.
Now that we know the local transformation, let us move to the question how the orbitals in the full lattice transform. It is this step, where we *induce a representation in the full space group G from the irreps of the point group:* $\rho_G = \rho \uparrow G$:

$$h\psi_{i\alpha}(\boldsymbol{r} - \boldsymbol{t}_\mu) = [\rho(g^h_{\alpha\beta})]_{ji}\psi_{j\beta}(\boldsymbol{r} - R\boldsymbol{t}_\mu - \boldsymbol{t}_{\alpha\beta}). \tag{9.2.15}$$

Let us analyze this formula step by step. First, under the action of h, the orbital might be transported into another unit cell

$$h\boldsymbol{q}_\alpha = \{\mathbb{1}|\boldsymbol{t}_{\alpha\beta}\}\boldsymbol{q}_\beta, \quad \text{with} \tag{9.2.16}$$

$$\boldsymbol{t}_{\alpha\beta} = h\boldsymbol{q}_\alpha - \boldsymbol{q}_\beta \tag{9.2.17}$$

We use (9.2.16) to obtain

$$\underbrace{g_\beta^{-1}\{\mathbb{1}| - \boldsymbol{t}_{\alpha\beta}\}hg_\alpha}_{g^h_{\alpha\beta}}\boldsymbol{q}_1 = \boldsymbol{q}_1, \tag{9.2.18}$$

which defines the group element g which leaves the Wyckoff position invariant and allows us to use the result (9.2.14) in (9.2.15).
With these results, we are in the position to determine how the Bloch functions transform

$$\begin{aligned}
[\rho_G(h)]_{j\beta,i\alpha}u_{j\beta}(\boldsymbol{k},\boldsymbol{r}) &= \frac{1}{\sqrt{N}}\sum_\mu e^{\mathrm{i}\boldsymbol{k}\cdot\boldsymbol{t}_\mu}[\rho_G(h)]_{j\beta,i\alpha}\psi_{j\beta}(\boldsymbol{r} - \boldsymbol{t}_\mu) \\
&\overset{(9.2.15)}{=} \frac{1}{\sqrt{N}}\sum_\mu e^{\mathrm{i}\boldsymbol{k}\cdot\boldsymbol{t}_\mu}[\rho(g^h_{\alpha\beta})]_{ji}\psi_{j\beta}(\boldsymbol{r} - R\boldsymbol{t}_\mu - \boldsymbol{t}_{\alpha\beta}) \\
&= [\rho(g^h_{\alpha\beta})]_{ji}\frac{1}{\sqrt{N}}\sum_\mu e^{\mathrm{i}(R^{-1}\boldsymbol{k})\cdot(R\boldsymbol{t}_\mu)}\psi_{j\beta}(\boldsymbol{r} - R\boldsymbol{t}_\mu - \boldsymbol{t}_{\alpha\beta}) \\
&= e^{-\mathrm{i}(R^{-1}\boldsymbol{k})\cdot\boldsymbol{t}_{\alpha\beta}}[\rho(g^h_{\alpha\beta})]_{ji}\frac{1}{\sqrt{N}}\sum_\mu e^{\mathrm{i}(R^{-1}\boldsymbol{k})\cdot(R\boldsymbol{t}_\mu + \boldsymbol{t}_{\alpha\beta})}\psi_{j\beta}(\boldsymbol{r} - R\boldsymbol{t}_\mu - \boldsymbol{t}_{\alpha\beta}) \\
&= e^{-\mathrm{i}(R^{-1}\boldsymbol{k})\cdot\boldsymbol{t}_{\alpha\beta}}[\rho(g^h_{\alpha\beta})]_{ji}u_{j\beta}(R^{-1}\boldsymbol{k},\boldsymbol{r}).
\end{aligned}$$

With this we achieved our goal! We have found a representation of the space group G of the form

$$[\rho^{\boldsymbol{k}}_G(h)]_{j\beta,i\alpha} = e^{-\mathrm{i}(R^{-1}\boldsymbol{k})\cdot\boldsymbol{t}_{\alpha\beta}}[\rho(g^h_{\alpha\beta})]_{ji}. \tag{9.2.19}$$

It is quadratic matrix of size $n_{\text{orbit}}d_{\text{orbitals}} \times n_{\text{orbit}}d_{\text{orbitals}}$ where n_{orbit} is the number of Wykoff positions in the orbit and d_{irrep} is the dimension of the irrep we place on these maximal Wyckoff positions. In $\boldsymbol{k}$-space it connects a pair of two momenta $\boldsymbol{k}$ and $R^{-1}\boldsymbol{k}$. We close this section by noting two things: (i) We did not yet introduce a Hamiltonian. So far, we only studied how Bloch bands will transform under the space group symmetries. (ii) The way we constructed the Bloch bands they are defined as a representation of the space group. We call it an *elementary band representation* (EBR).
Example: For our choice of placing the orbitals $\overline{E}_{1g}$ and $\overline{E}_{2u}$ at $1a$, this process of induction is particularly trivial: There is only one Wyckoff position in the orbit and all point group symmetries act within the unit cell. Hence all $\boldsymbol{t}_{\alpha\beta} \equiv 0$ and $g^h_{\alpha\beta} \equiv h$. Therefore, the representations given in (9.2.8) and (9.2.10) define one-to-one the induced band representation.

9.2.3 Subducing a representation at special momenta

Theory: We have seen that in general the band representations connect two momenta. However, for every $\boldsymbol{k}$-point there exists a subgroup $G_{\boldsymbol{k}}$ of the full space group, under which $R\boldsymbol{k} = \boldsymbol{k}$ for all $R \in G_{\boldsymbol{k}}$ (up to a reciprocal lattice vector). The interesting, i.e., high-symmetry, points and lines in the Brillouin zone are those where this $G_{\boldsymbol{k}}$ does contain more than the trivial element. $G_{\boldsymbol{k}}$ is called the *little group* of $\mathbf{k}$. We can see how the full band representation $[\rho^{\boldsymbol{k}}_G(h)]$ sub-duces irreps at these high-symmetry points.
Technically, the procedure is straight forward: Using the character table of the little group, we can reduce the full representation $[\rho^{\boldsymbol{k}}_G(h)]$ into the irreps $\sigma^{\boldsymbol{k}}_i$ of the little group via

$$[\rho^{\boldsymbol{k}}_G(h)] \downarrow G_{\boldsymbol{k}} = \bigoplus_i m_i \, \sigma^{\boldsymbol{k}}_i, \tag{9.2.20}$$

with

$$m_i = \frac{1}{n} \sum_h \chi^*_i(h) \chi_{[\rho^{\boldsymbol{k}}_G(h)]}(h), \tag{9.2.21}$$

where the sum is over all group elements h of the little group, $\chi_i(h)$ are the characters of the irreps $\sigma^{\boldsymbol{k}}_i$ and $\chi_{[\rho^{\boldsymbol{k}}_G(h)]}(h)$ is the character of the subduced representation. The parameter n is the order of the little group $G_{\boldsymbol{k}}$.
Example: Let us start with $\overline{E}_{1g}$. At the $\boldsymbol{\Gamma}$ point $\boldsymbol{k} = (0, 0)$ we have the full group D_{4h}. For later reference, we go with the convention to use the second name of the irreps in Tab. 9.1 when we refer to the irreps of the little groups. In fact, we call the irreps by the name of the high-symmetry point supplemented by the number. E.g., $\overline{E}_{1g}$ at $\boldsymbol{\Gamma}$ is referred to as $\boldsymbol{\Gamma}_7$ and $\overline{E}_{2u}$ as $\boldsymbol{\Gamma}_8$.
If we now go out along the line $(k_x, 0)$ for $k_x \in [0, \pi]$ we reduce the little group to the double point group C_s with only a mirror as a non-trivial element. Using the character table in Tab. 9.1 and Eq. (9.2.21), we immediately find

$$m_{_2\overline{E}} = \frac{1}{4}(1 \times 2 + \mathrm{i} \times 0 + (-1) \times (-2) + (-\mathrm{i}) \times 0) = 1, \tag{9.2.22}$$

$$m_{_1\overline{E}} = \frac{1}{4}(1 \times 2 + (-\mathrm{i}) \times 0 + (-1) \times (-2) + \mathrm{i} \times 0) = 1. \tag{9.2.23}$$

$$\tag{9.2.24}$$

The same holds for $\overline{E}_{2u}$. This in principle means that the both irreps $\boldsymbol{\Gamma}_{7/8}$ split to $\overline{\boldsymbol{\Gamma}\boldsymbol{X}}_3$ and $\overline{\boldsymbol{\Gamma}\boldsymbol{X}}_4$ on the line from $\boldsymbol{\Gamma}$ to $\boldsymbol{X}$. If we also force time reversal symmetry $\mathcal{T}$, however, these two irreps have to come together as they form a conjugate pair (apparent through the complex characters for the mirror symmetry). For the lines $\overline{\boldsymbol{X}\boldsymbol{M}}$ and $\overline{\boldsymbol{M}\boldsymbol{\Gamma}}$ the same conclusion holds.
At $\boldsymbol{X}$ the little group is D_{2h} which again contains inversion. From this we can readily read off that the band representation induced by $\overline{E}_{1g}$ will subduce to $\boldsymbol{X}_5$ and $\overline{E}_{2u}$ to $\boldsymbol{X}_6$.
The $\boldsymbol{M}$ point has the same little group as $\boldsymbol{\Gamma}$ and hence we again find for $\overline{E}_{1g}$ the orbital $\boldsymbol{\Gamma}_7$ and for $\overline{E}_{2u}$ it is $\boldsymbol{\Gamma}_8$. Fig. 9.2(a) summarizes these considerations. Using the tools of the last few sections we constructed an explicit EBR and analyzed how the bands follow certain rules due to symmetry constraints. The following question presents itself: what kind of bands can arise in a given space group? This work has been done [1, 4] and we quickly introduce it in the next section before we analyze what happens when we place both $\overline{E}_{1g}$ *and* $\overline{E}_{2u}$ orbitals at $1a$.

9.2.4 A complete list of possible elementary band representations

Theory: The possible connections of the different irreps at different high-symmetry points in the Brillouin zone are highly restricted due to compatibility requirements. A complete tabulation of all EBRs has been achieved using spectral graph theory [1, 4]. The outcome of this work is available on the Bilbao Crystallographic Server under Topological Quantum Chemistry.

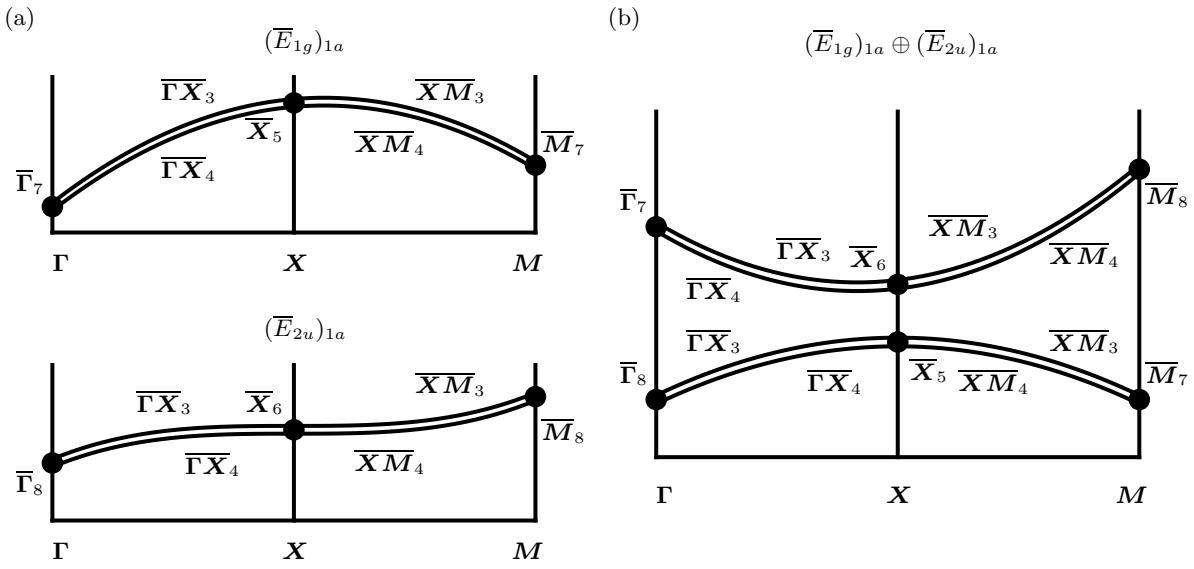

Figure 9.2: Band connectivities: (a) The bands induced by the orbitals $\overline{E}_{1g}$ and $\overline{E}_{2u}$ from Wyckoff position 1. Note that under time-reversal symmetry, the two irreps $\overline{\boldsymbol{AB}}_{3/4}$ are fused into a $2d$-irrep as they are conjugate to each other. (b) When the two EBRs of (a) overlap, one can connect the high-symmetry points in a way that gives rise to a stable topological insulator.

Example: Here we show in Tab 9.2 the results relevant for our example of spinful electrons in the planar version of $P4/mmm$. We see from this table that all induced representations from $1a$

Wyckoff pos.	$1a$	$1a$	$1a$	$1a$	$1b$	$1b$	$1b$	$1b$	$2c$	$2c$
Site symm.	D_{4h}	D_{4h}	D_{4h}	D_{4h}	D_{4h}	D_{4h}	D_{4h}	D_{4h}	D_{2h}	D_{2h}
Orbital	$\overline{E}_{1g}$	$\overline{E}_{1u}$	$\overline{E}_{2g}$	$\overline{E}_{2u}$	$\overline{E}_{1g}$	$\overline{E}_{1u}$	$\overline{E}_{2g}$	$\overline{E}_{2u}$	$\overline{E}_g$	$\overline{E}_u$
Decomposable	x	x	x	x	x	x	x	x	✓	✓
$\boldsymbol{\Gamma}$	$\boldsymbol{\Gamma}_7$	$\boldsymbol{\Gamma}_9$	$\boldsymbol{\Gamma}_6$	$\boldsymbol{\Gamma}_8$	$\boldsymbol{\Gamma}_7$	$\boldsymbol{\Gamma}_9$	$\boldsymbol{\Gamma}_6$	$\boldsymbol{\Gamma}_8$	$\boldsymbol{\Gamma}_6 \oplus \boldsymbol{\Gamma}_7$	$\boldsymbol{\Gamma}_8 \oplus \boldsymbol{\Gamma}_9$
$\boldsymbol{M}$	$\boldsymbol{M}_7$	$\boldsymbol{M}_9$	$\boldsymbol{M}_6$	$\boldsymbol{M}_8$	$\boldsymbol{M}_6$	$\boldsymbol{M}_8$	$\boldsymbol{M}_7$	$\boldsymbol{M}_9$	$\boldsymbol{M}_8 \oplus \boldsymbol{M}_9$	$\boldsymbol{M}_6 \oplus \boldsymbol{M}_7$
$\boldsymbol{X}$	$\boldsymbol{X}_5$	$\boldsymbol{X}_6$	$\boldsymbol{X}_5$	$\boldsymbol{X}_6$	$\boldsymbol{X}_6$	$\boldsymbol{X}_5$	$\boldsymbol{X}_6$	$\boldsymbol{X}_5$	$\boldsymbol{X}_5 \oplus \boldsymbol{X}_6$	$\boldsymbol{X}_5 \oplus \boldsymbol{X}_6$

Table 9.2: Little-group irrep content of the EBRs for spinful orbitals in the space group $P4/mmm$.

and $1b$ positions follow the same pattern as the ones we considered in these notes. In particular, the compatibility requirements force these band representations to be *connected*: All irreps at the different high-symmetry points have to be linked by a dispersion line.
The last two, which are induced from the Wyckoff position $2c$, with two sites in the orbit, are different. Here, the symmetry constraints allow for two sets of connected bands which are mutually disconnected. For the EBRs induced by $\overline{E}_g$ at $2c$ [which is often written as $(\overline{E}_g)_{2c}$] the options are

$$\begin{aligned} 1&: \boldsymbol{\Gamma}_6\text{—}\boldsymbol{M}_8\text{—}\boldsymbol{X}_5 \quad \text{and} \quad \boldsymbol{\Gamma}_7\text{—}\boldsymbol{M}_9\text{—}\boldsymbol{X}_6, \\ 2&: \boldsymbol{\Gamma}_6\text{—}\boldsymbol{M}_8\text{—}\boldsymbol{X}_6 \quad \text{and} \quad \boldsymbol{\Gamma}_7\text{—}\boldsymbol{M}_9\text{—}\boldsymbol{X}_5, \\ 3&: \boldsymbol{\Gamma}_7\text{—}\boldsymbol{M}_8\text{—}\boldsymbol{X}_5 \quad \text{and} \quad \boldsymbol{\Gamma}_6\text{—}\boldsymbol{M}_9\text{—}\boldsymbol{X}_6, \\ 4&: \boldsymbol{\Gamma}_7\text{—}\boldsymbol{M}_8\text{—}\boldsymbol{X}_6 \quad \text{and} \quad \boldsymbol{\Gamma}_6\text{—}\boldsymbol{M}_9\text{—}\boldsymbol{X}_5. \end{aligned} \tag{9.2.25}$$

For $(\overline{E}_u)_{2c}$ one finds

$$\begin{aligned} 1: &\boldsymbol{\Gamma}_8\text{—}\boldsymbol{M}_6\text{—}\boldsymbol{X}_5 \quad \text{and} \quad \boldsymbol{\Gamma}_9\text{—}\boldsymbol{M}_7\text{—}\boldsymbol{X}_6, \\ 2: &\boldsymbol{\Gamma}_8\text{—}\boldsymbol{M}_6\text{—}\boldsymbol{X}_6 \quad \text{and} \quad \boldsymbol{\Gamma}_9\text{—}\boldsymbol{M}_7\text{—}\boldsymbol{X}_5, \\ 3: &\boldsymbol{\Gamma}_9\text{—}\boldsymbol{M}_6\text{—}\boldsymbol{X}_5 \quad \text{and} \quad \boldsymbol{\Gamma}_8\text{—}\boldsymbol{M}_7\text{—}\boldsymbol{X}_6, \\ 4: &\boldsymbol{\Gamma}_9\text{—}\boldsymbol{M}_6\text{—}\boldsymbol{X}_6 \quad \text{and} \quad \boldsymbol{\Gamma}_8\text{—}\boldsymbol{M}_7\text{—}\boldsymbol{X}_5. \end{aligned} \tag{9.2.26}$$

We discuss the consequences of this table in the next section.

9.2.5 Stable and fragile topology

Theory: Table 9.2 together with Eq. (9.2.25) & (9.2.26) allows us to characterize bands in $P4/mmm$ according to their irrep content at high-symmetry points. There are three distinct scenarios:

Trivial bands

The irrep content of a given band structure can be written as a direct sum of the irreps in one of the EBRs in Tab. 9.2. This implies, that one can write a basis function of symmetric and localized orbitals, namely the ones from which these bands are induced.
For example, if we had a band structure with $\boldsymbol{\Gamma}_7 \oplus \boldsymbol{\Gamma}_7$, $\boldsymbol{M}_6 \oplus \boldsymbol{M}_7$, and $\boldsymbol{X}_5 \oplus \boldsymbol{X}_6$, we would immediately write

$$\left(\overline{E}_{1g}\right)_{1a} \oplus \left(\overline{E}_{1g}\right)_{1b}. \tag{9.2.27}$$

Stable topology

If, on the other hand, we need to make use of split bands [like the ones in Eq. (9.2.25) & (9.2.26)] to account for the irrep content of our bands, we cannot induce these bands from a set of symmetric localized orbitals: the definition of a topological system. We see one instance of such a stable topological set of bands in the example below.

Fragile topology

As a last option, there arises the possibility that one cannot reproduce the irrep content of the bands via a direct sum as in the trivial case above. However, as opposed to a split band, one might be able to collect the irreps of several EBRs in order to account for all irreps of the band under investigation. If in this process one accumulates too many degrees of freedom, one can maybe *subtract* the irreps of one or several other EBRs in order to account for the sought after types and multiplicities of irreps exactly. In this case one deals with *fragile topology*. Why is this topological: given that we need to add and subtract means that we cannot write a set of localized orbitals from which we can induce this set of bands. (There is no such thing as adding an atom with a minus sign). Why do we call it fragile: If one now adds a band induced by the orbital which appeared with a negative sign in the decomposition, we end up with a direct sum of elementary bands, and hence with a trivial system. One can summarize this by stating that a fragile topological system cannot be Wannierized, but becomes Wannierizable under the addition of a trivial band.

Example: As an example of how to use Tab. 9.2, we investigate what arises if we deal with a set of four bands induced by $(\overline{E}_{1g})_{1a}$ and $(\overline{E}_{2u})_{1a}$. In Fig. 9.2(b) we show what can happen if we bring the two EBRs close to each other. Remember that all lines are doubly degenerate because of the combination of the mirror symmetries with time reversal, i.e, all these double lines contain both mirror eigenvalues $\pm$i. As there are no further constraints, we can link up all irreps at $\boldsymbol{\Gamma}$, $\boldsymbol{M}$, and $\boldsymbol{X}$ at will.

The example shown in Fig. 9.2(b) can be understood has having exchanged the even and odd irreps (under inversion) at the $\boldsymbol{\Gamma}$ point, but not at the $\boldsymbol{X}$ or $\boldsymbol{M}$ points. In other words, we deal with the bands

$$\text{lower bands}: \boldsymbol{\Gamma}_7\text{—}\boldsymbol{M}_8\text{—}\boldsymbol{X}_6, \tag{9.2.28}$$

$$\text{upper bands}: \boldsymbol{\Gamma}_8\text{—}\boldsymbol{M}_7\text{—}\boldsymbol{X}_5. \tag{9.2.29}$$

When comparing to Tab. 9.2 we see that none of the EBRs fits this irrep content. However, when checking the split EBRs $(\overline{E}_g)_{2c}$ and $(\overline{E}_u)_{2c}$, we see that the two bands above and below the gap in Fig. 9.2(b) each arise from half an EBR! We deal with a stable topological system.

9.3 Finally: A Hamiltonian

So far, we have analyzed Bloch bands without making reference to a Hamiltonian. We got quite some mileage out of symmetry considerations alone! But now we would like to substantiate our findings on the stable topological system induced by $(\overline{E}_{1g})_{1a} \oplus (\overline{E}_{2u})_{1a}$. Let us remind ourselves of the time reversal invariant, doubled lattice Dirac Hamiltonian (4.3.2)

$$\mathcal{H} = \tau_0 \otimes \{[m - 2 + \cos(k_x) + \cos(k_y)]\sigma_z + \sin(k_y)\sigma_y\} + \sin(k_x)\tau_z \otimes \sigma_x. \tag{9.3.1}$$

For the purpose here, it is most convenient to transform to

$$\mathcal{H} \to U^\dagger \mathcal{H} U = \begin{pmatrix} \epsilon_0(\boldsymbol{k}) & 0 & l_+(\boldsymbol{k}) & 0 \\ 0 & \epsilon_0(\boldsymbol{k}) & 0 & -l_-(\boldsymbol{k}) \\ l_-(\boldsymbol{k}) & 0 & -\epsilon_0(\boldsymbol{k}) & 0 \\ 0 & -l_+(\boldsymbol{k}) & 0 & -\epsilon_0(\boldsymbol{k}) \end{pmatrix}, \quad \text{with} \quad U = \begin{pmatrix} 1 & 0 & 0 & 0 \\ 0 & 0 & 1 & 0 \\ 0 & 1 & 0 & 0 \\ 0 & 0 & 0 & 1 \end{pmatrix} \tag{9.3.2}$$

and

$$\epsilon_0(\boldsymbol{k}) = -2 + m + \cos(k_x) + \cos(k_y), \tag{9.3.3}$$

$$l_\pm = \sin(k_x) \pm \mathrm{i}\sin(k_y). \tag{9.3.4}$$

Written like this, it is apparent that the matrix elements $l_\pm(\boldsymbol{k})$ can raise (lower) the angular momentum quantum number by one. The Hamiltonian has the following symmetries

$$C_4^z: \quad (k_x, k_y) \to (k_y, -k_x) \qquad \rho(C_4^z) = \begin{pmatrix} e^{3\mathrm{i}\pi/4} & 0 & 0 & 0 \\ 0 & e^{-3\mathrm{i}\pi/4} & 0 & 0 \\ 0 & 0 & e^{\mathrm{i}\pi/4} & 0 \\ 0 & 0 & 0 & e^{-\mathrm{i}\pi/4} \end{pmatrix} \tag{9.3.5}$$

$$C_2^z: \quad (k_x, k_y) \to (-k_x, -k_y) \qquad \rho(C_2^z) = \begin{pmatrix} -\mathrm{i} & 0 & 0 & 0 \\ 0 & \mathrm{i} & 0 & 0 \\ 0 & 0 & -\mathrm{i} & 0 \\ 0 & 0 & 0 & \mathrm{i} \end{pmatrix} \tag{9.3.6}$$

$$C_2^y: \quad (k_x, k_y) \to (-k_x, k_y) \qquad \rho(C_2^y) = \begin{pmatrix} 0 & \mathrm{i} & 0 & 0 \\ \mathrm{i} & 0 & 0 & 0 \\ 0 & 0 & 0 & \mathrm{i} \\ 0 & 0 & \mathrm{i} & 0 \end{pmatrix} \tag{9.3.7}$$

$$I: \quad (k_x, k_y) \to (-k_x, -k_y) \qquad \rho(I) = \begin{pmatrix} -1 & 0 & 0 & \\ 0 & -1 & 0 & 0 \\ 0 & 0 & 1 & 0 \\ 0 & 0 & 0 & 1 \end{pmatrix} \tag{9.3.8}$$

Comparing this to the representations in $\overline{E}_{1g}$ (9.2.8) and $\overline{E}_{2u}$ (9.2.10) we immediately see that we deal with $P4/mmm$ and that the first two orbitals correspond to $\overline{E}_{2u}$, while the second two belong to $\overline{E}_{1g}$.
To determine the irrep content at the high-symmetry momenta $\boldsymbol{\Gamma}$, $\boldsymbol{X}$, and $\boldsymbol{M}$ we only need to look at the eigenvalues of $\rho(I)$, as inversion determines the difference between the involved irreps $\boldsymbol{\Gamma}_{7/8}$, $\boldsymbol{M}_{7/8}$, and $\boldsymbol{X}_{5/6}$, respectively. At the high-symmetry points, the Hamiltonian reads

$$\mathcal{H}(\boldsymbol{\Gamma}) = \mathrm{diag}(m, m, -m, -m), \tag{9.3.9}$$
$$\mathcal{H}(\boldsymbol{X}) = \mathrm{diag}(-2+m, -2+m, 2-m, 2-m), \tag{9.3.10}$$
$$\mathcal{H}(\boldsymbol{M}) = \mathrm{diag}(-4+m, -4+m, 4-m, 4-m). \tag{9.3.11}$$

$m < 0$: The first two states are odd under inversion. For $m < 0$, they form the lower two bands at all high-symmetry momenta. Therefore, we realize

$$\text{lower}: \quad (\overline{E}_{2u})_{1a} \qquad\qquad \text{upper}: \quad (\overline{E}_{1g})_{1a}. \tag{9.3.12}$$

$0 < m < 2$: Now, the inversion eigenvalue switches at $\boldsymbol{\Gamma}$. Hence we realize $\boldsymbol{\Gamma}_7$—$\boldsymbol{M}_8$—$\boldsymbol{X}_6$ in the lower and $\boldsymbol{\Gamma}_8$—$\boldsymbol{M}_7$—$\boldsymbol{X}_5$ in the upper band. We can write the bands as

$$\text{lower}: \quad \frac{1}{2}(\overline{E}_g)_{2c} \qquad\qquad \text{upper}: \quad \frac{1}{2}(\overline{E}_u)_{2c}, \tag{9.3.13}$$

from which we read off that we deal with a stable topological insulator.
$2 < m < 4$: At $m = 2$, the gap closes at $\boldsymbol{X}$ and now also at $\boldsymbol{X}$ the lower bands are even under inversion. Hence we realize $\boldsymbol{\Gamma}_7$—$\boldsymbol{M}_8$—$\boldsymbol{X}_5$ in the lower and $\boldsymbol{\Gamma}_8$—$\boldsymbol{M}_7$—$\boldsymbol{X}_6$ in the upper band. While different split versions of the EBRs induced at $2c$ are realized, the bands can still be written as

$$\text{lower}: \quad \frac{1}{2}(\overline{E}_g)_{2c} \qquad\qquad \text{upper}: \quad \frac{1}{2}(\overline{E}_u)_{2c}. \tag{9.3.14}$$

$m > 4$: For $m > 4$, finally, all irreps of the lower bands are even under inversion and we have

$$\text{lower}: \quad (\overline{E}_{1g})_{1a} \qquad\qquad \text{upper}: \quad (\overline{E}_{2u})_{1a}. \tag{9.3.15}$$

References

1. Bradlyn, B. *et al.* "Topological quantum chemistry". *Nature* **537,** 298. https://dx.doi/org/10.1038/nature23268 (2017).
2. Robredo, I., Bernevig, B. A. & Mañes, J. L. in (eds Bercioux, D., Cayssol, J., Vergniory, M. G. & Calvo, M.) 1 (Springer Nature Switzerland, 2018). https://doi.org/10.1007/978-3-319-76388-0_1.
3. Kohn, W. "Analytic properties of bloch waves and wannier functions". *Phys. Rev.* **115,** 809. http://link.aps.org/abstract/PR/v115/p809 (1959).
4. Bradlyn, B. *et al.* "Band connectivity for topological quantum chemistry: Band structures as a graph theory problem". *Phys. Rev. B* **97,** 035138. https://doi.org/10.1103/PhysRevB.97.035138 (2018).

Chapter 10

Topological semimetals

Learning goals

- We know Weyl semimetals, their Fermi arc surface states and chiral anomaly.
- We have an overview of other types of symmetry-enforced degeneracies in band structures, including point-like degeneracies of several bands and nodal lines.

- X. Wan, et al., Phys. Rev. B **83**, 205101 (2011)
- B. Bradlyn *et al.*, Science **353**, aaf5037 (2017)
- G. Chang *et al.*, Nature Mater. **17**, 978–985 (2018)

So far, this entire lecture was focussed on the topology in gapped ground states of matter. In this chapter we discuss gapless topological states, so-called topological semimetals. Remembering that topology was initially defined as (symmetry-protected) equivalence classes states under adiabatic deformations, this provokes the question what meaning we should attach to the adiabatic theorem in a gapless phase and – as a consequence – how topology should be defined at all in such a case. At least for the purpose of this lecture, we rescue the notion of topology by relying on translation symmetry. Hence we can label our Hamiltonian by momentum $\boldsymbol{k}$. (We used translation symmetry before, but mainly to obtain convenient formulas for topological invariants. The notion of the topological phases themselves was – with the exception of TQC – never dependent on translation symmetry.)
The story of topological semimetals is most interesting in three dimensions, which is why we focus on this case exclusively here. While the Hamiltonian, depending on three components of momentum, is then gapped almost everywhere in the BZ, the few points or lines where this is not the case are our main interest. At these nodal points or lines bands are degenerate and we will see that these degeneracies are *topologically stable*. They cannot be removed (yet potentially moved in the BZ), if the Hamiltonian is smoothly deformed while maintaining translation symmetry (and potentially some other protecting symmetries). Such a notion of robustness to deformations allows to define a *gapless phase* and a sense of topology.

10.1 Weyl semimetals

The Weyl semimetal is the most elementary topological semimetal, as we will see. A Hamiltonian for it can be motivated from several angles. Here we choose a perspective where we start from a three-dimensional topological insulator Hamiltonian in momentum space

$$\mathcal{H}_{\mathrm{TI}}(\boldsymbol{k}) = \sum_{i=x,y,z} \sin\, k_i\, \sigma_i \tau_x + \left(M - \sum_{i=x,y,z} \cos\, k_i \right) \sigma_0 \tau_z, \tag{10.1.1}$$

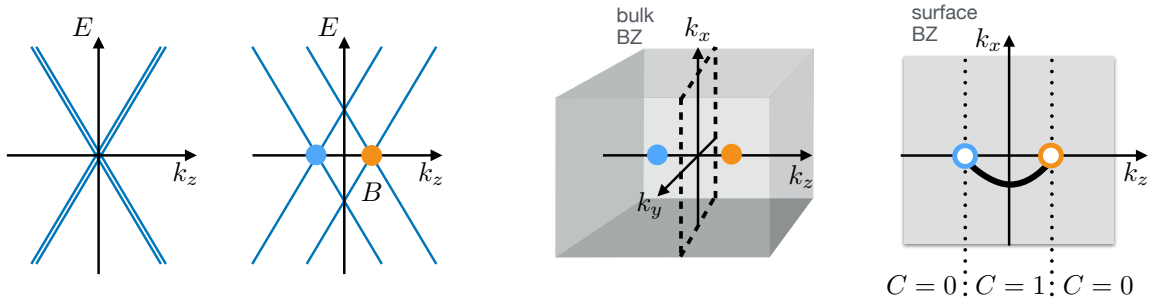

Figure 10.1: Momentum space picture of a Weyl semimetals. Left: The band structure of the critical point between a three-dimensional topological insulator and a trivial insulator is a gapless Dirac fermion. Upon the application of a Zeeman field, the Dirac fermion splits into two Weyl fermions (blue and orange) of opposite chiral charge. Right: The occupied bands on planes in momentum space that do not pass through the Weyl fermions carry a well-defined Chern number. This Chern number is $|\mathsf{C}^{(1)}| = 1$ between two two Weyl points and 0 for planes outside. Correspondingly, there is a Fermi arc surface state in the surface BZ connecting the projections of the bulk Weyl points.

with time-reversal symmetry defined as

$$(\sigma_y\tau_0)\mathcal{H}^*_{\mathrm{TI}}(\boldsymbol{k})(\sigma_y\tau_0)^{-1} = \mathcal{H}_{\mathrm{TI}}(-\boldsymbol{k}) \tag{10.1.2}$$

and inversion symmetry defined as

$$(\sigma_0\tau_z)\mathcal{H}_{\mathrm{TI}}(\boldsymbol{k})(\sigma_0\tau_z)^{-1} = \mathcal{H}_{\mathrm{TI}}(-\boldsymbol{k}). \tag{10.1.3}$$

Here, σ_i are the Pauli matrices acting on the spin degree of freedom and τ_i are Pauli matrices that can be though of as acting on an s/p orbital degree of freedom – consistent with the opposite inversion eigenvalue of the orbitals indicated by τ_z.
Hamiltonian (10.1.1) is constructed such that all terms anticommute, which makes it easy to obtain the doubly degenerate bands (the degeneracy is due to inversion and time-reversal, giving a local in $\boldsymbol{k}$ Kramers symmetry)

$$E_\pm(\boldsymbol{k}) = \pm\sqrt{\sum_{i=x,y,z}\sin^2 k_i + \left(M - \sum_{i=x,y,z}\cos k_i\right)^2}. \tag{10.1.4}$$

This indicates several gap-closing phase transitions, in particular for $1 < |M| < 3$ we have a topological insulator. At the phase transition, $M = 3$, we can expand the Hamiltonian to linear order in $\boldsymbol{k}$ and obtain a massless Dirac equation (we rotate the orbital basis $\tau_x \leftrightarrow \tau_z$ for convenience and signify this by a tilde)

$$\tilde{\mathcal{H}}_{\mathrm{TI,eff}}(\boldsymbol{k}) = \begin{pmatrix} \boldsymbol{k}\cdot\boldsymbol{\sigma} & 0 \\ 0 & -\boldsymbol{k}\cdot\boldsymbol{\sigma} \end{pmatrix}. \tag{10.1.5}$$

This block structure of the Dirac equation was noticed by Hermann Weyl (in Zurich), and the Fermion (two-spinor) described by each of the 2×2 blocks is known as Weyl fermion. We thus see that two Weyl fermions make up one massless Dirac fermion. The innocent minus sign between the two blocks is actually quite important, as we will see in a bit. Studying the effective theory of one Weyl fermion is now hindered by the fact that the two coincide both in energy and momentum. To "separate" them, we apply a Zeeman magnetic field, which could be sourced by

some spontaneous ferromagnetic order in the crystal. Choosing this, without loss of generality, to be oriented along the z direction, we have

$$\tilde{\mathcal{H}}_{2-\mathrm{Weyl}}(\boldsymbol{k}) = \begin{pmatrix} \boldsymbol{k}\cdot\boldsymbol{\sigma} + B\sigma_z & 0 \\ 0 & -\boldsymbol{k}\cdot\boldsymbol{\sigma} + B\sigma_z \end{pmatrix}. \tag{10.1.6}$$

This Hamiltonian has now momentum-separated Weyl fermions: one at $k_z = B$ and one at $k_z = -B$ (see Fig. 10.1). Near each of these two momenta, two bands touch with an effective $\boldsymbol{k}\cdot\boldsymbol{\sigma}$ dispersion around the touching point, while the other two bands are at energies $\pm 2B$, and thus not considered part of the low-energy theory. The $\boldsymbol{k}\cdot\boldsymbol{\sigma}$ linear touching of two bands in three-dimensional momentum space is a *Weyl point*.

A Weyl point has topological robustness. Any translation-symmetric *small* perturbation that we add to a Hamiltonian $\boldsymbol{k}\cdot\boldsymbol{\sigma}$ can only move, but never remove the Weyl point! We can see this by expanding an arbitrary small perturbation in the basis of the Pauli matrices as $\delta_0\sigma_0 + \boldsymbol{\delta}\boldsymbol{\sigma}$. Adding it to the Hamiltonian gives

$$\delta_0\sigma_0 + (\boldsymbol{k} + \boldsymbol{\delta})\cdot\boldsymbol{\sigma}, \tag{10.1.7}$$

which now has Weyl point at $\boldsymbol{k} = -\boldsymbol{\delta}$ at energy δ_0. Weyl points can, however, annihilate pairwise.

It is a nice exercise to analytically calculate the Berry curvature near a Weyl node with Hamiltonian $\pm\boldsymbol{k}\cdot\boldsymbol{\sigma}$. For the occupied band, it is given by

$$\boldsymbol{\mathcal{F}}(\boldsymbol{k}) = \mp\frac{\boldsymbol{k}}{4\pi|\boldsymbol{k}|^3}. \tag{10.1.8}$$

This results suggests the interpretation of the Weyl node as a *monopole* of Berry curvature in momentum space. The monopole charge is quantized: If we integrate the Berry flux over any closed surface that encloses one of these Weyl nodes (which amounts to calculating the Chern number of the occupied bands on such a surface) we obtain ∓ 1. The overall sign in the Weyl Hamiltonian is thus the sign of the monopole (or chiral) charge of the Weyl fermion.

It is instructive to consider the Hamiltonian $\tilde{\mathcal{H}}_{2-\mathrm{Weyl}}(k_x, k_y, k_z)$ as describing two-dimensional systems in x-y space, while k_z is a "tuning parameter" of these systems. Each of these two-dimensional Hamiltonians describes a sensible physical system (i.e., it is local), which is gapped except at $k_z = \pm B$. What is the topology of these systems and is there a topological phase transition at $k_z = \pm B$? First, we notice that for each of our two-dimensional systems, the Chern number is well defined – we denote is by $\mathsf{C}^{(1)}(k_z)$. To answer our topology question, we go back to the monopole property of the Weyl points and consider the one at $k_z = B$, for concreteness: We can enclose it with two (oppositely oriented) planes at $k_z = B - \epsilon$ and $k_z = B + \epsilon$. Since the system is gapped on each of these planes, they have each an integer Chern number $\mathsf{C}^{(1)}(B-\epsilon)$, $\mathsf{C}^{(1)}(B+\epsilon)$ (for $0 < \epsilon < 2B$). The Weyl monopole implies $\mathsf{C}^{(1)}(B+\epsilon) - \mathsf{C}^{(1)}(B-\epsilon) = \mathrm{sgn}B$, with the minus sign coming from the opposite orientation. From the lattice model, we can deduce that $\mathsf{C}^{(1)}(|k_z| > |B|) = 0$. Hence, we obtain

$$\mathsf{C}^{(1)}(k_z) = \begin{cases} 0 & |k_z| > |B| \\ \mathrm{sgn}(B) & |k_z| < |B| \end{cases}. \tag{10.1.9}$$

Between the Weyl points, the two-dimensional system is thus as Chern insulator. Crucial for this is the breaking of time-reversal symmetry through the magnetic field (which preserves inversion symmetry).

For the Berry curvature, inversion symmetry implies

$$\boldsymbol{\mathcal{F}}(\boldsymbol{k}) = \boldsymbol{\mathcal{F}}(-\boldsymbol{k}), \tag{10.1.10}$$

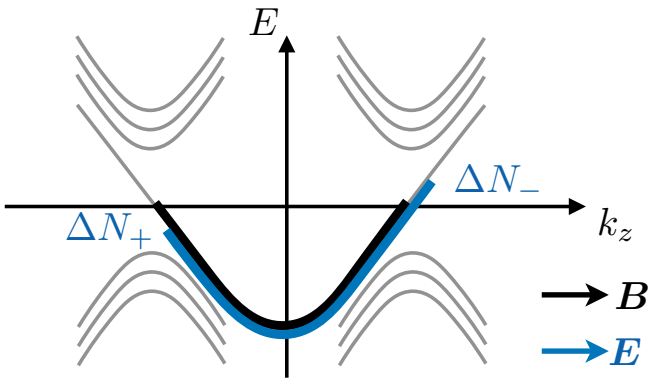

Figure 10.2: When a Weyl semimetal is expose to an orbital Zeeman field along the z direction, a k_z-dependent Landau level band structure forms (gray). In particular, one chiral and one antichiral Landau level pass through the Weyl points of monopole charge ± 1, respectively. When in addition an electrical field $\boldsymbol{E}$ is applied in parallel to the magnetic field, the resulting out-of-equilibrium, current-carrying state is depleting charge in one Weyl node and adding charge to the other Weyl node (blue). The chiral charge $N_+ - N_-$ is thus not conserved. This constitutes the chiral anomaly. The exchange of charge between the two Weyl nodes is allowed because the Landau levels at high energies connect the two Weyl nodes.

while time-reversal symmetry implies

$$\boldsymbol{\mathcal{F}}(\boldsymbol{k}) = -\boldsymbol{\mathcal{F}}(-\boldsymbol{k}). \tag{10.1.11}$$

One verifies that inversion (time-reversal) symmetry thus maps a Weyl cone of charge $+1$ at $\boldsymbol{k}$ to a cone at $-\boldsymbol{k}$ with charge -1 $(+1)$. Furthermore, the total charge of Weyl cones has to be zero in the entire BZ, due to its periodicity (a fact also conveyed by so-called Fermion doubling theorems). Thus, a time-reversal breaking Weyl semimetal (like our case), has at least two Weyl nodes, while an inversion-breaking Weyl semimetal has at least four Weyl nodes. Furthermore, the combination of inversion and time-reversal symmetry implies $\boldsymbol{\mathcal{F}}(\boldsymbol{k}) \equiv 0$, in which case no Weyl nodes can exist.
Another important property of Weyl semimetals are *Fermi arcs*, their topological surface states. Since, $\mathcal{H}_{2-\mathrm{Weyl}}(k_x, k_y, k_z)$, $|k_z| < |B|$ has a nonzero Chern number, it has, as a two-dimensional system, chiral boundary states. In the two-dimensional surface BZ of the three-dimensional system, these states combine into a chiral surface band. This band is anomalous, i.e., it can only exist on the surface of a thee-dimensional object. One way to see this is by considering the Fermi surface they form (see Fig. 10.1): At the energy of the bulk Weyl points, the surface band's Fermi surface is a line connecting the surface BZ projections of the two Weyl points, the Fermi arc. In two-dimensional systems, Fermi surfaces are always closed contours. The way the Fermi arc evades this paradigm is by moving the other half of the closed contour Fermi surface to the opposite surface of the material.

10.1.1 Transport properties and the chiral anomaly

Weyl semimetals have peculiar transport properties. Most immediate is the anomalous Hall effect. Considering each k_z as independently contributing to Hall transport, we obtain an anomalous Hall conductivity

$$\sigma_{xy} = \frac{2B}{2\pi}\frac{e^2}{h}. \tag{10.1.12}$$

Note that the three-dimensional Hall conductivity has units of inverse length times e^2/h, i.e., it depends on the crystal details. Here, we see that it is proportional to the distance of the Weyl

nodes in k_z direction ($2B$).
More surprising is the effect of an *orbital* magnetic field on transport (note that what is in the Hamiltonian so far is a Zeeman magnetic field). The phenomenon that we will describe here, the *chiral anomaly*, is present both for small and large magnetic fields, but it is easier to understand in a large field limit, where Landau levels are well established.
To appreciate the deep meaning of the chiral anomaly, we make a small excursion to field theory. An *anomaly* is in general defined as a symmetry of the classical equations of motion that is not respected once quantum fluctuations are taken into account. Mathematically, in a path integral formulation, this is enabled by a symmetry of the action which is broken by the path integral measure. Concretely, the action for Dirac electrons in three-dimensional space, represented by a spinor-valued field ψ, is given by

$$S_{\text{Dirac}} = \int \mathrm{d}^4x\, \psi^\dagger \not{\nabla} \psi \tag{10.1.13}$$

with the covariant kinetic operator $\not{\nabla} = \gamma^\mu(\partial_\mu - A_\mu)$, where γ^μ are the Gamma matrices fulfilling the Clifford algebra and A_μ is the electromagnetic vector potential. The equations of motion

$$\not{\nabla}\psi = 0, \qquad \psi^\dagger \overleftarrow{\not{\nabla}} = 0, \tag{10.1.14}$$

feature, besides the $U(1)$ rotations with a unit matrix, leading to the conservation of charge, a so-called chiral symmetry

$$\psi \to e^{\mathrm{i}\alpha\gamma_5}\psi, \tag{10.1.15}$$

where α is a real number. This leads to the chiral current

$$J_{\mu,5} := \psi^\dagger \gamma_\mu \gamma_5 \psi \tag{10.1.16}$$

to be classically conserved

$$\partial^\mu J_{\mu,5} = \psi^\dagger \overleftarrow{\not{\nabla}} \gamma_5 \psi - \psi^\dagger \gamma_5 \not{\nabla}\psi = 0. \tag{10.1.17}$$

However, when we compute the quantum average of this quantity with the full path integral

$$\begin{aligned} \langle \partial^\mu J_{\mu,5} \rangle =& \frac{\int \mathcal{D}[\psi]\mathcal{D}[\psi^\dagger] \left(\psi^\dagger \overleftarrow{\not{\nabla}} \gamma_5 \psi - \psi^\dagger \gamma_5 \not{\nabla}\psi \right) e^{S_{\text{Dirac}}}}{\int \mathcal{D}[\psi]\mathcal{D}[\psi^\dagger] e^{S_{\text{Dirac}}}} \\ =& \frac{1}{4\pi^2} \boldsymbol{E}\cdot\boldsymbol{B} \end{aligned} \tag{10.1.18}$$

we obtain a nonzero contribution if (non-orthogonal) electric and magnetic fields are simultaneously applied. The chiral current can be thought of as the difference between two currents of the chiral and antichiral part of the Fermion four-spinor. This is particularly apparent in the Dirac equation representation of Eq. (10.1.5), in which $\gamma_5 = \mathrm{diag}(1,1,-1,-1)$. It is thus the difference between the current of positive chirality Weyl fermions and the current of negative chirality Weyl fermions. Note that these currents are only well-defined in the continuum formulation of the Dirac equation. A fermion in a Weyl semimetal that lives at higher energies cannot be assigned to one or the other Weyl node.
This connection of the Weyl nodes at higher energies is what enables the chiral anomaly in a Weyl semimetal: Fermions can be pumped from one Weyl node to another through high-energy states when electric and magnetic fields are applied in parallel (see Fig. 10.2).
Finding unambiguous experimental proof of this fact has been proven difficult, with the most striking consequence found in semiclassical transport. One finds that the magnetoconductivity, i.e., the dependence of the conductivity on the applied magnetic field is highly anisotropic. It

has a quadratic magnetic field dependence that is maximal for transport along the magnetic field direction. Along the magnetic field direction the conductivity is modified from its zero field value σ_0 to

$$\sigma(B) = \sigma_0 + \frac{e^4 B^2 \tau_a}{4\pi^4 \nu(E_\mathrm{F})}, \tag{10.1.19}$$

where $\nu(E_\mathrm{F})$ is the density of states at the Fermi level and $1/\tau_a$ the rate of inter-Weyl node scattering. The most remarkable feature of this formula is the sign of the correction: this longitudinal magnetoconductivity is positive (and the longitudinal magnetoresistance thus negative). This is opposite to most other sources of magnetoresistance, where magnetic fields typically lead to increased localization and thus a larger resistivity.

10.1.2 Symmetry enforced Weyl nodes

We already discussed how time-reversal symmetry and inversion symmetry maps one Weyl node to another Weyl node of the same and opposite charge, respectively. This leaves the possibility open that a Weyl node is located at a time-reversal symmetric momentum. In fact, the generic time-reversal symmetric Hamiltonian of *any* spin-orbit coupled band around *any* time-reversal symmetric momentum takes the form $A_{i,j}\, k_i \sigma_j$ with material-specific coefficients $A_{i,j}$ and is thus a Weyl node. The degeneracy at $\boldsymbol{k} = 0$ is then protected by Kramers theorem. These so-called Kramers-Weyl nodes are thus very abundant in band structures. However, they are only relevant in cases where spin orbit coupling is so strong that it is not immediately overtaken by the next order (k^2) term in the Hamiltonian which comes from the normal band dispersion. Kramers-Weyl semimetals have the advantage of (potentially) very long Fermi arcs, since their Weyl nodes are maximally far apart in the BZ. Furthermore, many lattice symmetries, such as mirror and inversion, prevent spin-orbit coupling from being nonzero in all directions in momentum space around the time-reversal invariant momentum. Kramers-Weyl nodes are thus preferably found in low-symmetry crystal structures, in particular in all chiral space groups (those without any mirror or (roto-)inversion).
We continue with some further constraints that crystal symmetries pose for Weyl nodes.

- **Mirror symmetry**: Just as a real magnetic field, the component of the Berry curvature parallel to the mirror plane is conserved, while the other components are flipped. Thus, no Weyl node can lie on a mirror plane in momentum space and mirror-related Weyl nodes on opposite sides of the mirror plane have opposite chiral charge. Another way to argue is that no unitary operation can reverse the sign of only one of the three Pauli matrices, as would be required for $\boldsymbol{k} \cdot \boldsymbol{\sigma}$ to be mirror symmetric.

- **Rotation symmetry**: Weyl nodes can exist on a rotation axis. However, depending on the rotation eigenvalues of the two bands that are coming together, Weyl nodes of higher charge may appear. In general, for a n-fold rotation symmetry, let the two bands have eigenvalues $e^{\mathrm{i}l_1/n}$ and $e^{\mathrm{i}l_2/n}$, with $l_1, l_2 = 0, 1, \cdots, n-1$. The chiral charge c of possible Weyl nodes between these two bands on the rotation axis is given by the difference in "angular momentum" $e^{\mathrm{i}c/n} = e^{\pm\mathrm{i}(l_1-l_2)/n}$ (this relation also holds for spinful rotation symmetries where the eigenvalues are offset by a half-integer). An effective Hamiltonian for such a Weyl node of higher chiral charge is, for the case that the rotation axis is the z axis,

$$\mathcal{H}_{\mathrm{Weyl},c}(\boldsymbol{k}) = \begin{pmatrix} k_z & (k_x - \mathrm{i}k_y)^c \\ (k_x + \mathrm{i}k_y)^c & -k_z \end{pmatrix}. \tag{10.1.20}$$

10.2 Dirac semimetals

Much like Weyl semimetals are materials where a band touching is described by the Weyl equation, there exist Dirac semimetals, in which a band touching (of four bands) is described

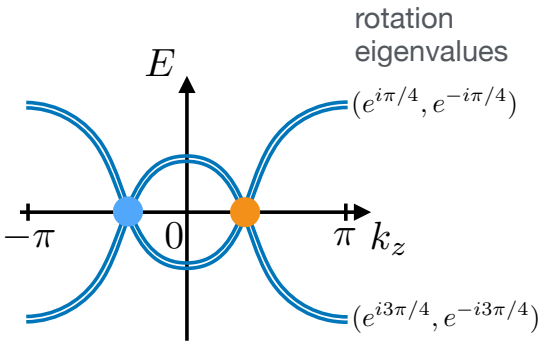

Figure 10.3: Band structure of the Dirac semimetal described by Eq. (10.2.2) for $k_x = k_y = 0$. The Dirac points are formed as doubly-degenerate pairs of bands with opposite rotation eigenvalues cross each other.

by the massless Dirac equation (10.1.5). We previously obtained Eq. (10.1.5) as a critical point between a topological insulator and a trivial insulator phase. As such, the Dirac fermion is not topologically stable. To obtain a topologically stable massless Dirac fermion, we have to impose some spatial symmetry on the system. We consider the case of four-fold rotation symmetry around the z axis as a concrete example and chose the representation

$$C_4^z = \tau_z \exp\left[\mathrm{i}\frac{\pi}{4}\sigma_z\right]. \tag{10.2.1}$$

One verifies that all terms in $\mathcal{H}_{\mathrm{TI}}(\boldsymbol{k})$ from Eq. (10.1.1) obey this C_4^z symmetry, except for the $\sin k_z$ term. We thus consider the Hamiltonian without this term,

$$\mathcal{H}_{\mathrm{Dirac-SM}}(\boldsymbol{k}) = \sin k_x\, \sigma_x\tau_x + \sin k_y\, \sigma_y\tau_x + \left(M - \sum_{i=x,y,z} \cos k_i\right) \sigma_0\tau_z, \tag{10.2.2}$$

which obeys

$$C_4^z \mathcal{H}_{\mathrm{Dirac-SM}}(R_4\boldsymbol{k})(C_4^z)^{-1} = \mathcal{H}_{\mathrm{Dirac-SM}}(\boldsymbol{k}), \tag{10.2.3}$$

where R_4 is the four-fold rotation matrix in three-dimensional Euclidian space.
All bands of $\mathcal{H}_{\mathrm{Dirac-SM}}(\boldsymbol{k})$ are doubly degenerate everywhere, since we still have time-reversal and inversion symmetry. These doubly degenerate bands can touch at two points in the BZ (see Fig. 10.3). To see this, it is sufficient to consider the spectrum at the $(k_x, k_y) = (0, 0)$ line. It is given by

$$E_\pm(0, 0, k_z) = \pm\left(M - 2 - \cos k_z\right). \tag{10.2.4}$$

For $1 < M < 2$, there are two of these degeneracy points, which are Dirac points. Let us denote their k_z momenta by $\pm k_z^{\mathrm{D}}$. They are the crossing points of two bands with different C_4^z eigenvalues (one band pair has $e^{\pm\mathrm{i}\pi/4}$, another one has $e^{\pm\mathrm{i}3\pi/4}$). Thus, as long as C_4^z symmetry is maintained, the degeneracies cannot be removed or split by small (time-reversal-, inversion- and translation-preserving) perturbations. These Dirac points are thus topologically stable, in contrast to the Dirac point that marked the phase transition point.
Another way to characterize their topological property is by noting that for $1 < M < 2$, the Hamiltonian $\mathcal{H}_{\mathrm{Dirac-SM}}(\boldsymbol{k})$ at fixed k_z describes a two-dimensional topological insulator at $k_z = 0$ and a trivial insulator at $k_z = \pi$. The Dirac point thus marks the phase transition point between the two (when k_z is viewed as a tuning parameter). This argument has one potential flaw: in contrast to the Weyl semimetal, where Chern insulator topology was well-defined at every k_z slice, we require time-reversal symmetry to define the two-dimensional topological insulator, which a priori is only true for $k_z = 0, \pi$.

10.3 New fermions

We observed that Kramers-Weyl fermions can form at (and are pinned to) high-symmetry points in the BZ as two-fold band degeneracies. One may ask which higher band degeneracies are possibly enforced at high-symmetry points in the BZ if crystalline symmetries are considered in addition to time-reversal. The answer to this question is rather rich and has been determined for spin-orbit coupled band structures. One finds examples for $2-$, $3-$, $4-$, $6-$ and even $8-$fold protected degeneracies of bands, also known as *new Fermions*. One intuitive example is a degeneracy of three bands with the effective Hamiltonian

$$\mathcal{H}_{\text{spin}-1}(\boldsymbol{k}) = \boldsymbol{k} \cdot \boldsymbol{S}, \tag{10.3.1}$$

where S_i are the generators of the rotation group SO(3) in the spin-1 representation, which are 3×3 matrices. (This example appears in space groups 199 and 214.) The Chern numbers of each of the bands, obtained by integrating the Berry curvature over any surface enclosing the degeneracy point, are $\mathsf{C}^{(1)} = \pm 2$ and $\mathsf{C}^{(1)} = 0$. The degeneracy is thus not characterized by a single charge anymore, but a set of such charges.

10.4 Nodal line semimetals

In addition to degeneracy points, we can also consider degeneracies of bands along lines in momentum space. There is ample literature analyzing many aspects of this subject. Here, we just mention that a frequent mechanism for the protection of such nodal lines is the existence of a mirror symmetry. The line degeneracy can then be deformed within the mirror plane in momentum space, but cannot be removed by a small perturbation. Concretely, let us consider a two-band effective Hamiltonian, and consider a mirror operation $z \to -z$, i.e.,

$$M_z \mathcal{H}(k_x, k_y, -k_z) M_z^{-1} = \mathcal{H}(k_x, k_y, k_z). \tag{10.4.1}$$

Without loss of generality, we further assume $M = \sigma_z$ (in a spin-orbit coupled system, we would have $M = \mathrm{i}\sigma_z$ for it to commute with time-reversal symmetry). On the mirror planes $k_z = 0, \pi$, the symmetry then prevents σ_x and σ_y from entering the Hamiltonian. Degeneracies are thus zeros of the real function $d_z(k_x, k_y)$ in a Hamiltonian of the form

$$\mathcal{H}(k_x, k_y; 0, \pi) = d_0(k_x, k_y)\sigma_0 + d_z(k_x, k_y)\sigma_z. \tag{10.4.2}$$

Zeros of a scalar real function in two-dimensional parameter space are generically lines – the nodal line band degeneracies. Away from the mirror plane, there is no local (in $\boldsymbol{k}$) symmetry constraint on the Hamiltonian and the line-like degeneracy can thus gap out. It is confined to the mirror plane.

References

1. Wan, X., Turner, A. M., Vishwanath, A. & Savrasov, S. Y. "Topological semimetal and Fermi-arc surface states in the electronic structure of pyrochlore iridates". *Phys. Rev. B* **83,** 205101. http://link.aps.org/doi/10.1103/PhysRevB.83.205101 (2011).
2. Bradlyn, B. *et al.* "Topological quantum chemistry". *Nature* **537,** 298. https://dx.doi.org/10.1038/nature23268 (2017).
3. Chang, G. *et al.* "Topological quantum properties of chiral crystals". *Nature Mat.* **17,** 978. https://www.nature.com/articles/s41563-018-0169-3 (2018).

Chapter 11

Kitaev's Honeycomb Model and the Toric code

Learning goals

- We know the physical motivation, Hamiltonian, and phase diagram of Kitaev's honeycomb model.
- We understand how some phases reduce to the toric code Hamiltonian.
- We know how to rewrite the ground state and low-lying excitations in terms of Majorana degrees of freedom.
- We know the toric code model Hamiltonian and understand its ground state manifold.
- We know the emergent excitations above the ground states, and how to derive their statistics.

- A. Kitaev, Annals of Physics **321**, 2–111 (2006)

So far, we have been concerned with symmetry protected topological states and considered examples that were motivated by the topological classification of free fermion Hamiltonians. The topological properties of these systems are manifest by the presence of protected boundary modes. In this Chapter, we want to familiarize ourselves with the concept of intrinsic topological order by ways of several examples. We will study the connections between different characterizations of topological order, such as fractionalized excitations in the bulk and the topological ground state degeneracy. Our examples will be in 2D space, as topologically ordered states do not exist in 1D and are best understood in 2D.

11.1 Definition of the model

We want to physically motivate the following Hamiltonian

$$H = -J_x \sum_{x-\text{links}} \sigma_j^x \sigma_k^x - J_y \sum_{y-\text{links}} \sigma_j^y \sigma_k^y - J_z \sum_{z-\text{links}} \sigma_j^z \sigma_k^z, \tag{11.1.1}$$

acting on spin 1/2 degrees of freedom on a honeycomb lattice, where the bonds in the 3 inequivalent directions have been labeled x, y, z. This Hamiltonian has been proposed to be relevant to the honeycomb iridates Na_2IrO_3 and Li_2IrO_3, see Fig. 11.1, and there is mounting experimental evidence that α-$RuCl_3$ is governed (in part) by this Hamiltonian. In addition, there is a Heisenberg term allowed and competing with this term in the materials, but since we are interested in the physics in some integrable limit, we consider the Hamiltonian (11.1.1) on its own right.
A model is called integrable if it has an extensive number of integrals of motion. In what we studied so far, we have simply used the powers of the primitive translation operator (or the momentum operator) as the conserved quantities. For Hamiltonian (11.1.1), we can construct

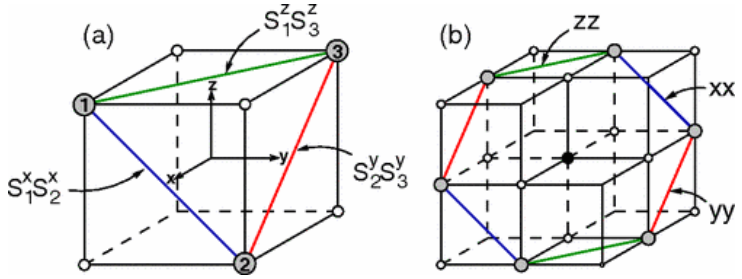

Figure 11.1: Examples of the structural units formed by 90 degree TM-O-TM bonds and corresponding spin-coupling patterns. Gray circles stand for magnetic ions (e.g., Ir), and small open circles denote oxygen sites, and black is sodium, for example. From [PRL **102**, 017205 (2009)]. Spins come from the Ir 5d orbitals, which in the octahedral coordination split in t_{2g} and e_g. The former further split into a $j = 1/2$ and a $j = 3/2$ sector by spin-orbit coupling. In the $j = 1/2$ sector, the 90 degree Ir-O-Ir bonds give rise to the Kitaev exchange interaction.

local conserved quantities as follows: consider around any plaquette p of the hexagonal lattice the operator

$$W_p = \sigma_1^x \sigma_2^y \sigma_3^z \sigma_4^x \sigma_5^y \sigma_6^z, \tag{11.1.2}$$

where $1 \cdots 6$ label the sites around the plaquette in such a way that the link leading out of the plaquette from site i is a $\alpha = x, y, z$ link if σ_i^α appears in W_p [see Fig. 11.2 a)]. Observe that W_p has eigenvalues ± 1 and commutes with the Hamiltonian. Thus the Hilbert space splits up in sectors with fixed eigenvalues $w_p = \pm 1$ of each operator W_p. The honeycomb lattice has $1/2$ plaquette per spin, hence for N vertices the total Hilbert space dimension 2^N is reduced to $2^{N/2}$ subspaces of dimension $2^{N/2}$. Hence, the problem is not completely solved by splitting it into w_p sectors, but we made some progress still.
Further progress can be made by representing the spins in terms of Majorana operators: Consider at every site j of the honeycomb lattice four Majorana operators b_j^x, b_j^y, b_j^z, and c_j, which obey the usual relations

$$\{b_j^\alpha, b_j^{\alpha'}\} = 2\delta_{\alpha,\alpha'}, \qquad \{b_j^\alpha, c_j\} = 0, \qquad c_j^2 = 1. \tag{11.1.3}$$

Four Majorana operators furnish a 4-dimensional Hilbert space $\tilde{\mathcal{M}}_j$ (one can build 2 complex fermions from them). This is twice as large as the Hilbert space of a single spin. We reduce $\tilde{\mathcal{M}}_j$ to a physical subspace $\mathcal{M}_j \subset \tilde{\mathcal{M}}_j$ by the following constraint

$$|\xi_j\rangle \in \mathcal{M}_j \qquad \Leftrightarrow \qquad D_j |\xi_j\rangle = |\xi_j\rangle, \tag{11.1.4}$$

where $D_j = b_j^x b_j^y b_j^z c_j$. We see that D_j is the total parity of the two fermionic levels defined from the four Majoranas. We now want to represent the Pauli operators on $\tilde{\mathcal{M}}_j$ such that the respective operators obey the same algebra on $\mathcal{M}_j$ and commute with D_j (i.e., they preserve the subspace $\mathcal{M}_j$). We choose

$$\tilde{\sigma}_j^\alpha = \mathrm{i} b_j^\alpha c_j, \qquad \alpha = x, y, z. \tag{11.1.5}$$

Observe that $\tilde{\sigma}_j^x \tilde{\sigma}_j^y \tilde{\sigma}_j^z = \mathrm{i} D_j$, and D_j is the identity on $\mathcal{M}_j$, compatible with $\sigma_j^x \sigma_j^y \sigma_j^z = \mathrm{i}$.
We can use this Majorana representation to rewrite all the terms in our Hamiltonian

$$\sigma_j^\alpha \sigma_k^\alpha \to (\mathrm{i} b_j^\alpha c_j)(\mathrm{i} b_k^\alpha c_k) = -\mathrm{i}(\mathrm{i} b_j^\alpha b_k^\alpha) c_j c_k, \tag{11.1.6}$$

where $\alpha = x, y, z$ is not summed over. We can rewrite

$$\tilde{H} = \frac{\mathrm{i}}{4} \sum_{j,k} \hat{A}_{jk} c_j c_k \tag{11.1.7}$$

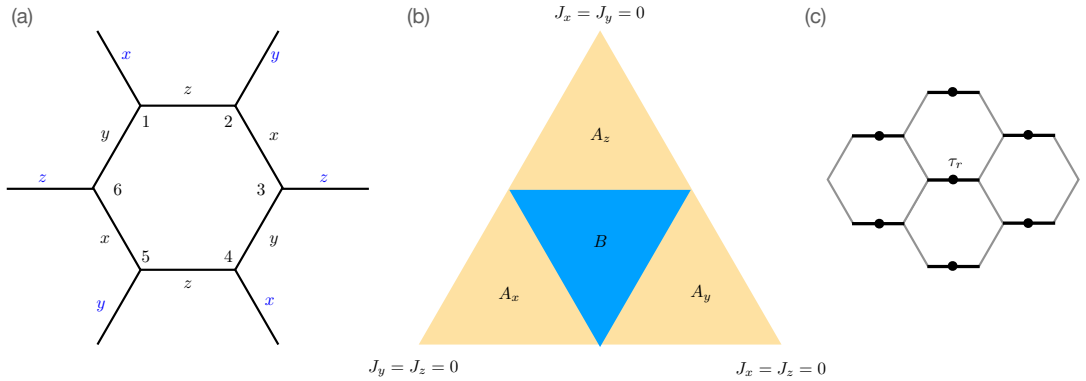

Figure 11.2: a) Definition of x, y, z type bonds for the Kitaev Hamiltonian (11.1.1) on the honeycomb lattice and of the numbering of sites within a plaquette that enter the W_p operator (11.1.2). b) Phase diagram of the Kitaev honeycomb model. c) Strong bonds that are replaced with an effective spin-1/2 degree of freedom in the limit $|J_z| \gg |J_x|, |J_y|$ to derive the toric code Hamiltonian.

where $\hat{A}_{jk} = 2J_{\alpha_{jk}} \hat{u}_{ik}$ is a hermitian operator when i and j are connected and 0 otherwise. We defined $\hat{u}_{jk} := \mathrm{i} b_j^\alpha b_k^\alpha$ which commutes with the Hamiltonian and with the other $\hat{u}_{j'k'}$. Each $\hat{u}_{jk}$ has eigenvalues $u_{jk} = \pm 1$ and in each sector we can simply obtain the Hamiltonian by replacing operators by numbers, i.e.,$\hat{A}_{jk} \to A_{jk} = 2J_{\alpha_{jk}} u_{ik}$. However, observe that $\{\hat{u}_{jk}, D_j\} = 0$, i.e., $\hat{u}_{jk}$ does not leave the subspace $\mathcal{M}_j$ invariant. Starting from a ground state $|\tilde{\Psi}_u\rangle$ of $\tilde{H}_u = \frac{\mathrm{i}}{4} \sum_{j,k} A_{jk} c_j c_k$, we can construct a state

$$|\Psi_w\rangle = \prod_j \left(\frac{1 + D_j}{2} \right) |\tilde{\Psi}_u\rangle, \tag{11.1.8}$$

where w is the collection of eigenvalues w_p for each plaquette operator W_p. In therms of the Majorana bilinear eigenvalues they are given by $w_p = \prod_{j,k \in \partial p; j<k} u_{jk}$.
The lowest energy state is obtained if all $u_{jk} = +1$, which is a nontrivial statement. The relevant Hamiltonian is given by

$$H_{\text{vortex-free}} = \frac{1}{4} \sum_{\boldsymbol{k}} \begin{pmatrix} c_{-\boldsymbol{k},A} & c_{-\boldsymbol{k},B} \end{pmatrix} \begin{pmatrix} 0 & \mathrm{i} f(\boldsymbol{k}) \\ -\mathrm{i} f(\boldsymbol{k})^* & 0 \end{pmatrix} \begin{pmatrix} c_{\boldsymbol{k},A} \\ c_{\boldsymbol{k},B} \end{pmatrix} \tag{11.1.9}$$

where

$$f(\boldsymbol{k}) = 2(J_x e^{\mathrm{i}\boldsymbol{k}\cdot\boldsymbol{a}_1} + J_y e^{\mathrm{i}\boldsymbol{k}\cdot\boldsymbol{a}_2} + J_z), \qquad \boldsymbol{a}_1 = \frac{1}{2}(1, \sqrt{3}), \quad \boldsymbol{a}_2 = \frac{1}{2}(-1, \sqrt{3}). \tag{11.1.10}$$

The spectrum corresponds to that of anisotropic graphene. Time-reversal symmetry and inversion symmetry, which protect the Dirac cones, are retained. Hence the system can only gap out if the anisotropy is large enough for two cones to meet (at one of the TRIM points). Said differently, zero energy solutions $J_x e^{\mathrm{i}\boldsymbol{k}\cdot\boldsymbol{a}_1} + J_y e^{\mathrm{i}\boldsymbol{k}\cdot\boldsymbol{a}_2} + J_z = 0$ are obtained if and only if

$$|J_x| \leq |J_y| + |J_z|, \qquad |J_y| \leq |J_x| + |J_z|, \qquad |J_z| \leq |J_x| + |J_y|. \tag{11.1.11}$$

This gives a phase diagram with three gapped phases A_x, A_y, A_z and a gapless phase B [see Fig. 11.2 b)]. The gapless phase has Majorana Dirac cones.

11.2 The gapped phases

Topological properties of a gapped phase are constant throughout the phase and we may study them in a parameter regime that is convenient for us. We will focus on the phase A_z and study it in the limit $|J_z| \gg |J_x|, |J_y|$. The Hamiltonian is given by $H = H_0 + V$ where

$$H_0 = -J_z \sum_{z-\text{links}} \sigma_j^z \sigma_k^z, \qquad V = -J_x \sum_{x-\text{links}} \sigma_j^x \sigma_k^x - J_y \sum_{y-\text{links}} \sigma_j^y \sigma_k^y, \tag{11.2.1}$$

is the dominant term and the perturbation, respectively. Out of two spins connected by a z-link, H_0 selects the states where these spins are both parallel or anti-parallel [see Fig. 11.2 c)]. We may thus replace these two spins by a single spin 1/2, which is acted upon with the V perturbation. Let us act on these spins with Pauli matrices τ_r^α to distinguish them from the original spins. The sites r live now on the links of a square lattice. It turns out that, to get back to the degenerate ground state subspace of H_0, one needs to apply the perturbation V 4 times. After going to fourth order in perturbation theory, and applying a unitary transformation, we obtain the Hamiltonian

$$H_{\text{eff}} = -J_{\text{eff}} \left(\sum_s A_s + \sum_p B_p \right) \tag{11.2.2}$$

where $J_{\text{eff}} = J_x^2 J_y^2 / (16|J_z|^3)$. Here, the four spins that sit on the bonds emanating from a given site r of the lattice are referred to as a star s. The four spins that sit on the bonds surrounding a square of the lattice are called a plaquette p. We defined two sets of operators

$$A_s := \prod_{r \in s} \tau_r^x, \qquad B_p := \prod_{r \in p} \tau_r^z. \tag{11.2.3}$$

We will analyze this exact same Hamiltonian in the following section.

11.3 Gapping the gapless phase

The gapless phase B has both vortex-like excitations which are gapped and fermionic excitations which are gapless (they live on a Majorana cone). The statistics of the vortices is not well defined due to the interaction with the gapless fermionic background. The gapless nature of the fermions is protected by (inversion times) time-reversal symmetry, just as in graphene. This is true for all flux sectors, as $\mathbb{Z}_2$ flux does not break time-reversal symmetry. The fermions can, however, be gapped out when breaking time-reversal symmetry. Consider applying an external magnetic field

$$\delta H_{\text{B}} = -\sum_j \boldsymbol{B} \cdot \boldsymbol{\sigma}_j. \tag{11.3.1}$$

Kitaev showed that in the vortex-free sector, the time-reversal symmetry breaking nature of this term manifests to third order in perturbation theory (for $J_x = J_y = J_z = J$) as

$$\delta H_{\text{B}}^{(3)} = -\frac{B_x B_y B_z}{J^2} \sum_{i,k,l} \sigma_j^x \sigma_k^y \sigma_l^z, \tag{11.3.2}$$

where sites j, k, l are clockwise neighbors belonging to s single hexagon (i.e., there are six such terms in each hexagon). In the fermionic language

$$\begin{aligned} \sigma_j^x \sigma_k^y \sigma_l^z =& (\mathrm{i} b_j^x c_j)(\mathrm{i} b_k^y c_k)(\mathrm{i} b_l^z c_l) \\ =& -\mathrm{i} b_j^x c_j \, b_k^x b_k^x \, b_k^y c_k \, b_k^z b_k^z \, b_l^z c_l \\ =& -\mathrm{i} (b_k^x b_k^y b_k^z c_k)(b_j^x b_k^x)(b_k^z b_l^z) c_j c_l \\ =& +\mathrm{i} D_k \hat{u}_{jk} \hat{u}_{kl} c_j c_l. \end{aligned} \tag{11.3.3}$$

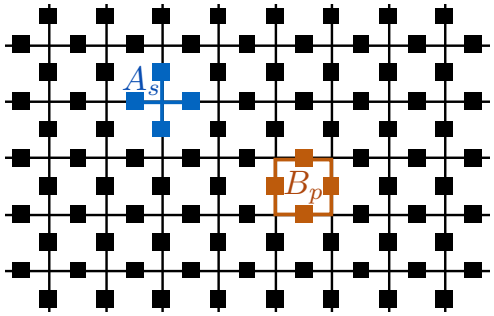

Figure 11.3: The toric code model is defined on a square lattice with spin-1/2 degrees of freedom on every bond (black squares). The operator A_s acts with σ_x on all four spins one the bonds that are connected to a lattice site (a star s). The operator B_p acts with σ_z on all four spins around a plaquette p.

Omitting D in the physical subspace and using the standard gauge, $\hat{u}_{jk} = \hat{u}_{kl} = 1$, we have a term $\mathrm{i}c_j c_l$ which is exactly the NNN hopping of the Haldane model with $\phi = \pi/2$ and $t_2 \sim B_x B_y B_z / J^2$. Thus, with the magnetic field switched on, the Majorana fermion bands acquire a Chern number ± 1. We thus have a model formally equivalent to the chiral p-wave superconductor, with the important difference that the $\mathbb{Z}_2$ vortices are *dynamic* objects this time, i.e., the system is properly topologically ordered with non-Abelian Majorana anyons σ (a vortex) and the same properties as discussed before.

11.4 The toric code

As an example of a topologically ordered state we study an exactly soluble model with vanishing correlation length. The significance of having zero correlation length is the following. The correlation functions of local operators decay exponentially in gapped quantum ground states in 1D and 2D with a characteristic length scale given by the correlation length ξ. In contrast, topological properties are encoded in quantized expectation values of nonlocal operators (for example the Hall conductivity) or the degeneracy of energy levels (such as the end states of the Su-Schrieffer-Heeger model). In finite systems, such quantizations and degeneracies are generically only exact up to corrections that are of order $e^{-L/\xi}$, where L is the linear system size. Models with zero correlation length are free from such exponential finite-size corrections and thus expose the topological features already for the smallest possible system sizes. The down-side is that their Hamiltonians are rather contrived.
We define the toric code model on a square lattice with a spin-1/2 degree of freedom on every *bond* j (see Fig. 11.3). The four spins that sit on the bonds emanating from a given site of the lattice are referred to as a star s. The four spins that sit on the bonds surrounding a square of the lattice are called a plaquette p. We define two sets of operators

$$A_s := \prod_{j \in s} \sigma_j^x, \qquad B_p := \prod_{j \in p} \sigma_j^z, \tag{11.4.1}$$

that act on the spins of a given star s and plaquette p, respectively. Here, $\sigma_j^{x,z}$ are the respective Pauli matrices acting on the spin on bond j.
These operators have two crucial properties which are often used to construct exactly soluble models for topological states of matter

1. All of the A_s and B_p commute with each other. This is trivial for all cases except for the commutator of A_s with B_p if s and p have spins in common. However, any star shares with

any plaquette an even number of spins (edges), so that commuting A_s with B_p involves commuting an even number of σ^z with σ^x, each of which comes with a minus sign.

2. The operators
$$\frac{1-B_p}{2}, \qquad \frac{1-A_s}{2} \tag{11.4.2}$$
are projectors. The former projects out plaquette states with an even number of spins polarized in the positive z-direction. The latter projects out stars with an even number of spins in the positive x-direction.

11.4.1 Ground states

The Hamiltonian is defined as a sum over these commuting projectors

$$H = -J_{\mathrm{e}} \sum_s A_s - J_{\mathrm{m}} \sum_p B_p, \tag{11.4.3}$$

where the sums run over all stars s and plaquettes p of the lattice. Let us assume that both J_{e} and J_{m} are positive constants. Then, the ground state is given by a state in which all stars s and plaquettes p are in an eigenstate with eigenvalue $+1$ of A_s and B_p, respectively. (The fact that all A_s and B_p commute allows for such a state to exist, as we can diagonalize each of them separately.) Let us think about the ground state in the eigenbasis of the σ^x operators and represent by bold lines those bonds with spin up and and draw no lines along bonds with spin down. Then, A_s imposes on all spin configurations with nonzero amplitude in the ground state the constraint that an even number of bold lines meets at the star s. In other words, we can think of the bold lines as connected across the lattice and they may only form closed loops. Bold lines that end at some star ("open strings") are not allowed in the ground state configurations; they are excited states. Having found out which spin configurations are allowed in the ground state, we need to determine their amplitudes. This can be inferred from the action of the B_p operators on these closed loop configurations. The B_p flips all bonds around the plaquette p. Since $B_p^2 = 1$, given a spin configuration $|c\rangle$ in the σ^x-basis, we can write an eigenstate of B_p with eigenvalue 1 as

$$\frac{1}{\sqrt{2}} \left(|c\rangle + B_p |c\rangle \right), \tag{11.4.4}$$

for some fixed p. This reasoning can be extended to all plaquettes so that we can write for the ground state

$$|\mathrm{GS}\rangle = \left(\prod_p \frac{1+B_p}{\sqrt{2}} \right) |c\rangle, \tag{11.4.5}$$

where $|c\rangle$ is a closed loop configuration [see Fig. 11.4 a)]. Is $|\mathrm{GS}\rangle$ independent of the choice of $|c\rangle$? In other words, in the ground state unique? We will see that the answer depends on the topological properties of the manifold on which the lattice is defined and thus reveals the topological order imprinted in $|\mathrm{GS}\rangle$.

To answer these questions, let us consider the system on two topologically distinct manifolds, the torus and the sphere. To obtain a torus, we consider a square lattice with $L_x \times L_y$ sites and impose periodic boundary conditions. This lattice hosts $2L_xL_y$ spins (2 per unit cell for they are centered along the bonds). Thus, the Hilbert space of the model has dimension $2^{2L_xL_y}$. There are L_xL_y operators A_s and just as many B_p. Hence, together they impose $2L_xL_y$ constraints on the ground state in this Hilbert space. However, not all of these constraints are independent. The relations

$$1 = \prod_s A_s, \qquad 1 = \prod_p B_p \tag{11.4.6}$$

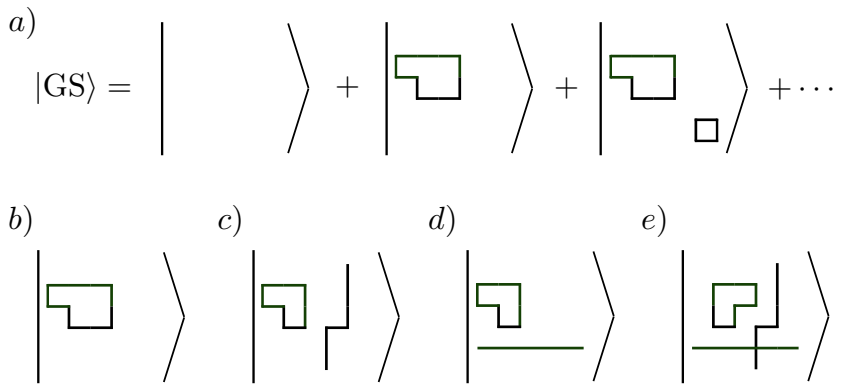

Figure 11.4: Visualization of the toric code ground states on the torus. a) The toric code ground state is the equal amplitude superposition of all closed loop configurations. b)-e) Four base configurations $|c\rangle$ entering Eq. (11.4.5) that yield topologically distinct ground states on the torus.

make two of the constraints redundant, yielding $(2L_xL_y - 2)$ independent constraints. The ground state degeneracy (GSD) is obtained as the quotient of the Hilbert space dimension and the subspace modded out by the constraints

$$\text{GSD} = \frac{2^{2L_xL_y}}{2^{2L_xL_y-2}} = 4. \tag{11.4.7}$$

The four ground states on the torus are distinguished by having an even or an odd number of loops wrapping the torus in the x and y direction, respectively. Four configurations $|c\rangle$ that can be used to build the four degenerate ground states are shown in Fig. 11.4 b)-e). This constitutes a set of "topologically degenerate" ground states and is a hallmark of the topological order in the model.

Let us contrast this with the ground state degeneracy on the sphere. Since we use a zero correlation length model, we might as well use the smallest convenient lattice with the topology of a sphere. We consider the model (11.4.3) defined on the edges of a cube. The same counting as above yields that there are 12 degrees of freedom (the spins on the 12 edges), 8 constraints from the A_s operators defined on the corners and 6 constraints from the B_p operators defined on the faces. Subtracting the 2 redundant constraints (11.4.6) yields $12-(8+6-2) = 0$ remaining degrees of freedom. Hence, the model has a unique ground state on the sphere.

On a general manifold, we have

$$\text{GSD} = 2^{\text{number of noncontractible loops}}. \tag{11.4.8}$$

An important property of the topologically degenerate ground states is that any local operator has vanishing off-diagonal matrix elements between them in the thermodynamic limit. Similarly, no local operator can be used to distinguish between the ground states. We can, however, define *nonlocal* operators that transform one topologically degenerate ground state into another and that distinguish the ground states by topological quantum numbers. (Notice that such operators may not appear in any physical Hamiltonian due to their nonlocality and hence the degeneracy of the ground states is protected.) On the torus, we define two pairs of so-called Wilson loop operators as

$$W^{\text{e}}_{x/y} := \prod_{j\in l^{\text{e}}_{x/y}} \sigma^z_j, \qquad W^{\text{m}}_{x/y} := \prod_{j\in l^{\text{m}}_{x/y}} \sigma^x_j. \tag{11.4.9}$$

Here, $l^{\text{e}}_{x/y}$ are the sets of spins on bonds parallel to a straight line wrapping the torus once along the x- and y-direction, respectively. The $l^{\text{m}}_{x/y}$ are the sets of spins on bonds perpendicular to a

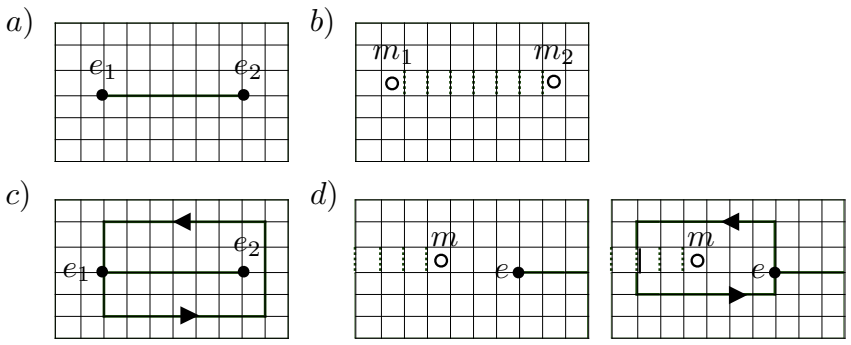

Figure 11.5: Visualization of operations to compute the braiding statistics of toric code anyons. a) Two e excitations above the ground state. b) Two m excitations above the ground state. c) Loop created by braiding e_1 around e_2. c) Loop created by braiding e around m. A phase of -1 results for this process because there is a single bond on which both a σ^x operator (dotted line) and a σ^z operator (bold line) act.

straight line that connects the centers of plaquettes and wraps the torus once along the x and y-direction, respectively. We note that the $W^{\mathrm{e}}_{x/y}$ and $W^{\mathrm{m}}_{x/y}$ commute with all A_s and B_p

$$\left[W^{\mathrm{e/m}}_{x/y}, A_s\right] = \left[W^{\mathrm{e/m}}_{x/y}, B_p\right] = 0, \tag{11.4.10}$$

and thus also with the Hamiltonian. Furthermore, they obey

$$W^{\mathrm{e}}_x W^{\mathrm{m}}_y = -W^{\mathrm{m}}_y W^{\mathrm{e}}_x. \tag{11.4.11}$$

This algebra must be realized in any eigenspace of the Hamiltonian. However, due to Eq. (11.4.11), it cannot be realized in a one-dimensional subspace. We conclude that all eigenspaces of the Hamiltonian, including the ground state, must be degenerate. In the σ^x basis that we used above, $W^{\mathrm{m}}_{x/y}$ measures whether the number of loops wrapping the torus is even or odd in the x and y direction, respectively, giving 4 degenerate ground states. In contrast, $W^{\mathrm{e}}_{x/y}$ changes the number of loops wrapping the torus in the x and y direction between even and odd.

11.4.2 Topological excitations

To find the topological excitations of the system above the ground state, we ask which are the lowest energy excitations that we can build. Excitations are a violation of the rule that all stars s are eigenstates of A_s and all plaquettes p are eigenstates of B_p. Let us first focus on star excitations which we will call e. They appear as the end point of open strings, i.e., if the closed loop condition is violated. Since any string has two end points, the lowest excitation of this type is a pair of e. They can be created by acting on the ground state with the operator

$$W^{\mathrm{e}}_{l^{\mathrm{e}}} := \prod_{j \in l^{\mathrm{e}}} \sigma^z_j, \tag{11.4.12}$$

where l^{e} is a string of bonds connecting the two excitations e_1 and e_2 [see Fig. 11.5 a)]. The state

$$|e_1, e_2\rangle := W^{\mathrm{e}}_{l^{\mathrm{e}}} |\mathrm{GS}\rangle \tag{11.4.13}$$

has energy $4J_{\mathrm{e}}$ above the ground state energy. Similarly, we can define an operator

$$W^{\mathrm{m}}_{l^{\mathrm{m}}} := \prod_{j \in l^{\mathrm{m}}} \sigma^x_j, \tag{11.4.14}$$

that creates a pair of plaquette defects m_1 and m_2 connected by the string l^{m} of perpendicular bonds [see Fig. 11.5 b)]. (Notice that the operator $W^{\mathrm{m}}_{l^{\mathrm{m}}}$ does not flip spins when the ground state is written in the σ^x basis. Rather, it gives weight $+1/-1$ to the different loop configurations in the ground state, depending on whether an even or an odd number of loops crosses l^{m}.) The state

$$|m_1, m_2\rangle := W^{\mathrm{m}}_{l^{\mathrm{m}}}|\mathrm{GS}\rangle \tag{11.4.15}$$

has energy $4J_{\mathrm{m}}$ above the ground state energy. Notice that the excited states $|e_1, e_2\rangle$ and $|m_1, m_2\rangle$ only depend on the positions of the excitations and not on the particular choice of string that connects them. Furthermore, the energy of the excited state is independent of the separation between the excitations. The excitations are thus "deconfined", i.e., free to move independent of each other.

It is also possible to create a combined defect when a plaquette hosts a m excitation and one of its corners hosts a e excitation. We call this combined defect f and formalize the relation between these defects in a so-called fusion rule

$$e \times m = f. \tag{11.4.16a}$$

When two e-type excitations are moved to the same star, the loop l^{e} that connects them becomes a closed loop and the state returns to the ground state. For this, we write the fusion rule

$$e \times e = 1, \tag{11.4.16b}$$

where 1 stands for the ground state or vacuum. Similarly, moving two m-type excitations to the same plaquette creates a closed loop l^{m}, which can be absorbed in the ground state, i.e.,

$$m \times m = 1. \tag{11.4.16c}$$

Superimposing the above processes yields the remaining fusion rules

$$m \times f = e, \qquad e \times f = m, \qquad f \times f = 1. \tag{11.4.16d}$$

It is now imperative to ask what type of quantum statistics these emergent excitations obey. We recall that quantum statistics are defined as the phase by which a state changes if two identical particles are exchanged. Rendering the exchange operation as an adiabatically slow evolution of the state, in three and higher dimensions only two types of statistics are allowed between point particles: that of bosons with phase $+1$ and that of fermions with phase -1. In 2D, richer possibilities exist and the exchange phase ϑ can be *any* complex number on the unit circle, opening the way for *any*ons. While the exchange is only defined for quantum particles of the same type, the double exchange (braiding) is well defined between any two deconfined anyons. We can compute the braiding phases of the anyons e, m, and f that appear in the toric code one by one. Let us start with the phase resulting from braiding e_1 with e_2. The initial state is $W^{\mathrm{e}}_{l^{\mathrm{e}}}|\mathrm{GS}\rangle$ depicted in Fig. 11.5 a). Moving e_1 around e_2 leaves a loop of flipped σ^x bonds around e_2 [see Fig. 11.5 c)]. This loop is created by applying B_p to all plaquettes enclosed by the loop $l^{\mathrm{e}}_{e_1}$ along which e_1 moves. We can thus write the final state as

$$\begin{aligned}\left(\prod_{p\in l^{\mathrm{e}}_{e_1}} B_p\right) W^{\mathrm{e}}_{l^{\mathrm{e}}}|\mathrm{GS}\rangle &= W^{\mathrm{e}}_{l^{\mathrm{e}}}\left(\prod_{p\in l^{\mathrm{e}}_{e_1}} B_p\right)|\mathrm{GS}\rangle \\ &= W^{\mathrm{e}}_{l^{\mathrm{e}}}|\mathrm{GS}\rangle.\end{aligned} \tag{11.4.17}$$

Flipping the spins in a closed loop does not alter the ground state as it is the equal amplitude of all loop configurations. We conclude that the braiding of two e particles gives no phase. Similar considerations can be used to conclude that the braiding of two m particles is trivial as well.

In fact, not only the braiding, but also the exchange of two e particles and two m particles is trivial. (We have not shown that here.)
More interesting is the braiding of m with e. Let the initial state be $W^{\mathrm{m}}_{l^{\mathrm{m}}} W^{\mathrm{e}}_{l^{\mathrm{e}}} |\mathrm{GS}\rangle$ and move the e particle located on one end of the string $l^{\mathrm{e}}_{\mathrm{in}}$ around the magnetic particle m on one end of the string l^{m}. Again this is equivalent to applying B_p to all plaquettes enclosed by the path l^{e}_e of the e particle, so that the final state is given by

$$\begin{aligned}\left(\prod_{p\in l^{\mathrm{e}}_e} B_p\right) W^{\mathrm{m}}_{l^{\mathrm{m}}} W^{\mathrm{e}}_{l^{\mathrm{e}}} |\mathrm{GS}\rangle &= -\, W^{\mathrm{m}}_{l^{\mathrm{m}}} \left(\prod_{p\in l^{\mathrm{e}}_e} B_p\right) W^{\mathrm{e}}_{l^{\mathrm{e}}} |\mathrm{GS}\rangle \\ &= -\, W^{\mathrm{m}}_{l^{\mathrm{m}}} W^{\mathrm{e}}_{l^{\mathrm{e}}} |\mathrm{GS}\rangle .\end{aligned} \tag{11.4.18}$$

The product over B_p operators anticommutes with the path operator $W^{\mathrm{m}}_{l^{\mathrm{m}}}$, because there is a single bond on which a single σ^x and a single σ^z act at the crossing of l^{m} and l^{e}_e [see Fig. 11.5 d)].
As a result, the initial and final state differ by a -1, which is the braiding phase of e with m. Particles with this braiding phase are called (mutual) semions.
Notice that we have moved the particles on contractible loops only. If we create a pair of e or m particles, move one of them along a noncontractible loop on the torus, and annihilate the pair, we have effectively applied the operators $W^{\mathrm{e}}_{x/y}$ and $W^{\mathrm{m}}_{x/y}$ to the ground state (although in the process we have created finite energy states). The operation of moving anyons on noncontractible loops thus allows to operate on the manifold of topologically degenerate groundstates. This exposes the intimate connection between the presence of fractionalized excitations and topological groundstate degeneracy in topologically ordered systems.
From the braiding relations of e and m we can also conclude the braiding and exchange relations of the composite particle f. This is most easily done in a pictorial way by representing the particle worldlines as moving upwards. For example, we represent the braiding relations of e and m as

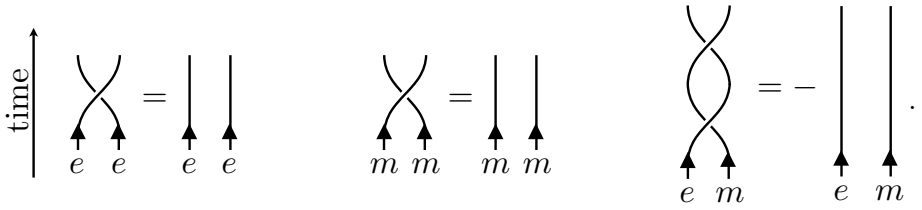

(11.4.19)

The exchange of two f, each of which is composed of one e and one m is then

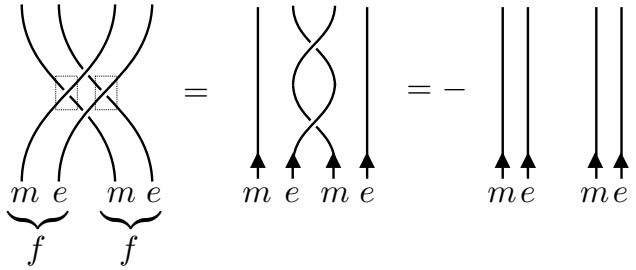

(11.4.20)

Notice that we have used Eq. (11.4.19) to manipulate the crossing in the dotted rectangles. Exchange of two f thus gives a phase -1 and we conclude that f is a fermion.
In summary, we have used the toric code model to illustrate topological ground state degeneracy and emergent anyonic quasiparticles as hallmarks of topological order. We note that the toric code model does not support topologically protected edge states.

References

1. Kitaev, A. Y. & Preskill, J. "Topological Entanglement Entropy". *Phys. Rev. Lett.* **96,** 110404. http://dx.doi.org/10.1103/PhysRevLett.96.110404 (2006).

Chapter 12

The fractional quantum Hall effect I

Learning goals

- We are acquainted with the basic phenomenology of the fractional quantum Hall effect.
- We know the Laughlin wave function.
- We can explain the mutual statistic of Laughlin quasi-particles

- D.C. Tsui, H.L. Stormer, and A.C. Gossard, Phys. Rev. Lett. 48, 1559 (1982)

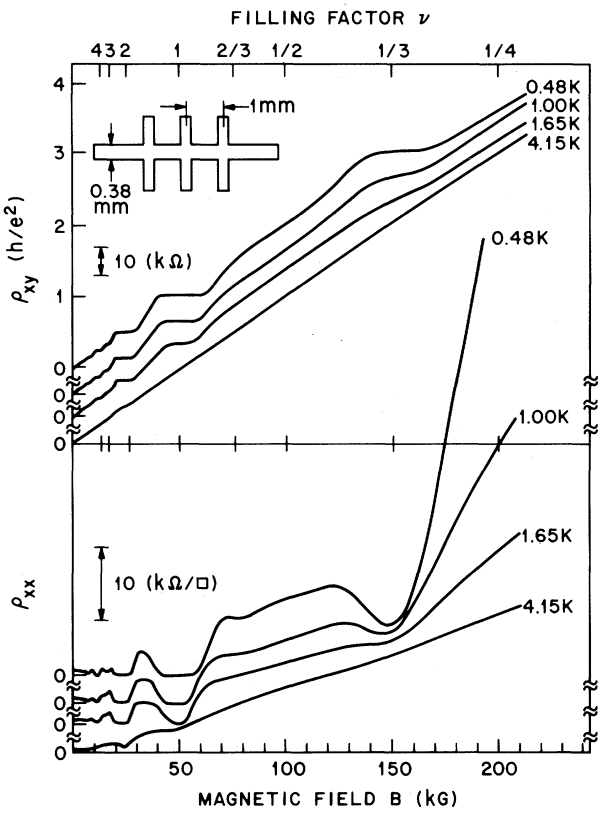

Figure 12.1: Measurements of the longitudinal and transverse resistance in a semiconductor heterostructure. At low temperatures a Hall plateau develops at a filling fraction $\nu = 1/3$ together with a dip in the transverse conductance. Figure take from Ref. [1] (Copyright (1982) by The American Physical Society).

We have seen that the Hall conductance in a large magnetic field is quantized to multiples of the

quantum of conductance e^2/h. We could explain this quantization via a mapping of the linear response expression for the Hall conductance to the calculation of the Chern number of ground state wave function. The seminal experiment of Tsui et al. [1] showed, however, that in a very clean sample, the Hall conductance develops a fractional plateau at one third of a quantum of conductance, see Fig. 12.1. In this chapter we try to understand how this can come about and how it is compatible with our derivation of the integer-quantized Hall conductance. So far we have only dealt with free fermion systems where the ground state was a Slater determinant of single particle states. Let us start from such a ground state and see how we might understand the fractional quantum Hall effect via a wave function inspired by such a Slater determinant.

12.1 Many particle wave functions

In the symmetric gauge, where $\boldsymbol{A} = -\frac{1}{2}\boldsymbol{r} \wedge \boldsymbol{B}$, the lowest Landau level wave function can be written as

$$\psi_m(z) \propto z^m e^{-\frac{1}{4}|z|^2}, \qquad z = \frac{1}{l}(x + \mathrm{i}y), \qquad l = \sqrt{\frac{\hbar}{eB}}. \tag{12.1.1}$$

The m'th wave function is peaked on a ring that encircles m flux quanta. A direct consequence of (12.1.1) is that any function

$$\psi(z) = f(z)e^{-\frac{1}{4}|z|^2} \tag{12.1.2}$$

with an analytic $f(z)$ is in the lowest Landau level. Let us make use of that to address the many-body problem at fractional filling. At fractional fillings, there is no single-particle gap as the next electron can also be accommodated in the same, degenerate, Landau level. Hence, we need interactions to open up a gap. Let us assume a rotational invariant interaction, e.g., $V(r) = e^2/\epsilon r$. Moreover, we start with the two-particle problem. Requiring relative angular momentum m and total angular momentum M, the only *analytic* wave function is

$$\psi_{m,M}(z_1, z_2) = (z_1 - z_2)^m (z_1 + z_2)^M e^{-\frac{1}{4}\left(|z_1|^2 + |z_2|^2\right)}. \tag{12.1.3}$$

Given the azimuthal part (angular momentum), no radial problem had to be solved! The requirement to be in the lowest Landau level fixes the radial part. ⇒ All we need to know about $V(r)$ are the Haldane pseudo-potentials[1]

$$v_m = \langle Mm|V|Mm\rangle. \tag{12.1.4}$$

12.1.1 The quantum Hall droplet

Let us now construct the many-body state for the two-particle state centered around $z = 0$. For $\nu = 1$ we construct the Slater determinant with the orbits $m = 0, 1$

$$\psi(z_1, z_2) = f(z_1, z_2)e^{-\frac{1}{4}\sum_{j=1}^{2}|z_j|^2} \qquad \text{with} \qquad f(z_1, z_2) = \begin{vmatrix} 1 & 1 \\ z_1 & z_2 \end{vmatrix} = -(z_1 - z_2). \tag{12.1.5}$$

The generalization to N particles with $m = 0, \ldots, N-1$ will fill a circle of radius $\sqrt{2N}$ and f is given by the Vandermonde determinant

$$f = -\prod_{i<j}(z_i - z_j). \tag{12.1.6}$$

[1] If we neglect Landau level mixing!

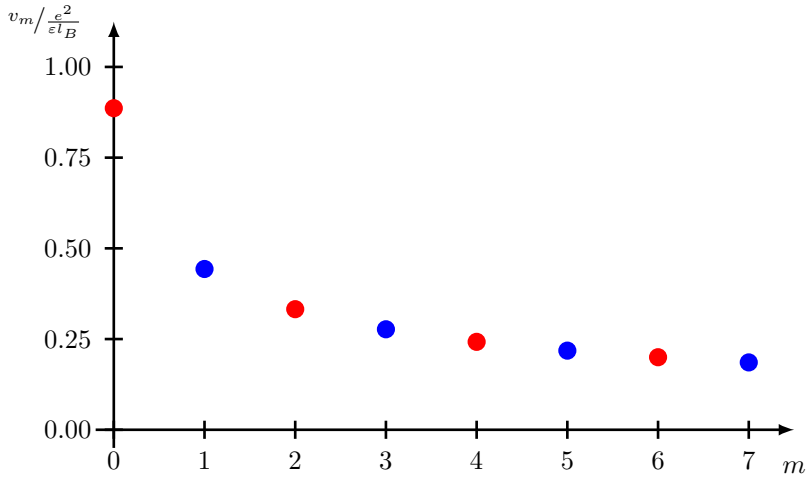

Figure 12.2: Haldane pseudo potentials for the Coulomb interaction in the lowest Landau level as a function of relative angular momentum m. The even relative angular momenta (red) are irrelevant for a fermionic system. In the following we approximate the full Coulomb potential with the first pseudo potential by setting $v_{m>1} \equiv 0$

Therefore, the many-body wave function of a filled lowest Landau level is given by

$$\psi(\{z_i\}) = \prod_{i<j}(z_i - z_j)e^{-\frac{1}{4}\sum_{j=1}^{N}|z_j|^2}. \tag{12.1.7}$$

Building on this form of the ground state wave function R. Laughlin made the visionary step [2] of proposing the following wave function for the one third filled Landau level[2]

$$\psi_{\mathrm{L}}(\{z_i\}) = \prod_{i<j}(z_i - z_j)^3 e^{-\frac{1}{4}\sum_{j=1}^{N}|z_j|^2}. \tag{12.1.8}$$

Before we embark on a detailed analysis of this wave function, let us make a few simple comments: (i) No pair of particles has a relative angular momentum $m < 3!$ $\Rightarrow$ if we only keep the smallest non-trivial Haldane pseudo potential v_1, ψ_{L} is an exact ground state wave function in the lowest Landau level. (ii) if $g(\{z_i\})$ is a symmetric (under exchange $i \leftrightarrow j$) polynomial, then $\psi = g\psi_{\mathrm{L}}$ is also in the lowest Landau level. In particular

$$\psi_{\{w_s\}}(\{z_i\}) = \prod_{s=1}^{n}\prod_{j=1}^{N}(z_j - w_s)\psi_{\mathrm{L}}(\{z_i\}) \tag{12.1.9}$$

is a wave function of N particles depending on the n (two dimensional) parameters $w_n = x_n + \mathrm{i}y_n$ and is in the lowest Landau level. We will study this generalization of the Laughlin wave-function in the following. Keep in mind that the ground-state shall be described by $\psi_{\mathrm{L}}(\{z_i\})$ and we will argue that $\psi_{\{w_s\}}(\{z_i\})$ corresponds to an excited state with quasi-holes at the positions w_s.

[2]It is maybe interesting to state here the *full* abstract of this paper: *This Letter presents variational ground-state and excited-state wave functions which describe the condensation of a two-dimensional electron gas into a new state of matter.* Keep its length in mind when you write your Nobel paper...

12.2 The plasma analogy

In order to better understand the Laughlin wave function we make use of a very helpful analogy called the "plasma analogy" [3]. We write the probability distribution in the form

$$|\psi_{\{w_s\}}(\{z_i\})|^2 = \exp\left[-6E_{\{w_s\}}(\{z_i\})\right] = e^{-\beta E}, \quad Z = \int d\boldsymbol{z} e^{-\beta E}, \tag{12.2.1}$$

with

$$E_{\{w_s\}}(\{z_i\}) = -\frac{1}{3}\sum_{sj}\log|z_j - w_s| - \sum_{i<j}\log|z_i - z_j| + \sum_j \frac{|z_j|^2}{12}. \tag{12.2.2}$$

We will argue in the following that $|\psi_{\{w_s\}}(\{z_i\})|^2$ is given by the Boltzmann weight of a *fake* classical plasma at inverse temperature $\beta = 6$. Note that this is just a way of interpreting a quantum mechanical wave function. There is no plasma involved. Moreover, when we speak of "charges" in the following, we mean the fake charges of our plasma analogy. When we are interested in real, electronic charges, we will calculate (electron) densities with the help of the plasma analogy. From these real electron densities we will infer the actual real charge.
Let us remind ourselves of two-dimensional electrodynamics. From Gauss' law we find

$$\int d\boldsymbol{s}\, \boldsymbol{E} = 2\pi Q \quad \Rightarrow \quad \boldsymbol{E}(\boldsymbol{r}) = \frac{Q\hat{\boldsymbol{r}}}{r} \quad \Rightarrow \quad \phi(\boldsymbol{r}) = -Q\log(r/r_0) \tag{12.2.3}$$

and the two dimensional Poisson equation is given by

$$\nabla\cdot\boldsymbol{E} = -\nabla^2\phi = 2\pi Q\delta(\boldsymbol{r}). \tag{12.2.4}$$

We can now interpret the terms in $E_{\{w_s\}}(\{z_i\})$:

1. $-\log|z_i - z_j|$: electrostatic repulsion between two unit charges (fake charges...).
2. $-\frac{1}{3}\log|z_i - w_s|$: interaction of a unit charge at z_i with a charge $1/3$ at w_s.
3. $-\nabla^2|z|^2/12 = -1/3l^2 = 2\pi\rho_{\mathrm{b}}$ with $\rho_{\mathrm{b}} = -\frac{1}{3}\frac{1}{2\pi l^2}$. Hence, $\sum_j |z_j|^2/12$ is a background potential to keep the plasma (in the absence of w_s) charge neutral (Jellium).

With these interpretations we are in the position to analyze the properties of $\psi_{\{w_s\}}(\{z_i\})$:

1. $\log r$ – interactions make density variations extremely costly. Therefore the ground state, i.e., $\psi_{\mathrm{L}}(\{z_i\})$ has uniform density:

$$\Rightarrow \rho = \frac{1}{3}\frac{1}{2\pi l^2} \Rightarrow \nu = \frac{1}{3}. \tag{12.2.5}$$

   This we could have also inferred from the fact that the largest monomial z_j^M appearing in $\psi_{\{w_s\}}(\{z_i\})$ has $M = 3N$. Hence, the radius of the droplet would be $\propto\sqrt{3N}$ and hence the area three times larger than for the $\nu = 1$ case.

2. Each w_s corresponds to a charge $1/3$. Therefore, it will be screened by the z-Plasma with a compensating charge $-1/3$. $\Rightarrow$ each w_s corresponds to a *quasi-hole* with $e^* = -\frac{e}{3}$.

3. The plasma analogy also allows us to find the normalization of the wave function $\psi_{\{w_s\}}(\{z_i\})$:

$$\psi_{\{w_s\}}(\{z_i\}) = C\prod_{s<p}|w_s - w_p|^{1/3}\prod_{sj}(z_j - w_s)\prod_{i<j}(z_i - z_j)^3 e^{-\sum_j\frac{|z_j|^2}{4}} e^{-\sum_s\frac{|w_s|^2}{12}}. \tag{12.2.6}$$

For this normalization we find a new plasma energy

$$E = -\frac{1}{9}\sum_{s<p}\log|w_s - w_p| - \frac{1}{3}\sum_{sj}\log|z_j - w_s| - \sum_{i<j}\log|z_j - z_i| + \sum_j \frac{|z_j|^2}{12} + \sum_s \frac{|w_s|^2}{36}. \quad (12.2.7)$$

We see that all "forces" between w_s, z_j are mediated by two-dimensional Coulomb electrodynamics $\Rightarrow$ all forces on w_s are screened $\Rightarrow$

$$F_{w_s} = \frac{\partial \log Z}{\partial w_s} \approx 0 \qquad \text{for} \qquad |w_s - w_p| \gg 1. \quad (12.2.8)$$

Hence $Z = \int d\boldsymbol{z}\,|\psi|^2 = \text{const}$, and we can normalize it with an appropriate C.

Before we calculate the charge of a quasi particle in another way that highlights the relation to their mutual statistics, σ_{xy}, and eventually the ground-state degeneracy on the torus, we want to convince ourselves that ψ_{L} is describing a ground state with a gapped excitation spectrum above it: If we want to make an *electronic* excitation we have to change the relative angular momentum by one. Therefore, we will have to pay the cost v_1 corresponding to the first Haldane pseudo potential! How did ψ_{L} manage to be such a good candidate wave function? One argument is due to Halperin [3]:
Fix all z_j except for z_i. Take z_i around the whole droplet. ψ_{L} needs to pick up an Aharonov-Bohm phase $2\pi N/\nu = 2\pi N 3$. ψ_{L} must also have N zeros (whenever $z_i \to z_j$) due to the Pauli principle. $\Rightarrow$ $2N$ zeros could be somewhere else, not bound to any special particle configuration (like to the coincidence of two particles as above) to pick up the proper Aharonov-Bohm phase. However, the *Laughlin wave function does not "waste" any zeros but uses them all to avoid interactions.*

12.3 Mutual statistics

We want to move the quasi-particle described by the location w_s around and see what Aharonov-Bohm and statistical phase they pick up. For this we calculate the Berry phase

$$\phi = \oint \mathcal{A}_\mu du^\mu \qquad \text{with} \qquad \mathcal{A}_\mu = \mathrm{i}\,\langle\psi|\partial_{u^\mu}\psi\rangle\,. \quad (12.3.1)$$

Our "slow" parameters u^μ are the x and y coordinates of the positions w_s of the quasi-holes. There is a problem with the above formula, however: At $w_s \to w_p$, the normalized $\psi_{\{w_s\}}(\{z_i\})$ is not differentiable. In order to make it differentiable we apply a gauge transformation

$$\tilde{\psi}_{\{w_s\}}(\{z_i\}) = e^{\frac{\mathrm{i}}{3}\sum_{s<p}\arg(w_s - w_p)}\psi_{\{w_s\}}(\{z_i\}). \quad (12.3.2)$$

For fixed positions $\{w_s\}$ it is clear that this amounts to a simple global phase change. However, through

$$e^{\frac{\mathrm{i}}{3}\sum_{s<p}\arg(w_s - w_p)} = \prod_{s<p}\frac{(w_s - w_p)^{1/3}}{|w_s - w_p|^{1/3}} \quad (12.3.3)$$

it cures the problem with differentiability for $w_s \to w_p$ and we can use (12.3.1) to calculate Berry phases. Note, however, that we made $\tilde{\psi}_{\{w_s\}}(\{z_i\})$ multivalued. The requirement of global integrability necessitated this step: a phenomena we saw already for example in the calculation of the Chern number for a spin 1/2 in a magnetic field in Chapter 2.

The calculation of the Berry curvature is now straight forward. We use $w_s = x_s + \mathrm{i}y_s$ and $\bar{w}_s = x_s - \mathrm{i}y_s$ as our coordinates. Let us start with

$$\mathcal{A}_{\bar{w}_s} = \mathrm{i}\langle\psi|\partial_{\bar{w}_s}\psi\rangle \tag{12.3.4}$$

$$= \mathrm{i}|C|^2 \int d\boldsymbol{z} \int d\bar{\boldsymbol{z}} \prod_{a<b}\prod_{cd}\prod_{e<f} (\bar{w}_a - \bar{w}_b)^{1/3}(\bar{w}_c - \bar{z}_d)(\bar{z}_e - \bar{z}_f)^3 e^{-\frac{\sum_g z_g \bar{z}_g}{4}} e^{-\frac{\sum_h w_h \bar{w}_h}{12}}$$

$$\times \partial_{\bar{w}_s} \prod_{i<j}\prod_{kl}\prod_{m<n} (w_i - w_j)^{1/3}(w_k - z_l)(z_m - z_n)^3 e^{-\frac{\sum_o z_o \bar{z}_o}{4}} e^{-\frac{\sum_p w_p \bar{w}_p}{12}} \tag{12.3.5}$$

$$= -\mathrm{i}\frac{w_s}{12}. \tag{12.3.6}$$

For $\mathcal{A}_{w_s}$ we use the fact that our wave function is normalized

$$0 = \partial_{w_s}\langle\psi|\psi\rangle = \langle\partial_{w_s}\psi|\psi\rangle + \langle\psi|\partial_{w_s}\psi\rangle \qquad \Rightarrow \mathcal{A}_{w_s} = \mathrm{i}\langle\psi|\partial_{w_s}\psi\rangle = -\mathrm{i}\langle\partial_{w_s}\psi|\psi\rangle. \tag{12.3.7}$$

The last term, however, is now easy to calculate as $\langle\psi|$ depends on w_s only through the exponential factor. Hence the calculation of $\mathcal{A}_{w_s}$ is analogous to the one of $\mathcal{A}_{\bar{w}_s}$ and we find

$$\mathcal{A}_{w_s} = \mathrm{i}\frac{\bar{w}_s}{12}. \tag{12.3.8}$$

The Berry curvature is then given by

$$\mathcal{F}_{w_s\bar{w}_s} = \partial_{w_s}\mathcal{A}_{\bar{w}_s} - \partial_{\bar{w}_s}\mathcal{A}_{w_s} = -\frac{\mathrm{i}}{6}. \tag{12.3.9}$$

From this we can calculate the Berry phase for bringing the coordinate w_s around an area A

$$\varphi_A = -\mathrm{i}\oiint_A dw_s d\bar{w}_s\, \mathcal{F}_{w_s\bar{w}_s} = -\frac{1}{6}\oiint_A dxdy\frac{2}{l^2} = -\frac{\Phi_A}{3}, \tag{12.3.10}$$

where Φ_A is the magnetic flux through the area A. This confirms again the finding that each w_s in the wave-function $\psi_{\{w_s\}}(\{z_i\})$ describes a quasi-particle of charge[3]

$$e^* = -\frac{e}{3}. \tag{12.3.11}$$

Note, that hand-in-hand with the appearance of a fractional charge e^*, we also picked up a non-trivial mutual statistics: If we move w_s once around w_p, we go back to the same wave-function up to a phase factor $\exp(2\pi\mathrm{i}/3)$. This readily leads to a mutual statistical phase of $\exp(\pi\mathrm{i}/3)$. Therefore our $e/3$ quasi-particles are neither bosons nor fermions but anyons with a statistical angle of $\pi/3$.

Figure 12.3: Mutual statistics.

To elucidate the connection between σ_{xy}, $e^* = -e/3$ and $\exp(\mathrm{i}\pi/3)$ further we go through a Gedankenexperiment in analogy to Laughlin's pumping argument for the integer quantum Hall

[3]Remember that if a particle of charge q goes around a region containing a flux Φ_A, it will pick up an Aharonov-Bohm phase $\exp(\mathrm{i}q\Phi_A)$.

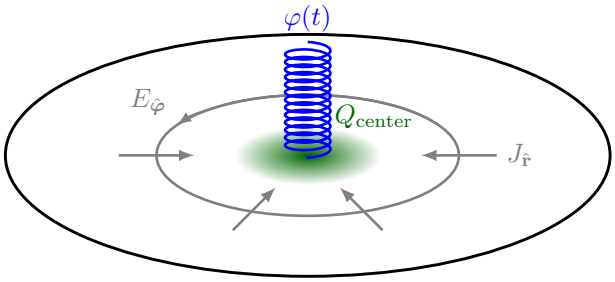

Figure 12.4: Pumping argument. Inserting a flux quantum h/e leads to an accumulation of charge $-e/3$. In the limit of an infinitely small solenoid we can gauge h/e away and we end up with a stable excitation in the form of a quasi-hole carrying one third of an electronic charge.

effect, cf. Fig 12.4. Let us consider a disk displaying the 1/3 fractional quantum Hall effect. We insert a flux quantum through a thin solenoid in the center. The induced current in radial direction is then given by

$$J_{\hat{\mathbf{r}}} = \sigma_{xy} E_{\hat{\varphi}} = -\sigma_{xy} \frac{\partial \varphi}{\partial t}. \tag{12.3.12}$$

Therefore the charge accumulated on the center of the disk is given by

$$Q_{\text{center}} = \int dt\, J_{\hat{\mathbf{r}}} = -\frac{1}{3}\frac{e^2}{h} \int dt\, \frac{\partial \varphi}{\partial t} = -\frac{e}{3}. \tag{12.3.13}$$

After we inserted a full flux quantum h/e through the solenoid, we can gauge the phase away and we arrive at the same Hamiltonian. However, we do not necessarily reach the same state but we might end up in another *eigenstate* of the Hamiltonian. The accumulated charge $-e/3$ in the center must therefore be a *stable* quasi-hole after the system underwent spectral flow!
Let us bring a test quasi-hole around the solenoid: Either we think of $\exp(2\pi \mathrm{i}/3)$ as a statistical flux after we gauged away the h/e. Equivalently we can think of the additional flux of the solenoid spread over a finite area. We can then not gauge the flux away and hence we did not induce a stable quasi-hole. In contrary, the test particle accumulated a $\exp(2\pi \mathrm{i}/3)$ Aharonov-Bohm phase. This links the properties

$$\sigma_{xy} = \frac{1}{3}\frac{e^2}{h} \quad \Leftrightarrow \quad e^* = -\frac{e}{3} \quad \Leftrightarrow \quad e^{\mathrm{i}\pi/3} - \text{anyons}. \tag{12.3.14}$$

12.4 Ground state degeneracy on the torus

During the discussion of the integer quantum Hall effect we found that the Hall conductivity has to be an integer multiple of e^2/h. How can we reconcile this with the fractionally quantized plateau at $\nu = 1/3$ in Fig. 12.1? The key issue was the assumption of a unique ground state on the torus with a finite gap to the first excited state. We are now proving that this is not the case for a state described by Laughlin's wave function for the $\nu = 1/3$ plateau.
Consider an operator T_x (T_y) that creates a quasi-particle – quasi-hole pair, moves the quasi-hole around the torus in x (y) direction an annihilates the two again, cf. Fig. 12.5(a). We consider now the action of $T_x T_y T_x^{-1} T_y^{-1}$. T_x shall create the pair in the middle of the chart in Fig. 12.5(b), T_y close to a corner. Moreover, we perform the T_y movements on a given chart directly on the quasi-particle – quasi-hole pair, whereas for the T_x movements we move the whole chart in the opposite direction rather than moving the quasi-hole created in the middle of the chart. From this we see that one quasi-hole encircles the other! $\Rightarrow$ $T_x T_y = \exp(2\pi \mathrm{i}/3) T_y T_x$. In addition, we have the following property $T_x^3 = T_y^3 = \mathbb{1}$ as moving a full electron around the

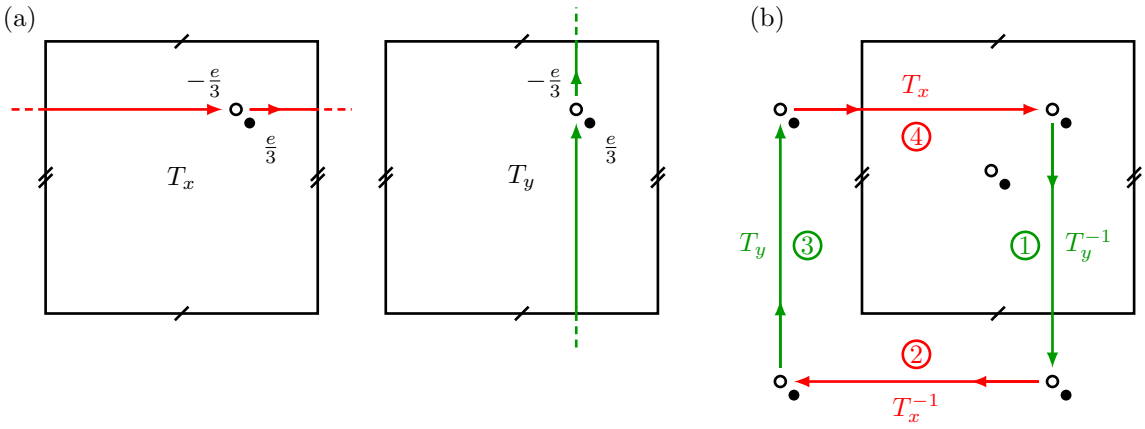

Figure 12.5: Illustration of the actions of (a) $T_{x(y)}$ and (b) $T_xT_yT_x^{-1}T_y^{-1}$ (see text).

torus has to be harmless as this is what we demand for the boundary conditions.[4] The fact that $[T_x, T_y] \neq 0$ means they act on a space which is more than one-dimensional. However, they act on the ground-state manifold of the fractional quantum Hall effect on the torus. *This requires that there are several ground state sectors for the $\nu = 1/3$ state.* One can show that

$$T_x = \begin{pmatrix} 0 & 1 & 0 \\ 0 & 0 & 1 \\ 1 & 0 & 0 \end{pmatrix} \qquad T_y = \begin{pmatrix} 1 & 0 & 0 \\ 0 & e^{2\pi \mathrm{i}/3} & 0 \\ 0 & 0 & e^{4\pi \mathrm{i}/3} \end{pmatrix} \tag{12.4.1}$$

are the unique irreducible representation of the algebra defined by the above conditions. We conclude that the $\nu = 1/3$ state is threefold degenerate on the torus.
We conclude this chapter by stating that X.-G. Wen generalized the observation that ground-state degeneracy on the torus and fractional statistics are deeply linked and give rise to a new classification scheme of intrinsically topologically states (as opposed to non-interaction topological states such as the integer quantum Hall effect or more generally topological insulators) [4].

References

1. Tsui, D. C., Stormer, H. L. & Gossard, A. C. "Two-Dimensional Magnetotransport in the Extreme Quantum Limit". *Phys. Rev. Lett.* **48,** 1559. http://dx.doi.org/10.1103/PhysRevLett.48.1559 (1982).
2. Laughlin, R. B. "Anomalous Quantum Hall Effect: An Incompressible Quantum Fluid with Fractionally Charged Excitations". *Phys. Rev. Lett.* **50,** 1395. http://link.aps.org/doi/10.1103/PhysRevLett.50.1395 (1983).
3. Halperin, B. I. "Theory of quantized Hall conductance". *Helv. Phys. Acta* **56,** 75. http://dx.doi.org/10.5169/seals-115362 (1983).
4. Wen, X.-G. "Topological orders and edge excitations in fractional quantum Hall states". *Adv. in Phys.* **44,** 405. http://dx.doi.org/10.1080/00018739500101566 (1995).

[4] Remember the gluing phase in Chapter 2.

Chapter 13

The fractional quantum Hall effect II

Learning goals

- We know what a coherent state path integral is.
- We know the concept of a composite fermion.
- We know how to get from composite fermions to a Chern-Simons theory.

- Willett, R. et al., Phys. Rev. Lett. **59**, 1776 (1987)

13.1 Path integrals

13.1.1 Why do we need a path integral

In this section we try to argue why we need a path integral representation of the partition sum

$$Z = \int D[\bar{\phi}\phi] e^{-S[\bar{\phi},\phi]}. \tag{13.1.1}$$

First of all, we trade non-commuting bosonic *operators* with an integral over all "field" configurations, i.e.,

$$[.,.] \to D[\bar{\phi},\phi]. \tag{13.1.2}$$

Moreover, we replace complicated anti-commutations for fermions we a simple tool called Grassmann numbers. Before we are going to explain what we exactly mean with expression (13.1.1), we list a few nice properties that we will gain from a path integral formalism.

1. We can use Gaussian integrals

$$\int D[\bar{\phi}\phi] e^{-\bar{\phi}^{\mathrm{T}} A \phi} = \frac{1}{\det A}. \tag{13.1.3}$$

2. We can complete the square

$$\int D[\bar{\phi}\phi] e^{-\bar{\phi}^{\mathrm{T}} A \phi + \vartheta^{\mathrm{T}}\bar{\phi} + \bar{\vartheta}^{\mathrm{T}}\phi} = \int D[\bar{\phi}\phi] e^{-(\bar{\phi}-A^{-1}\bar{\vartheta})^{\mathrm{T}} A (\phi - A^{-1}\vartheta) + \bar{\vartheta}^{\mathrm{T}} A^{-1}\vartheta} = \frac{e^{\bar{\vartheta}^{\mathrm{T}} A^{-1}\vartheta}}{\det A}. \tag{13.1.4}$$

   This completing of the square in turn has three important applications:

   (a) Greens functions (or more generally, two-point correlators) in a quadratic theory can be calculated by coupling sources ϑ

$$\langle \bar{\phi}_i \phi_j \rangle = \frac{\int D[\bar{\phi}\phi] \bar{\phi}_i \phi_j e^{-S[\bar{\phi},\phi]}}{\int D[\bar{\phi}\phi] e^{-S[\bar{\phi},\phi]}} = \frac{\delta^2}{\delta\vartheta_i \delta\bar{\vartheta}_j}\bigg|_{\vartheta=\bar{\vartheta}=0} e^{\bar{\vartheta}^{\mathrm{T}} A^{-1}\vartheta} = [A^{-1}]_{ij}. \tag{13.1.5}$$

(b) "Integrating out" linearly coupled quadratic degrees of freedom

$$\int D[\bar{\phi}\phi]D[\bar{\vartheta}\vartheta]e^{-S[\bar{\phi},\phi]+\phi^{\mathrm{T}}\bar{\vartheta}+\bar{\phi}^{\mathrm{T}}\vartheta-\bar{\vartheta}^{\mathrm{T}}B\vartheta} = \int D[\bar{\phi}\phi]e^{-S[\bar{\phi},\phi]+\bar{\phi}^{\mathrm{T}}B^{-1}\phi} = \int D[\bar{\phi}\phi]e^{-S_{\mathrm{eff}}[\bar{\phi},\phi]}. \quad (13.1.6)$$

(c) Or the reverse of it, called *Hubbard Stratonovich transformation*

$$\int D[\bar{\phi}\phi]e^{-\bar{\phi}^{\mathrm{T}}A\phi+\bar{\phi}^{\mathrm{T}}\phi\bar{\phi}^{\mathrm{T}}\phi} = \int D[\bar{\phi}\phi]D[\vartheta]e^{-(\bar{\vartheta}-\bar{\phi}^{\mathrm{T}}\phi)(\vartheta-\bar{\phi}^{\mathrm{T}}\phi)-\phi^{\mathrm{T}}A\phi+\bar{\phi}^{\mathrm{T}}\phi\bar{\phi}^{\mathrm{T}}\phi} \quad (13.1.7)$$

$$= \int D[\bar{\phi}\phi]D[\vartheta]e^{-\bar{\vartheta}\vartheta+2\vartheta\bar{\phi}^{\mathrm{T}}\phi-\bar{\phi}^{\mathrm{T}}\phi\bar{\phi}^{\mathrm{T}}\phi-\bar{\phi}^{\mathrm{T}}A\phi+\bar{\phi}^{\mathrm{T}}\phi\bar{\phi}^{\mathrm{T}}\phi} \quad (13.1.8)$$

$$= \int D[\bar{\phi}\phi]D[\vartheta]e^{-\bar{\vartheta}\vartheta-\bar{\phi}^{\mathrm{T}}(A+2\vartheta)\phi} \quad (13.1.9)$$

$$= \int D[\vartheta]e^{-\bar{\vartheta}\vartheta-\mathrm{tr}\log[A+2\vartheta]}. \quad (13.1.10)$$

This is still not a quadratic theory, but the logarithm can be expanded step by step to get an effective theory.

3. We can do mean-field calculations

$$\frac{\delta S[\bar{\phi},\phi]}{\delta\bar{\phi}} = 0 \qquad \Rightarrow \qquad \phi_{\mathrm{MF}}. \quad (13.1.11)$$

After all these expected profits, let us start introducing such a path integral representation of the partition sum.

13.1.2 Coherent state path integral

Given a quantum mechanical problem defined by a Hamiltonian H, we want to express the partition sum

$$Z = \mathrm{tr}\, e^{-\beta H} = \sum_n \langle m|e^{-\beta H}|m\rangle, \quad (13.1.12)$$

as a path integral. For this we use coherent states

$$|\phi\rangle = e^{\eta\sum_i \phi_i c_i^\dagger}|\mathrm{vac}\rangle \quad \Rightarrow c_i|\phi\rangle = \phi_i|\phi\rangle, \quad (13.1.13)$$

and we used $\eta = \pm 1$ for bosons (fermions), respectively. Remember that they are not orthogonal

$$\langle\phi|\vartheta\rangle = e^{\bar{\phi}^{\mathrm{T}}\vartheta}. \quad (13.1.14)$$

For bosons, $\phi_i \in \mathbb{C}$. For fermions we need to take care of anti-commutations. This can be achieved by requiring ϕ_i to be Grassmann numbers.
Grassmann numbers are defined by

$$\phi_i\phi_j = -\phi_j\phi_i; \quad \partial_{\phi_i}\phi_j = 0; \quad \int d\phi_i = 0; \quad \int d\phi_i\phi_i = 1. \quad (13.1.15)$$

From this follows immediately

$$\int d\bar{\phi}_i d\phi_i\, e^{-\bar{\phi}_i a\phi_i} = \int d\bar{\phi}_i d\phi_i\,[1-\phi_i\phi_i a] = a. \quad (13.1.16)$$

Which immediately leads to

$$\int d(\bar{\phi}\phi)\, e^{-\bar{\phi}^{\mathrm{T}} A\phi} = \prod_n \int d\bar{\phi}_n d\phi_n\, e^{-\sum_{rs}\bar{\phi}_r A_{rs}\phi_s} = \det A. \tag{13.1.17}$$

Note that this is similar to the bosonic case, however $[\det A]^{-1}$ is replaced with $\det A$.
With the help of the coherent states $|\phi\rangle$ we can now write a complicated but tremendously useful resolution of the unity

$$\mathbb{1} = \int d(\bar{\phi}\phi)\, e^{-\bar{\phi}^{\mathrm{T}}\phi} |\phi\rangle\langle\phi|. \tag{13.1.18}$$

To prove this identity, we have to show that c_i and $c_i^\dagger$ commute with the right-hand side:

$$c_i \int d(\bar{\phi}\phi)\, e^{-\bar{\phi}^{\mathrm{T}}\phi} |\phi\rangle\langle\phi| = \int d(\bar{\phi}\phi)\, e^{-\bar{\phi}^{\mathrm{T}}\phi} c_i |\phi\rangle\langle\phi| = \int d(\bar{\phi}\phi)\, e^{-\bar{\phi}^{\mathrm{T}}\phi} \phi_i |\phi\rangle\langle\phi| \tag{13.1.19}$$

$$= -\int d(\bar{\phi}\phi)\, [\partial_{\bar{\phi}_i} e^{-\bar{\phi}^{\mathrm{T}}\phi}] |\phi\rangle\langle\phi| \tag{13.1.20}$$

$$\overset{\text{P.I.}}{=} \int d(\bar{\phi}\phi)\, e^{-\bar{\phi}^{\mathrm{T}}\phi} [\underbrace{(\partial_{\bar{\phi}_i}|\phi\rangle)}_{=0}\langle\phi| + |\phi\rangle(\partial_{\bar{\phi}_i}\langle\phi|)] \tag{13.1.21}$$

$$= \int d(\bar{\phi}\phi)\, e^{-\bar{\phi}^{\mathrm{T}}\phi} |\phi\rangle\langle\phi| c_i. \tag{13.1.22}$$

In the last line we used

$$c_i^\dagger |\phi\rangle = \partial_{\phi_i}|\phi\rangle \qquad \Rightarrow \qquad \partial_{\phi_i}\langle\phi| = \langle\phi_i| a_i. \tag{13.1.23}$$

With this we showed that c_i indeed commutes with the alleged unity. For $c_i^\dagger$ one starts from the other end end and goes through the same manipulations (show!). As all operators in the Fock space can be written as products (and sums) of the creation and annihilation operators, we have shown that indeed

$$\int d(\bar{\phi}\phi)\, e^{-\bar{\phi}^{\mathrm{T}}\phi} |\phi\rangle\langle\phi| \propto \mathbb{1}. \tag{13.1.24}$$

Let us check for the proportionality factor

$$\langle \mathrm{vac}|\mathbb{1}|\mathrm{vac}\rangle = 1 = \int d(\bar{\phi}\phi)\, e^{-\bar{\phi}^{\mathrm{T}}\phi} \langle \mathrm{vac}|\phi\rangle\langle\phi|\mathrm{vac}\rangle. \tag{13.1.25}$$

Let us now rewrite the trace in the partition sum

$$Z = \sum_n \langle n|e^{-\beta H}|n\rangle = \int d(\bar{\phi}\phi) \sum_n \langle n|\phi\rangle\langle\phi|e^{-\beta H}|n\rangle e^{-\bar{\phi}^{\mathrm{T}}\phi} \tag{13.1.26}$$

$$= \int d(\bar{\phi}\phi)\, e^{-\bar{\phi}^{\mathrm{T}}\phi} \sum_n \langle\eta\phi|n\rangle\langle n|e^{-\beta H}|\phi\rangle = \int d(\bar{\phi}\phi)\, e^{-\bar{\phi}^{\mathrm{T}}\phi} \langle\eta\phi|e^{-\beta H}|\phi\rangle. \tag{13.1.27}$$

Now we need to fix an important property. In order for our path integral approach to go through, we need to normal order our Hamiltonian. This means, we arrange all operators in H such that all $c_i^\dagger$ stand to the left of all c_i. As the fields ϕ_i are just complex numbers (for bosons, at least), this will be the last time we can take care of the operator nature of second quantized quantum mechanics. We write for the normal ordered Hamiltonian explicitly

$$Z = \int d(\bar{\phi}\phi)\, e^{-\bar{\phi}^{\mathrm{T}}\phi} \langle\eta\phi|e^{-\beta H(c^\dagger, c)}|\phi\rangle. \tag{13.1.28}$$

Next, we re-write

$$\beta H(c^\dagger, c) = \frac{\beta}{N} \sum_{i=1}^{N} H(c^\dagger, c) \tag{13.1.29}$$

and we insert a unity in between all resulting factors

$$Z = \int_{\phi^1=\eta\phi^N,\,\bar\phi^1=\eta\bar\phi^N} \prod_{i=1}^{N} d(\bar\phi^i\phi^i) e^{\frac{\beta}{N}\sum_{i=1}^{N}\frac{(\bar\phi^i-\bar\phi^{i+1})\phi^i}{\beta/N}+H(\bar\phi^i,\phi^i)}. \tag{13.1.30}$$

Note that the superscript i labels the i'th insertion of the unity. One often calls β the "imaginary time" in relation to the real time propagator $\exp(\mathrm{i}tH)$. Within this interpretation, i corresponds to the i'th time slice. If we now take the limit $N \to \infty$, we are taking a continuum limit in imaginary time where

$$\phi^i \to \phi(\tau) \qquad \text{and} \qquad \frac{\beta}{N}\sum_i \to \int_0^\beta d\tau. \tag{13.1.31}$$

We can now write down our sought path integral

$$Z = \int D[\bar\phi\phi] e^{-S[\bar\phi,\phi]}, \tag{13.1.32}$$

$$S[\bar\phi,\phi] = \int_0^\beta d\tau\, \bar\phi^{\mathrm{T}}\partial_\tau\phi + H(\bar\phi,\phi), \tag{13.1.33}$$

$$D[\bar\phi,\phi] = \lim_{N\to\infty}\prod_{i=1}^{N} d(\bar\phi^i\phi^i); \quad \bar\phi(0) = \eta\bar\phi(\beta), \;\; \phi(0) = \eta\phi(\beta). \tag{13.1.34}$$

13.1.3 Kubo formula

We already got acquainted with the Kubo formula in Chap. 2. We want to revisit it here in the language of our newly introduced coherent state path integral. Imagine a "force" $F(\boldsymbol{r},\omega)$ coupled to the "coordinate"

$$\hat X = \sum_{\alpha\beta} c^\dagger_\alpha X_{\alpha\beta} c_\beta. \tag{13.1.35}$$

We then ask for the linear response coefficient

$$X(\boldsymbol{r},\omega) = \int dr' \chi(\boldsymbol{r}-\boldsymbol{r}',\omega) F(\boldsymbol{r}',\omega). \tag{13.1.36}$$

In path integral formalism the expectation value on the right hand side is expressed as

$$X(\tau) = \sum_{\alpha\beta}\langle\bar\phi_\alpha(\tau) X_{\alpha\beta}\phi_\beta(\tau)\rangle_F, \tag{13.1.37}$$

where the subscript F indicates that we have to evaluate this expression in the presence of the force F

$$\delta S_F = \int_0^\beta d\tau\, F(\tau)\bar\phi_\alpha(\tau) X_{\alpha\beta}\phi_\beta(\tau). \tag{13.1.38}$$

To generate the expectation value (13.1.37) we can add another ficticious force F' to the action

$$\delta S_{F'} = \int_0^\beta d\tau\, F'(\tau)\bar\phi_\alpha(\tau) X'_{\alpha\beta}\phi_\beta(\tau). \tag{13.1.39}$$

With this addition, one can write

$$X(\tau) = -\frac{\delta}{\delta F'(\tau)}\Big|_{F'=0}\log(Z[F,F']). \tag{13.1.40}$$

For the sake of linear response, we imagine F to be small. Therefore, we can apply a Taylor expansion

$$X(\tau) = \int d\tau' \left[\frac{\delta^2}{\delta F'(\tau)\delta F(\tau')}\Big|_{F=F'=0}\log(Z[F,F'])\right] F(\tau') \tag{13.1.41}$$

With this expression we can immediately indentify the linear response coeffiecient. If we assume at $X(\tau) = 0$ in the absence of the force

$$\chi(\tau, \tau') = -\frac{1}{Z} \frac{\delta^2}{\delta F'(\tau) \delta F(\tau')} \bigg|_{F=F'=0} Z[F, F']. \tag{13.1.42}$$

Electromagnetic response

We consider a system subject to an electromagnetic field $A^\mu = (\mathrm{i}\varphi, \boldsymbol{A})$. The system might react via a redistribution of charge ρ or via an onset of a current $\boldsymbol{j}$. We write $j_\mu = (\mathrm{i}\rho, \boldsymbol{j})$ and look for

$$j_\mu(x) = \int_{t'<t} dx' K_{\mu\nu}(x - x') A^\nu(x'), \tag{13.1.43}$$

where x describes the four-coordinate $(\mathrm{i}t, \boldsymbol{x})$. We remember that we coupled the A^μ-field as $j_\mu A^\mu$ to the Hamiltonian. Therefore,

$$j_\mu = \frac{\delta S}{\delta A^\mu} \qquad \Rightarrow \qquad F = F' = A^\mu. \tag{13.1.44}$$

With this we find

$$K_{\mu\nu}(x - x') = -\frac{1}{Z} \frac{\delta^2}{\delta A^\mu(x) \delta A^\nu(x')} Z[A^\mu]. \tag{13.1.45}$$

Effective theories

If we have a system of charged particles, $H(c^\dagger, c)$, and we are interested in its electro-magnetic response, all we need to know is $K_{\mu\nu}$. In a path integral language, we say we *integrate out the fermions* to obtain an *effective action* in terms of the A^μ-field alone. The peculiar structure of $K_{\mu\nu}$ will fully describe our system in terms of its electro-magnetic system

$$S_{\text{eff}}[A^\mu] = \int_0^\beta d\tau \int dx dx' \, A^\mu(x) K_{\mu\nu}(x - x') A^\nu(x'). \tag{13.1.46}$$

13.2 Composite fermions

13.2.1 From a wave functions to a field theory

In the last chapter we got to know the Laughlin wave function for filling fractions $\nu = \frac{1}{2p+1}$ with $p \in \mathbb{N}$

$$\psi(\{z_i\}) = \prod_{i<j} (z_i - z_j)^{\frac{1}{\nu}} e^{-\frac{1}{4}\sum_i |z_i|^2}. \tag{13.2.1}$$

These wave functions are manifestly in the lowest Landau level and in addition to the $(z_i - z_j)^1$ term needed for the Pauli principle there are two (for $\nu = 1/3$) more zeros attached to the coincidence of two particles. This observation is identical to attaching $1/\nu - 1$ fluxes of 2π to each particle[1]

In the last chapter, we only considered the Laughlin wave function and analyzed its properties. Here, we follow a more ambitious goal. Building on the insight gained through the Laughlin

[1] Up to the fact that a pure flux attachment would require a factor

$$e^{-2\mathrm{i}\sum_{i<j} \arg(z_i - z_j)} = \prod_{i<j} \frac{(z_i - z_j)^2}{|z_i - z_j|^2}. \tag{13.2.2}$$

The absence of the factor $1/|z_i - z_j|^2$ in the Laughlin wave function can be seen as the effect of the projection to the lowest Landau level.

wave function, we want to construct an effective theory for the fractional quantum Hall effect including the Hamiltonian! However, we want to assume that the important players are not electrons, but the "bound states of electrons with statistical fluxes" that were at the heart of the Laughlin wave function [**Jain:2007**]. In other words, we want to go from an electron wave function (theory), to one of *composite fermions* by

$$\psi(\{\boldsymbol{x}_i\}) \mapsto \psi(\{\boldsymbol{x}_i\}) e^{2\mathrm{i}s\sum_{i<j}\arg(\boldsymbol{x}_i-\boldsymbol{x}_j)} \quad \text{with} \quad s\in\mathbb{Z}. \tag{13.2.3}$$

This amounts to attaching $2s$ phase vortices to each electron[2]

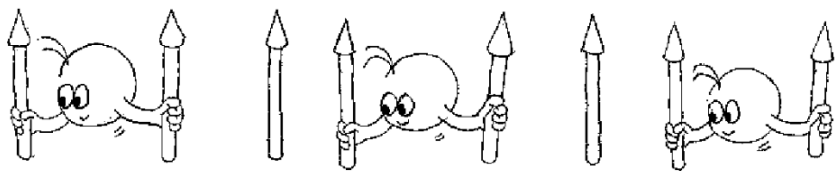

Our task is now to find a many-body theory formulated in terms of this new degrees of freedom. In a second quantized version, Eq (13.2.3) looks like

$$c^\dagger(\boldsymbol{x}) \quad \mapsto \quad c^\dagger(\boldsymbol{x}) \exp\left[-2\mathrm{i}s\int d\boldsymbol{x}' \arg(\boldsymbol{x}-\boldsymbol{x}')\rho(\boldsymbol{x}')\right]. \tag{13.2.4}$$

Substituted into the Hamiltonian this leads to

$$H \quad \mapsto \quad \int d\boldsymbol{x}\, c^\dagger(\boldsymbol{x}) \left[\frac{1}{2m}\left(-\partial_{\boldsymbol{x}}+\hat{\boldsymbol{A}}(\boldsymbol{x})\right)^2 + V(\boldsymbol{x})\right] c(\boldsymbol{x}) + H_{\mathrm{int}}[\rho], \tag{13.2.5}$$

where

$$\hat{\boldsymbol{A}}(\boldsymbol{x}) = \boldsymbol{A}_{\mathrm{ext}}(\boldsymbol{x}) + \hat{\boldsymbol{a}}(\boldsymbol{x}) \quad \text{with} \quad \hat{\boldsymbol{a}}(\boldsymbol{x}) = -2s\int d\boldsymbol{x}' \, \frac{(x_1-x_1')\hat{\boldsymbol{x}}_1 + (x_2-x_2')\hat{\boldsymbol{x}}_2}{|\boldsymbol{x}-\boldsymbol{x}'|^2}\rho(\boldsymbol{x}'). \tag{13.2.6}$$

This is very annoying! The kinetic energy operator became highly non-local and depends on six operators. Let us fix this. We can relocate the condition (13.2.6) to another place in the action. Two observations are needed for this:

(i) Eq. (13.2.6) is only giving rise to the transversal part of $\boldsymbol{A}$: $\hat{\boldsymbol{a}} = \hat{\boldsymbol{a}}_\perp$ as $\sum_i \partial_i \hat{a}_i = 0$.

(ii) $b = \epsilon^{ij}\partial_i a_{\perp,j}$ fulfills $b = -4\pi s\rho(\boldsymbol{x})$.

Using these two observations we can write

$$Z = \int D[\bar\psi\psi]D[a_\perp]D[\phi] e^{\mathrm{i}S_{\mathrm{CF}}[\bar\psi,\psi,a_\perp,\phi] + \mathrm{i}\frac{\Theta}{2}S'_{\mathrm{CS}}[a_\perp,\phi]}, \tag{13.2.7}$$

where $\Theta = 1/2\pi s$. Furthermore,

$$S_{\mathrm{CF}}[\bar\psi,\psi,a_\perp,\phi] = \int d\boldsymbol{x}\int dt\, \bar\psi\left[\mathrm{i}\partial_t + \mu - \phi + \frac{1}{2m}\left(-\mathrm{i}\partial_{\boldsymbol{x}}+\hat{\boldsymbol{A}}\right)^2 - V\right]\psi + S_{\mathrm{int}}[\bar\psi,\psi]. \tag{13.2.8}$$

$$S'_{\mathrm{CS}}[a_\perp,\phi] = -\int d\boldsymbol{x}\int dt\, \phi \underbrace{\epsilon_{ij}\partial_i a_{\perp,j}}_{b}. \tag{13.2.9}$$

$\hat{\boldsymbol{A}}$ is still given by $\boldsymbol{A}_{\mathrm{ext}} + \hat{\boldsymbol{a}}$, but the constraint (13.2.6) is replaced by the functional δ-function

$$\int D[\phi] e^{\mathrm{i}\int d\boldsymbol{x}\int dt\,\phi\left(\frac{b}{4\pi s}+\rho\right)}. \tag{13.2.10}$$

[2] Cartoon due Kwon Park.

With this we are almost done. We see that $a_\perp = (\phi, \boldsymbol{a}_\perp)$ enters Z like a gauge field. However, $S'_{\rm CS}$ is not gauge invariant. Hence, we propose to use

$$S_{\rm CS}[a] = -\int dx^\mu \epsilon_{\mu\nu\sigma} a^\mu \partial_\nu a^\sigma. \tag{13.2.11}$$

with $x^\mu = (x^0, x^1, x^2)$; $\partial_\mu = (-\partial_0, \partial_1, \partial_2)$ which is gauge invariant. The old $S'_{\rm CS}$ is nothing but $S_{\rm CS}$ evaluated in the Coulomb gauge $\partial_\mu a^\mu = 0$. Therefore, our full effective theory is now given by

$$Z = \int D[\bar\psi\psi] D[a] \exp\left\{ \mathrm{i} S_{\rm CF}[\bar\psi, \psi, a] + \mathrm{i}\frac{\Theta}{4} S_{\rm CS}[a] \right\}, \tag{13.2.12}$$

with

$$S_{\rm CF}[\bar\psi, \psi, a] = \int d\boldsymbol{x} \int dt\, \bar\psi \left[\mathrm{i}\partial_t + \mu - \phi + \frac{1}{2m}\left(-\mathrm{i}\partial_{\boldsymbol{x}} + \boldsymbol{A}_{\rm ext} + \boldsymbol{a}\right)^2 - V \right] \psi + S_{\rm int}[\bar\psi, \psi]. \tag{13.2.13}$$

13.2.2 Analyzing the composite fermion Chern-Simons theory

Before we embark on the analysis of the above effective theory, let us make a hand-waving mean-field analysis. We see that for $s = 1$, each electron binds two flux quanta. If we *assume* the density to be homogeneous (recall the plasma analogy for the Laughlin wave function), and if we neglect fluctuations, then the electrons see *on average* a flux corresponding to $\boldsymbol{A}_{\rm ext} - \langle \boldsymbol{a} \rangle$. In other words, the composite fermions see a smaller $\boldsymbol{B}$-field! Several scenarios are possible

(i) $\boldsymbol{A}_{\rm ext} = \langle \boldsymbol{a} \rangle \;\Rightarrow$ no magnetic field. This happens at $\nu = 1/2$. The fact that the composite fermion prediction at $\nu = 1/2$ looks like a Fermi liquid is one of the great successes of the composite fermion construction [1].

(ii) Maybe, for some filling fraction ν, the effective $\boldsymbol{B}$-field corresponding to $\boldsymbol{A}_{\rm ext} - \langle \boldsymbol{a} \rangle$ leads to an effective new filling fraction $\nu^* \in \mathbb{Z}$, i.e., the fractional quantum Hall effect for electrons would be mapped to an integer quantum Hall effect for composite fermions.

We are now trying to analyze the composite-fermion Chern-Simons (CF-CS) theory in mean-field. The only term which gives a real headache is the interaction term $S_{\rm int}[\bar\psi, \psi]$. We re-write it using a Hubbard-Stratanovich transformation

$$e^{\mathrm{i}S_{\rm int}} = \int D[\sigma] \exp\left\{ \frac{\mathrm{i}}{2} \int dx^3 dx'^3\, \sigma(x) [V^{-1}](x, x') \delta(x_0 - x'_0) \sigma(x') + \mathrm{i} \int dx^3 (\rho(x) - \rho_0) \sigma(x) \right\}. \tag{13.2.14}$$

For the interpretation of the σ-field it helps to note that when completing the square, it appears as next to $\bar\psi\psi$, hence it describes a (rescaled) density field.[3] Now ψ and $\bar\psi$ (and $\rho = \bar\psi\psi$) only appear quadratically (linearly) in the action and we can integrate out $\bar\psi, \psi$. With this we obtain an effective theory

$$S_{\rm eff}[\sigma, a] = \underbrace{-\mathrm{i}\,\mathrm{tr}\log\left[\mathrm{i}\partial_0 + \mu - a_0 - \sigma + \frac{1}{2m}(-\mathrm{i}\nabla + A)^2 \right]}_{S_\psi[a, A]} \tag{13.2.15}$$

$$- \rho_0 \int dx^3\, \sigma(x) + \frac{1}{2} \int dx^3 dx'^3\, \sigma(x) [V^{-1}](x, x') \delta(x_0 - x'_0) \sigma(x') \tag{13.2.16}$$

$$+ \frac{\Theta}{4} S_{\rm CS}[a], \tag{13.2.17}$$

where $A = A_{\rm ext} + a$. The first line arises from integrating out the fermions ψ. On this effective theory we want to apply a mean-field, or saddle-point, approximation. As there are no ψ-fields present anymore, it can be difficult to interpret the different terms in the theory. To

[3] We also say that we decouple the action in the density-density channel.

provide remedy to this problem, we note that the local density of fermions is given by taking the derivative of the original fermionic action with respect to $a_0(x)$. This property obviously survives the elimination of the ψ field. Therefore, we can get an "effective" expression for the density by

$$\frac{\delta S_\psi}{\delta a_0} = \rho[a,\sigma]. \tag{13.2.18}$$

Therefore,

$$\rho[a,\sigma] = \left[\mathrm{i}\partial_0 + \mu - a_0 - \sigma + \frac{1}{2m}(-\mathrm{i}\nabla + A)^2\right]^{-1}(x,x). \tag{13.2.19}$$

Next, let us write down the saddle-point (Euler-Lagrange) equations. We start with

$$\left.\frac{\delta S_{\text{eff}}}{\delta a_o}\right|_{\bar\sigma,\bar a} = 0: \qquad \rho[\bar a,\bar\sigma] = \frac{1}{4\pi s}\bar b. \tag{13.2.20}$$

This is nothing but the expected relation between the $\bar b$ field and the density.[4]
Next, we also need to minimize the action with respect to the field σ

$$\frac{\delta S_{\text{eff}}}{\delta\sigma}|_{\bar\sigma,\bar a} = 0 \qquad \Rightarrow \qquad \rho(x) - \rho_0 = -\int dx'^3 [V^{-1}](x,x')\sigma(x')\delta(x_0 - x_0'), \tag{13.2.21}$$

or

$$\sigma(x) = -\int dx'^3 V(x-x')[\rho(x') - \rho_0]\big|_{x_0'=x_0}. \tag{13.2.22}$$

Here we recognize that deviations of $\rho(x)$ from its mean value give rise to an "interaction potential" $\sigma(x)$. We can solve the mean-field equations by

$$\rho[\bar a, 0] = \rho_0 \tag{13.2.23}$$

$$\bar\sigma = \bar a = 0 \tag{13.2.24}$$

$$\bar b = 4\pi s\rho_0 \quad \Rightarrow \boldsymbol{a} = 2s\nu \boldsymbol{A}_{\text{ext}}. \tag{13.2.25}$$

When can we expect this mean-field calculation to be reliable? Certainly, if the resulting ground-state is gapped, we can hope that fluctuations around the mean-field solutions will not do too much harm. One way to ensure a gapped mean-field solution is by asking for the effective $A - A_{\text{ext}} - a$ to give rise to a *filled effective Landau level*. Therefore we ask

$$\nu_{\text{eff}} = p \quad \text{or} \quad \Phi_{\text{eff}} = \frac{2\pi N}{p} \quad \text{with} \quad \Phi_{\text{eff}} = (B_{\text{ext}} - \bar b)L^2. \tag{13.2.26}$$

Inserting $b = 4\pi sN/L^2$ we immediately obtain

$$\nu = \frac{2\pi N}{B_{\text{ext}}L^2} = \frac{2\pi N}{\frac{2\pi N}{p} + 4\pi sN} \qquad \Rightarrow \qquad \nu = \frac{p}{1+2sp}. \tag{13.2.27}$$

We can summarize the mean-field discussion with the following list and Fig. 13.1

(i) We can explain many fractions which are symmetrically distributed around $1/2s$ by an integer quantum Hall effect for composite fermions. Note, however, that the gap is entirely due to interactions!

(ii) For $\nu = p/2s$, CF-CS predicts a Fermi-liquid theory in $B_{\text{eff}} = 0$

  (a) This seems to describe $\nu = 1/2$ well [1].
  (b) For $3/2 = 1/2+1$ and $5/2 = 1/2+2$ one could have expected the same Fermi-liquid as they are nothing but the $1/2$ plateaus in higher (real) Landau levels. This is however not the case. One can imagine that in these cases, residual interactions beyond the mean-field descriptions lead to an instability of the Fermi surface.

[4] Check that the minimization of the action with respect to a_1 and a_2 only provides the continuity equation of the density and does not give any further constraints in the mean-field value of a.

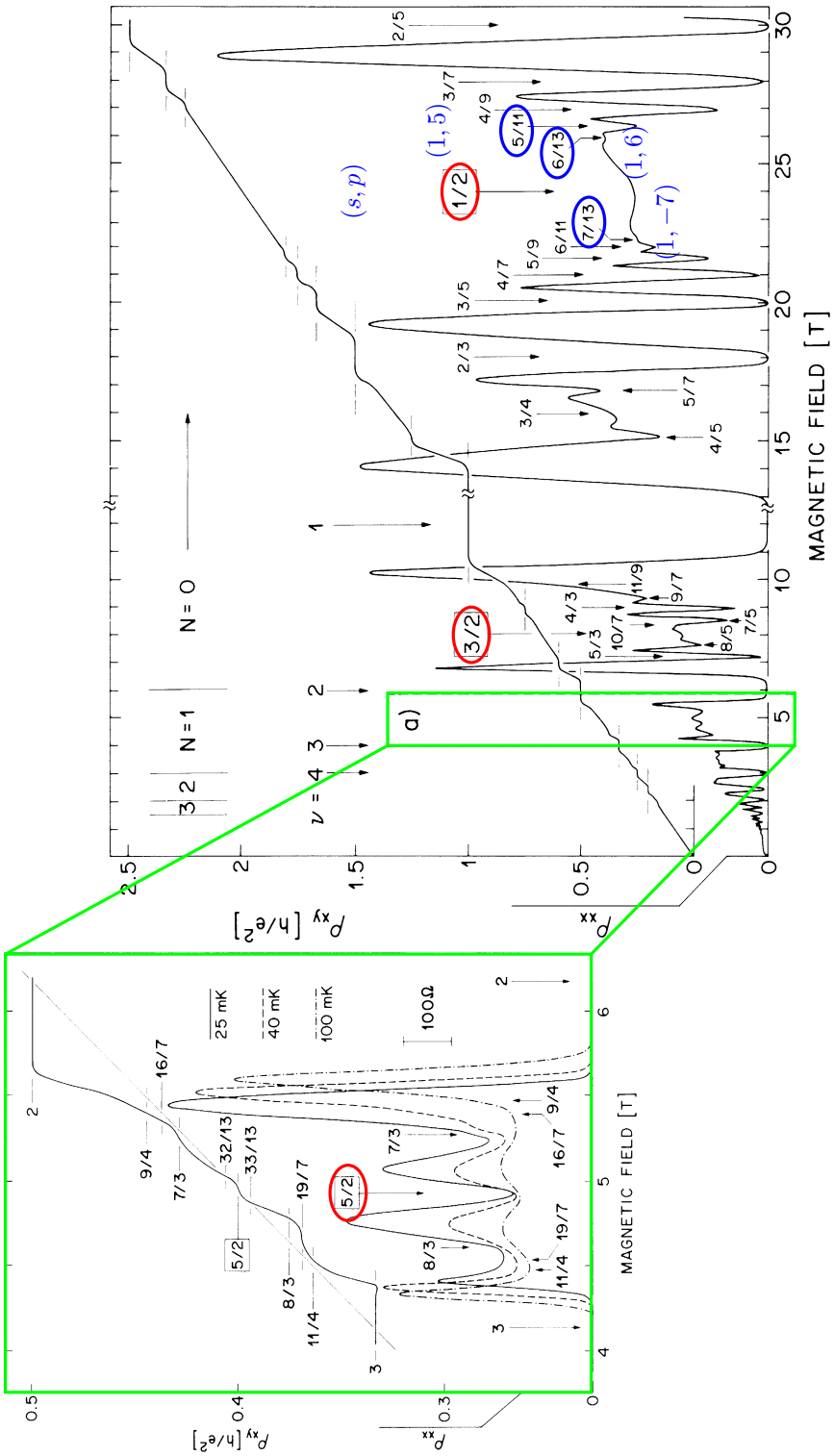

Figure 13.1: Overview of diagonal resistivity ρ_{xx} and Hall resistance ρ_{xy}. The blue numbers denote the fractions which are well explained by an integer quantum Hall plateau of composite fermions. The inset shows the details around $\nu = 5/2$. Figure adapted from Ref. [2] (Copyright (1987) by The American Physical Society).

13.2.3 Fluctuations around the mean-field solution

We want to take a step beyond the mean-field considerations. For this, let us expand $S[a, A]$ to second order in a.[5] We could take the CF-CS action and expand to leading order around $\bar{a}$. However, we can do a much simpler thing. Let us just say that

$$S^{(2)}[a, A] = \frac{1}{2}\int dx^3 dx'^3\, (A+a)^\mu(x) K_{\mu\nu}(x-x')(A+a)^\nu(x') + \frac{\Theta}{4} S_{\text{CS}}[a]. \tag{13.2.28}$$

Without actually calculating $K_{\mu\nu}$, we try to constrain it from general considerations

- $K_{\mu\nu}$ has to be gauge invariant.
- $K_{\mu\nu}(q)$ can be expanded in q.
- Via the Kubo formula (13.1.46), we know that $K_{\mu\nu}$ encodes the electromagnetic response.

We know that $\sigma_{11} = 0$ due to the gap for composite fermions. The transverse response, σ_{12}, however, can be non-zero. Recall, that

$$\sigma_{12} = -\mathrm{i} \lim_{\boldsymbol{q}\to 0} \frac{1}{\omega} K_{12}(\omega, \boldsymbol{q}). \tag{13.2.29}$$

From this we conclude that we have

$$K_{\mu\nu} = -\mathrm{i}\sigma_{12}^{(0)} \epsilon_{\mu\sigma\nu} q_\sigma. \tag{13.2.30}$$

Here $\sigma_{12}^{(0)}$ denotes the composite fermion mean-field value for the transverse response. Inserted into the expression for $S^{(2)}[a, A]$ we find

$$S^{(2)}[a, A] = \frac{\sigma_{12}^{(0)}}{2} S_{\text{CS}}[a + A] + \frac{\Theta}{4} S_{\text{CS}}[a]. \tag{13.2.31}$$

This effective action is clearly (i) gauge invariant, (ii) the lowest order expansion in q, and (iii) provides $K_{\mu\nu}$ that reproduces the electromagnetic of the effective theory. Actually, we would expect that

$$\frac{\delta^2 Z}{\delta A_\mu \delta A_\nu} \tag{13.2.32}$$

provides us with the desired response function. However, this is only true after we integrated out the fluctuations in a! What we need in the following is the formula valid for quadratic actions (Show!)

$$\int D[a]\, e^{c_1 S[a+b] + c_2 S[b]} = e^{\frac{1}{\frac{1}{c_1}+\frac{1}{c_2}} S[b]}. \tag{13.2.33}$$

Using this formula we obtain after integrating over the field a

$$S_{\text{eff}}[A] = \frac{1}{\frac{1}{\sigma_{12}^0} + \frac{2}{\Theta}} S_{\text{CS}}[A]. \tag{13.2.34}$$

And hence,

$$\sigma_{12} = \frac{e^2}{h} \frac{p}{1+2sp} \qquad s, p \in \mathbb{Z}. \tag{13.2.35}$$

[5] Why not in σ?

13.3 $\nu = 5/2$

We have seen that composite fermions allow us to extend the idea of the Laughlin wave function to many other fillings in a simple way. We also mentioned that the prediction of a Fermi-liquid at zero effective magnetic field was one of the great successes of the composite fermion approach. There is, however, even more interesting physics emerging from half-filled Landau levels.
In the presence of interactions, a Fermi surface is generically unstable towards symmetry breaking. At least at low enough temperatures. It seems, however, that for the lowest Landau level, the attached fluxes already account for all interaction effects (recall that the Laughlin wave-function is exact if we neglect pseudo-potentials v_s with $s > 1$).[6] A natural question that arises is what happens in higher Landau levels. Let us go through a chain of (somewhat handwaving) arguments

- For the lowest Landau level the flux attachment "exactly" accounts for interaction effects and renders the $\nu = 1/2$ state a gapless Fermi liquid.
- In the next Landau level, the free Hamiltonian is less optimized. Hence we can expect it to be slightly better tailored to satisfy the interaction effects.
- If we optimally absorbed the interaction effects in the lowest Landau level, we overdue in the second Landau level.
- To compensate for the over-accounted interactions, there is a residual *attraction* between composite fermions.

[6] Let us examine the two-particle problem on top of a Fermi surface

$$\left[-\frac{\hbar^2}{m}\nabla^2 + V(\boldsymbol{r})\right]\psi(\boldsymbol{r}) = \left(E + \frac{\hbar^2 k_{\mathrm{F}}^2}{m}\right)\psi(\boldsymbol{r}), \tag{13.3.1}$$

where $\boldsymbol{r}$ is the relative coordinate of the two-particle wave-function of a singlet of electrons. The energy E is measured with respect to the Fermi energy $\hbar^2 k_{\mathrm{F}}^2/2m$. We use the Fourier transform of the wave-function and the interaction potential

$$g(\boldsymbol{k}) = \int d\boldsymbol{r}\, e^{-\mathrm{i}\boldsymbol{k}\cdot\boldsymbol{r}}\psi(\boldsymbol{r}) \qquad \text{and} \qquad V(\boldsymbol{k}) = \int d\boldsymbol{r}\, e^{-\mathrm{i}\boldsymbol{k}\cdot\boldsymbol{r}}V(\boldsymbol{r}). \tag{13.3.2}$$

Inserted into the above equation we obtain

$$\frac{\hbar^2 k^2}{m}g(\boldsymbol{k}) + \int \frac{d\boldsymbol{k}'}{(2\pi)^2}V(\boldsymbol{k}-\boldsymbol{k}')g(\boldsymbol{k}') = \left(E + \frac{\hbar^2 k_{\mathrm{F}}^2}{m}\right)g(\boldsymbol{k}). \tag{13.3.3}$$

If now assume $V(\boldsymbol{k})$ to be attractive with a strength $-V_0$ in a shell around the Fermi-surface we find

$$\left(-\frac{\hbar^2 k^2}{m} + E + \frac{\hbar^2 k_{\mathrm{F}}^2}{m}\right)g(\boldsymbol{k}) = -V_0 \int_{E_{\mathrm{F}}<(\hbar k')^2/2m<E_{\mathrm{F}}+\Lambda} d\boldsymbol{k}' g(\boldsymbol{k}'). \tag{13.3.4}$$

We can now divide by the bracket on the left and integrate over $\boldsymbol{k}$ in the shell around the Fermi-surface. With this we find the equation

$$1 = V_0 \int_{E_{\mathrm{F}}<(\hbar k')^2/2m<E_{\mathrm{F}}} \frac{d\boldsymbol{k}}{(2\pi)^2}\frac{1}{\frac{\hbar^2 k^2}{m} - E - \frac{\hbar^2 k_{\mathrm{F}}^2}{m}}. \tag{13.3.5}$$

We now use the constant density of states to go from a momentum integral over to an integral over the energy $\xi = \hbar^2 k^2/2m - E_{\mathrm{F}}$, where $N(0)$ is the density if states (at the Fermi level)

$$1 = V_0 N(0)\int_0^{\Lambda} d\xi\, \frac{1}{2\xi - E} = \frac{V_0 N(0)}{2}\log\left(-\frac{2\Lambda}{E}\right) \tag{13.3.6}$$

and therefore

$$E = -2\Lambda e^{-\frac{1}{V_0 N(0)}}. \tag{13.3.7}$$

In other words, two electrons bind into a Cooper pair [3]. Consequently, the Fermi-surface is unstable towards the formation of such pairs. It is the content of the Bardeen Cooper Schrieffer theory [4] to determine the resulting physics.

- Due to the strong magnetic field, it is profitable to form a superconductor out of spin-polarized composite fermions.
- The pairing has to be odd as the spin is symmetric.
- The resulting phase is a $p_x + ip_y$ superconductor of composite fermions.
- We end up with a filling $1+1+1/2 = 5/2$. The two ones correspond to the two spin-species filling the lowest Landau level.
- We have seen in Chap. 6 that this state has non-abelian excitations in the form of Majorana zero modes bound to vortices.

It is important to note that due to the fact that we are dealing with a p-wave superconductor of *composite fermions* the resulting state and excitations are significantly more complicated than in the non-interacting case discussed in Chap. 6. In particular, $\nu = 5/2$ state is an intrinsically topologically ordered state with fractionally charged excitation with a charge $e^* = e/4$ [5]. The link between the full theory of the 5/2-state in terms of the famous Moore-Read state [6] and the p-wave superconductor interpretation was established by Read and Green [7]. In the framework of the superconductor language it was shown in a particularly transparent way that the quasiparticles exhibit non-abelian statistics by Ivanov [8].

References

1. Halperin, B. I., Lee, P. A. & Read, N. "Theory of the half-filled Landau level". *Phys. Rev. B* **47,** 7312. http://link.aps.org/doi/10.1103/PhysRevB.47.7312 (1993).
2. Willett, R. *et al.* "Observation of an even-denominator quantum number in the fractional quantum Hall effect". *Phys. Rev. Lett.* **59,** 1776. http://dx.doi.org/10.1103/PhysRevLett.59.1776 (1987).
3. Cooper, L. N. "Bound Electron Pairs in a Degenerate Fermi Gas". *Phys. Rev.* **104,** 1189. http://link.aps.org/doi/10.1103/PhysRev.104.1189 (1956).
4. Bardeen, J., Cooper, L. N. & Schrieffer, J. R. "Theory of Superconductivity". *Phys. Rev.* **108,** 1157. http://link.aps.org/doi/10.1103/PhysRev.108.1175 (1957).
5. Dolev, M., Heiblum, M., Umansky, V., Stern, A. & Mahalu, D. "Observation of a quarter of an electron charge at the $\nu = 5/2$ quantum Hall state". *Nature* **452,** 829. http://dx.doi.org/10.1038/nature06855 (2008).
6. Moore, G. & Read, N. "Nonabeloans in the fractional quantum Hall effect". *Nucl. Phys. B* **360,** 362. http://dx.doi.org/10.1016/0550-3213(91)90407-O (1991).
7. Read, N. & Green, D. "Paired states of fermions in two dimensions with breaking of parity and time-reversal symmetries and the fractional quantum Hall effect". *Phys. Rev. B* **61,** 10267. http://link.aps.org/doi/10.1103/PhysRevB.61.10267 (2000).
8. Ivanov, D. A. "Non-Abelian Statistics of Half-Quantum Vortices in p-Wave Superconductors". *Phys. Rev. Lett.* **86,** 268. http://link.aps.org/doi/10.1103/PhysRevLett.86.268 (2001).

Chapter 14

Summary

Learning goals

- We understand how all the models and systems discussed in the lecture can be systematized as part of the known types of topological phases.
- We understand the fundamental differences and the connections between noninteracting topological phases and intrinsic topological order.
- We can embed the contents of the lecture in the historical context of the field.

This chapter consists of two parts: We will first give a short historical account of topological condensed matter physics. Then, we will attempt to put the models and types of systems that we studied in this lecture in a systematic structure.

14.1 A historical recap of the lecture

This review is somewhat biased to experiments, since the ultimate relevance of physical insights lies in the connection to the real world, i.e., to experiments. There is much more theory work that often foreshadowed experimental developments.
Topology entered condensed matter physics in the form of topological defects. Specifically, Skyrmions (Tony Skyrme, 1962) were predicted as hypothetical particles, and much later confirmed in magnetic systems. Another topological defect – which found its experimental verification sooner – is a vortex in a superconductor or superfluid. It is at the basis of the Berezinskii-Kosterlitz-Thouless transition (1971/1973; Nobel prize), which is understood as a vortex-antivortex condensation in 2D (for instance in the XY spin model). The mechanism describes well 2D or quasi-2D (disordered) superconductors and Josephson junction arrays. Another early point where topological concepts entered condensed matter research is the study of defects in crystalline solids.
Then came the revolution of the quantum Hall effects, spearheaded by the integer quantum Hall effect (von Klitzing 1980; Nobel prize). They introduced quantized topological response functions, i.e., universally quantized observables that are expressed in constants of nature and do not depend on the system details. (Note that this is a stricter quantization constraint than in quantum mechanics, where for instance the energy quanta a system can absorb do depend on the system's details.) The mathematical understanding of the integer quantum Hall effect was soon delivered by Laughlin, Thouless, Kohmoto, Nightingale, Den Nijis (1892), defining the Chern number in a physical context by connecting it to the Hall conductivity $\sigma_{xy} = ne^2/h$, $n \in \mathbb{Z}$. In essentially the same system, the fractional quantum Hall effect was discovered (Laughlin, Störmer, Tsui 1982; Nobel prize) with Hall conductivities $\sigma_{xy} = \frac{p}{q}e^2/h$, with $p, q \in \mathbb{Z}$. This is a remarkable coincidence, as the integer and fractional effects are radically different from a theoretical perspective. The new paradigms coming with the fractional effect

(intrinsic topological order and emergent quantum statistics) where therefore not understood until a few years later, with important contributions from X.-G. Wen at the beginning of the 1990s. There followed many studies that aimed to understand the cuprate high-temperature superconductors using topological physics in terms of anyons models and chiral spin liquids, but no experimental confirmation could be found.
In a somewhat parallel development, spin models were studied for their topological properties. Notably, Haldane conjectured that the spin-1 Heisenberg chains is gapped and supports topological spin-1/2 end excitations. An exactly soluble, but less natural model was conceived by Affleck, Kennedy, Lieb, Tasaki (AKLT model, 1987). The Haldane conjecture was experimentally confirmed in 1D spin chain materials in the 1990s.
While theoretical efforts in topological quantum matter diversified at the end of the 1990s, one important realization was the description of non-Abelian statistics of vortices in p-wave superfluids (Reed, Moore, Ivanov). All of this paved the way for Kitaev to write his most influential papers: on the honeycomb spin model and its reduction to the toric code as well as the work on Majorana chains. They proposed, respectively, the vision for topological software and topological hardware of a quantum computer. In particular, the Majorana wire was still a very abstract idea that was sharpened in several iterations by the community and eventually fueled the effort on Majorana fermions at Microsoft, with Leo Kouwenhoven and Charles Marcus as the lead experimentalists.
In parallel to researchers exploiting Kitaev's insights, 2005/06 marked the time where a revolution in topological band theory started, with the prediction of the QSHE by Bernevig-Hughes-Zhang and the experimental verification by Molenkamp as well as the theoretical discovery of $\mathbb{Z}_2$ topological insulators in 2D by Kane and Mele. In quick succession the 3D versions of the latter where predicted and found, setting in motion a back and forth between theoretical predictions and experimental verifications of new topological band structures that has not stopped since. Milestones are the discovery of Weyl semimetals in 2015 and the formalism of topological quantum chemistry in 2017. Furthermore, initiated by the work of Kane and Lubensky in 2013, researchers started to look for topological physics in classical systems, such as phononic, acoustic, or photonic metamaterials.
One influential name that has not been mentioned so far is Grigory E. Volovik, who's book "The universe in a helium droplet" anticipated much of the ideas described above. In addition, there has been a fruitful influx or exchange of ideas with high-energy and mathematical physicists over the years. For instance, Roman Jackiw published solutions to domain wall and vortex bound states (based on the Dirac equation) before they made an appearance in condensed matter. Juerg Froehlich, Leonard Susskind, Edward Witten brought important field-theoretical ideas, inspired often by quantum Hall physics where topological matter is the "cleanest".

14.2 A systematizing recap of the lecture

We close by organizing the lecture contents according to our current physical understanding of topological phases. Figure 14.1 attempts such a summary for gapped quantum phases at zero temperature. The biggest differentiation is between topological phases with or without intrinsic topological order: Those with intrinsic topological order *always* have a manifold-dependent topological ground state degeneracy. The others, so-called symmetry-protected topological phases (SPT) *always* gapless boundary modes if the boundary does not break the protecting symmetry, but never such a topological degeneracy in the ground state. (Note that some spatial symmetries give problems with the emergence of boundary modes, as any boundary may break them.). The only phases that do not quite fit in here are the integer quantum Hall phases (which exist both for fermions and for bosons). If we do not care about charge conservation (i.e., we are not interested in the quantized Hall conductivity), these phases are still topological with anomalous boundary modes that transport heat, but there is no symmetry needed to protect their topology.

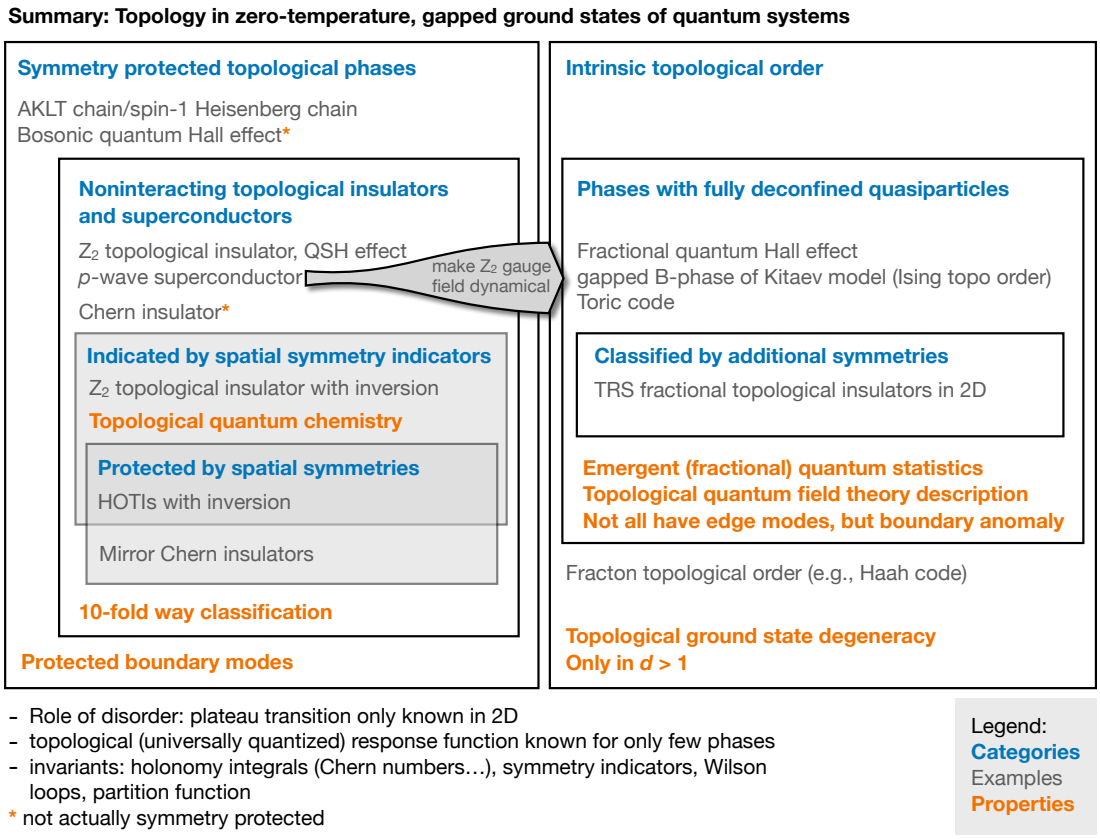

Figure 14.1: Overview of the lecture contents

Bosonic SPT phases always need interactions to be stabilized, as noninteracting Bosons fall into a boring Bose condensate ground state. For fermionic SPTs we know of examples that require interactions, but the ones we encountered in this lecture can all be defined for non-interacting systems. (The superconductors are somewhat of an exception – physically, they require interactions, but we considered only their mean-field BDG description which is effectively a non-interacting theory.) Foundational for the understanding of noninteracting fermionic SPTs is the 10-fold way. If spatial symmetries are added, their representation theory can be used to detect in which topological phase from the 10-fold way classification a system is (e.g., the inversion symmetry criterion for topological insulators), in which case we say the phase is symmetry-indicated. Furthermore, spatial symmetries can be used to protect new topological phases, such as a mirror Chern insulator. Some of these are indicated by representation theory invariants, but not all of them (for instance, in a C_n-symmetric TRS system, the mirror Chern number is symmetry indicated modulo n).

Turning to intrinsic topological order, we have to state a few things that have not been shown in the lecture. Intrinsic topological order exists for fermionic and bosonic systems in dimensions $d \geq 2$. In $d = 2$, the phases are fully classified and can always be understood from a topological quantum field theory and from their content of emergent quasiparticles (anyons) with fractional statistics. We have seen this at work in the FQHE and the toric code. In presence of additional symmetries such as charge conservation, fractional quantized response functions (e.g., fractional Hall conductivity) reflect the fractionalization. In $d > 2$ other types of intrinsic topological orders, so-called *fracton phases* exist, which also have topologically degenerate ground states but no quasiparticle picture can (fully) describe them.

It is important to realize that *all* intrinsic topological orders *are not* adiabatically connectable to a trivial phase, even if no symmetries are imposed. (Symmetries only offer a refinement of the

classification of intrinsic topological order phases among themselves.) This is in stark contrast to the SPTs: With the exception of the Hall effect type phases, *all* of them *are* adiabatically connected to a trivial phase if no symmetries are imposed.

Appendix A

Scaling theory of localization*

Learning goals

- We appreciate the role of the dimensions for the localization of electrons.
- We can reproduce the gang-of-four scaling plot.

- M. A. Paalanen G. A. Thomas, Helv. Phys. Acta **56**, 27 (1983)

A.1 Conductance versus conductivity*

We want to study the influence of disorder on the electrical resistance R relating the applied voltage U to the electrical current I

$$U = RI. \tag{A.1.1}$$

R connects two macroscopic observables and therefore characterizes a macroscopic sample. The conductance g is defined as the inverse of the resistance

$$g = \frac{1}{R}. \tag{A.1.2}$$

These quantities have to be contrasted with the microscopic quantities such as the conductivity σ

$$j = \sigma E, \tag{A.1.3}$$

where E is the electric field and j the microscopic current density. In this chapter we want to understand if there is a simple bridge between the microscopic quantity σ (which we might be able to calculate from first principles in simple model situations) and the macroscopic conductance g. We try to do so by starting from a relatively small system where we are in principle up to the task of calculating g exactly. We then want to successively increase the system size and see what we can deduce.

A.2 One parameter scaling*

The key step in the program of successively increasing the system size dates back to the very influential paper by what we now call the the "gang of four": Abrahams, Anderson, Licciardello, and Ramakrishnan [1]. Their key insight was that the conductance $g(2L)$of a block of size $2L$ only depends on one parameter, namely the conductance $g(L)$ of the block of size L out of which the larger was formed, cf. Fig. A.1. In other words

$$g(2L) = f[g(L)] \qquad \text{and not} \qquad g(2L) = h[g(L), L, \dots]. \tag{A.2.1}$$

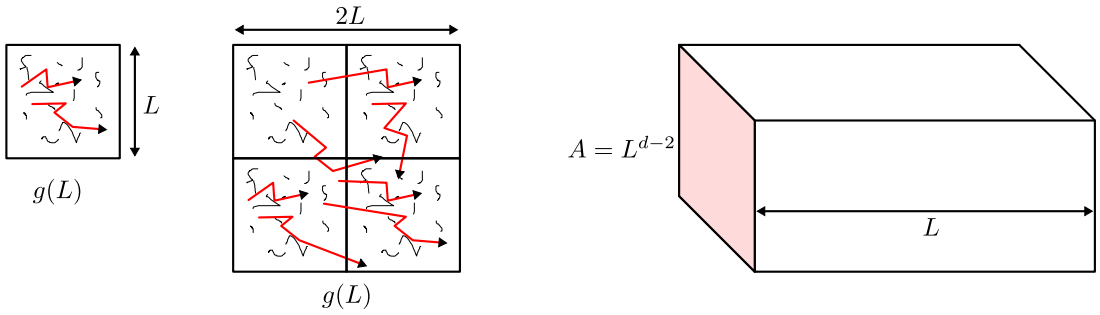

Figure A.1: Setup for the renormalization of the conductance.

This statement is not easy to motivate in a systematic way. Instead of attempting to legitimate (A.2.1), we want to analyze its consequences in the following. To make further progress we write (A.2.1) in a form that contains no scales

$$\frac{L}{g}\frac{dg(L)}{dL} = \frac{d\log(g)}{d\log(L)} = \beta(g). \tag{A.2.2}$$

Let us have a look at simple limiting cases.
For a good conductor $g \gg 1$ we know that the "one parameter scaling" holds in the form of Ohm's law

$$R = \rho\frac{L}{A} = \rho\frac{L}{L^{d-1}} \qquad \Rightarrow \qquad g = \sigma_0 L^{2-d}. \tag{A.2.3}$$

From this we immediately obtain

$$\frac{d\log(g)}{d\log(L)} = d-2 \qquad \Rightarrow \qquad \lim_{g\to\infty}\beta(g) = d-2. \tag{A.2.4}$$

In the other limit of very strong disorder, all wave-function will be exponentially localized. Therefore, we expect the conductance to behave as

$$g(L) \propto e^{-L/\xi} \qquad \Rightarrow \qquad \frac{d\log(g)}{d\log(L)} = -\frac{L}{\xi} = \log(g). \tag{A.2.5}$$

Hence in the limit of vanishingly small conductance, the β function reads

$$\lim_{g\to 0}\beta(g) = \log(g). \tag{A.2.6}$$

We summarize these results in Fig. A.2. Due to the dependence of the β-function on the dimension d, disorder seems to have very different effects depending on the spatial dimension. Let us discuss the consequences of Fig. A.2 for one, two, and three dimensions separately.

A.2.1 One dimension*

In one dimension, $\beta(g) < 0$ is always negative. In other words, by increasing the system size, the conductance g always flows to zero, irrespective of the conductance of a short section of the wire.
Let us define a localization length ξ, where $g(L=\xi) = 1$. We find

$$\frac{d\log(g)}{d\log(L)} = -1 \qquad \Rightarrow \qquad g(L) = \frac{g_0}{L} \qquad \Rightarrow \qquad \xi \sim g_0, \tag{A.2.7}$$

where g_0 is the conductance calculated for a small segment.

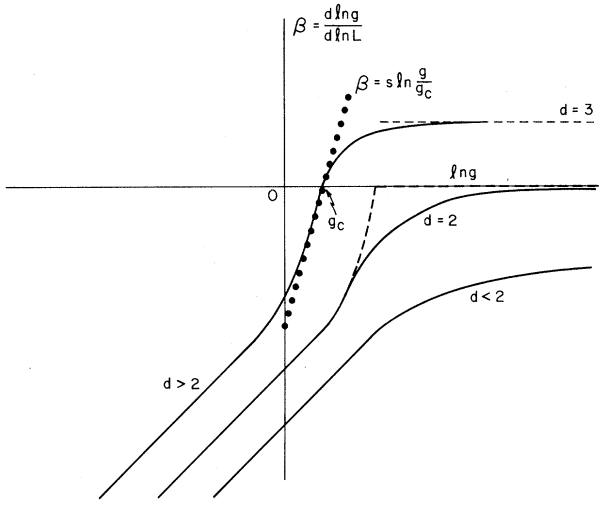

Figure A.2: Plot of $\beta(g)$ as a function of $\log(g)$ for various dimensions. Figure take from Ref. [1] (Copyright (1979) by The American Physical Society).

A.2.2 Two dimensions*

In two dimensions we encounter a somewhat more intriguing situation. For large values of g the β-function is zero. In other words, to first order in $1/g$, the conductance does not change under a change in L. Such a situation is called marginal. As we have identified the limit $g \gg 1$ as the classical regime where Ohm's law holds, this means quantum corrections will play a crucial role in how $\beta(g)$ behaves away from $g \gg 1$. These quantum corrections are called "weak (anti-) localization". Their detailed calculation is beyond the scope of this course. However, we can estimate them using a simple trick. Let us just calculate the probability for a particle to return to the point where we inject it into the system

$$P = |\langle \psi^\dagger(x)\psi(x)\rangle|^2. \tag{A.2.8}$$

When we calculate $\langle \psi^\dagger(x)\psi(x)\rangle$, we have to sum over all path the particle can take from x, back to the same point x. In quantum mechanics, each path is associated with an amplitude and a phase. Due to the disorder (which we try to study, after all), all paths sum up incoherently. If we have a time-reversal invariant system, however, there are paths who's amplitude and phase are correlated as shown in Fig. A.3. Owing to the time-reversal symmetry the blue and the red path have a well defined phase relation. If we now calculate P the sum contains the following contributions shown in Fig. A.4.

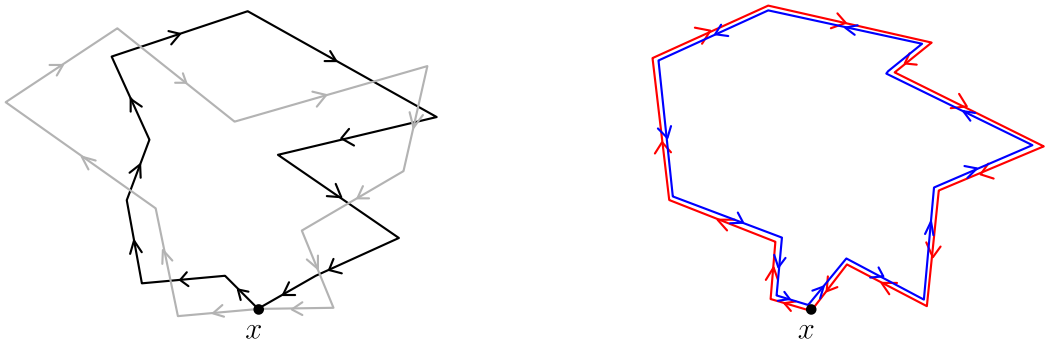

Figure A.3: Return probability.

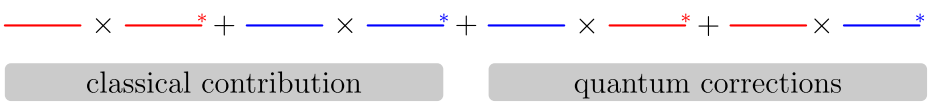

The endpoints of any segment are related to some state $|\phi\rangle$. In order to invert the arrow of time we use the time reversal operator $\mathcal{T}$ on these states:

Figure A.4: Interference in the return probability.

From this we conclude that we can have two distinctly different situations

1. $\mathcal{T}^2 = -\mathbb{1}$ $\Rightarrow$ the return probability P is reduced, hence quantum mechanical effects lead to more extended states and we deal with weak *anti-localzation*.
2. $\mathcal{T}^2 = \mathbb{1}$ $\Rightarrow$ the return probability P is enhanced, i.e., the states are more localization: weak *localization*.

However, a word of caution is in order here! When applying this argument for spin-1/2 fermions we generically have $\mathcal{T}^2 = -\mathbb{1}$. But if the Hamiltonian does not mix the spin degrees of freedom, we can go to the individual spin sectors and describe the physics as two spin-0 problems. In this case however, $\mathcal{T}^2 = \mathbb{1}$. The situation changes if we deal with *spin-orbit* coupling. In this case we have to stick with the spin-1/2 description and therefore we generically expect *anti-localization* in this case.
Let us now analyze the case of no spin-orbit interactions, i.e., weak localization. We solve the equation

$$\frac{d\log(g)}{d\log(L)} = -\frac{C}{g} \qquad \text{or} \qquad \frac{dg}{d\log(L)} = -C < 0. \tag{A.2.9}$$

We find

$$g = g_0 - C\log(L/l), \tag{A.2.10}$$

where l is the small length at which we managed to solve the problem exactly and found $g(l) = g_0$. We can now again determine the localization length by equating $g(\xi) = 1$ to find

$$\xi \sim l e^{g_0/C}. \tag{A.2.11}$$

Indeed, all states are localized. However, $g \gg g_0$ and the localization length is astronomical.

A.2.3 Three dimensions*

Three dimensions (or two with spin-orbit) are the most interesting cases. Depending on the initial value g_0, $\beta(g)$ is either positive or negative, i.e., a macroscopic sample can either be conducting or insulating. In other words, there is a metal-insulator transition as a function of g_0. For the time being three dimensions are not in the scope of the course and we will come back to it (and spin-orbit in two dimensions) later.

References

1. Abrahams, E., Anderson, P. W., Licciardello, D. C. & Ramakrishnan, T. V. "Scaling Theory of Localization: Absence of Quantum Diffusion in Two Dimensions". *Phys. Rev. Lett.* **42,** 673. http://link.aps.org/doi/10.1103/PhysRevLett.42.673 (1979).

Appendix B

A more historical route to time reversal invariant topological insulators*

B.1 The Haldane Chern insulator*

In his seminal paper [1], Haldane considered a honeycomb model with no net magnetic flux but with complex phases $e^{\pm i\varphi}$ on the next-to-nearest neighbor hoppings. A possible *staggered* flux pattern giving rise to such a situation is shown in Fig. B.1. In Fig. B.1 we also indicate the sign structure of the phases. The model can be written as

$$H = \sum_{\langle i,j\rangle} c_i^\dagger c_j + t \sum_{\langle\langle i,j\rangle\rangle} e^{\pm \mathrm{i}\varphi} c_i^\dagger c_j + m \sum_i \epsilon_i c_i^\dagger c_i, \tag{B.1.1}$$

where $\epsilon_i = \pm 1$ for the two sub-lattices of the honeycomb lattice. Written in $\boldsymbol{k}$-space we find $\mathcal{H} = \epsilon(\boldsymbol{k}) + \sum_i d_i(\boldsymbol{k})\sigma_i$ with

$$d_1(\boldsymbol{k}) = \cos(\boldsymbol{k}\cdot\boldsymbol{a}_1) + \cos(\boldsymbol{k}\cdot\boldsymbol{a}_2) + 1, \tag{B.1.2}$$

$$d_2(\boldsymbol{k}) = \sin(\boldsymbol{k}\cdot\boldsymbol{a}_1) + \sin(\boldsymbol{k}\cdot\boldsymbol{a}_2), \tag{B.1.3}$$

$$d_3(\boldsymbol{k}) = m + 2t\sin(\varphi)\left[\sin(\boldsymbol{k}\cdot\boldsymbol{a}_1) - \sin(\boldsymbol{k}\cdot\boldsymbol{a}_2) - \sin(\boldsymbol{k}\cdot(\boldsymbol{a}_1 - \boldsymbol{a}_2))\right], \tag{B.1.4}$$

with $\boldsymbol{a}_1 = a(1,0)$ and $\boldsymbol{a}_2 = a(1/2, \sqrt{3}/2)$. We ignore the shift $\epsilon(\boldsymbol{k})$ in the following. What are the symmetries of this Hamiltonian? First, d_1 and d_2 are compatible with the time-reversal $\mathcal{T}$. However, $d_3(\boldsymbol{k}) = d_3(-\boldsymbol{k})$ holds only for $\varphi = 0, \pi$. We can therefore expect a non-vanishing Chern number for a general φ. The Hamiltonian has C_3 symmetry. Hence, the gap closings have to happen at the K or K' point, see Fig. B.2 (Prove!),

$$K = \frac{2\pi}{a}\left(1, \frac{1}{\sqrt{3}}\right), \qquad K' = \frac{2\pi}{a}\left(1, -\frac{1}{\sqrt{3}}\right),$$

where a denotes the lattice constant. To calculate the Chern number we follow the same logic as in the last chapter. We start from the limit $m \to \infty$ and track the gap-closings at the Dirac points at K and K'. The low energy expansion at these two points read

$$\mathcal{H}_K = \frac{3}{2}(k_y\sigma_x - k_x\sigma_y) + \left(m - 3\sqrt{3}t\sin(\varphi)\right)\sigma_z, \tag{B.1.5}$$

$$\mathcal{H}_{K'} = -\frac{3}{2}(k_y\sigma_x + k_x\sigma_y) + \left(m + 3\sqrt{3}t\sin(\varphi)\right)\sigma_z. \tag{B.1.6}$$

Note that the gap-closings at K and K' happen at different values of m (for $\varphi \neq 0, \pi$). Moreover, the two Dirac points give rise to a change in σ_{xy} of opposite sign has $\det(A)$ as a different sign. We can now construct the phase diagram

- $m > 3\sqrt{2}t\sin(\varphi)$: $\sigma_{xy} = 0$
- $-3\sqrt{2}t\sin(\varphi) < m \geq 3\sqrt{2}t\sin(\varphi)$ for $\varphi > 0$: At $m = 3\sqrt{2}t\sin(\varphi)$ the gap closes at K and we have a $\Delta\sigma_{xy} = -\frac{e^2}{h}$. The gap at K' stays open.
- $m \leq -3\sqrt{2}t\sin(\varphi)$ for $\varphi > 0$: The gap at K' closes at $m - 3\sqrt{2}t\sin(\varphi)$ and hence the Chern number changes back to 0.

For $\varphi < 0$ the signs of the Chern numbers are inverted. The resulting phase diagram is summarized in Fig. B.3.
The model of Haldane breaks time-reversal invariance $\mathcal{T}$. How can we build a model which is $\mathcal{T}$-symmetric? The easiest way is by doubling the degrees of freedom:

$$\mathcal{T}H\mathcal{T}^{-1} = H' \neq H \Rightarrow H_{\text{doubled}} = \begin{pmatrix} H & \\ & H' \end{pmatrix}.$$

We will see in the next section how Kane and Mele [2] took this step.

B.2 The Kane-Mele model*

In the last chapter we have seen that we can construct lattice models where the Bloch bands have a non-vanishing Chern number despite the absence of a net magnetic field. Here we try to build a time-reversal invariant version based on Haldane's honeycomb model for a Chern insulator.
We start from the low energy version of graphene

$$\mathcal{H}_0 = -\mathrm{i}\hbar v_{\mathrm{F}} \left[\sigma_x\tau_z\partial_x + \sigma_y\partial_y\right], \tag{B.2.1}$$

where $\boldsymbol{\sigma}$ acts on the sub-lattice index and $\boldsymbol{\tau}$ on the valley (K, K') space.
Let us add spin $\boldsymbol{s}$ to the game. With this we arrive at an 8×8 problem. The question is what kind of terms can we add in order to open a "non-trivial" gap. We have seen that $m\sigma_z + \tau_z\sigma_z 3\sqrt{3}t\sin(\varphi)$ does the job. However, this is not time-reversal symmetric for $\varphi \neq 0, \pi$ and m alone opens trivial gaps with $\mathsf{C}^{(1)} = 0$.
We construct a "non-trivial" time-reversal invariant gap step by step. First, in the sub-lattice space we need a σ_z term, otherwise we just move around the K and K' Dirac points in $\boldsymbol{k}$-space. Next, we need a spin dependent ($\boldsymbol{s}$) part to couple the two copies of the Haldane model. Let us try for the K point

$$\sigma_z \otimes s_z = \begin{pmatrix} \sigma_z & 0 \\ 0 & -\sigma_z \end{pmatrix}, \tag{B.2.2}$$

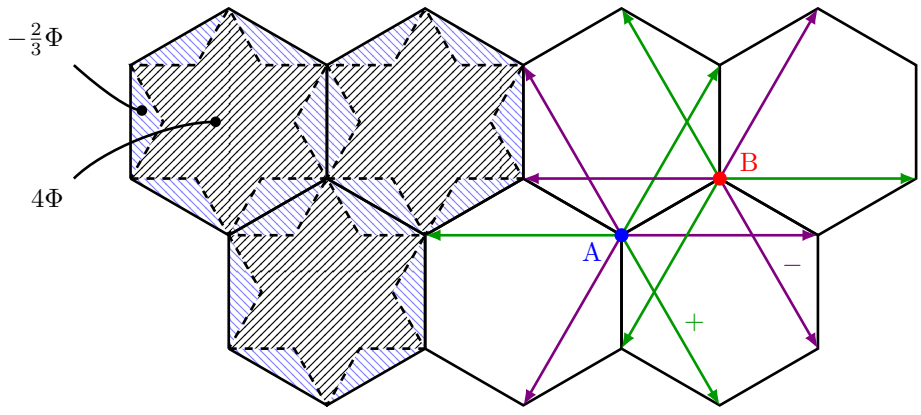

Figure B.1: The Haldane Chern insulator model.

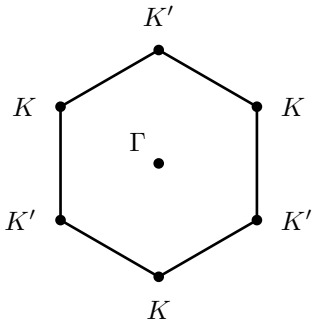

Figure B.2: Gap closings for the Haldane Chern insulator.

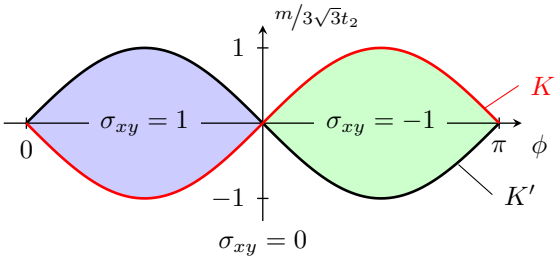

Figure B.3: Phase diagram of the Haldane model.

which gives us different gaps [with different "sign(m)"] for the two spins. How do we now add the valley degree of freedom ($\boldsymbol{\tau}$) in order to make it time-reversal invariant? The $\mathcal{T}$-operator acts in sub-lattice and spin space as

$$\mathcal{T} = \mathbb{1}_\sigma \otimes \mathrm{i}s_y K = \begin{pmatrix} 0 & -\mathbb{1}_\sigma \\ \mathbb{1}_\sigma & 0 \end{pmatrix}. \tag{B.2.3}$$

Therefore, the term $\propto \sigma_z \otimes s_z$ transforms as

$$\begin{aligned} \mathcal{T}\sigma_z \otimes s_z \mathcal{T}^{-1} &= \begin{pmatrix} 0 & -\mathbb{1}_\sigma \\ \mathbb{1}_\sigma & 0 \end{pmatrix} \begin{pmatrix} \sigma_z & 0 \\ 0 & -\sigma_z \end{pmatrix} \begin{pmatrix} 0 & \mathbb{1}_\sigma \\ -\mathbb{1}_\sigma & 0 \end{pmatrix} \\ &= \begin{pmatrix} 0 & -\mathbb{1}_\sigma \\ \mathbb{1}_\sigma & 0 \end{pmatrix} \begin{pmatrix} 0 & \sigma_z \\ \sigma_z & 0 \end{pmatrix} = \begin{pmatrix} -\sigma_z & 0 \\ 0 & \sigma_z \end{pmatrix} = -\sigma_z \otimes s_z. \end{aligned} \tag{B.2.4}$$

Under time reversal, $K \to K'$. Hence, we need the gap opening term in K' to be $\mathcal{T}\sigma_z \otimes s_z \mathcal{T}^{-1} = -\sigma_z \otimes s_z$ to have $\mathcal{T}\mathcal{H}(\boldsymbol{k})\mathcal{T}^{-1} = \mathcal{H}(-\boldsymbol{k})$. From this we conclude that the full gap opening term should be of the form

$$\mathcal{H}_{\mathrm{KM}} = \lambda_{\mathrm{SO}} \sigma_z \otimes \tau_z \otimes s_z. \tag{B.2.5}$$

We labelled the interaction with spin-orbit (λ_{SO}) to stress that $\mathcal{H}_{\mathrm{KM}}$ couples spin (s_z) and orbital (τ_z) degrees of freedom. Moreover, $\mathcal{H}_{\mathrm{KM}}$ is time-reversal invariant (TRI) by construction. Reverse engineering to a full lattice model we find

$$H_{\mathrm{KM}} = \sum_{\langle i,j\rangle,\alpha} c^\dagger_{i\alpha} c_{j\alpha} + \mathrm{i}\lambda_{\mathrm{SO}} \sum_{\langle\langle i,j\rangle\rangle,\alpha\beta} \nu_{ij} c^\dagger_{i\alpha} s^z_{\alpha\beta} c_{j\beta} + \lambda_v \sum_{i\alpha} \epsilon_i c^\dagger_{i,\alpha} c_{i,\alpha}, \tag{B.2.6}$$

where ϵ_i and the sign strucutre of ν_{ij} are the same as in Haldane's '88 model [1]. The above model was the first TRI topological insulator proposed by Kane and Mele in 2005 [2]. As it is TRI, the total Chern number cannot be non-zero. However, in the form (B.2.6), the spin

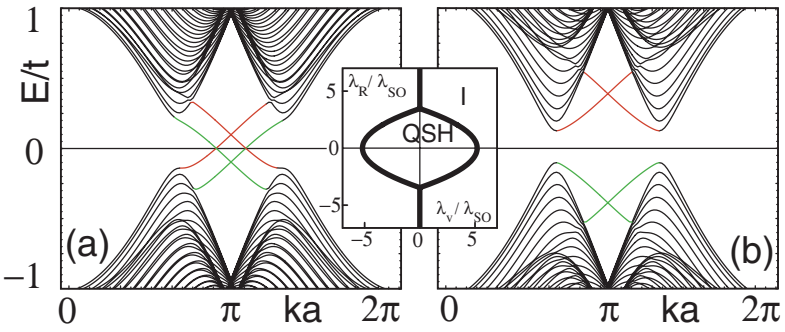

Figure B.4: Edge spectrum of the Kane Mele model for two different values of λ_R. On the left, two edge states cross the gap (colors label the edge). On the right, no edge states cross the gap. The inset shows the phase diagram as a function of λ_v and λ_R. Figure take from Ref. [2] (Copyright (2005) by The American Physical Society).

projections $|\uparrow\rangle, |\downarrow\rangle$ are good eigenstates. Therefore, we can use the Chern number $\mathsf{C}_\sigma^{(1)}$ in each spin-sector to characterize the phases. Indeed

$$\nu = \frac{\mathsf{C}_\uparrow^{(1)} - \mathsf{C}_\downarrow^{(1)}}{2} \bmod 2 \quad \in \mathbb{Z}_2 \tag{B.2.7}$$

defines a good topological index as we will see below [3]. The addition of a Rashba term

$$\mathcal{H}_R = \lambda_R \left[\sigma_x \tau_z s_x - \sigma_y s_x\right] \tag{B.2.8}$$

removes this conserved quantity. While $\mathcal{H}_R$ does not open a gap by itself (why?), it can influence the λ_{SO} induced gap, see Fig. B.4. However, the above topological index ν is not well defined anymore. In the following section we aim at deriving a $\mathbb{Z}_2$ index which does not rely on spin-Chern numbers.

References

1. Haldane, F. D. M. "Model for a Quantum Hall Effect without Landau Levels: Condensed-Matter Realization of the "Parity Anomaly"". *Phys. Rev. Lett.* **61,** 2015. http://link.aps.org/doi/10.1103/PhysRevLett.61.2015 (1988).
2. Kane, C. L. & Mele, E. J. "Quantum Spin Hall Effect in Graphene". *Phys. Rev. Lett.* **95,** 226801. http://link.aps.org/abstract/PRL/v95/e226801 (2005).
3. Sheng, D. N., Weng, Z. Y., Scheng, L. & Haldane, F. D. M. "Quantum Spin-Hall Effect and Topologically Invariant Chern Numbers". *Phys. Rev. Lett.* **97,** 036808. http://dx.doi.org/10.1103/PhysRevLett.97.036808 (2006).

Appendix C

An explicit example of dimensional reduction*

This appendix is following the derivation in Ref. [1].

C.1 Class D*

Our goal is to take the step of dimensional reduction to relate the $\mathbb{Z}$ index of symmetry class D in three dimensions to the $\mathbb{Z}_2$ index of the same symmetry class in one spatial dimension. in this section. We consider one dimensional lattice systems where the Hamiltonian matrix fulfills

$$U_{\mathcal{C}}^{\dagger}\mathcal{H}^{*}(-k)U_{\mathcal{C}} = \mathcal{H}(k) \qquad \text{with} \qquad U_{\mathcal{C}} = U_{\mathcal{C}}^{\mathrm{T}}. \tag{C.1.1}$$

We now try to establish an equivalence relation between two such Hamiltonians $\mathcal{H}_1(k)$ and $\mathcal{H}_2(k)$. To borrow the Chern number from one dimension higher, we construct a path, or interpolation $\mathcal{H}(k,\vartheta)$, with $\vartheta \in [0,\pi]$ connecting the two Hamiltonians

$$\mathcal{H}(k,0) = \mathcal{H}_1(k) \qquad \text{and} \qquad \mathcal{H}(k,\pi) = \mathcal{H}_2(k). \tag{C.1.2}$$

In general, the Hamiltonian for an arbitrary $\vartheta \in [0,\pi]$ will not posses the symmetry (C.1.1). We correct for this by explicitly constructing the cyclic interpolation for $\vartheta \in [\pi, 2\pi]$

$$\mathcal{H}(k,\vartheta) = -U_{\mathcal{C}}^{\dagger}\mathcal{H}^{*}(-k, 2\pi-\vartheta)U_{\mathcal{C}}. \tag{C.1.3}$$

Interpreted as a two-dimensional problem, $H(k,\vartheta)$ is now manifestly particle-hole symmetric. By requiring for the whole interpolation the system to be gapped we can define the Chern number of this cyclic interpolation[1]

$$\mathsf{C}_{\mathcal{H}} = \oint d\vartheta \frac{\partial \mathsf{P}(\vartheta)}{\partial \vartheta}, \tag{C.1.6}$$

[1] To see that these formula indeed corresponds to our known result we first state that (we drop the label and sum over n for simplicity)

$$\begin{aligned}\mathcal{F}_{\vartheta k} &= \partial_\vartheta \mathrm{i}\langle\varphi_k|\partial_k\varphi_k\rangle - \partial_k \mathrm{i}\langle\varphi_k|\partial_\vartheta\varphi_k\rangle = \mathrm{i}\langle\partial_\vartheta\varphi_k|\partial_k\varphi_k\rangle + \mathrm{i}\langle\varphi_k|\partial_\vartheta\partial_k\varphi_k\rangle - \mathrm{i}\langle\partial_k\varphi_k|\partial_\vartheta\varphi_k\rangle - \mathrm{i}\langle\varphi_k|\partial_k\partial_\vartheta\varphi_k\rangle \\ &= \mathrm{i}\langle\partial_\vartheta\varphi_k|\partial_k\varphi_k\rangle - \mathrm{i}\langle\partial_k\varphi_k|\partial_\vartheta\varphi_k\rangle.\end{aligned}$$

We now write

$$\begin{aligned}\oint d\vartheta \frac{\partial \mathsf{P}(\vartheta)}{\partial\vartheta} &= \oint d\vartheta \frac{\partial}{\partial\vartheta}\oint \frac{dk}{2\pi}\mathrm{i}\langle\varphi_k|\partial_k\varphi_k\rangle = \oint d\vartheta\oint\frac{dk}{2\pi}\left(\mathrm{i}\langle\partial_\vartheta\varphi_k|\partial_k\varphi_k\rangle + \mathrm{i}\langle\varphi_k|\partial_\vartheta\partial_k\varphi_k\rangle\right) \\ &\overset{\text{P.I.}}{=} \oint d\vartheta\oint\frac{dk}{2\pi}\left(\mathrm{i}\langle\partial_\vartheta\varphi_k|\partial_k\varphi_k\rangle - \mathrm{i}\langle\partial_k\varphi_k|\partial_\vartheta\varphi_k\rangle\right) + \oint d\vartheta \underbrace{\mathrm{i}\langle\varphi_{k=2\pi}|\partial_\vartheta\varphi_{k=2\pi}\rangle}_{\mathcal{A}_\vartheta(k=2\pi)} + \oint d\vartheta \underbrace{\mathrm{i}\langle\varphi_{k=0}|\partial_\vartheta\varphi_{k=0}\rangle}_{\mathcal{A}_\vartheta(k=0)}.\end{aligned}$$

From the discussion of fiber bundles we know that we cannot necessarily choose a smooth gauge such that $\boldsymbol{\mathcal{A}}$ is a single-valued function over the whole torus. However, we can always choose a gauge where $\mathcal{A}_\vartheta$ is single valued

where as before we defined the charge polarization as a function of the pumping parameter ϑ

$$\mathsf{P}(\vartheta) = \oint \frac{dk}{2\pi} \sum_{n\,\text{filled}} \mathrm{i}\langle\varphi_{nk}|\partial_k\varphi_{nk}\rangle \tag{C.1.7}$$

To make further progress in establishing an equivalence relation between one dimensional Hamiltonians of class D we note that owing to the particle-hole symmetry, eigenstates of different locations in the Brillouin zone are related to each other. Without showing the full algebraic manipulations [1], we state that

$$\mathsf{P}(\vartheta) = -\mathsf{P}(2\pi - \vartheta). \tag{C.1.8}$$

An immediate consequence is

$$\int_0^\pi d\vartheta \mathsf{P}(\vartheta) = \int_\pi^{2\pi} d\vartheta \mathsf{P}(\vartheta). \tag{C.1.9}$$

We remind ourselves that these two equations rely crucially on the presence of the particle-hole symmetry. Consider now another particle-hole symmetric interpolation $\mathcal{H}'(k,\vartheta)$ between $\mathcal{H}_1(k)$ and $\mathcal{H}_2(k)$. We denote the corresponding polarization with $\mathsf{P}'(\vartheta)$. The relative Chern number of the two interpolations is then given by

$$\mathsf{C}_{\mathcal{H}} - \mathsf{C}_{\mathcal{H}'} = \oint d\vartheta \left(\frac{\partial \mathsf{P}(\vartheta)}{\partial\vartheta} - \frac{\partial \mathsf{P}'(\vartheta)}{\partial\vartheta} \right). \tag{C.1.10}$$

One can define two yet different interpolations $\mathcal{G}_1(k,\vartheta)$ and $\mathcal{G}_2(k,\vartheta)$ (not particle-hole symmetric!) via

$$\mathcal{G}_1(k,\vartheta) = \begin{cases} \mathcal{H}(k,\vartheta) & \vartheta \in [0,\pi] \\ \mathcal{H}'(k,2\pi-\vartheta) & \vartheta \in [\pi,2\pi] \end{cases}, \tag{C.1.11}$$

and

$$\mathcal{G}_2(k,\vartheta) = \begin{cases} \mathcal{H}'(k,2\pi-\vartheta) & \vartheta \in [0,\pi] \\ \mathcal{H}(k,\vartheta) & \vartheta \in [\pi,2\pi] \end{cases}. \tag{C.1.12}$$

These interpolations are shown in Fig. C.1. We see that $\mathcal{G}_1$ is obtained by reconnecting $\mathcal{H}$ and $\mathcal{H}'$ such that it always runs in the upper half-space and vice-versa for $\mathcal{G}_2$. It is straightforward to see that

$$\mathsf{C}_{\mathcal{G}_1} = \int_0^\pi d\vartheta \left(\frac{\partial \mathsf{P}(\vartheta)}{\partial\vartheta} - \frac{\partial \mathsf{P}'(\vartheta)}{\partial\vartheta} \right), \tag{C.1.13}$$

and

$$\mathsf{C}_{\mathcal{G}_2} = \int_\pi^{2\pi} d\vartheta \left(\frac{\partial \mathsf{P}(\vartheta)}{\partial\vartheta} - \frac{\partial \mathsf{P}'(\vartheta)}{\partial\vartheta} \right). \tag{C.1.14}$$

From this it is easy to see that $\mathsf{C}_{\mathcal{H}} - \mathsf{C}_{\mathcal{H}'} = \mathsf{C}_{\mathcal{G}_1} + \mathsf{C}_{\mathcal{G}_2}$. Moreover, if we use the symmetry (C.1.9) we see that $\mathsf{C}_{\mathcal{G}_1} = \mathsf{C}_{\mathcal{G}_2}$ and hence

$$\mathsf{C}_{\mathcal{H}} - \mathsf{C}_{\mathcal{H}'} = 2\nu \qquad \text{with} \qquad \nu \in \mathbb{Z}. \tag{C.1.15}$$

How can we understand this result? Remember that each interpolation gives rise to a two-dimensional band-structure. The Chern number of this band-structure, $\mathsf{C}_{\mathcal{H}}$ can only change if

(akin the Landau gauge for the electro-magnetic gauge potential). For such a gauge the integrals

$$\oint d\vartheta \mathcal{A}_\vartheta(k) = 0 \tag{C.1.4}$$

for both $k = 0$ and $k = 2\pi$. With this we established

$$\oint d\vartheta \frac{\partial \mathsf{P}(\vartheta)}{\partial\vartheta} = \oint d\vartheta \oint \frac{dk}{2\pi} \left(\mathrm{i}\langle\partial_\vartheta\varphi_k|\partial_k\varphi_k\rangle - \mathrm{i}\langle\partial_k\varphi_k|\partial_\vartheta\varphi_k\rangle \right) = \frac{1}{2\pi} \oint d\vartheta \oint dk\, \mathcal{F}_{\vartheta k} = \mathsf{C}^{(1)}, \tag{C.1.5}$$

as we tried to prove.

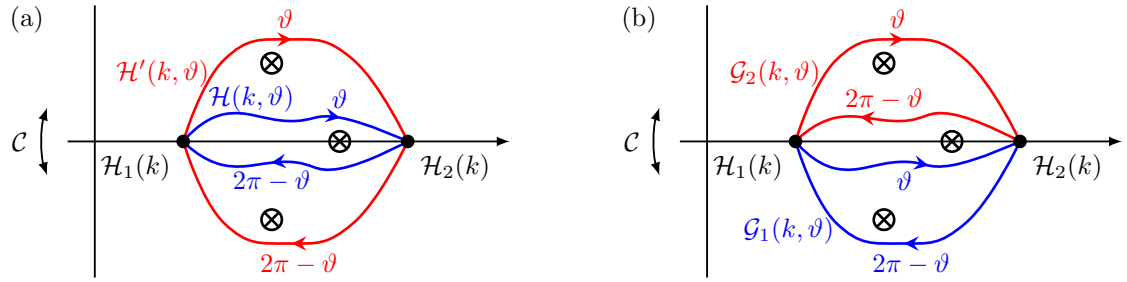

Figure C.1: (a) Interpolation between two particle-hole symmetric one dimensional Hamiltonians $\mathcal{H}_{1/2}(k)$. Along the horizontal axis we move between different one-dimensional Hamiltonians. Along the vertical axis, the particle-hole symmetry operation on the one-dimensional Hamiltonians corresponds to a mirroring around the horizontal axis. Hence, we see that the blue (red) interpolation paths are constructed such that the interpolation, interpreted as a two-dimensional Hamiltonian, is manifestly symmetric under $\mathcal{C}$. The crosses correspond to gap closings in $\mathcal{H}(k,\vartheta)$ and hence the interpolations are not allowed to touch them in order for $\mathcal{H}(k,\vartheta)$ to have a well defined Chern number. Due to symmetry constraints, all gap closings away from the particle-hole symmetric line appear in pairs. Consequently, we might change the Chern number by deforming the interpolation, but always by two. Hence, independently of how $\mathcal{H}_1(k)$ and $\mathcal{H}_2(k)$ are connected, the Chern number parity is independent of the interpolation and hence can be used as a $\mathbb{Z}_2$ index. (b) Different interpolation paths to make the arguments in (a) formal.

when going from $\mathcal{H} \to \mathcal{H}'$ we close a gap. However, due to the particle-hole symmetry, such gap closings always occur in two points in the Brillouin zone, see Fig. C.1. Therefore, for all possible interpolations between our original one dimensional problems $\mathcal{H}_1(k)$ and $\mathcal{H}_2(k)$ the parity of the Chern number is conserved. We can thus write the *relative Chern parity*

$$N[\mathcal{H}_1(k),\mathcal{H}_2(k)] = (-1)^{\mathsf{C}_{\mathcal{H}(k,\vartheta)}}. \tag{C.1.16}$$

It is easy to prove that this relative Chern parity has the property

$$N[\mathcal{H}_1(k),\mathcal{H}_2(k)]N[\mathcal{H}_2(k),\mathcal{H}_3(k)] = N[\mathcal{H}_1(k),\mathcal{H}_3(k)] \tag{C.1.17}$$

and consequently defines an equivalence relation. Equivalence classes are given by Hamiltonians in symmetry class D which have the same relative Chern parity. We can moreover define an absolute $\mathbb{Z}_2$ index by choosing a naturally "trivial" Hamiltonian $\mathcal{H}_0$ and then define

$$\mathcal{H}(k) \in \mathrm{D} \quad \text{trivial} \quad \Leftrightarrow \quad N[\mathcal{H}(k),\mathcal{H}_0] = 1, \tag{C.1.18}$$

$$\mathcal{H}(k) \in \mathrm{D} \quad \text{non-trivial:} \quad \Leftrightarrow \quad N[\mathcal{H}(k),\mathcal{H}_0] = -1. \tag{C.1.19}$$

While the above developments might appear somewhat formal, they have a direct physical consequence. Imagine a one dimensional system $\mathcal{H}_{\mathrm{nt}}$ which is non-trivial according to (C.1.19). The two dimensional system given by the interpolation between $\mathcal{H}_0$ and $\mathcal{H}_{\mathrm{nt}}$ therefore has an odd Chern number and correspondingly an odd number of surface modes traversing the gap on a each side of a finite cylinder. Let us imagine ϑ to be the momentum along the edge of the cylinder. Due to the particle hole symmetry between ϑ and $2\pi-\vartheta$, zero levels always appear in pairs at ϑ and $2\pi-\vartheta$. As we need an odd number of them, there has to be one either at $\vartheta = 0$ or π. As $\vartheta = 0$ corresponds to the trivial atomic Hamiltonian $\mathcal{H}_0$, there are no end states at $\vartheta = 0$. In other words, a non-trivial $\mathbb{Z}_2$ index in class D guarantees the existence of zero energy end states for a one dimensional system with an end.

References

1. Qi, X.-L., Hughes, T. L. & Zhang, S.-C. "Topological field theory of time-reversal invariant insulators". *Phys. Rev. B* **78,** 195424. http://link.aps.org/doi/10.1103/PhysRevB.78.195424 (2008).

Appendix D

Irreducible representations of non-symmorphic space groups*

Learning goals

- We know the difference between interior and exterior points of the Brillouin zone.
- We know the Herring construction of irreps of non-symmorphic little groups.

- T. Inui et al., Group theory and its applications to physics, Springer Berlin, Heidelberg

In large parts of this chapter we follow reference [1]. We assume that the reader is familiar with the concept of space groups. If this is not the case, Chap. 11 of Ref. [1] will provide the background needed for this chapter.

D.1 Outline

For non-symmorphic groups, some of the symmetry operations interweave point group operations with translations in a non-trivial way. This presents a challenge when classifying the representations, as one cannot simply use the well-known irreps of the standard point groups in combination with the one-dimenasional irreps of the abelian translation group. It turns out that this complication only arises at high-symmetry points on the boundary of the Brillouin zone. The key idea we want to apply here is to enlarge the unit cell in order to fold these zone-boundary momenta to an effective Γ-point. Once we do that one can use the standard tools to derive the irreps. However, in order to be faithful to the orginal (small) real-space unit cell, we need to post-select some of the so-obtained irreps. The goal of this appendix is to formalize this idea, which goes by the name of *Herring's method* [2].

D.2 Space group symmetries

The symmetry groups of crystalline systems are called space groups in three dimensions or wallpaper groups in two dimensions. Their elements can be written as

$$g = \{R|\boldsymbol{t}\}, \tag{D.2.1}$$

with R a member of the crystalline point group and $\boldsymbol{t}$ a translation. Amongst the members of the various space groups we have both pure point group opertions $\{R|0\}$, pure translations $\{E|\boldsymbol{t}\}$ with $\boldsymbol{t} = n_i\boldsymbol{a}_i$, where the $\boldsymbol{a}_i$ denote the lattice vectors, $n_i \in \mathbb{Z}$, and E is the neutral element of the point group. Some groups contain non-symmorphic elements $\{R|\boldsymbol{b}\}$, which involve a point group operation combined with a (fraction of a lattice-) translation $\boldsymbol{b}$.

If R is a rotation and $\boldsymbol{b}$ points along the rotation axis, we talk about a screw symmetry. If R is a mirror operation and $\boldsymbol{b}$ lies in the mirror plane, we denote this a glide symmetry. If the translation is orthogonal to the rotation axis or the mirror plane, respectively, the group element can be made symmorphic by a suitable choice of rotation center (mirror plane).
Multiplication of group elements are defined as

$$\{R_2|\boldsymbol{b}_2\}\circ\{R_1|\boldsymbol{b}_1\}=\{R_2R_1|R_2\boldsymbol{b}_1+\boldsymbol{b}_2\}, \tag{D.2.2}$$

from which follows that

$$\{R|\boldsymbol{b}\}^{-1}=\{R^{-1}|-R^{-1}\boldsymbol{b}\}. \tag{D.2.3}$$

A change of origin would amount to $\{e|\boldsymbol{\eta}\}\circ\{R|\boldsymbol{b}\}\circ\{e|-\boldsymbol{\eta}\}=\{R|\boldsymbol{b}+\boldsymbol{\eta}-R\boldsymbol{\eta}\}$. Moreover, the group's action on functions of spatial coordinates is given by

$$[\{R|\boldsymbol{b}\}]\psi(\boldsymbol{r})=\psi(R^{-1}(\boldsymbol{r}-\boldsymbol{b})). \tag{D.2.4}$$

We now want to embark on the description of the irreducible represenation (irreps) of the space group G. We start by the discrete translation group.

D.3 Translations

The translations can be written as a direct product of the abdelian one dimensional groups

$$T=T_1\times T_2\times T_3, \tag{D.3.1}$$

$$\{E|\boldsymbol{a_n}=n_i\boldsymbol{a}_i\}=\{E|n_1\boldsymbol{a}_1\}\circ\{E|n_2\boldsymbol{a}_2\}\circ\{E|n_3\boldsymbol{a}_3\}. \tag{D.3.2}$$

Moreover, we assume periodic boundary conditions $\{E|\boldsymbol{a}_i\}^N=\{E|0\}$, such that the characters of the one-dimensional represenations have to fulfill

$$[\chi(\{E|\boldsymbol{a}_i\})]^N=1. \tag{D.3.3}$$

This immediately defines the characters to be

$$\chi^{\mathbf{k}}(\{E|\boldsymbol{a_n}\})=e^{\mathrm{i}\boldsymbol{k}\cdot\boldsymbol{a_n}}, \tag{D.3.4}$$

where we took the limit $N\to\infty$ to obtain a continuous lattice momentum $\boldsymbol{k}$. It is simple to check that Bloch wave functions indeed transform in the so-obtained irrep

$$\begin{aligned}[\{E|\boldsymbol{a_n}\}]\psi_{\boldsymbol{k}}(\boldsymbol{r})&=[\{E|\boldsymbol{a_n}\}]e^{-\mathrm{i}\boldsymbol{k}\cdot\boldsymbol{r}}u(\boldsymbol{r})=e^{-\mathrm{i}\boldsymbol{k}\cdot(\boldsymbol{r}-\boldsymbol{a_n})}u(\boldsymbol{r}-\boldsymbol{a_n})\\&=e^{\mathrm{i}\boldsymbol{k}\cdot\boldsymbol{a_n}}e^{-\mathrm{i}\boldsymbol{k}\cdot\boldsymbol{r}}u(\boldsymbol{r})=e^{\mathrm{i}\boldsymbol{k}\cdot\boldsymbol{a_n}}\psi_{\boldsymbol{k}}(\boldsymbol{r}),\end{aligned} \tag{D.3.5}$$

where in the step to the second line we made use of the periodicity of $u(\boldsymbol{r}-\boldsymbol{a_n})=u(\boldsymbol{r})$. Let us now consider how such Bloch wave functions transform under the full group G.

D.4 Little groups and their irreps

Let us see what happens to an irrep of the group T under the action of $\{R_i|\boldsymbol{b}_i\}$

$$[\{E|\boldsymbol{a_n}\}][\{R_i|\boldsymbol{b}_i\}]\psi_{\boldsymbol{k}}(\boldsymbol{r})=[\{R_i|\boldsymbol{a_n}+\boldsymbol{b}_i\}]\psi_{\boldsymbol{k}}(\boldsymbol{r})=[\{R_i|\boldsymbol{b}_i\}]\underbrace{[\{E|R^{-1}\boldsymbol{a_n}\}]\psi_{\boldsymbol{k}}(\boldsymbol{r})}_{e^{-\mathrm{i}\boldsymbol{k}\cdot R^{-1}\boldsymbol{a_n}}\psi_{\boldsymbol{k}}(\boldsymbol{r})} \tag{D.4.1}$$

$$=e^{\mathrm{i}R\boldsymbol{k}\cdot\boldsymbol{a_n}}[\{R_i|\boldsymbol{b}_i\}]\psi_{\boldsymbol{k}}(\boldsymbol{r}). \tag{D.4.2}$$

We see that $[\{R_i|\boldsymbol{b}_i\}]\psi_{\boldsymbol{k}}(\boldsymbol{r})$ transforms under T as $\psi_{\boldsymbol{k}}$, however, it belongs to the irrep of $R\boldsymbol{k}$ rather than $\boldsymbol{k}$!

There may be some operations $\{R_i|\boldsymbol{b}_i\}$ which leave $\boldsymbol{k}$ invariant up to the addition of a reciprocal lattice vector

$$R_i\boldsymbol{k} = \boldsymbol{k} + n_j\boldsymbol{K}_j. \tag{D.4.3}$$

According to (D.4.2) $[\{R_i|\boldsymbol{b}_i\}]\psi_{\boldsymbol{k}}(\boldsymbol{r})$ then belongs to the same representation as $\psi_{\boldsymbol{k}}(\boldsymbol{r})$. The set of $\{R_i|b_i\}$ where (D.4.3) holds defines the symmetry group $G_{\boldsymbol{k}}$ of the wave vector $\boldsymbol{k}$. It is typically called the little group of $\boldsymbol{k}$. We now try to obtain the irreps $D^{\boldsymbol{k}}$ of these little groups. The first constraint is, that $D^{\boldsymbol{k}}(\{e|\boldsymbol{a_n}\}) = e^{\mathrm{i}\boldsymbol{k}\cdot\boldsymbol{a_n}}\mathbb{1}$. Motivated by this observation we now try to construct a representation of the little group. We propose irreps of $G_{\boldsymbol{k}}$ by writing

$$D^{\boldsymbol{k}}(\{R_i|\boldsymbol{b}_i\}) = e^{\mathrm{i}\boldsymbol{k}\cdot\boldsymbol{b}_i}\Gamma(R_i), \tag{D.4.4}$$

where $\Gamma(R_i)$ is an irrep of the point group $G^0_{\boldsymbol{k}}$ of $G_{\boldsymbol{k}}$. In other words, we just compose the irreps of $G_{\boldsymbol{k}}$ by combining the Bloch states with the irreps of the well-know point groups. Let us see when the above construction leads to an actual representation of $G_{\boldsymbol{k}}$. For this we check the defining property of a represenation:

$$D^{\boldsymbol{k}}(\{R_2|\boldsymbol{b}_2\})D^{\boldsymbol{k}}(\{R_1|\boldsymbol{b}_1\}) = e^{\mathrm{i}\boldsymbol{k}\cdot(\boldsymbol{b}_1+\boldsymbol{b}_2)}\Gamma(R_2R_1), \tag{D.4.5}$$

which should be the same as

$$D^{\boldsymbol{k}}(\{R_2,\boldsymbol{b}_2\}\circ\{R_1|\boldsymbol{b}_1\}) = D^{\boldsymbol{k}}(\{R_2R_1|R_2\boldsymbol{b}_1+\boldsymbol{b}_2\}) = e^{\mathrm{i}\boldsymbol{k}\cdot(R_2\boldsymbol{b}_2+\boldsymbol{b}_1)}\Gamma(R_2R_1). \tag{D.4.6}$$

Obvioulsy, we define a valid linear representation if, and only if

$$\exp[\mathrm{i}(R_2^{-1}\boldsymbol{k}-\boldsymbol{k})\cdot\boldsymbol{b}_1] = 1. \tag{D.4.7}$$

We deduce that

- $D^{\boldsymbol{k}}(\{R_i|\boldsymbol{b}_i\}) = e^{\mathrm{i}\boldsymbol{k}\cdot\boldsymbol{b}_i}\Gamma(R_i)$ defines a representation for all $\boldsymbol{k}$ in the interior of the Brillouin zone, as in this case $R_2^{-1}\boldsymbol{k} = \boldsymbol{k}$ without the addition of a reciprocal lattice vector $n_j\boldsymbol{K}_j$.
- For symmorphic groups, where all $\boldsymbol{b}_i = 0$, the above prescription also defines a legitimate represention.

Which leaves us with the actual task of this chapter: to construct the irreps of non-symmorphic little groups at the Brillouin zone boundaries.
As pointed out in the introduction, we now enlarge the unit cell by selecting a subset $T_{\boldsymbol{k}}$ of the translation group corresponding to an effective enlargment of the unit cell. The criterion is that

$$e^{\mathrm{i}\boldsymbol{k}\cdot\boldsymbol{a_n}} = 1. \tag{D.4.8}$$

In other words, the irreps of the reduced translation group $T_{\boldsymbol{k}}$ are just simple identities $\mathbb{1}$. This will come in handy, because we can consider the factor group $G_{\boldsymbol{k}}/T_{\boldsymbol{k}}$ and all irreps of $G_{\boldsymbol{k}}$ will be contained in it. Let us illustrate this on the wallpaper group $P4gm$.
$P4gm$ contains the pure translations of a simple square lattice with $\boldsymbol{a}_1 = (1,0)$ and $\boldsymbol{a}_2 = (0,1)$ and the following generators of the further symmetry operations

$$\begin{aligned}
\{E|0\}: &\quad \text{the neutral element,}\\
\{C_2|0\}: &\quad \text{inversion,}\\
\{C_4|0\}: &\quad \text{a four-fold rotation,}\\
\{m_{10}|\boldsymbol{b}_m = (1/2,1/2)\}: &\quad \text{a mirror on the y-axis combined with half-lattice translations.}
\end{aligned}$$

It is easy to check that for $X = 2\pi(1/2,0)$, at the edge of the Brillouin zone, the little group is given by

$$G_{\mathbf{k}} = T\{E|0\} + T\{C_2|0\} + T\{m_{10}|\boldsymbol{b}_m\} + T\{m_{01}|\boldsymbol{b}_m\}. \tag{D.4.9}$$

Moreover, for X we can check that $T_{\boldsymbol{k}}$ contains all translations

$$\boldsymbol{a_n} = 2n_1\boldsymbol{a}_1 + n_2\boldsymbol{a}_2 \quad \text{with} \quad n_i \in \mathbb{Z}. \tag{D.4.10}$$

The factor of two in front of n_1 corresponds to the anticipated enlargment of the unit cell. As promised, we now treat $\{E|\boldsymbol{a}_1\}$ as a member of the point group by writing

$$\begin{aligned} G_{\boldsymbol{k}} = \; & T_{\boldsymbol{k}}\{E|0\} + T_{\boldsymbol{k}}\{C_2|0\} + T_{\boldsymbol{k}}\{m_{10}|\boldsymbol{b}_m\} + T_{\boldsymbol{k}}\{m_{01}|\boldsymbol{b}_m\} \\ & + T_{\boldsymbol{k}}\{E|\boldsymbol{a}_1\} + T_{\boldsymbol{k}}\{C_2|\boldsymbol{a}_1\} + T_{\boldsymbol{k}}\{m_{10}|\boldsymbol{b}_m + \boldsymbol{a}_1\} + T_{\boldsymbol{k}}\{m_{01}|\boldsymbol{b}_m + \boldsymbol{a}_1\}. \end{aligned}$$

Thanks to (D.4.8), all irreps of $G_{\boldsymbol{k}}$ will be contained in the factor group $G_{\boldsymbol{k}}/T_{\boldsymbol{k}}$. It remains to be determined to which finite group of eight elements $G_{\boldsymbol{k}}/T_{\boldsymbol{k}}$ is isomorphic to. By comparing the multiplication table of the members of the factor group $G_{\boldsymbol{k}}/T_{\boldsymbol{k}}$ with those of the five inequivalent groups of order eight we deduce that $G_{\boldsymbol{k}}/T_{\boldsymbol{k}}$ is isomorphic to $4mm$ with the identification

$$\{E|0\} \to E, \qquad \{E|\boldsymbol{a}_1\} \to C_2, \tag{D.4.11}$$

$$\{m_{01}|\boldsymbol{b}_m\} \to C_4^+, \qquad \{m_{01}|\boldsymbol{b}_m + \boldsymbol{a}_1\} \to C_4^-, \tag{D.4.12}$$

$$\{C_2|0\} \to m_{10}, \qquad \{C_2|\boldsymbol{a}_1\} \to m_{01}, \tag{D.4.13}$$

$$\{m_{10}|\boldsymbol{b}_m\}, \to m_{11}, \qquad \{m_{10}|\boldsymbol{b}_m + \boldsymbol{a}_1\} \to m_{1-1}. \tag{D.4.14}$$

We are now in the position to consult the character table of $4mm$ in Tab. D.1. Special attention is required for the group element $\{E|\boldsymbol{a}_1\}$. While this was added as a point group element in the factor group $G_{\boldsymbol{k}}/T_{\boldsymbol{k}}$, we should recall that $\{E|\boldsymbol{a}_1\}$ is a pure translation and as such should transform as

$$\exp(\mathrm{i}\boldsymbol{k}\cdot\boldsymbol{a}_1)\mathbb{1} \overset{\boldsymbol{k}=X}{=} -\mathbb{1}.$$

In other words, only X_5 is admissible as an irrep for the little group of $P4gm$ at the X-point!

		E $\{E\|0\}$	C_4 $\{m_{01}\|\boldsymbol{b}_m\}$	C_2 $\{E\|\boldsymbol{a}_1\}$	m_{10} $\{C_2\|0\}$	m_{11} $\{m_{10}\|\boldsymbol{b}_m\}$
A_1	X_1	1	1	1	1	1
A_2	X_2	1	1	1	-1	-1
B_1	X_3	1	-1	1	1	-1
B_2	X_4	1	-1	1	-1	1
E_g	X_5	2	0	-2	0	0

Table D.1: Character table for the group $4mm$ and the identifaction of the group elements of $4mm$ with the members of the factor group $G_{\boldsymbol{k}}/T_{\boldsymbol{k}}$.

Quite remarkably, only two-dimensional irreps occur at the X point of structures in $P4gm$. Luckily, we do not have to go through Herring's construction for all high-symmetry points of non-symmorphic space groups. As usual, all of this data is tabulated on the Bilbao Crystallographic Server.

D.5 Space group symmetry induced Kramer's pairs

We conclude this appendix by the observation that space group symmetries may induce degeneracies beyond the usual higher-dimensional irreps of finite groups. We cover two such options here. First, a set of anti-commuting symmetries may be responsible for degeneracies, or, second, anti-unitary symmetries squaring to $-\mathbb{1}$ give rise to effective Kramer's pairs. Let us start with the second scenario.

D.5.1 $\mathcal{M}^2 = -\mathbb{1}$

One option is that an anti-unitary symmetry squares to $-\mathbb{1}$. This often occurs in conjunction with time reversal symmetry. To construct an effective Kramer's pair we use that for an antiunitary operator $\mathcal{M}$ we have $\langle \mathcal{M}v|\mathcal{M}w\rangle = \langle w|v\rangle$. If $\mathcal{M}^2 = -\mathbb{1}$ we can use

$$-\langle v|\mathcal{M}v\rangle = \langle \mathcal{M}^2 v|\mathcal{M}v\rangle = \langle v|\mathcal{M}v\rangle,$$

which implies $\langle v|\mathcal{M}v\rangle = 0$ and hence all eigenvalues come in pairs of two.
In the above example of $P4gm$, we can construct such an antiunitary operator along the line $\overline{XM}$ where $\boldsymbol{k} = (\pi, k_y)$ with $k_y \in [0, \pi]$. In the wall paper group $P4gm$, we may use the fact, that the combined action of bosonic time reversal[1] $\mathcal{T}$ with $\{m_{01}|\boldsymbol{b}_m\}$ is a symmetry of $\boldsymbol{k}$ on $\overline{XM}$:

$$\mathcal{M} = \mathcal{T} \circ \{m_{01}|\boldsymbol{b}_m\} : (\pi, k_y) \to (-\pi, k_y) = (\pi, k_y). \tag{D.5.1}$$

Note, that $\{m_{01}|\boldsymbol{b}_m\}$ alone, unlike $\{m_{10}|\boldsymbol{b}_m\}$, is not a symmetry of the line $\overline{XM}$. We further use that

$$(x, y) \overset{m_{01}}{\to} (x, -y) \overset{T_{\boldsymbol{b}_m}}{\to} (x + 1/2, -y + 1/2) \overset{m_{01}}{\to} (x + 1/2, y - 1/2) \overset{T_{\boldsymbol{b}_m}}{\to} (x + 1, y). \tag{D.5.2}$$

Or in other words

$$(\{m_{01}|\boldsymbol{b}_m\})^2 = T_{\boldsymbol{a}_1} = e^{\mathrm{i}k_x} \overset{k_x=\pi}{=} -1. \tag{D.5.3}$$

As we also have that $[\mathcal{T}, \{m_{01}|\boldsymbol{b}_m\}] = 0$, we find

$$\mathcal{M}^2 = (\mathcal{T} \circ \{m_{01}|\boldsymbol{b}_m\})^2 = \mathcal{T}^2 (\{m_{01}|\boldsymbol{b}_m\})^2 \overset{k_x=\pi}{=} -1. \tag{D.5.4}$$

We conclude that the presence of a bosonic (or spinless) time reversal symmtery makes bands in $P4gm$ along $\overline{XM}$ stick to each other.

D.5.2 $\{\mathcal{A}, \mathcal{B}\} = 0$

Quite similar to the above case, the anticommutation of two unitary symmetries can be used to construct an effective Kramer's pair. Assuming $\mathcal{A}$ and $\mathcal{B}$ to be unitary symmetries of the Hamiltonian with $\mathcal{A}|v\rangle = \lambda_{\mathcal{A}}|v\rangle$ and $\mathcal{B}|v\rangle = \lambda_{\mathcal{B}}|v\rangle$ we can write

$$\langle v|\mathcal{A}\mathcal{B}|v\rangle = \lambda_{\mathcal{A}}\lambda_{\mathcal{B}}\langle v|v\rangle = \langle v|\mathcal{B}\mathcal{A}|v\rangle = -\langle v|\mathcal{A}\mathcal{B}|v\rangle, \tag{D.5.5}$$

from which follows that $\mathcal{A}\mathcal{B}|v\rangle$ has to be orthogonal to $|v\rangle$ and hence we obtain a degenerate subspace of the Hamiltonian.
As an illustration, we can use the following model of a quadrupole insulator [3] with $\Gamma_i = -\sigma_y \otimes \sigma_i$, where $i = 1, 2, 3$ denote the three Pauli matrices, $\Gamma_4 = -\sigma_x \otimes \mathbb{1}_{2\times 2}$, and $\Gamma_{24} = [\Gamma_1, \Gamma_4]/(2\mathrm{i})$. With these definitions we can write

$$\mathcal{H}(k_x, k_y) = \left[1 + \frac{1}{2}\cos(k_x)\right]\Gamma_4 + \frac{1}{2}\sin(k_x)\Gamma_3 + \left[1 + \frac{1}{2}\cos(k_y)\right]\Gamma_2 + \frac{1}{2}\sin(k_y)\Gamma_1 + \Gamma_{24}. \tag{D.5.6}$$

This Hamiltonian is symmetric under the mirrors $m_{10} = \sigma_x \otimes \sigma_z$ and $m_{01} = \sigma_x \otimes \sigma_x$ with $m_{10}\mathcal{H}(k_x, k_y)m_{10}^\dagger = \mathcal{H}(-k_x, k_y)$ and $m_{01}\mathcal{H}(k_x, k_y)m_{01}^\dagger = \mathcal{H}(k_x, -k_y)$. The three points in the Brillouin zone with both these mirrors in the little group are $\Gamma = (0, 0)$, $X = (\pi, 0)$, and $M = (\pi, \pi)$. The spectrum along the high-symmetry lines is shown in Fig. D.1.

[1] $\mathcal{T} = K$ with K denoting complex conjugation and $\mathcal{T}^2 = 1$.

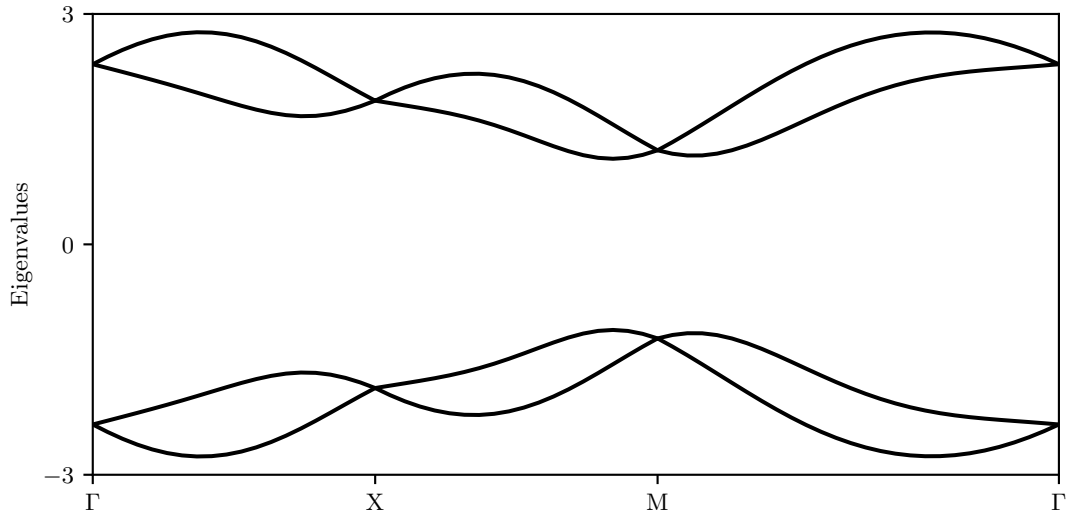

Figure D.1: Spectrum of the quadrupole insulator where anticommuting mirrors m_{10} and m_{01} lead to degeneracies at the mirror symmetric points Γ, X and M.

References

1. Inui, T., Tanabe, Y. & Onodera, Y. *Group Theory and Its Applications in Physics*. https://doi.org/10.1007/978-3-642-80021-4 (Springer-Verlag Berlin, 1990).
2. Herring, C. "Character tables for two space groups". *J. of the Franklin Inst.* **233,** 525. https://doi.org/10.1016/S0016-0032(42)90462-9 (1942).
3. Benalcazar, W. A., Bernevig, B. A. & Hughes, T. L. "Quantized Electric Multipole Insulators". *Science* **357,** 61. https://dx.doi.org/10.1126/science.aah6442 (2017).